Fouling Control in Anaerobic Membrane Bioreactors by Flux Enhancer Dosing

Odriozola, Magela

Important note
To cite this publication, please use the final published version (if applicable).
Please check the document version above.

Fouling Control In Anaerobic Membrane Bioreactors By Flux Enhancer Dosing

Magela Odriozola Arbiza

FOULING CONTROL IN
ANAEROBIC MEMBRANE BIOREACTORS
BY FLUX ENHANCER DOSING

Dissertation

for the purpose of obtaining the degree of doctor
at Delft University of Technology
by the authority of the Rector Magnificus Prof. dr. ir. T.H.J.J. van der Hagen,
chair of the Board for Doctorates
to be defended publicly on
Friday 8 April 2022 at 12:30 o'clock

by

Magela ODRIOZOLA ARBIZA

Magíster en Ingeniería Química, Universidad de la República, Uruguay
born in Artigas, Uruguay

This dissertation has been approved by the promotors:
Prof. dr. ir. J.B. van Lier
Dr. ir. H.L.F.M. Spanjers

Composition of the doctoral committee:

Rector Magnificus,	chairperson
Prof. dr. ir. J.B. van Lier,	Delft University of Technology, promotor
Dr. ir. H.L.F.M. Spanjers,	Delft University of Technology, promotor

Independent members:

Prof. dr. P. Le-Clech,	University of South Wales, Australia
Prof. dr. D.A. Jeison Nuñez,	Pontificia Universidad Católica de Valparaíso, Chile
Prof. dr. I. López Moreda,	Universidad de la República, Uruguay
Dr. A. Robles Martínez,	Universitat de València, Spain
Prof. dr. M.K. de Kreuk,	Delft University of Technology

Reserve member:

Prof. dr. ir. L.C. Rietveld	Delft University of Technology

To my family

TABLE OF CONTENTS

SUMMARY

Anaerobic membrane bioreactor (AnMBR) technology is increasingly researched for wastewater treatment in a circular economy scenario to recover nutrients, water, and biogas. AnMBR couples the advantages of anaerobic digestion, such as low sludge production, no aeration requirement and biogas production, with the benefits of membrane technology, that is, complete solids removal and a high removal degree of pathogenic organisms. Nevertheless, membrane fouling remains the major operational challenge, limiting the economic feasibility and applicability of AnMBRs. Membrane fouling is responsible for lower flux, higher transmembrane pressure, the need for intensive biogas sparging or increased crossflow velocities for membrane scouring, and increased frequency of membrane cleaning and membrane replacement; consequently, increasing energy and operational costs.

Researchers extensively studied the causes and mitigation of membrane fouling in both aerobic and anaerobic membrane bioreactors. Membrane fouling mitigation strategies have focused on optimisation of membrane operational variables, such as: gas sparging, crossflow velocity, filtration-relaxation cycle, permeate flux and frequency and intensity of chemical cleaning. Although optimisation of operational variables might be suitable when the sludge has good or moderate filterability, it may not be adequate or sufficient when fouling is caused by a sludge with poor filterability. The application of flux enhancers for fouling control has been extensively investigated. Flux enhancers are adsorbents, coagulants and flocculants that decrease fouling by changing the sludge characteristics, thereby improving sludge filterability. Particularly, cationic polymers have been successfully applied as flux enhancers in short-term tests on large-scale aerobic membrane bioreactors (MBRs), whereas in AnMBRs research is scarce, and so far, only done at lab-scale. Results from MBRs cannot be directly translated to AnMBRs because the extent and nature of membrane fouling under anaerobic and aerobic conditions are different.

This thesis studies the feasibility of dosing cationic polymers into large-scale AnMBRs for fouling mitigation, focusing on long-term effects, possible side effects, optimal dosing strategy and variation of required dosage. Dosing the cationic polymer Adifloc KD451 was a suitable strategy for fouling mitigation in a pilot-scale AnMBR, because it had a long-term improvement of filtration performance and sludge filterability, while having no significant adverse effects on permeate quality and COD removal efficiency.

Scarce, and contradictory reports are published on the effect of cationic polymers on the microbial community. This thesis analyses the inhibitory effect of the cationic polymer Adifloc KD451 on the biological activity of anaerobic sludge. Batch tests showed that the cationic polymer presented a significant inhibitory effect on the specific methanogenic activity of the sludge. Mathematical modelling was used as a tool to reveal the underlying inhibition mechanism. The inhibition was successfully predicted by the non-competitive and un-competitive inhibition models. These models describe a biostatic inhibition, namely a

reversible process. Accordingly, dosing the cationic polymer to a pilot-scale AnMBR had an immediate negative effect on the specific methanogenic activity, but this was a reversible process that had no adverse effect on permeate quality or chemical oxygen demand (COD) removal efficiency.

In large-scale membrane bioreactors, the sludge characteristics are constantly changing due to variations in the membrane and reactor operational conditions. These variations can affect the required optimal dosage of flux enhancer. Previous research revealed a high variability of the required optimal dosage of cationic polymers as flux enhancers for different types of sludge; however, studies analysing the causes for such variability are lacking. This thesis identifies the main factors affecting the optimal required dosage of cationic polymer for sludge filterability improvement in AnMBRs. Guidelines for adequate continuous application of cationic polymers in full-scale AnMBRs for fouling control are provided.

Researchers have suggested the possible application of in-situ and online measurement of sludge filtration characteristics (such as filterability) for automatic flux enhancer dosing control in membrane bioreactors. However, this has not been further studied or tested. In this thesis, in-situ sludge filterability measurements allowed to identify the cause of filtration performance deterioration and improvement in a pilot-scale AnMBR, and thus provided an appropriate input variable for manipulating flux enhancer dosage for fouling control in AnMBRs. The sludge filterability was measured with a dedicated installation, — the anaerobic Delft filtration characterisation method (AnDFCm) — connected on-line to a pilot-scale AnMBR.

Flux enhancer has been mostly added to membrane bioreactors using an initial pulse-dosage that is followed by periodic dosing to compensate for the flux enhancer loss by biodegradation and sludge withdrawal. However, this dosing strategy does not consider possible disturbances and is based on assumptions that might lead to flux enhancer underdose or overdose. This thesis proposes and compares three feedback and two feedforward control tools to manipulate flux enhancer dosing into AnMBRs. The comparison was done in a simulation environment with an integrated model that predicted the effect of cationic polymer dosing on sludge filterability and membrane fouling rate. The integrated model coupled filtration, flocculation, and biochemical processes and it was developed, calibrated, and validated in this thesis. The most appropriate control tool was a feedback sludge filterability controller that dosed cationic polymer continuously. This strategy achieved more stable sludge filterability and fouling rate by rejecting disturbances.

Samenvatting

De anaerobe membraanbioreactor (AnMBR) technologie biedt interessante mogelijkheden voor waterzuivering in een circulaire economie om zo voedingstoffen, water en biogas terug te winnen. AnMBR koppelt de voordelen van anaerobe gisting, zoals lage slibproductie, geen noodzaak voor beluchting, en biogasproductie, aan de voordelen van membraantechnologie. Deze voordelen zijn de volledige verwijdering van deeltjes en een hoge verwijdering van pathogene organismen. Desondanks blijft membraanvervuiling (*fouling*) de belangrijkste operationele uitdaging die de economische haalbaarheid en toepasbaarheid van AnMBRs beperkt. Het optreden van membraanvervuiling leidt tot een lagere flux, hogere transmembraandruk, en vereist aanpassingen in de bedrijfsvoering om deze vervuiling te beheersen, zoals recirculatie van biogas of opvoeren van de vloeistof snelheid langs het membraan. Daarnaast leidt deze vervuiling tot een verhoogde reinigingsfrequentie en het vroegtijdig vervangen van de membranen, wat vervolgens de energie- en operationele kosten verhoogt.

Diverse onderzoekers hebben uitgebreid onderzoek verricht naar de oorzaken en mogelijkheden tot vermindering van membraanvervuiling in zowel aerobe als anaerobe MBRs. De meest toegepaste strategieën om membraanvervuiling tegen te gaan zijn gericht op het optimaliseren van membraan-gerelateerd operationele variabelen zoals: opvoeren van de biogas recirculatie en vloeistofsnelheid langs het membraan, aanpassen van de filtratie-relaxatie cyclus en de permeaatflux, en de frequentie en intensiteit van het chemisch reinigen. Hoewel de optimalisatie van deze operationele variabelen wellicht zeer geschikt zijn indien het slib wordt gekarakteriseerd door een goede of middelmatige filtreerbaarheid, zijn ze wellicht minder of niet geschikt indien de membraanvervuiling juist wordt veroorzaakt door slib met een slechte filtreerbaarheid. Om verlies van een goede membraanflux te voorkomen, is de toevoeging van fluxverbeteraars uitgebreid in de literatuur bestudeerd. Fluxverbeteraars zijn adsorbentiemiddelen, coagulatiemiddelen en vlokmiddelen die de membraanvervuiling verminderen doordat ze de karakteristieken van het slib zodanig aanpassen dat ze de filtreerbaarheid van het slib verbeteren. Met name kationische polymeren worden met succes toegepast als fluxverbeteraars in aerobe membraanbioreactoren (MBRs) op praktijkschaal, terwijl het onderzoek in AnMBRs zich beperkt tot labschaal reactoren. Daarbij kunnen de resultaten behaald in aerobe MBRs niet direct worden vertaald naar AnMBRs, omdat zowel de mate en aard van de membraanvervuiling anders zijn onder aerobe en anaerobe omstandigheden.

Dit proefschrift bestudeert de haalbaarheid van dosering van kationische polymeren in AnMBRs op praktijkschaal om membraanvervuiling te verminderen, waarbij het onderzoek is toegespitst op de langetermijneffecten, mogelijke neveneffecten, optimale doseerstrategie, en de variatie in de benodigde dosis. Het doseren van het kationische polymeer Adifloc KD451 bleek een geschikte strategie om membraanvervuiling te verminderen in een AnMBR op pilootschaal. Behaalde resultaten lieten een verbetering zien van de membraanfiltratiestap en de filtreerbaarheid van het slib op de lange termijn, terwijl er geen significante bijwerkingen

waren op de kwaliteit van het permeaat en het verwijderingsrendement van het chemisch zuurstofverbruik (CZV).

Er is slechts weinig gepubliceerd, terwijl resultaten zich soms tegenspreken wat betreft de effecten van kationische polymeren op de biologische activiteit en microbiële samenstelling van het slib. Dit proefschrift analyseert het remmende effect van het kationische polymeer Adifloc KD451 op de biologische activiteit van het anaerobe slib. Batchtesten laten zien dat kationische polymeren een significant remmend effect hebben op de specifieke methanogene activiteit van het slib. Met behulp van wiskundige niet-competitieve (*non-competitive* en *un-competitive)* modellen werd aangetoond dat de remming door polymeren biostatisch is, dat wil zeggen een omkeerbaar proces. In overeenstemming hiermee had de toevoeging van het kationische polymeer aan de AnMBR op pilootschaal in eerste instantie een negatief effect op de specifieke methanogene activiteit, echter dit bleek ook hier omkeerbaar en de toevoeging had geen bijwerkingen op de permeaatkwaliteit of de verwijderingsefficiëntie van CZV op de langere termijn.

In membraanbioreactoren op praktijk- en pilootschaal, zijn de slibkarakteristieken voortdurend aan veranderingen onderhevig vanwege wijzigingen in de operationele bedrijfsvoering van de membraan-unit en de bioreactor zelf. Deze wijzigingen kunnen tevens van invloed zijn op de optimale dosis van de toe te passen fluxverbeteraar. Eerder onderzoek liet een grote variatie zien van de benodigde optimale dosis van kationische polymeren als fluxverbeteraar voor verschillende soorten slib. Echter, tot dusver ontbreken verdergaande studies die de oorzaken van deze variabiliteit analyseren. Dit proefschrift identificeert de belangrijkste factoren die de optimale dosis van kationische polymeren voor de verbetering van de slibfiltreerbaarheid in AnMBRs beïnvloeden. Er zijn tevens richtlijnen ontwikkeld ten behoeve van de juiste en continue toepassing van kationische polymeren om membraanvervuiling in AnMBRs op praktijkschaal te beheersen.

Diverse onderzoekers hebben gesuggereerd dat in-situ en online metingen van slibfiltratiekarakteristieken (zoals de slibfiltreerbaarheid) een mogelijkheid kan zijn om de dosering van fluxverbeteraars in membraanbioreactoren te kunnen automatiseren met behulp van een regeling. Echter, dit is tot dusver nog niet verder onderzocht of getest. In dit proefschrift, zijn in-situ slibfiltreerbaarheidsmetingen toegepast om de oorzaak van de verslechtering dan wel verbetering van de filtratieprestatie in een AnMBR op pilootschaal te kunnen vaststellen. De verkregen resultaten laten zien dat in AnMBRs de slibfiltreerbaarheid inderdaad een geschikte ingangsvariabele is om de dosering van fluxverbeteraars te kunnen sturen met als doel de membraanvervuiling te kunnen regelen. De slibfiltreerbaarheid is gemeten met een speciaal hiervoor ontwikkelde installatie - the *anaerobic Delft filtration characterisation method* (AnDFCm) – die online werd verbonden met de AnMBR op pilootschaal.

Fluxverbeteraars worden meestal door middel van een pulsdosering toegevoegd aan membraanbioreactoren, gevolgd door een periodieke dosering om te compenseren voor het verlies van fluxverbeteraars door biologische afbraak en door verwijdering middels spuislib. Echter, deze doseerstrategie houdt geen rekening met mogelijke verstoringen en is gebaseerd op aannames die er wellicht toe leiden dat fluxverbeteraars worden over- of ondergedoseerd.

Dit proefschrift presenteert en vergelijkt drie regelstrategieën gebaseerd op een teruggekoppeling en twee regelstrategieën gebaseerd op een voorwaartse koppeling om de dosis fluxverbeteraars in AnMBRs te manipuleren. Deze vergelijking is gedaan in een simulatieomgeving met een geïntegreerd model dat het effect beschrijft van kationische polymeerdosering op slibfiltreerbaarheid en membraanvervuilingssnelheid. Het geïntegreerde model koppelt filtratie, flocculatie en biochemische processen. De ontwikkeling, kalibratie en validatie van dit model is in dit proefschrift in detail beschreven. Resultaten laten zien dat de meest geschikte regelstrategie een slibfiltreerbaarheidregeling met terugkoppeling betreft, die het kationische polymeer continu doseert. Met behulp van deze strategie kon mede op basis van storingsonderdrukking een stabielere slibfiltreerbaarheid en membraanvervuilingssnelheid worden behaald.

Resumen

La tecnología de biorreactores anaerobios de membrana (AnMBR, por sus siglas en inglés) está siendo crecientemente investigada para el tratamiento de aguas residuales en un marco de economía circular para recuperar nutrientes, agua y biogás. AnMBR acopla las ventajas de la digestión anaerobia, como ser la baja producción de lodos, ausencia de aireación y producción de biogás, con los beneficios de la tecnología de membranas, a saber, remoción completa de sólidos y alto grado de remoción de organismos patógenos. Sin embargo, el ensuciamiento de la membrana, referido como *fouling* en inglés, es aún el mayor desafío operacional que limita la viabilidad económica y aplicabilidad de los AnMBRs. El ensuciamiento reduce el flujo transmembrana y aumenta la presión transmembrana, la demanda del efecto abrasivo por burbujeo de biogás o velocidad de flujo cruzado, y las frecuencias de limpieza y reemplazo de las membranas; elevando así los costos operacionales y de energía.

Las causas del ensuciamiento y estrategias para mitigarlo han sido extensamente investigadas tanto en biorreactores de membranas aerobios como anaerobios. Las estrategias de mitigación se han enfocado en la optimización de la operación de la membrana, como ser: intensidad de burbujeo de gas, velocidad de flojo cruzado, ciclos de filtración y relajación, flujo de permeado y frecuencia e intensidad de limpieza química. La optimización de variables operacionales puede ser apropiada cuando el lodo tiene una capacidad a ser filtrado (referida como filtrabilidad) buena o moderada, no obstante, esta estrategia puede resultar inadecuada o insuficiente cuando el ensuciamiento es causado por lodos con baja filtrabilidad. El uso de mejoradores de flujo ha sido extensamente investigado. Los mejoradores de flujo son adsorbentes, coagulantes o floculantes capaces de atenuar el ensuciamiento de la membrana mejorando la filtrabilidad mediante cambios en las características del lodo. Particularmente, polímeros catiónicos han sido utilizados como mejoradores de flujo en ensayos de corto plazo en biorreactores aerobios de membrana (MBR, por sus siglas en inglés) de escala real y piloto, mientras que la investigación en AnMBRs es escasa, y hasta la fecha únicamente realizada en escala laboratorio. Los resultados obtenidos en MBRs no pueden ser directamente traducidos a AnMBRs dado que la magnitud y naturaleza del ensuciamiento bajo condiciones aerobias y anaerobias es diferente.

Esta tesis estudia la viabilidad de dosificar polímeros catiónicos para mitigar el ensuciamiento en AnMBRs de escala piloto, enfocándose en los efectos a largo plazo, los posibles efectos secundarios, la estrategia de dosificación optima y la variación de la dosis requerida. El polímero catiónico Adifloc KD451 resultó apropiado para mitigar el ensuciamiento en un reactor AnMBR escala piloto dado que sostuvo una mejora en el desempeño de la filtración y la filtrabilidad de lodo por un largo plazo. A su vez, dicho polímero no produjo efectos adversos significativos en la calidad del permeado y en la eficiencia de remoción de la demanda química de oxígeno (DQO).

Las publicaciones que estudian el efecto de polímeros catiónicos sobre la comunidad microbiana son escasas y presentan resultados contradictorios. Esta tesis analiza el efecto

inhibitorio del polímero catiónico Adifloc KD451 sobre la actividad biológica de lodos anaerobios. En ensayos en discontinuo, el polímero inhibió significativamente la actividad metanogénica específica del lodo. Con el uso de modelos matemáticos, se reveló que la inhibición del polímero es bioestática, es decir, un proceso reversible, evidenciado por modelos de inhibición no competitivos, referidos en inglés como *non-competitive* y *un-competitive*. En concordancia, la dosificación del polímero en un reactor AnMBR escala piloto tuvo un efecto negativo inmediato sobre la actividad metanogénica específica, pero el efecto fue reversible, y no afectó la calidad del permeado ni la eficiencia de remoción de DQO.

En biorreactores de membrana de escala real y piloto, las características del lodo cambian constantemente debido a variaciones en las condiciones de operación de la membrana y del reactor. Dichas variaciones pueden alterar la dosis optima requerida de mejoradores de flujo. Particularmente, investigaciones previas revelaron una alta variabilidad en la dosis optima de polímeros catiónicos, al ser usados como mejorador de flujo, en diferentes tipos de lodos. Sin embargo, hacen falta estudios que analicen las causas de dicha variabilidad. Esta tesis identifica los factores principales que afectan la variabilidad de la dosis optima de polímero catiónico requerida para mejorar la filtrabilidad de lodos provenientes de AnMBRs. A su vez, en esta tesis se brindan pautas para el uso continuo de polímeros catiónico para mitigar el ensuciamiento en AnMBRs de escala piloto y real.

Investigaciones previas han sugerido el posible uso de mediciones en línea e *in situ* de características de filtración del lodo (como ser la filtrabilidad) para controlar la dosificación de mejoradores de flujo en biorreactores de membrana. No obstante, esta estrategia no ha sido probada ni estudiada. En esta tesis, mediciones de filtrabilidad del lodo *in situ* permitieron identificar las causas de deterioro y mejora de la filtración en un AnMBR escala piloto y, por lo tanto, estas mediciones resultaron ser una variable adecuada para un sistema de control que manipule la dosis de mejoradores de flujo en AnMBRs. Las medidas de filtrabilidad del lodo se realizaron usando el instrumento de caracterización de la filtración de Delft (AnDFCm, por sus siglas en inglés) conectado en línea a un reactor AnMBR de escala piloto.

La adición de mejoradores de flujo en biorreactores de membrana se realiza usualmente mediante un pulso, seguido de adiciones periódicas para compensar la presunta perdida del mejorador de flujo por biodegradación o causada por la purga de lodos. Sin embargo, esta estrategia no toma en consideración posibles perturbaciones, y se basa en supuestos que podrían causar una sobredosis o una dosis insuficiente del mejorador de flujo. Esta tesis propone y compara distintos sistemas de control, tres de retroalimentación y dos anticipativos, para manipular la dosificación de mejoradores de flujo en AnMBRs. La comparación se realizó en un entorno de simulación con un modelo capaz de predecir el efecto de la adición de un polímero catiónico sobre la filtrabilidad del lodo y sobre la tasa de ensuciamiento de la membrana. El modelo acopla procesos de filtración, floculación y bioquímicos, y fue desarrollado, calibrado y validado en esta tesis. El sistema de control de filtrabilidad por retroalimentación fue el más apropiado. Este sistema proporcionó una dosificación continua del polímero al AnMBR, lo que resultó en una filtrabilidad del lodo y una tasa de ensuciamiento de la membrana más estable comparado con los resultados alcanzados con los restantes sistemas de control.

1

GENERAL INTRODUCTION [*]

[*] This chapter is partially based on:

Odriozola, M., Lousada-Ferreira, M., Spanjers, H., and van Lier, J. B. (2021). Effect of sludge characteristics on optimal required dosage of flux enhancer in anaerobic membrane bioreactors. J. Memb. Sci. 619, 118776. doi:10.1016/j.memsci.2020.118776.

Odriozola, M., Abraham, E., Lousada-Ferreira, M., Spanjers, H., and van Lier, J. B. (2019). Identification of the Methanogenesis Inhibition Mechanism Using Comparative Analysis of Mathematical Models. Front. Bioeng. Biotechnol. 7, 93. doi:10.3389/fbioe.2019.00093.

Odriozola, M., Morales, N., Vázquez-Padín, J. R., Lousada-Ferreira, M., Spanjers, H., and van Lier, J. B. (2020). Fouling Mitigation by Cationic Polymer Addition into a Pilot-Scale Anaerobic Membrane Bioreactor Fed with Blackwater. Polymers (Basel). 12, 2383. doi:10.3390/polym12102383.

Odriozola, M., van Lier, J. B., and Spanjers, H. (2022). Optimising the flux enhancer dosing strategy in a pilot-scale anaerobic membrane bioreactor by mathematical modelling. *Membranes* 12, 151. doi.org/10.3390/membranes12020151.

1.1 ANAEROBIC MEMBRANE BIOREACTOR (ANMBR) TECHNOLOGY

Anaerobic digestion has become a competitive technology for wastewater treatment in the last decades (van Lier et al., 2020). The degradation of organic matter under anaerobic conditions yields biogas (mainly composed of methane and carbon dioxide) that can be used to e.g., generate heat and electric power. Anaerobic digestion does not require oxygen supply and consequently the energy consumption is significantly reduced. Additionally, anaerobic digestion has a lower sludge production than degradation under aerobic conditions.

The development of anaerobic digestion was driven by decoupling the hydraulic and solids retention times, HRT and SRT, which was achieved by sedimentation, granulation, or immobilization in fixed or moving beds. In AnMBRs the microorganisms are retained inside the bioreactor by membranes, which provides a perfect SRT control, enabling the design of smaller reactors operating at high SRT. The membranes keep all the microorganisms inside the reactor, regardless of whether they are forming flocs or granules, allowing the retention of species that would be washed-out from bioreactors with gravity separation technique (Ben Aim and Semmens, 2002). This complete retention enables the application of anaerobic technologies for high diversity wastewater types, including wastewaters containing slowly biodegradables or persistent pollutants, which require the acclimation and growth of specific microorganisms. Therefore, AnMBR couples the advantages of anaerobic digestion, that is: low sludge production, no aeration requirement and biogas production, with the benefits of membrane technology, that is, retention of microorganisms, complete solids removal and a high degree of removal of pathogenic organisms (Skouteris et al., 2012).

AnMBR is an innovative technology for municipal wastewater treatment (Hu et al., 2020; Smith et al., 2012) and an established technology for industrial wastewater treatment with several full-scale AnMBRs treating wastewater from food processing industries (Dereli et al., 2012; Dvořák et al., 2016). AnMBR has been increasingly researched for wastewater treatment in a circular economy scenario to recover nutrients, water and biogas.

1.2 MEMBRANE FOULING

Membrane fouling remains the major operational challenge limiting applicability and economic feasibility of AnMBRs (Ozgun et al., 2013). Fouling is the coverage of the membrane surface, external and internal, by deposits that adsorb or simply accumulate during filtration. It can occur by several mechanisms: pore blocking, adsorption and cake layer formation and concentration polarisation. The latter is negligible in membrane bioreactors when compared to the other fouling mechanisms. During AnMBR operation, fouling is responsible for decreased fluxes and increased transmembrane pressure (TMP), and the need of more intensive biogas sparging, increased crossflow velocities, more frequent membrane cleaning and membrane replacement (Ozgun et al., 2013), and thus increasing energy and operational costs.

Membrane fouling in membrane bioreactors has been quantified by different process state variables and is expressed using different indicators, such as permeability, TMP development, filtration resistance, specific resistance and fouling rate (de La Torre, 2013).

Membrane fouling can be classified into reversible, irreversible, and irrecoverable fouling according to the required type of cleaning to remove it. Reversible fouling can be removed by physical cleaning, such as back-flushing or relaxation, irreversible fouling can be removed by chemical cleaning but not by physical cleaning, and irrecoverable fouling cannot be removed by either physical or chemical cleaning. The fouling rate for each type of fouling is significantly different: 0.1-1, 0.001-0.1 and 0.0001-0.001 mbar min^{-1} for reversible, irreversible and irrecoverable fouling, respectively (Kraume et al., 2009). Therefore, different time intervals should be considered to study each type of fouling, for example, reversible fouling can be assessed in a few minutes, whereas irreversible fouling needs weeks or months, and irrecoverable several years (Kraume et al., 2009). Figure 1.1 shows a schematic representation of TMP during constant flux operation in a membrane bioreactor and presents the different types of fouling that will develop during membrane filtration. Maintenance cleanings are regular chemical cleanings performed in-situ to reduce irreversible fouling. Main cleanings are intensive chemical cleanings performed once or twice a year.

Factors impacting membrane fouling have been widely studied (Choo et al., 2000; Deng et al., 2016; Dereli et al., 2012; Drews, 2010; Judd and Judd, 2011; Meng et al., 2017; Stuckey, 2012; Wang et al., 2013). Literature shows that fouling is sensitive to sludge characteristics, membrane operation and membrane properties, as shown in Figure 1.2. Membrane operation refers to the operational variables, such as imposed flux or TMP, frequency and characteristics of mechanical and chemical cleaning, crossflow velocity and gas sparging rate. The sludge characteristics are determined by the bioreactor operation conditions, such as solids and hydraulic retention times, and substrate type, that is the concentration and characteristics of the organic and inorganic materials in the influent. Additionally, certain sludge characteristics, such as particle size distribution and floc structure, can be affected by the shear rate caused by crossflow velocity or gas sparging rate. The concentration of soluble and
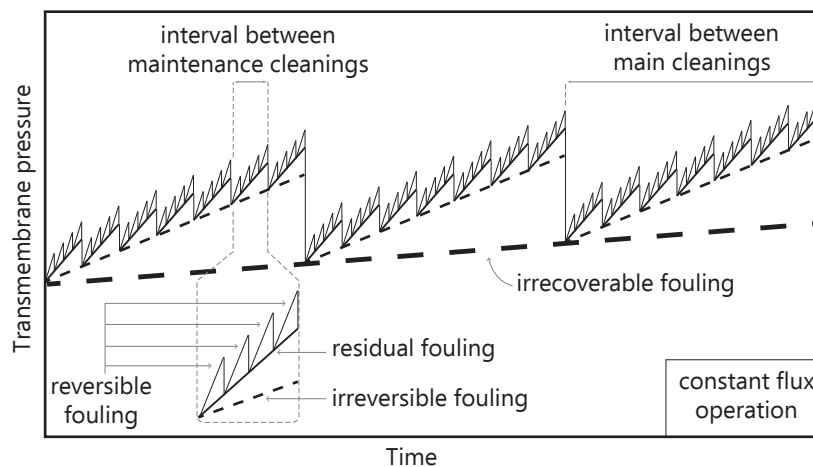
Figure 1.1. Scheme of different fouling mechanisms during long-term operation at constant flux (Kraume et al., 2009).

colloidal organic matter plays a major role in membrane fouling (Christensen et al., 2018; Judd and Judd, 2011; Shi et al., 2018); high concentrations increase fouling by pore blocking, cake layer formation, and decrease in cake layer porosity.
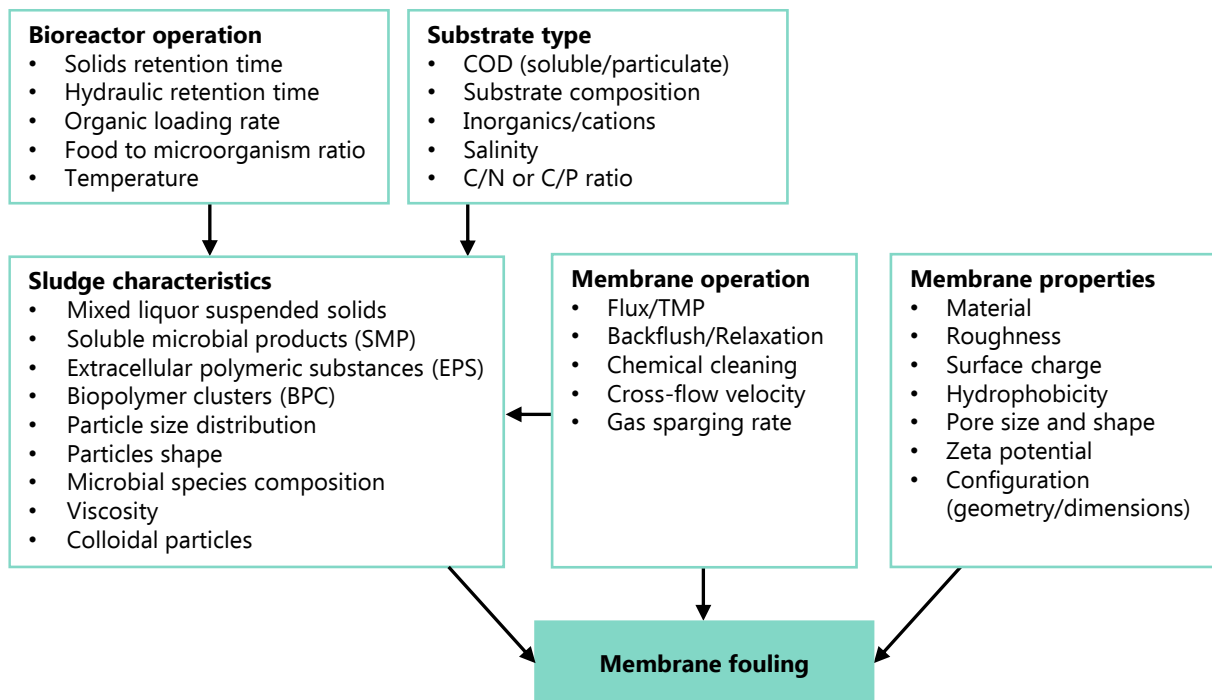
Figure 1.2. Factors affecting membrane fouling in AnMBRs (adapted from Deng et al. (2016), Dereli et al. (2012) and Stuckey (2012)).

1.3   SLUDGE FOULING POTENTIAL QUANTIFICATION

The fouling potential is a sludge characteristic that reflects the propensity of the sludge to cause fouling under reference operational conditions and membrane properties. Several methods have been developed to quantify, and sometimes qualify fouling potential of activated sludge using different indicators, such as filterability, critical flux and resistance to filtration (de La Torre, 2013; Lousada-Ferreira et al., 2014). These methods can be divided in dead-end filtration and filtration test cells methods.

Dead-end filtration methods include: time to filter test, capillary suction time test, sludge volume index test and stirred test cell (de La Torre, 2013). Membrane bioreactors use crossflow filtration, therefore, the fouling mechanisms expected from dead-end filtration methods are not truly representative of those occurring in membrane bioreactors.

Filtration test cell methods, using crossflow filtration, include the Delft filtration characterization method (DFCm) (Evenblij et al., 2005) developed at the TU Delft, the MBR VITO fouling measurement (MBR-VFM) (Huyskens et al., 2008), the Berlin filtration method (BFM) (de La Torre et al., 2010) and the critical flux determination by the flux-step method (Le Clech et al., 2003). The main output is the sludge quality filtration parameter, ΔR_{20} and cake compressibility factor in the DFCm, reversible and irreversible fouling resistances in the MBR-VFM and critical flux in both the BFM and the flux-step method. The

ΔR_{20} is the additional resistance when 20 L of permeate per m^2 of membrane surface are obtained during filtration at constant flux and crossflow velocity in the DFCm installation, and it is inversely proportional to sludge filterability.

The filtration test cell methods have been applied in-situ and ex-situ and they are developed and implemented in lab-, pilot- and full-scale MBRs. In a pilot MBR, the MBR-VFM was able to detect an increase in the fouling potential of the mixed liquor approximately two days before it became apparent in the online TMP measurements (Huyskens et al., 2008).

The DFCm was developed at the TU Delft and it has been researched in several PhD theses, which show results from activated sludge samples of pilot and full-scale MBRs (Evenblij, 2006; Geilvoet, 2010; Lousada-Ferreira, 2011; Moreau, 2010). In the framework of the Bio-Water-Methanisation project, the TU Delft modified the DFCm for anaerobic sludge filterability assessment (Lousada-Ferreira et al., 2017). The anaerobic DFCm (AnDFCm) has been used to measure anaerobic sludge filterability both in-situ and ex-situ. The AnDFCm uses a dedicated set-up that comprises a tubular side-stream ultrafiltration membrane, combined with a well-defined measurement and cleaning protocol, allowing comparison of the filterability of sludge samples.

The use of in-situ methods to quantify fouling potential has been mainly applied to characterise and monitor fouling potential. Furthermore, researchers had suggested its potential applicability as measured variable for fouling control in membrane bioreactors (Brauns et al., 2011; de La Torre et al., 2010; Huyskens et al., 2008). Nevertheless, to the authors' best knowledge, there is only one published research that used fouling potential quantification in a control tool. In a pilot MBR, Huyskens et al. (2011a) applied a membrane permeability control tool that used the MBR-VITO reversible fouling potential as measured variable to manipulate the aeration flow and relaxation duration. The control tool was unable to correct the membrane permeability when the sludge fouling potential was elevated, because the manipulated variables (aeration flow and relaxation duration) did not have an unambiguous effect on the sludge characteristics. Therefore, the use of fouling potential quantification for fouling control tools should be further researched, particularly by coupling the fouling potential measurements with a manipulated variable that has a direct effect on membrane fouling and sludge fouling potential.

1.4 STRATEGIES TO MITIGATE MEMBRANE FOULING

Researchers have extensively studied the causes and mitigation of membrane fouling in both aerobic and anaerobic membrane bioreactors (Bérubé et al., 2006; Bouhabila et al., 2001; Drews, 2010; Hamedi et al., 2019; Judd and Judd, 2011; Lin et al., 2013; Meng et al., 2017; Wang et al., 2013).

The most implemented strategies to mitigate fouling in AnMBRs are (Robles et al., 2018; Shin and Bae, 2018): (1) high shear stress near the membrane surface, (2) increased frequency and duration of backwashing and relaxation, (3) reduced permeate flux, and (4) increased frequency of chemical cleaning. The first strategy is achieved through increased biogas

sparging or crossflow velocity, which are energy intensive processes causing an increased energy demand. Additionally, these processes may promote the production of extracellular polymeric substances, floc breakage and detachment of soluble and colloidal material (Judd and Judd, 2011) which exacerbates fouling. The second and third strategies decrease the treatment capacity, namely the daily volume of wastewater treated. The fourth strategy reduces the lifespan of the membranes.

Furthermore, although these four strategies are usually suitable during stable operation of the membrane bioreactor, they may not be adequate or sufficient when the fouling is caused by sludge with a high fouling potential (Huyskens et al., 2011a). The application of flux enhancers for fouling mitigation by changing sludge characteristics and decreasing the sludge fouling potential has been extensively investigated and it is further discussed in the next section.

1.5   FLUX ENHANCERS FOR MEMBRANE FOULING MITIGATION

1.5.1   Definition, application, and mechanisms

Flux enhancers (FE) are adsorbents, coagulants and flocculants that mitigate membrane fouling by modifying the sludge characteristics. Over the last two decades, extensive research has been done on the application of FE in membrane bioreactors.

One of the most comprehensive studies with FE was performed by Iversen, Koseoglu and collaborators (Iversen, 2010; Iversen et al., 2009b; Koseoglu et al., 2008). The research started with batch experiments using 30 different FE and culminated in the application of three of them into a pilot-scale aerobic membrane bioreactor (MBR): the starch Mylbond168, and the synthetic cationic polymers MPE50 and Adifloc KD452. The cationic polymers improved the filtration performance in the MBR, whereas starch had a detrimental effect. Nevertheless, in short-term lab experiments performed with a crossflow filtration test cell, the filtration performance was improved with the three chemicals, and the improvement obtained with the cationic polymers was higher than in subsequent studies in the pilot. The authors postulated that the different results in lab-scale and pilot-scale experiments might have been due to the hydrodynamic differences between the installations (test cell and MBR). Moreover, the authors emphasized the need for more research on FE addition in long-term and large-scale trials (i.e., pilot and full scale), which was also addressed by other authors (Kulesha et al., 2018; Ozgun et al., 2013). Ozgun et al. (2013) reviewed the AnMBR applications for municipal wastewater treatment and indicated the need for assessing the feasibility of continuous addition of FE during long-term operation.

Table 1.1 summarises the published applications of FE in large-scale (i.e., pilot- and full-scale) membrane bioreactors. MPE50 was the most commonly employed FE, mostly used by researchers at Nalco, the supplier of the polymer (Collins et al., 2006; Wozniak, 2010; Yoon and Collins, 2006). In all the studies that applied cationic polymers, namely MPE50 and KD452, membrane filtration was improved, which was shown by a TMP decrease or flux increase. Therefore, it can be concluded that cationic polymers are suitable FE for fouling mitigation.

Table 1.1. Literature review of flux enhancers (FE) applied to pilot and full-scale MBRs and AnMBRs fed with real wastewater.

Reactor reference	FE type [a], dosage (mg L⁻¹)	Dosing control [b]	Dosing strategy [c]	Reactor type	V (m³)	A_m (m²)	Wastewater fed	t (d)	Main effects of FE presence [g]	Reference
R1	FeCl₃, 26	FF	Step in influent	AnMBR	0.55	5.4	Municipal	90	↓fouling, ↑thickness and porosity fouling layer, ↓PR and CH on membrane surface, ↑COD removals, ↓colloidal COD ↓soluble COD, ↑particle size.	Dong et al. (2015)
R2	FeCl₃, 12–21, 43	FF	Step in influent	AnMBR	0.55	5.4	Municipal	70	↓reversible fouling, ↓colloidal COD, ↓VSS biodegradability.	Dong et al. (2018)
R3	PACl, 12.5 mg gTS S⁻¹	FF	P+C(W)	MBR	-	1	Domestic and textile	65	↓fouling rate, ↓cake resistance, ↑filtration stability, ↕SMP-PR, ↕SMP-CH,↓extracted EPS-PR and EPS-CH.	Teli et al. (2012)
R4	Mylbond168, 1,500–2,000	FF	P+C (W)	MBR	1	22	Municipal	50	↑TMP, washed out with permeate, ↑floc size, ↓CST.	Iversen et al. (2009)
R4	KD452, 70	FF	P+C (W)	MBR	1	22	Municipal	63	↓TMP, retarded fouling, ↕nutrient removal, ↓SMP, ↑floc size, ↓biopolymers.	Iversen et al. (2009)
R4	MPE50, 500	FF	P+C (W)	MBR	1	22	Municipal	74	↓TMP, retarded fouling, ↕nutrient removal, ↓SMP, ↑ floc size, ↓CST.	Iversen et al. (2009)
R5	MPE50, 250	FF; FB	P+C (W & B); Pulses	MBR	0.12	0.9	Refinery effluent	220	↓fouling resistance, ↓TTF, ↑PSD, ↓colloidal TOC, ↓SMP, ↓EPS.	Alkmim et al. (2016)
R6	MPE50, 400	FF	P+C(B)	MBR	10.2	60	Municipal	20	↑flux, ↓TMP, ↓foam.	Collins et al. (2006)
R7	MPE50, 400	FF	P+C (-)	MBR	-	1000	Leachate	30	↓TMP, ↑permeability, ↑flow, ↓permeate COD, ↓chemical cleaning frequency, ↓foam.	Wozniak (2010)

(continued)

Table 1.1. continued. Literature review of flux enhancers (FE) applied to pilot and full-scale MBRs and AnMBRs fed with real wastewater.

Reactor reference	FE type[a], dosage (mg L⁻¹)	Dosing control[b]	Dosing strategy[c]	Reactor type	V (m³)	A_m (m²)	Wastewater fed	t (d)	Main effects of FE presence[g]	Reference
R8	MPE50, 600	FF	P+C (-)	MBR	125	-	Food Industry	12	↓TMP, ↑permeability, ↓ permeate COD, ↓chemical cleaning frequency, ↓foam.	Wozniak (2010)
R9	MPE50, 500	FF	P+C (-)	MBR	0.2	0.5	Municipal	14	↑critical flux.	Yoon and Collins (2006)
R10	MPE50, 400	FF	P+C (-)	MBR	750[d]	-	Municipal	>1[f]	↑permeability, ↑one-day peak flux.	Yoon and Collins (2006)
R11	MPE50, 200	FF	P	MBR	-	6.4	Municipal	35	↑flux, ↓permeate COD.	Yoon and Collins (2006)
R12	MPE50, 300	FF	P+C (W)	MBR	-[e]	-	Municipal with waxes	35	↑flux, ↓shuts down triggered by high TMP, ↑one-day peak flux.	Yoon and Collins (2006)
R13	PAC, 1,500, 3,000	FF	P+C (-)	MBR	0.52	6	Tannery Industry	139	↓fouling rate, ↓chemical cleanings, COD removal stabilisation.	Munz et al. (2007)
R14	PAC, 500	FF	Ramp up	MBR	0.085	0.1	Municipal	140	↑critical flux, ↑sustainable filtration period, ↓gel-cake deposition, ↑removability of gel-cake, ↑permeate quality.	Remy (2012)

[a] MPE50 and KD452 are cationic polymers; PACl is polyaluminum chloride; and Mylbond168 is a starch.

[b] FF: feedforward dosing, where FE is dosed to achieve a target concentration. FB: feedback dosing, where FE is added based on the value of an input variable.

[c] P, pulse-dosage: reactor spiked with FE; P+C, pulse and compensation: initial pulse dosage that is followed by periodic additions to compensate loss of FE with sludge withdrawal (W) and 1% biodegradable fraction (B), or the cause was not specified by the authors (-).

[d] Total bioreactor volume calculated based on total MPE50 added (300 kg) and target concentration (400 mg L⁻¹).

[e] Design operational volume 50 m³ d⁻¹.

[f] Reported results for 1 day, but MPE50 remained in the system.

[g] Nomenclature: ↑, increase; ↓, decrease; ↕, no significant change. Abbreviations: COD, chemical oxygen demand; CST, capillary suction time; EPS, extracellular polymeric substances; PR, proteins; CH, carbohydrates; PSD, particle size distribution; SMP, soluble microbial products; TMP, transmembrane pressure; TTF, time-to-filter; VSS, volatile suspended solids.

However, all those studies were performed in (aerobic) MBRs. The extent and nature of the membrane fouling mechanisms in MBRs and AnMBRs can be very different because of the very different biomass developments and the different characteristics of the potential foulants under aerobic and anaerobic conditions (Judd and Judd, 2011; Xiong et al., 2016). Particularly, under anaerobic conditions, higher concentrations of colloidal organic matter are reported compared to aerobic conditions, which might result in higher fouling rates (Judd and Judd, 2011). Therefore, the results from aerobic MBRs cannot be directly translated to AnMBRs, and it is important to study the feasibility of using cationic polymers for fouling mitigation in AnMBRs.

To the authors' best knowledge, to date there are only two publications about the application of cationic polymers in AnMBRs, both performed at lab scale—Diaz et al. (2014) achieved a flux increase by dosing 1.5 g L^{-1} of MPE50 to a 4.5 L AnMBR fed with synthetic wastewater, and Kooijman et al. (2017) obtained a decrease in the specific resistance to filtration (SRF) by applying 10 g kg^{-1} of the cationic polymer Calfloc P1502, combined with 40% FeCl$_3$, to an anaerobic dynamic membrane bioreactor (AnDMBR) fed with waste activated sludge. Furthermore, cationic polymers have been studied in batch tests with anaerobic sludge samples, leading to improved filtration characteristics in dead-end filtration tests (Braguglia et al., 2006; Díaz et al., 2014; Kooijman et al., 2017b) and cross-flow filtration tests (Díaz et al., 2014; Zhang et al., 2017). Therefore, cationic polymers are suitable FE for fouling mitigation in lab-scale AnMBRs and large-scale MBRs (Table 1.1). However, these FE should be further studied in long-term large-scale AnMBRs.

Figure 1.3 illustrates the interaction between cationic polymers and colloidal particles. Electrostatic repulsion between the negatively charged colloidal particles prevent them from agglomerating, whereas the intermolecular attraction promotes bonding. Cationic polymers promote colloidal agglomeration by bridge flocculation or electrostatic patch mechanisms (Bratby, 2016). In bridge flocculation, the polymer segments are adsorbed onto the surface of different colloid particles linking them together. In electrostatic patch mechanisms, the polymer is adsorbed onto the particle surface creating positively charged patches that interact, upon collision, with the negative surface of other colloidal particles to form flocs.
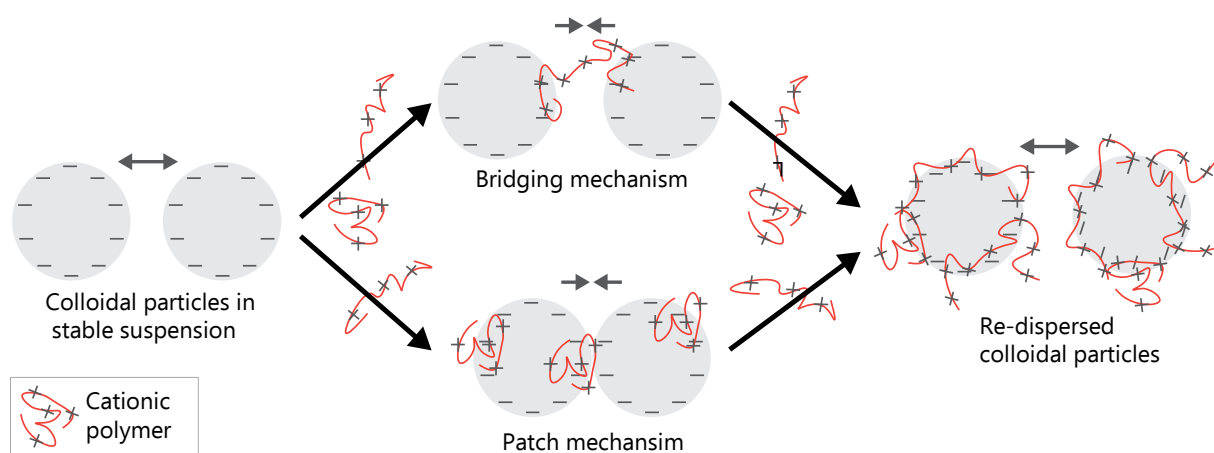

Figure 1.3. Schematic representation of mechanisms of destabilization and re-dispersion of negatively charged colloidal particles by cationic polymers.

Moreover, excessive cationic polymer dosages can cause particle redispersion, also designated as deflocculation or re-stabilisation, by saturation of bridging sites or charge reversal due to complete surface coverage (Bratby, 2016).

1.5.2 Optimal dosage

Researchers have determined the optimal required dosage of different cationic polymers in a variety of sludge samples and obtained significantly different results. For aerobic sludge samples, reported dosages of Adiflocs range from 10 (Gkotsis et al., 2017) to 70 mg L^{-1} (Iversen et al., 2009b; Koseoglu et al., 2008), and of MPE50 from 100 (Collins et al., 2006) to 600 mg L^{-1} (Wozniak, 2010). For anaerobic sludge, dosages of MPE50 from 300 to 1500 mg L^{-1} have been applied. Wozniak (2010) has recommended to evaluate weekly the optimal dosage for a continuous application of FE to an MBR, to adapt the dosage to the variable conditions. Díaz et al. (2014) determined the optimal dosage of MPE50 based on specific resistance to filtration (SRF) measurements during biodegradability tests of waste activated sludge. The latter authors obtained different values for the optimal dosage during the biodegradation test due to an increase in protein concentration in the soluble fraction. Despite the variability of the optimal dosage required for different sludge samples that has been reported in literature, there are no studies analysing the cause for such variability.

In large-scale membrane bioreactors the sludge characteristics are constantly changing due to variations in the membrane and reactor operational conditions, for example by fluctuations in organic loading rate or in the air/gas sparging rate, or even due to shock loads and seasonal changes (Drews, 2010). For example, Koseoglu et al. (2008) reported fluctuations in permeability between 844 and 2077 L $m^{-2}\,h^{-1}\,bar^{-1}$ under constant operational conditions in a pilot MBR within a 2-week period. The authors also indicate the importance of long-term studies to assess the irreversible fouling. The former aforementioned variations can impact the required dosage of FE (Iversen et al., 2009b).

The required FE dosage would be ideally determined by adding FE directly to membrane bioreactors and quantifying membrane fouling. However, this approach is not feasible because if the FE is applied at high dosages, adverse effects on the membrane filtration performance, biological activity and permeate quality may arise (Section 1.5.4). Alternatively, quantifying the sludge fouling potential of sludge samples might be a more appropriate method to determine optimal dosage. In previous research, optimal dosages were mostly determined based on soluble or colloidal organic matter removal, or using dead-end filtration measurements such as: time-to-filter, specific resistance to filtration, capillary suction time and volume of filtrate collected after a defined filtration time. However, crossflow filtration mode methods, as mostly applied in full-scale membrane bioreactors, are expected to represent more accurately the fouling mechanisms occurring in membrane bioreactors than dead-end filtration methods.

1.5.3 Dosing strategies

The most common strategy of dosing FE to membrane bioreactors, as presented in Table **1.1**, is to establish and sustain a desired concentration of FE inside the reactor based on different assumptions, such as FE biodegradability and optimal dosage. The term "feedforward dosing" is introduced to describe this strategy, which was previously referred to as preventive FE use (Alkmim et al., 2016). Feedforward dosing has been applied by performing an initial pulse of FE to achieve the desired concentration, followed by periodic additions to compensate for the loss of FE due to sludge withdrawal and possible FE biodegradation. The desired concentrations have been estimated in batch tests with sludge samples from the reactor before FE addition or based on reported values. FE biodegradation has been considered negligible or based on supplier's recommendation; for example, Nalco suggests that 1% of the MPE50 is biodegraded daily (Alkmim et al., 2016). Furthermore, all researchers in Table 1.1 who performed feedforward dosing, did not explicitly consider the possible FE loss in the permeate and used a unique target FE dosage that did not change over the reactor's operation. Moreover, feedforward dosing does not consider possible unmeasured disturbances, such as fluctuations in the influent characteristics, which can be present in full-scale plants even when operating under design conditions. Therefore, despite being the most used dosing strategy, feedforward dosing is based on assumptions that might lead to under- or overdose of FE. Overdosing FE can have detrimental effects on filtration performance, permeate quality and biological activity (Section 1.5.4), whereas underdosing FE may result in insufficient improvement of the sludge filtration performance.

An alternative FE dosing strategy is to adjust the dosage of FE based on an input variable that quantifies the sludge fouling potential, such as filterability. The term "feedback dosing" is introduced for this strategy, which was previously referred to as corrective FE use (Alkmim et al., 2016). In feedback dosing, a pulse of FE is applied to the reactor only when the sludge filterability is deteriorated. Feedback dosing does not require the assumptions made in feedforward dosing and it can reject possible unmeasured disturbances on the sludge filtration characteristics, and thus avoid under- or overdosing of FE. Nevertheless, the major challenge in feedback dosing is to identify an appropriate variable to quantify sludge fouling potential that could be measured at an appropriate frequency, preferably in-situ and online. Various researchers suggested the possible application of the online measurement of sludge fouling potential for automatic FE dosing control in membrane bioreactors (Brauns et al., 2011; Iversen, 2010). However, this has never been further studied or tested.

1.5.4 Side effects

Dosing inorganic coagulants, such as polyaluminium chloride, $FeCl_3$, $Al_2(SO_4)_3$ and polymeric ferric sulphate may decrease pH when increasing their dosage, when no pH correction is applied, whereas organic polymers and adsorbents do not affect pH (Bratby, 2016; Song et al., 2008; Zhang et al., 2017).

Powdered activated carbon (PAC) is the most widely applied adsorbent for fouling control in lab-scale experiments. The PAC with adsorbed sludge has reduced adsorbent capacity and

needs regular replacement (Skouteris et al., 2015); consequently, the sludge adsorbed to the PAC is lost during replacement. Avoiding sludge loss is crucial in anaerobic processes because the biomass has a low growth rate and a low sludge yield. Moreover, Iversen (2010) reported adverse effects of the residuals from chemical activation of PAC on biomass activity.

Excess dosage of FE could lead to adverse effects (Drews, 2010). Several researchers have observed an adverse effect at FE dosages higher than the optimal dosage on different response variables (Braguglia et al., 2006; Collins et al., 2006; Díaz et al., 2014; Koseoglu et al., 2008; Wozniak, 2010; Zhang et al., 2017), such as filtration performance. Particularly, for cationic polymers, an excessive dosage can cause colloidal particle deflocculation (Figure 1.3) resulting in deteriorated sludge filtration characteristics. Moreover, when overdosing FE, a fraction of FE remains unbonded in the bulk liquid and can cause intense fouling by FE adsorption on the membrane surface and inside the pores (Iversen et al., 2008) or potentially contaminate the permeate by passing through the membrane.

Iversen et al. (2008) studied the biological inhibition of 12 FE on aerobic sludge, namely one polyaluminium chloride, two chitosans, two activated carbons, five polymers and two starches. Their results showed no or only slightly inhibitory effect on the endogenous oxygen uptake rate with all the FE tested. For the exogenous oxygen uptake rate, six FE were shown to present no inhibitory effect, four had a slightly inhibitory effect and two polymers (i.e., Adiflocs KD451 and KD452) had a considerable inhibitory effect (50-70% inhibition). Polydiallyldimethylammonium chloride (polyDADMAC) is the component of several cationic polymers used as FE, such as Adifloc KD451, Adifloc KD452, and MPE50. In different research fields, polyDADMAC has been reported as an anti-microbial agent (Tran et al., 2017; Wang et al., 2017; Zhao et al., 2016) that can physically disrupt the prokaryotic cell wall. Therefore, scarce, and contradictory reports are published on the effect of FE on the microbial community. Another possible effect of FE on the sludge biological activity is the decrease in substrate availability caused by mass transfer limitation inside the formed larger aggregates (Kooijman et al., 2017b). The increased particle size caused by some FE may decrease the surface to volume ratio and a diffusion limitation inside the aggregate could be observed.

1.6   Membrane fouling control tools

The main goal of a control tool is to maintain the controlled variable at a desired value despite the disturbances that may arise from other inputs. The elements of the control tool are a sensor (measuring device), a controller and an actuator (final control element). The controlled variable is the variable to be regulated, the setpoint is the desired value of the controlled variable, the manipulated variable is an input variable that can be adjusted by the controller, disturbances are input variables that influence the controlled variable and can be measured or unmeasured, and the measured variable is the value of the controlled variable (feedback control) or disturbances (feedforward control) to be used by the controller to take a control action. Basic or advanced controllers can be used, basic controllers are on-off or PID (proportional integral derivative), and advanced controllers are fuzzy logic, neural network, hybrid systems and model predictive control.

Figure 1.4 illustrates three basic control configurations, that is: feedback control (also called closed-loop control), feedforward control, and open-loop control. Feedback and feedforward control also can be used in combination. Feedback control is the most widely used configuration, it measures the controlled variable and takes a control action based on the difference between the measured value and the desired value. Feedforward control measures the disturbances and takes a control action to reduce or eliminate the effect of disturbances on the controlled variable. Feedforward control requires a mathematical model of the effect of disturbances and manipulated variables on the controlled variable. Open-loop control sets the manipulated variable to a given value with the expectation that it will result in the desired value of the controlled variable. Open-loop cannot reject any disturbance and feedforward cannot reject unmeasured disturbances, and both configurations are sensitive to modelling errors and parameter changes in the process. The main advantages of feedback control are that it does not require a mathematical model and it can reject all the disturbances without requiring identification and measurement of any disturbance. However, feedback control can only be applied when the controlled variable can be measured with a sensor suited for or adapted to in-, on- or at-line measurement, able to transmit that measurement as an electrical signal back to the controller, and to generate data at a higher frequency than that at which changes in the controlled variable occur.

The first step to design a control tool is to formulate the control objective based on operational requirements; then input and output variables must be identified and classified into controlled, manipulated, disturbance, and measured variables; followed by identification of constrains, operating characteristics, and environmental, safety and economic considerations; and finally, determine the best control configuration (Bequette, 2003). Furthermore, the actuator must be able to receive the controller output signal and trigger a corrective action (manipulated variable) that impacts the process quickly and significantly. The sensor must have the characteristics previously mentioned. Thus, it is essential to know the dynamics of the control elements.

Researchers have published various control tools for energy savings and improvement of permeate quality successfully applied in pilot and full-scale MBRs (Krzeminski et al., 2017). These strategies include open- and closed-loop applications and focus on energy savings by different aeration strategies. In closed-loop control strategies the measured and controlled variables are usually TMP change in time, resistance, permeability and permeate flux. The manipulated variables are: duration of aeration cycle, aeration flow rate, permeate flux, filtration cycle (duration and initiation) and frequency of chemical and mechanical cleaning (Ferrero et al., 2012). Although these controlled variables provide information about the consequence of fouling, they are not strong variables for fouling control tools because they do not provide information about the cause of fouling (Ferrero et al., 2012) and cannot discriminate between fouling and clogging (Drews, 2010). For example, a sudden increase in the TMP development could be caused either by a currently high sludge fouling potential or by the cumulative effect of past fouling events (Huyskens et al., 2011a).

Relating the sludge fouling potential measurements with the membrane filtration process state variables, such as flux and TMP development, allows to identify the cause of the problem when the membrane performance is deteriorated (Kraume et al., 2009), that is, identify whether the problem is caused by a high sludge fouling potential or by inadequate setting of membrane operational parameters, such as low gas sparging rate, high flux, insufficient mechanical or chemical cleaning frequency. Therefore, a control tool that couples fouling rate measurements with membrane filtration performance could identify the cause of the problem and decide on the appropriate intervention, namely manipulate either the sludge characteristics or the membrane operation.

Brauns et al. (2011) presented an advanced control tool based on fuzzy set logic, which uses the MBR-VFM in-situ fouling measurement tool as measured variable and manipulates the setpoint of 17 different variables, each setpoint having an individual fuzzy set logic control block. The control tool uses the typical manipulated variables in an MBR, such as backwash/aeration/relaxation frequency and duration, and dosage and dosing frequency of FEs. This control tool was validated in a pilot-scale MBR fed with municipal wastewater, using
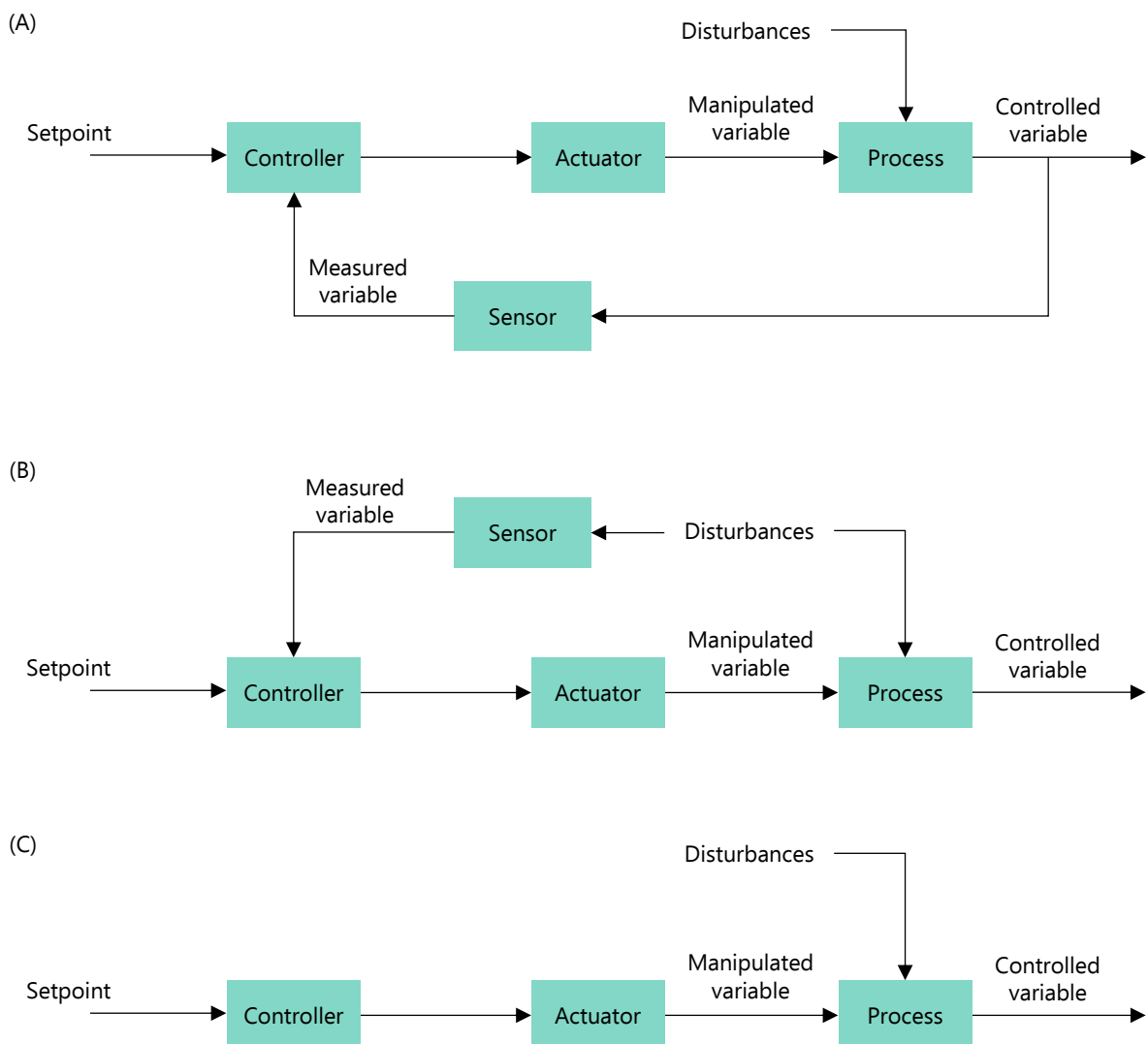
Figure 1.4. Block flow diagrams (A) feedback (close-loop) control, (B) feedforward control, and (C) open-loop control.

aeration flow and relaxation duration as manipulated variables (Huyskens et al., 2011a). They observed a correlation between in-situ permeability and reversible fouling potential, indicating that the in-situ reversible fouling potential measured by MBR-VFM is an appropriate input variable for the control tool. However, the control tool was not able to correct the membrane permeability when the sludge fouling potential was elevated, because the manipulated variable (aeration flow) did not have an unambiguous effect on the sludge characteristics.

Although several control strategies have been presented for aerobic MBRs only a few have been developed for AnMBR. Jeison and van Lier (2006) presented an online control of cake layer formation by manipulating gas sparging and backflush frequency based on TMP measurements in a lab-scale AnMBR fed with synthetic wastewater. The control tool was able to keep the pressure increase below 20 mbar and resulted in an efficient tool for cake layer formation control.

Robles et al. (2013) developed and validated a fuzzy logic and knowledge-based advanced control tool to optimise the filtration process (maintaining sub-critical filtration conditions and minimising operational costs) in a submerged pilot AnMBR fed with municipal wastewater. The control tool controls the fouling rate (measured online as changes in TMP) by manipulating gas sparging and mechanical cleaning frequency (backwash and ventilation). Results showed low fouling rates and reduction in mechanical cleaning downtimes achieved by control actions. In a later work the authors integrated this control tool with a model-based supervisory controller for minimising operational costs by automatic tuning of the controller parameters and set points (Robles et al., 2014a). With this real-time optimisation strategy, a 25 % energy saving was achieved during membrane scouring.

1.7 Scope and outline of the thesis

Membrane fouling is a major challenge for the economic feasibility and applicability of AnMBRs. For the last two decades, extensive research has been done on the application of flux enhancers (FE) to improve sludge filtration properties and mitigate fouling by modifying sludge characteristics. The main objective of this thesis is to develop a fouling control tool for AnMBRs that manipulates the flux enhancer dosing. To achieve this objective the following knowledge gaps were addressed in the thesis:

- feasibility of FE dosing in long-term and large-scale AnMBRs;
- effect of FE on biological activity under anaerobic conditions;
- causes of optimal FE dosage variation;
- feasibility of using in-situ fouling potential measurements (such as ΔR_{20}) for FE dosage control;
- identification of best control configuration.

Chapter 2 analyses the effect of sludge characteristics on the optimal required dosage of FE for sludge filterability improvement in AnMBRs. Experiments using sludge samples from five municipal and industrial pilot and full-scale AnMBRs were performed, located in four different countries in Europe and Africa. The optimal dosage was measured using the AnDFCm installation shown in Figure 1.5. The main factors affecting the required dosage of FE for different sludges were identified, and empirical models were provided to potentially estimate the optimal dosage of cationic polymer in new sludge samples by a simple sludge characterisation. Furthermore, this chapter provides guidelines for adequate continuous application of FE in full-scale AnMBR for fouling control.

Chapter 3 studies the inhibitory effect of FE on the biological activity of anaerobic sludge. Mathematical modelling was used as a tool to reveal the underlying inhibition mechanism which allows to understand the long-term implications of FE dosing in a continuous reactor. The chapter presents a critical assessment of various inhibition models widely used in literature.

Chapter 4 studies the long-term effect of dosing FE to the pilot AnMBR in Figure 1.6, that was fed with source-separated domestic blackwater. The chapter analyses the effects on permeate quality, sludge characteristics, biological activity and AnMBR filtration performance. Additionally, this chapter discusses the applicability of in-situ measurements of sludge filterability as an input variable in an FE feedback dosing control tool.

Chapter 5 compares three feedback and two feedforward control tools to manipulate FE dosing to an AnMBR. The comparison was done in a simulation environment with an integrated model that predicts the effect of FE dosing on sludge filterability and membrane fouling rate. The integrated model couples filtration, flocculation, and biochemical processes and it was developed, calibrated, and validated.

Chapter 6 summarises the main conclusions of this thesis and presents recommendations for future research and applications.

Figure 1.5. AnDFCm installation at the TU Delft waterlab. Left and right are pictures taken form different angles.

Figure 1.6. Pilot AnMBR plant (FCC-Aqualia) including the AnDFCm installation connected in bypass for in-situ sludge filterability measurements. The pilot was located at the Business Centre Porto do Molle, Nigrán, Pontevedra, Spain. Left and right are pictures taken form opposite sides.

2

Optimal dosage of flux enhancers for filterability improvement in municipal and industrial anaerobic membrane bioreactors [*]

ABSTRACT

Fouling is a major challenge for the economic feasibility and applicability of membrane bioreactors. Several strategies have been proposed for fouling control, and among them, addition of flux enhancers (FE) have shown promising results. Previous research revealed a high variability of the required optimal dosage of FE for different types of sludge; however, studies analysing the causes for such variability are lacking. Therefore, this research examines the effect of sludge characteristics on the optimal FE dosage required for sludge filterability improvement (D_{opt}). The cationic polymer Adifloc KD451 was applied as FE, and determined D_{opt} with short-term cross-flow filtration tests. Sludge samples were obtained from five different pilot and full-scale anaerobic membrane bioreactors (AnMBRs) treating municipal or industrial wastewater. Results showed that D_{opt} was significantly correlated with colloidal organic matter concentration, sludge filterability, capillary suction time, and concentration of soluble polysaccharides. Furthermore, empirical models to predict D_{opt} were derived based on the significantly correlated sludge characteristics as input variables. This research identifies the factors affecting the required dosage of FE for different sludges and provides guidelines for safe continuous dosing of FE in AnMBR for fouling control.

2.1   INTRODUCTION

Researchers have determined the optimal required dosage of different cationic polymers in a variety of sludge samples and obtained significantly different results. Knowing the optimal dosage is crucial to avoid (accidental) deterioration of the filtration performance and permeate quality. For aerobic sludge samples, reported dosages of Adiflocs range from 10 (Gkotsis et al., 2017) to 70 mg L^{-1} (Iversen et al., 2009b; Koseoglu et al., 2008), and of MPE50 from 100 (Collins et al., 2006) to 600 mg L^{-1} (Wozniak, 2010). For anaerobic sludge, dosages of MPE50 from 300 to 1500 mg L^{-1} have been applied. Wozniak (2010) has recommended to evaluate weekly the optimal dosage for a continuous application of FE to an MBR, to adapt the dosage to the variable conditions. Díaz et al. (2014) obtained different optimal MPE50 dosage values during the biodegradability tests of waste activated sludge due to an increase in protein concentration in the soluble fraction. Despite the variability of the optimal dosage required for different sludge samples that has been reported in literature, there are no studies analysing the cause for such variability.

The goal of this research is to study the effect of sludge characteristics on the optimal required dosage of FE for sludge filterability improvement (D_{opt}) and to provide guidelines for dosing FE to AnMBRs. D_{opt} was determined based on sludge filterability measurements applying the AnDFCm, on seven sludge samples collected from five pilot and full-scale AnMBRs treating municipal or industrial wastewater.

2.2   MATERIALS AND METHODS

2.2.1   Flux enhancer selection

In a previous study (results not shown here, manuscript in preparation), six potential FEs were compared for their effect on the filterability of sludge obtained from a full-scale anaerobic digester at a local sewage treatment plant, including powder-activated carbon (PAC), polyaluminium chloride PAX14, polyaluminium chloride PAX18, and the cationic polymers Adifloc KD352, Adifloc KD451 and MPE50. Optimal dosages were determined as the concentration at which the maximum soluble COD removal was achieved, through jar-test experiments. Afterwards, the sludge filterability in the sludge samples, without FE addition and with FE addition at its optimal dosage, was measured, applying the AnDFCm. Except for PAC, the remaining FEs considerably improved the sludge filterability, with improvements ranging from 72% to 96%. Particularly, Adifloc KD451 improved filterability by 96%, and its optimal dosage was between 1/44 and 1/3 of the optimal dosages for the remaining FEs. Therefore, Adifloc KD451 (Adipap SA, France) was selected as the FE for this research.

Adifloc KD451 is a cationic polymer with low molecular weight and high charge density. The concentration of the FE stock solution was 30 g L^{-1}, and it was prepared by mixing the polymer with demineralised water for at least 2 hours and prepared one day before use to provide enough time for chain opening.

Table 2.1. Sludge samples details.

Sludge name	Reactor (configuration, membrane surface area)	Fed	Location	Time between sludge collection and testing (d)
LiqOFMSW	Pilot-scale AnMBR (sidestream, 20.5 m^2)	Liquid fraction of OFMSW digestate [b]	Spain	7
BWa, BWb, BWc [a]	Pilot-scale AnMBR (submerged, 6.25 m^2)	Source separated blackwater	Spain	0 [c]
Food1	Full-scale AnMBR (sidestream, 1,452 m^2)	Wastewater from confectionery factory	the Netherlands	0.5
Food2	Full-scale AnMBR (sidestream, 1,584 m^2)	Wastewater and waste from confectionery and pet food factory	Poland	7, 8
Food3	Full-scale AnMBR (sidestream, 3,432 m^2)	Whey and wash water	South Africa	14, 15

[a] BWa, BWb and BWc were collected from one AnMBR at different operational conditions.
[b] OFMSW is the organic fraction of municipal solid waste.
[c] Tests performed at the AnMBR site immediately after sampling.

2.2.2 Sludge samples

Sludge samples were collected from five different AnMBRs, as summarised in Table 2.1. Sludges Bwa, BWb and BWc were collected from one AnMBR at different operational periods, as follows. The AnMBR was spiked (pulse-addition) with the FE Adifloc KD451; Bwa and BWb were collected before and three weeks after dosing FE, respectively. BWc was collected one year after BWb, assuming that the FE had been removed with the excess sludge. When samples Bwa and BWb were collected, the AnMBR was operated without sludge withdrawal, implying an infinite sludge retention time (SRT), whereas when BWc was collected, 30 L d^{-1} of sludge was withdrawn, resulting in an SRT of 70-80 days.

2.2.3 Analytical methods

Chemical oxygen demand (COD), total phosphorus (TP), total nitrogen (TN) and ammonium-nitrogen (NH4-N) were measured with Hach Lange test kits. Because no oxidised N compounds were present, the total organic nitrogen (TON) was calculated as the difference between TN and NH$_4$-N. COD was measured in different fractions of the sample, obtained by consecutive filtration steps (Zhang et al., 2017). The COD measured in the unfiltered sample was designated as total COD (tCOD). The submicron COD (csCOD), which includes both colloidal and soluble COD, and soluble COD (sCOD) were measured in fractions below 1 μm and 0.45 μm, respectively. The supracolloidal COD (scCOD) is the fraction above 1 μm and it was calculated by subtracting csCOD from tCOD. The colloidal COD (cCOD) is the fraction between 0.45 and 1 μm and was calculated as the difference between csCOD and sCOD. To obtain the csCOD fraction the unfiltered sludge sample was centrifuged at 6,500g for 10 minutes, and the supernatant filtrated through a 1 μm paper filter Whatman GF/B (GE

Healthcare, USA). A second filtration was made through a 0.45 μm syringe filter CHROMAFIL® Xtra PES-45/25 (MACHEREY-NAGEL, Germany) to obtain the sCOD.

Soluble microbial products (SMP) were measured in the soluble fraction, obtained by centrifuging the sludge sample at 15,772g for 15 minutes and filtering the supernatant through a 0.45 μm pore syringe filter. SMP were characterised as carbohydrates (SMP-CH), proteins (SMP-PR) and humic substances (SMP-HS). Carbohydrates were determined with the phenol-sulphuric acid method (Dubois et al., 1956), using D-Glucose monohydrate as standard. Proteins and humic substance were determined with the modified Lowry method (Frølund et al., 1995), using bovine serum albumin and humic acid sodium salt as standards.

Particle size distribution (PSD) was measured in the range 0.01-2000 μm with a Microtrac Bluewave diffraction analyser (Malvern Instruments Ltd., UK). This analyser uses a light scattering technique providing results as volume-based PSD and, in samples with multiple particle sizes together, volume-based distributions neglecting the smallest particles even when they are present in large numbers. For example, assuming spherically shaped particles, the volume distribution of a sample with equal number of particles with diameters of 1, 10 and 100 μm is 0.0001%, 0.0999% and 99.9%, respectively. Thus, it was assumed that the PSD represents the size of the larger particles, which are the flocs, and not of the submicron particles. PSD was reported as percentiles $D10$, $D50$ and $D90$, where $D50$ is the median diameter.

Electrical conductivity and pH were measured with a benchtop multi-meter WTW Multi 9620 IDS (Xylem Analytics, Germany). Sludge dewaterability was measured as CST with a Type 304M CST apparatus and filter paper (Triton Electronics Ltd, UK) at 21°C following Standard Methods (APHA, 1999). The concentrations of total suspended solids (TSS) and volatile suspended solids (VSS) were measured following Standard Methods (APHA, 1999), applying a 0.7 μm pore size filter (AP4007000, Merck Millipore Ltd., Ireland).

2.2.4 Sludge filterability

Sludge filterability was measured with the AnDFCm in the side-stream ultrafiltration crossflow filtration unit (AnDFCm installation) shown in Figure 2.1. The AnDFCm consists of three steps: (1) filtering water to determine the resistance to water filtration ($R_{T,water}$), (2) sludge filtration to estimate the additional resistance obtained when 20 L of permeate per m^2 of membrane area are produced (ΔR_{20}), and (3) mechanical membrane cleaning. $R_{T,water}$ includes the membrane intrinsic resistance and the irreversible and irrecoverable fouling resistances. Sludge filterability is inversely related to ΔR_{20}.

Moreover, ΔR_{20} values can only be directly compared when the AnDFCm sludge filtration operational conditions (flux and crossflow velocities) are the same. In this study, two different operational conditions were applied for different sludge samples, which are explicitly shown in the output measurement. The $\Delta R_{20(1.5,60)}$ and $\Delta R_{20(0.5,60)}$ are ΔR_{20} measured at 60 L m^{-2} h^{-1} flux, with 1.5 m s^{-1} and 0.5 m s^{-1} crossflow velocities, respectively. Moreover, ΔR_{20} was used to refer to $\Delta R_{20(0.5,60)}$ and $\Delta R_{20(1.5,60)}$ simultaneously.
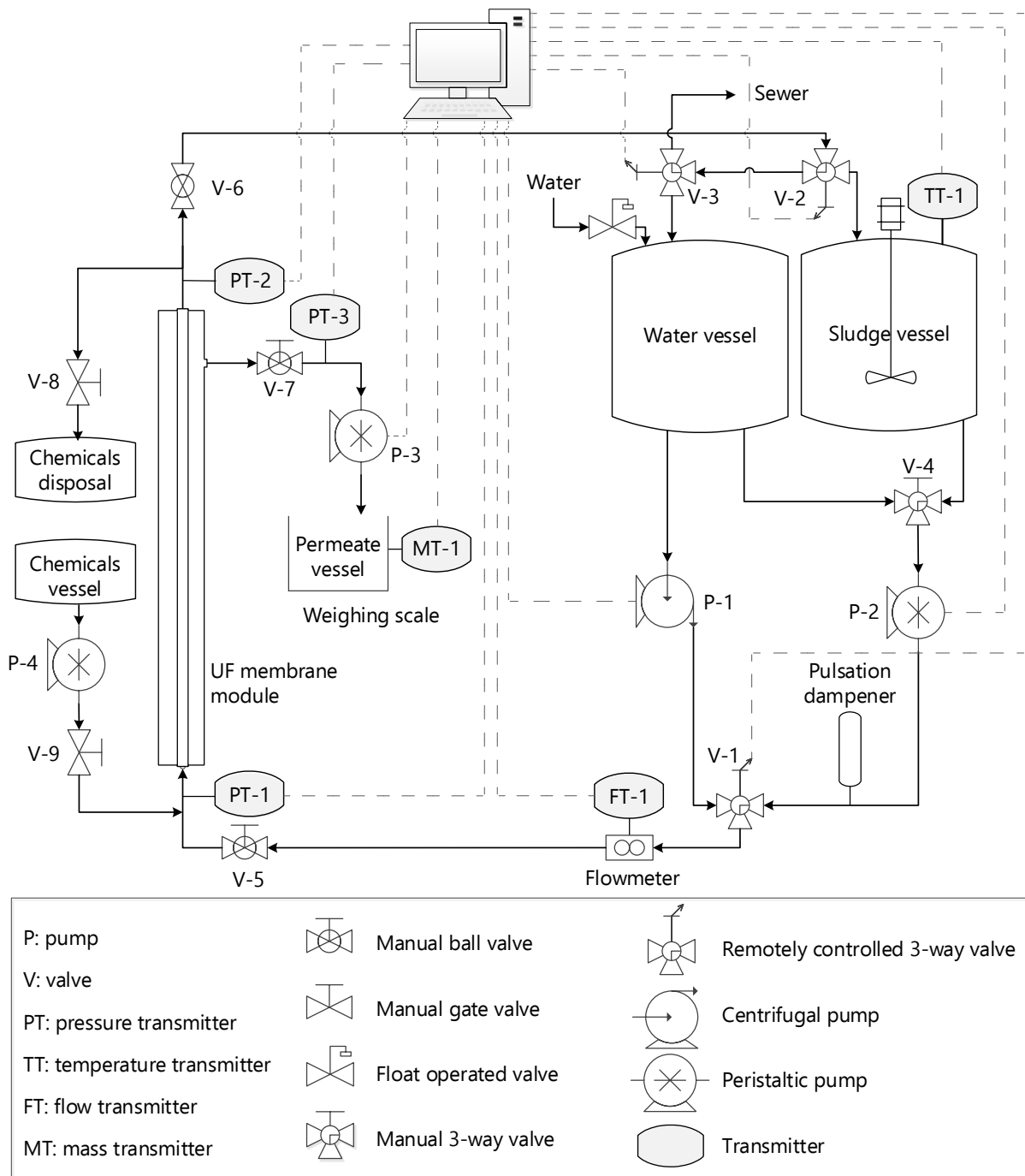
Figure 2.1. Scheme of the anaerobic Delft filtration characterisation method (AnDFCm) installation used for sludge filterability assessment. The ultrafiltration (UF) membrane was an X-Flow (Pentair, the Netherlands): tubular, 30 nm pore size, 8 mm internal diameter, and 95 cm length.

2.2.5 Flux enhancer dosage-step experiments

Dosage-step tests were performed for all sludge samples shown in Table 2.1, to determine D_{opt}. To assess the reproducibility of D_{opt} determination, the total volume of each sludge, i.e., BWc, Food2 and Food3, was divided in two samples of equal volume prior to performing the dosage-step tests; the resulting samples were further designated as: BWc, BWc-II, Food2, Food2-II, Food3 and Food3-II. D_{opt} was individually determined in each resulting sample.
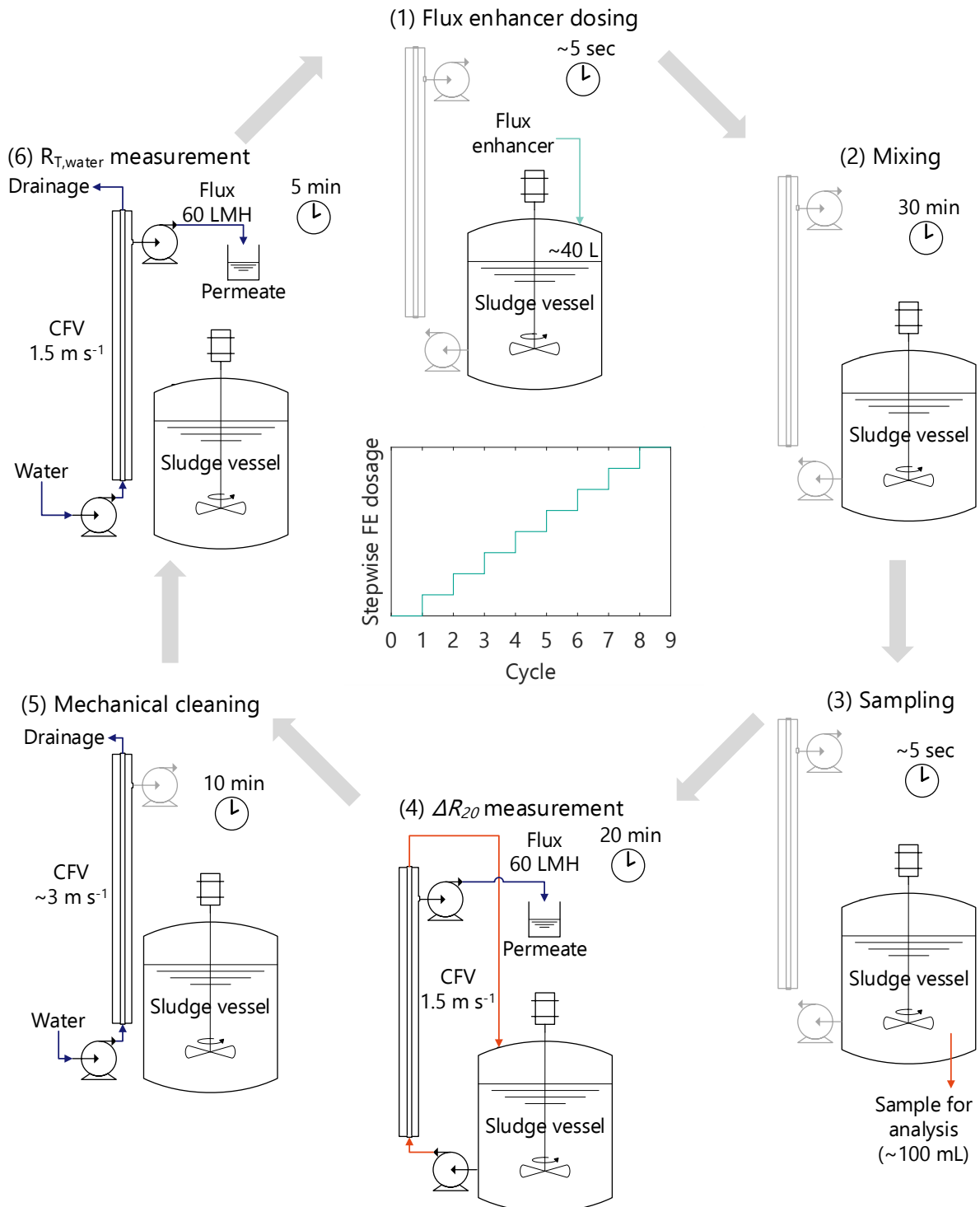
Figure 2.2. Scheme of the flux enhancer dosage-step protocol performed in the AnDFCm installation. The centre figure represents the increasing stepwise FE dosage. The total number of cycles was not fixed.

The dosage-step test consisted of consecutive stepwise increasing additions of FE into a sludge sample. The protocol, shown in Figure 2.1, was an iterative process that comprised: (1) dosing FE, (2) mixing, (3) sampling for characterisation (PSD, csCOD, sCOD and CST), (4) $\Delta R_{20(1.5,60)}$ measurement, (5) mechanical cleaning, and (6) determination of resistance to water filtration ($R_{T,water}$); Step 1 to Step 6 were performed consecutively for each dosage. During Step 4, $\Delta R_{20(1.5,60)}$ was measured for all sludge samples except Food2, where $\Delta R_{20(0.5,60)}$ was measured instead, because Food2 presented such good filtration quality that no cake build-up was obtained when a crossflow velocity of 1.5 m s^{-1} was applied.

2.2.6 Unbonded flux enhancer filtration tests

To study the effect of unbonded polymer on filtration performance and permeate quality, demineralised water with different concentrations of polymer were filtered in a crossflow filtration installation, the AnDFCm installation. The polymer Adifloc KD451 was used at three different concentrations: 0.1, 0.5, 1.0 g L^{-1} corresponding to 0.1, 0.6, 1.1 gCOD L^{-1}, respectively. The filtration test comprises: (1) measurement of resistance to water filtration ($R_{T,water}$) at 1.5 m s^{-1} crossflow velocity and 60 L m^{-2} h^{-1} flux, (2) addition of polymer to the water vessel followed by 1-minute mixing with an external pallet mixer at 50 rpm while recirculating the mixture through the AnDFCm installation, without permeate extraction, (3) measurement of total filtration resistance of the polymer solution (R_T) at 1.5 m s^{-1} crossflow velocity and 60 L m^{-2} h^{-1} flux, while collecting permeate in a vessel, and (4) measurement of total COD in the collected permeate solution ($C_{p,meas}$).

The membrane was mechanically and chemically cleaned between filtration tests at different polymer concentrations. Firstly, a flush forward at approximately 3 m s^{-1} crossflow velocity was performed during 5 minutes without permeate extraction. Secondly, the membrane was filled with 0.5 g L^{-1} NaOCl solution and left for 1 hour. Thirdly, a second flush forward was performed while extracting permeate for 5 minutes to clean the permeate side of the membrane.

2.2.7 Data analysis

2.2.7.1 Selection of optimal and critical dosages

The optimal and critical dosages were calculated based on sludge filterability improvement as response variable. Filterability improvement was defined as ΔR_{20} decrease, calculated as follows:

$$y = 100 \frac{x_{raw} - x}{x_{raw}},$$
(2.1)

where y is the response variable ΔR_{20} decrease, x_{raw} is ΔR_{20} of the raw sludge (without FE), and x is ΔR_{20} measured after each FE dosage; ΔR_{20} is $\Delta R_{20(0.5,60)}$ for Food2 and $\Delta R_{20(1.5,60)}$ for the other sludge samples.

Several researchers defined optimal dosage as the dosage which provides the highest improvement in the response variable (Braguglia et al., 2006; Díaz et al., 2014; Koseoglu et al., 2008; Lee et al., 2007; Malamis et al., 2014; Wang et al., 2014; Wozniak, 2010; Zhang et al., 2017); for further discussion, this dosage was referred to as critical dosage (D_{crit}). All these authors observed an adverse effect on the response variable at dosages higher than D_{crit}; thus, applying a dosage below D_{crit} is advisable to avoid (accidental) deterioration of the filtration performance. Furthermore, as observed in the same publications, the rate of improvement of response variables decreases when the dosage approaches D_{crit}. Ideally, optimal dosage should be calculated by minimising the cost of operation of a continuous AnMBR, but this is a challenging approach and varies between installations.

Moreover, D_{opt} has been also defined as the dosage at which the improvement of the response variable reaches a plateau (saturation behaviour), above which no further significant improvement is observed with higher dosages (Alkmim et al., 2016; Díaz et al., 2014; Fan et al., 2007; Koseoglu et al., 2008; Wang et al., 2016; Zhou et al., 2019). By applying this definition, the authors minimised the required dosage while achieving an improvement similar to the maximum. Therefore, this approach was applied to calculate the D_{opt}.

Most authors select the D_{opt} manually by looking at the plotted response variables as a function of dosage, but this approach is subjective. Therefore, a mathematical approach was used to determine the D_{opt} objectively. The hyperbolic response curve, of ΔR_{20} decrease as a function of dosage, was approximated by two lines with the following model:

$$y = \begin{cases} K_1 D, & D < K_2/K_1 \\ K_2, & D \geq K_2/K_1 \end{cases}, \tag{2.2}$$

where y is the response variable ΔR_{20} decrease (%), D is the FE dosage (g L^{-1}), and K_1 (% L g^{-1}) and K_2 (%) are empirical coefficients. The first line in the model ($y = K_1 D$) represents the linear increase at lower dosages that have been typically observed in the literature. The second line ($y = K_2$) represent the previously observed saturation behaviour. D_{opt} was defined as the dosage corresponding to the intersection of both lines ($D_{opt} = K_2/K_1$).

The parameters of the model (K_1 and K_2) were estimated to fit the experimental data for each dosage-step test, by minimising the residual sum of squares (RSS):

$$RSS = \sum_i \left(y_{e,i} - y_{m,i}\right)^2, \tag{2.3}$$

where $y_{e,i}$ is the experimental observation i, and $y_{m,i}$ the corresponding model prediction. RSS was minimised with a nonlinear constrained optimisation function, *fmincon*, in Matlab® R2019b. The upper limit for K_2 was set to 100, because ΔR_{20} decrease should be below 100%.

D_{opt} was determined with a crossflow filtration method; however, in previous research, optimal dosages were mostly determined based on soluble or colloidal organic matter removal and dead-end filtration measurements. Therefore, D_{opt} was compared with $D_{opt,csCOD}$,

$D_{\mathrm{opt,sCOD}}$ and $D_{\mathrm{opt,CST}}$, which are determined based on the response variables: csCOD removal, sCOD removal and CST decrease, respectively. The response variables were calculated with Equation (2.1), where y is the response variable (CST decrease, sCOD removal or csCOD removal), x_{raw} is CST, sCOD or csCOD of the raw sludge (without FE), and x is CST, sCOD or csCOD measured after each FE dosage.

As mentioned above, previous research shows that high FE dosages can cause an adverse effect on the response variables. Accordingly, the critical dosage (D_{crit}) was defined as the dosage above which an adverse effect on filterability is observed; D_{crit} was selected from the plotted ΔR_{20} decrease versus dosage as the last experimental data before filterability started deteriorating. Moreover, $D_{\mathrm{crit,csCOD}}$, $D_{\mathrm{crit,sCOD}}$ and $D_{\mathrm{crit,CST}}$ were determined with csCOD removal, sCOD removal and CST decrease, respectively.

2.2.7.2 Correlation and regression analyses

Kendall's correlation coefficient (τ) was used to identify which of the raw sludge characteristics, if any, had a statistically significant relationship with D_{opt}. Field (Field, 2009) recommends using τ, which is a non-parametric rank correlation, for small data sets such as the one in this study (10 points). The statistical significance was assessed by comparing the probability value (p) with two levels of significance: 0.01 and 0.05. τ and p were computed with *corr* function in Matlab® R2019b.

Afterwards, the sludge characteristics that significantly correlated with D_{opt} were used to derive empirical models: $D_{\mathrm{opt}} = f(x)$, where x is a significantly correlated variable and f is the model (for example: linear or exponential); f was selected based on the graphical representation of the results. The models were calibrated in Matlab® R2019b with *fit* function. The goodness-of-fit was assessed based on the coefficient of determination (R^2). The prediction bounds (or prediction interval) for new observations were obtained with *fit*, considering all predictor values (simultaneous bounds), and a 95% confidence level (The MathWorks, 2018).

2.3 RESULTS

2.3.1 Raw sludge characteristics

The physicochemical characteristics of the raw sludges are presented in Table 2.2 and the particle size distribution in Figure 2.3. The time lapses between collection and testing for LiqOFMSW, Food2, Food2-II, Food3 and Food3-II were sufficiently long to assume that sludge characteristics might have changed due to physicochemical and biochemical processes taking place during transportation and storage, such as degradation of substrates. Therefore, the physicochemical characteristics presented in Table 2.2 of the abovementioned samples might not be identical to the characteristics of the sludges at the moment of collection from the AnMBRs. Nevertheless, filterability was significantly worse (higher $\Delta R_{20(1.5,60)}$) for LiqOFMSW and Food1 than for the remaining samples, which was in accordance with the deteriorated permeability (=Flux/TMP) observed by the plant operators at the moment of collection (data not shown).

LiqOFMSW was noticeably different from other sludges, that is: it had considerably higher $\Delta R_{20(1.5,60)}$, CST, cCOD, sCOD, NH_4-N, conductivity, SMP-HS and SMP-CH. Moreover, in LiqOFMSW, SMP-PR was negligible compared to SMP-HS; thus, it was not possible to determine SMP-PR with the modified Lowry method because this method cannot measure proteins independently from humic substances.

The median floc size, represented by the median diameter $D50$, was similar for all samples, except Food1. The volume fraction for particles below 1 µm was zero in all samples tested, Figure 2.3. Govoreanu et al. (2004) showed that when measuring particle size distribution of activated sludge with a light scattering technique, the distribution of small particles are likely to have errors. Therefore, the values measured below 1 µm were likely not realistic. Therefore, the fraction of organic material below 1 µm was characterised through cCOD.
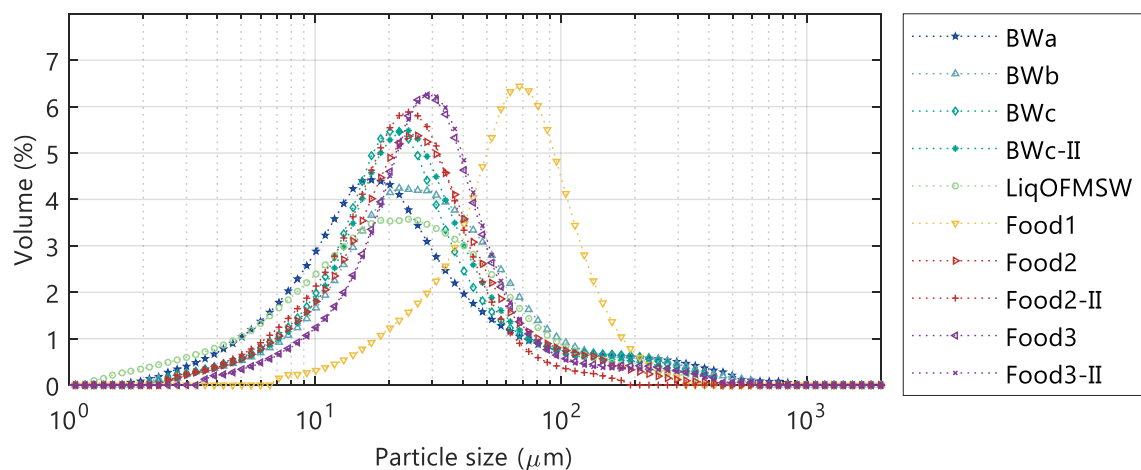
Figure 2.3. Volume-based particle size distribution of raw sludge samples.

Table 2.2. Characteristics of raw sludges.

Variable	Unit	BWa	BWb	BWc	BWc-II	LiqOFMSW	Food1	Food2	Food2-II	Food3	Food3-II
$\Delta R_{20}(_{1.5,60})$	$\times 10^{12}$ m^{-1}	13.2	6.5	3.1	3.4	30	24.8	3	0.6	14.2	15.3
$\Delta R_{20}(_{0.5,60})$	$\times 10^{12}$ m^{-1}	ND	ND	ND	12.2	ND	ND	14.1	ND	ND	17
CST	s	ND	76	64	72	3,712	1,458	204	204	393	497
tCOD	g L^{-1}	10.5	10.5	6.7	6.7	26.1	31.4	19.1	19.1	13.9	13.9
scCOD	g L^{-1}	9.6	10	6.2	6.2	14.9	ND	18.8	18.8	12.4	12.5
csCOD	g L^{-1}	0.9	0.47	0.52	0.48	11.22	ND	0.25	0.31	1.47	1.39
sCOD	g L^{-1}	0.14	0.1	0.28	0.28	4.36	ND	0.11	0.1	0.35	0.44
cCOD	g L^{-1}	0.76	0.37	0.24	0.21	6.86	ND	0.14	0.21	1.12	0.95
TP	mg L^{-1}	77.9	77.9	38	36	35	87	127	189	139	145
TN	mg L^{-1}	588	588	349	404	1616	755	627	710	1,290	1,190
NH$_4$-N	mg L^{-1}	166	141	82	72	862	38	140	159	246	227
TON	mg L^{-1}	421	446	267	332	754	717	486	551	1,044	963
pH	-	7.2	7.2	7.5	6.9	8.1	7.2	7.2	7.2	7.2	7.2
Conductivity	S m^{-1}	0.21	0.24	0.11	0.11	3	ND	0.45	0.45	0.42	0.42
VSS	g L^{-1}	7.6	7.5	3.7	3.3	9	15.2	11.2	13.2	8.9	9.7
TSS	g L^{-1}	8.6	8.7	4.2	3.9	12.4	17.2	14.4	17.8	9.5	10.7
SMP-PR	mg L^{-1}	50	15	74	71	NA [a]	140	0	0	109	117
SMP-HS	mg L^{-1}	80	71	89	83	5,164	47	32	33	0	0
SMP-CH	mg L^{-1}	14	7	19	19	339	62	16	16	20	22
D10	μm	6.5	9.3	8.9	9.2	5.5	23.8	8.2	8.3	11.7	11.9
D50	μm	19	27	22	23	21	61	21	21	27	28
D90	μm	107	99	80	75	73	120	46	46	69	66

Abbreviations: ND, not determined; NA, not applicable.
[a] SMP-PR could not be determined because SMP-HS was too high and the sample had to be diluted 20 times.

2.3.2   Flux enhancer dosage-step experiments

Figure 2.4 shows the effect of increasing FE dosage on ΔR_{20} obtained during the dosage step experiments for each sludge sample. The FE improved filterability showing a saturation behaviour for all sludges. The required dosage of FE to improve filterability was noticeably different for each sludge: the ones with better filterability required less FE. Furthermore, high dosages caused an adverse effect, i.e., increased ΔR_{20}, in LiqOFMSW, BWc, BWc-II, Food1, Food2 and Food3; for a more detailed visualisation is shown in Figure 2.5. The dosages above which this adverse effect was observed, i.e., D_{crit}, varied from 0.10 to 2.5 g L^{-1}. Moreover, the observed ΔR_{20} decrease that was achieved for LiqOFMSW (52%) and Food1 (82%) was smaller than for the other samples (> 90%). Therefore, sludges with worse filterability do not only require more FE, but also present a more limited improvement on filterability by FE addition.

Figure 2.5 shows that FE decreased csCOD, sCOD and CST, and increased $D50$. Comparison between Figure 2.5A and Figure 2.4 shows that for most sludge samples, except for LiqOFMSW, the csCOD and ΔR_{20} had a similar behaviour, that is: dosing FE decreased csCOD with a saturation behaviour and had an adverse effect at high dosages, which was observed in BWc, BWc-II, and Food3. Moreover, Figure 2.5B shows that sCOD presented a behaviour similar to ΔR_{20} and csCOD, which was characterised as decrease-saturation-increase. Nevertheless, in Food3, the sCOD increased at a lower dosage (0.5 g L^{-1}) than the csCOD and ΔR_{20} (1.0 g L^{-1}).

CST is a dead-end filtration method used to assess sludge dewaterability and has been previously used as an indicator of sludge filterability. In this study, CST (Figure 2.5C)
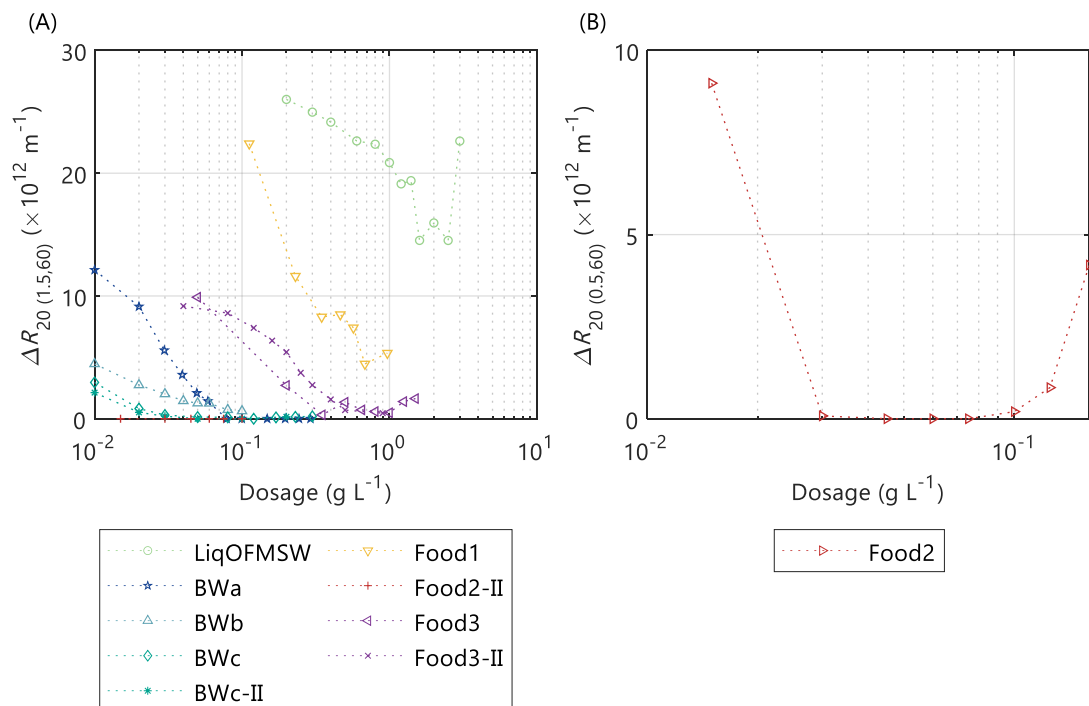
Figure 2.4. ΔR_{20} during FE dosage-step test in the AnDFCm installation for sludge samples from different sources. ΔR_{20} was measured by applying a flux of 60 L m^{-2} h^{-1} and crossflow velocities of (A) 1.5 m s^{-1} and (B) 0.5 m s^{-1}.

presented a similar saturation behaviour as ΔR_{20} (Figure 2.4) for most sludges tested. However, the adverse effect on ΔR_{20} and csCOD at high dosages, was not reflected in the CST measurements.

In the FE dosage ranges tested for each sample, the $D50$ versus dosage curve displayed the saturation behaviour, observed in ΔR_{20}, CST and csCOD, only in Food1. Moreover, the adverse effect at high dosages was only present in LiqOFMSW and BWc (Figure 2.5D). Therefore, floc size, as quantified in this research, might not be a direct indication of filterability improvement and deterioration.

$R_{\text{T,water}}$ was measured in each cycle of the dosage-step test, after filtering sludge with different dosages of FE and cleaning the membrane, see protocol in Figure 2.2. In Figure 2.6, the $R_{\text{T,water}}$ increased after filtering sludges with high FE dosages. For most sludges, the
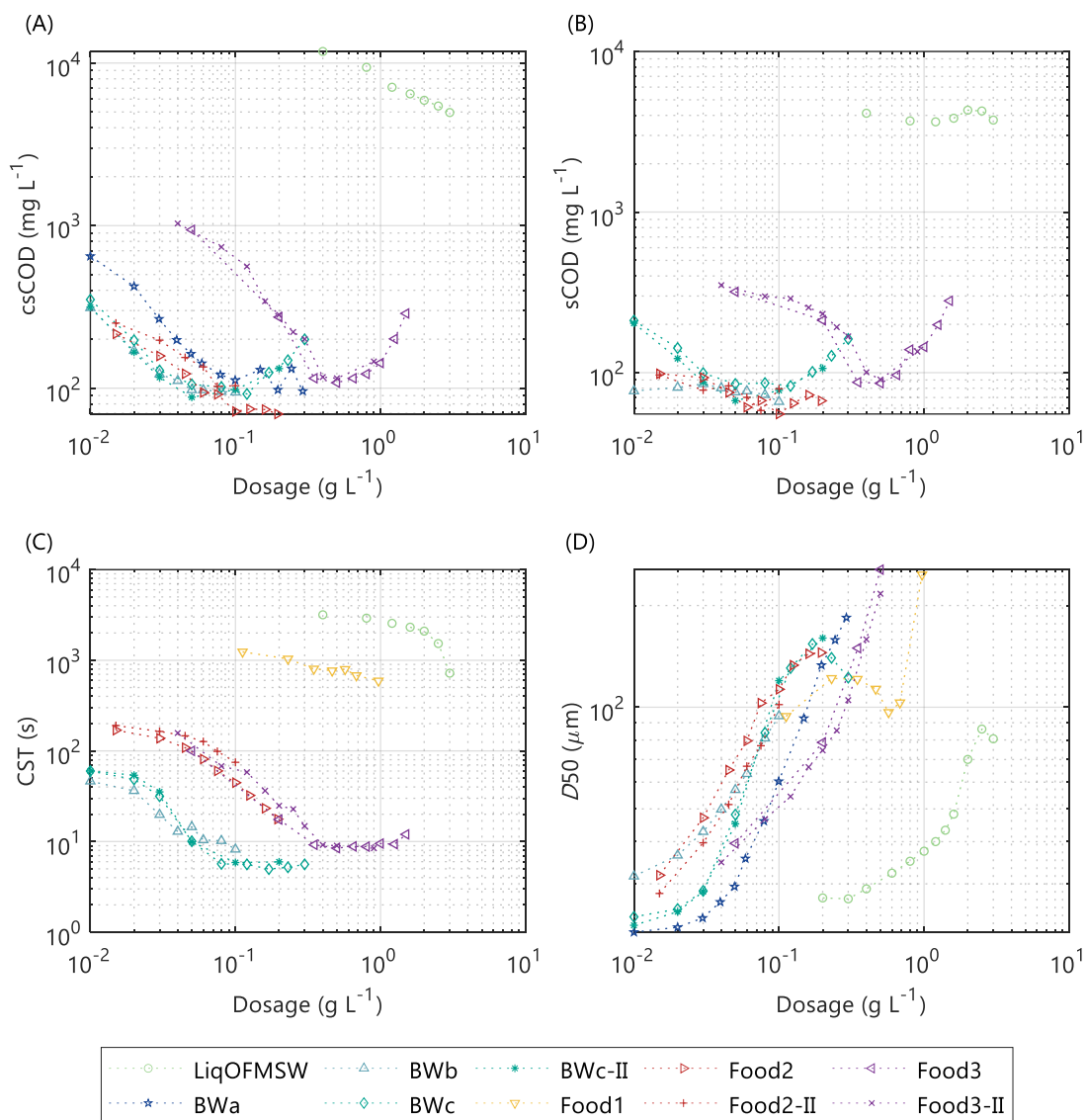
Figure 2.5. Sludge characteristics during FE dosage-step test in the AnDFCm installation for sludge samples from different sources: (A) submicron organic matter concentration, (B) soluble organic matter concentration, (C) capillary suction time, and (D) floc size expressed as median diameter. The csCOD of Food1, CST of BWa, and sCOD of BWa and Food1 were not measured.
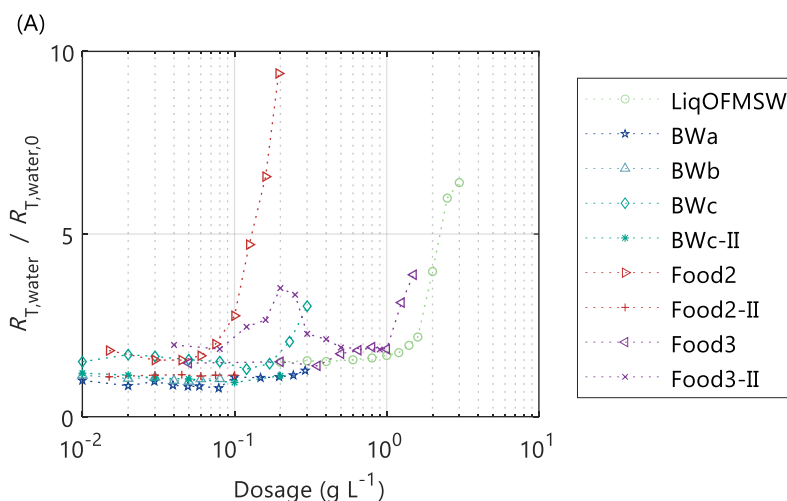
Figure 2.6. Resistance to water filtration after each step ($R_{T,water}$) during FE dosage-step test in the AnDFCm installation for sludges from different sources. The $R_{T,water}$ was normalised by resistance to water filtration before starting each test ($R_{T,water,0}$). For Food3-II, the membrane was chemically cleaned with 2 g L^{-1} of citric acid during 1 hour between the FE dosages 0.2 g L^{-1} and 0.25 g L^{-1}.

dosage above which $R_{T,water}$ rapidly increased was similar to D_{crit} (Table 2.3) of each sludge sample. However, in Food3-II, $R_{T,water}$ rapidly increased at dosages above 0.08 g L^{-1} while no adverse effect was observed on ΔR_{20} in the whole range tested, 0.04 – 0.90 g L^{-1}. The membrane was chemically cleaned after measuring Food3-II with 0.20 g L^{-1} of FE, causing a slight decrease in $R_{T,water}$ at the next dosage step (0.25 g L^{-1} of FE). Surprisingly, at dosages above 0.25 g L^{-1}, $R_{T,water}$ continuously decreased with increasing dosages. This observation could not be explained and the cause should be further investigated. Nevertheless, this behaviour was not observed in other sludges, including Food3 that originated from the same sample as Food3-II.

2.3.3   Optimal and critical dosages

Figure 2.7 to Figure 2.10 show the graphical representation of optimal and critical dosages determination based on ΔR_{20} decrease, sCOD removal, csCOD removal and CST decrease, respectively. The optimal and critical dosages values are summarised in Table 2.3.

The dosages differed considerably between samples; particularly D_{opt} ranged from 0.02 to 1.16 g L^{-1} and D_{crit} from 0.10 to 2.5 g L^{-1}, which were determined based on ΔR_{20} decrease.

D_{opt} was compared with $D_{opt,csCOD}$, $D_{opt,sCOD}$ and $D_{opt,CST}$, that were determined with csCOD, sCOD and CST, respectively. The average relative differences of $D_{opt,csCOD}$, $D_{opt,sCOD}$ and $D_{opt,CST}$ with D_{opt} were 47%, 52% and 78%, respectively; where the relative difference is the absolute value of the difference between the correspondent optimal dosage and D_{opt}, divided by D_{opt}.

D_{crit} was determined in 6 out of 10 performed dosage-step tests, because for Bwa, BWb, Food2-II and Food3-II no adverse effect on filterability was observed. Apparently, with the latter 4 sludges, the charge-saturation level of the applied FE was not reached and hence D_{crit}

Table 2.3. Optimal and critical FE dosages for: ΔR_{20} decrease (D_{opt} and D_{crit}), csCOD removal ($D_{opt,csCOD}$ and $D_{crit,csCOD}$), sCOD removal ($D_{opt,sCOD}$ and $D_{crit,sCOD}$), and CST decrease ($D_{opt,CST}$ and $D_{crit,CST}$). All dosages are in g L^{-1}.

Sludge name	Dosage range	D_{opt}	$D_{opt,csCOD}$	$D_{opt,sCOD}$	$D_{opt,CST}$	D_{crit}	$D_{crit,csCOD}$	$D_{crit,sCOD}$	$D_{crit,CST}$
BWa	0.01 - 0.30	0.06	0.03	ND [c]	ND [c]	NA [d]	NA [d]	ND [c]	ND [c]
BWb	0.01 - 0.10	0.03	0.02	0.09	0.03	NA [d]	NA [d]	NA [d]	NA [d]
BWc	0.01 - 0.30	0.03	0.02	0.03	0.06	0.12	0.12	0.12	NA [d]
BWc-II	0.01 - 0.20	0.02	0.02	0.03	0.05	0.10	0.10	0.05	NA [d]
LiqOFMSW	0.2 – 3.0	1.16	1.88	0.76	3.00	2.5	NA [d]	NA [d]	NA [d]
Food1	0.11 - 1.00	0.38	ND [c]	ND [c]	0.40	0.68	ND [c]	ND [c]	NA [d]
Food2	0.02 - 0.20	0.03 [a]	0.06	0.06	0.09	0.10	NA [d]	0.10	NA [d]
Food2-II	0.02 - 0.10	NA [b]	0.06	0.06	0.10	NA [d]	NA [d]	0.08	NA [d]
Food3	0.05 - 1.50	0.15	0.21	0.30	0.07	1.0	1.0	0.5	NA [d]
Food3-II	0.04 - 0.90	0.23	0.17	0.29	0.06	NA [d]	NA [d]	0.5	NA [d]

Abbreviations: ND, not determined; NA, not applicable.
[a] Optimal dosage determined using $\Delta R_{20} = \Delta R_{20(0.5,60)}$ instead of $\Delta R_{20} = \Delta R_{20(1.5,60)}$.
[b] Optimal dosage was not estimated because ΔR_{20} decrease was 100% immediately after the lower dosage tested.
[c] The corresponding characteristic was not measured during this dosage-step test.
[d] Critical dosage could not be estimated because no adverse effect was observed.

could not be identified. However, for Food2-II and Food3-II the maximum dosages tested were possibly too low to achieve an adverse effect, moreover these maximum dosages were lower than D_{crit} obtained with Food2 and Food3, respectively. Accordingly, for BWb the filterability improvement was below saturation at the maximum dosage tested (0.10 g L^{-1}); thus, the D_{crit} might be above 0.10 g L^{-1}. Surprisingly, for Bwa the adverse effect was not observed despite applying a dosage 5-folds above D_{opt}. Therefore, Bwa might be the only sludge that did not present an adverse effect at high dosages of FE.

D_{crit} was compared with their corresponding $D_{crit,csCOD}$, $D_{crit,sCOD}$ and $D_{crit,CST}$, presented in Table 2.3. $D_{crit,csCOD}$ was equal to D_{crit} for 3 sludges (BWc, BWc-II and Food3) and differed for 2 sludges (LiqOFMSW and Food2); whereas $D_{crit,sCOD}$ was equal to D_{crit} for 2 sludges (BWc and Food2) and differed for 5 sludges (LiqOFMSW, BWc-II, Food2-II, Food3 and Food3-II). Furthermore, $D_{crit,CST}$ was not detected in any sample because there was no adverse effect on CST.
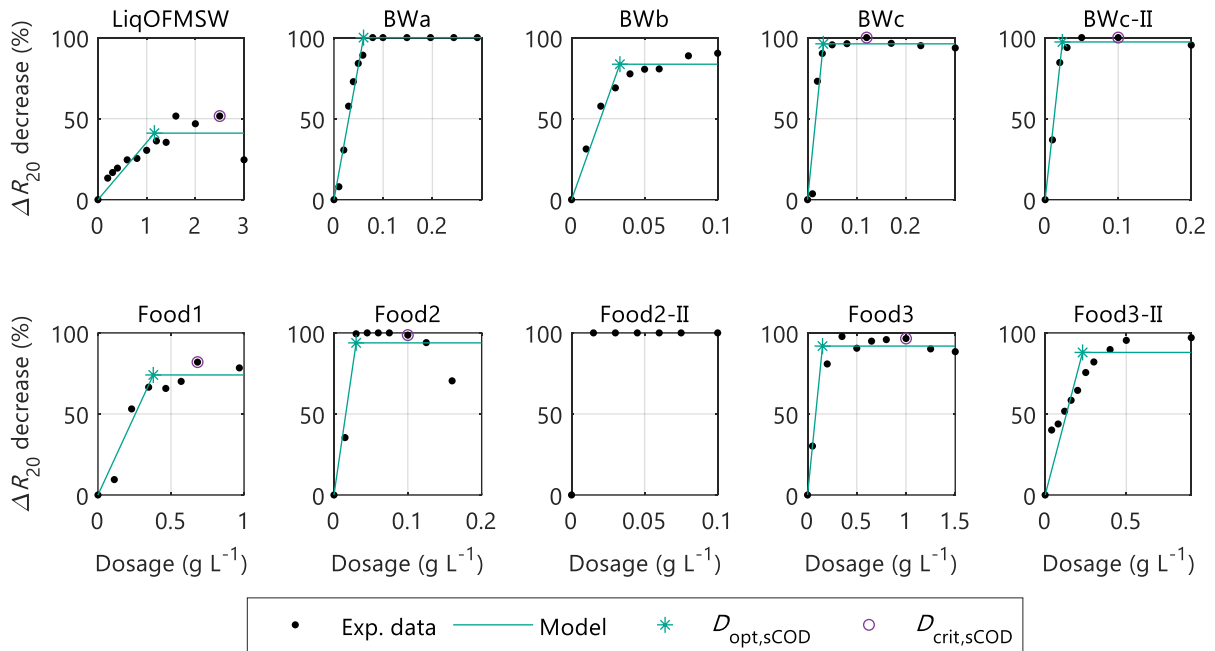
Figure 2.7. Sludge filterability improvement, expressed as ΔR_{20} decrease, during FE dosage-step test in the AnDFCm installation for sludge samples from different sources. The optimal dosage (D_{opt}) was determined with the model in Equation (2.2); and the critical dosage (D_{crit}), if existent, was selected as the last experimental dosage before an adverse effect on filterability was observed.
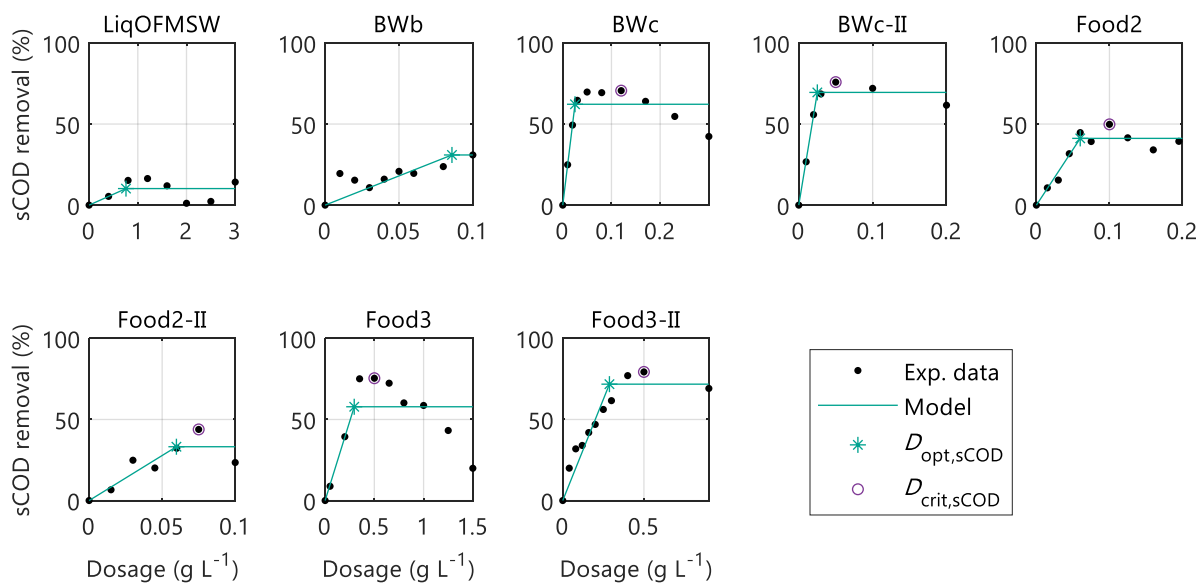
Figure 2.8. Removal of soluble COD during FE dosage-step test in the AnDFCm installation for sludge samples from different sources. The optimal dosage (D_{opt}) was determined with the model in Equation (2.2); and the critical dosage (D_{crit}), if existent, was selected as the last experimental dosage before an adverse effect on sCOD was observed.
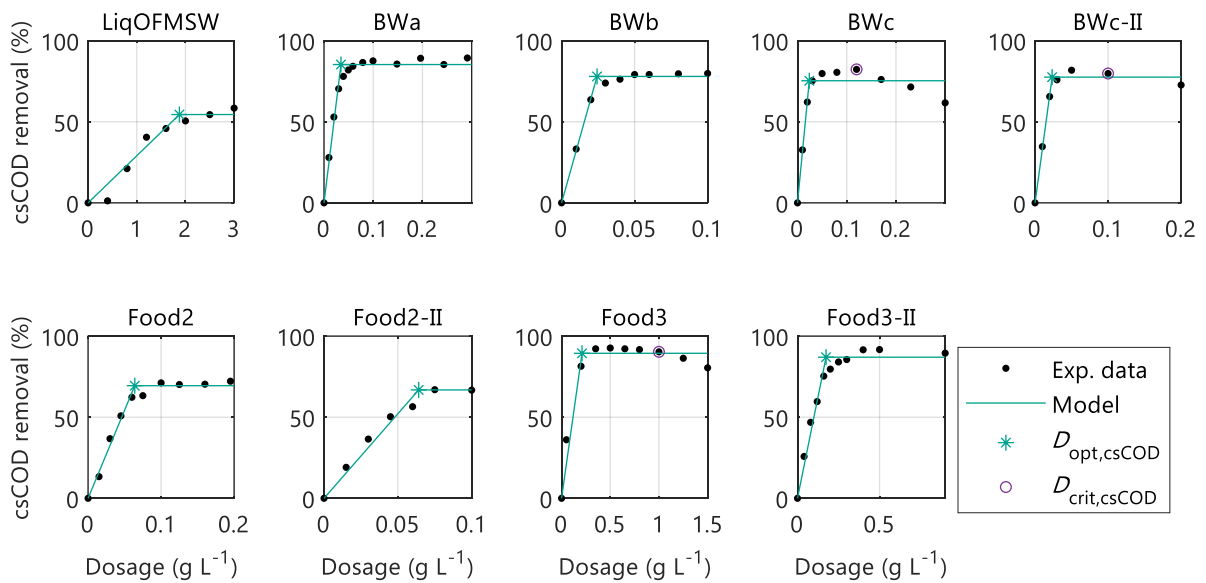
Figure 2.9. Removal of submicron COD, which includes colloidal and soluble COD, during FE dosage-step test in the AnDFCm installation for sludge samples from different sources. The optimal dosage (D_{opt}) was determined with the model in Equation (2.2); and the critical dosage (D_{crit}), if existent, was selected as the last experimental dosage before an adverse effect on csCOD was observed.
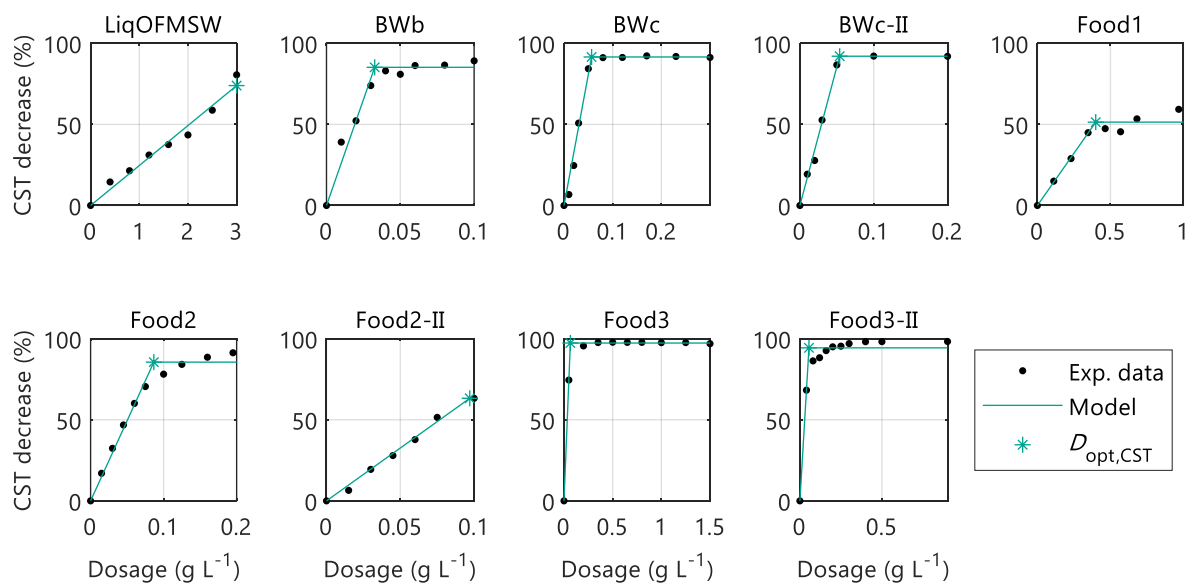
Figure 2.10. Capillary suction time (CST) decrease during FE dosage-step test in the AnDFCm installation for sludge samples from different sources. The optimal dosage (D_{opt}) was determined with the model in Equation (2.2).

2.3.4 Correlation analysis

Kendall's correlation (Table 2.4) revealed that D_{opt} had a statistically high significant correlation ($p < 0.01$) with: $\Delta R_{20,(1.5,60)}$, CST and cCOD. These correlations were all positive ($\tau > 0$), indicating that a sample with higher $\Delta R_{20,(1.5,60)}$ (lower filterability), CST or cCOD required higher FE dosages to mitigate fouling.

Moreover, D_{opt} was statistically significantly correlated with SMP-CH, contrary to SMP-PR and SMP-HS. Furthermore, D_{opt} had a non-significant correlation with NH_4-N, TON, TP, conductivity, pH and $D50$. In addition, there was a significant correlation between D_{opt} and TSS (>0.7 µm) but not between D_{opt} and scCOD (<1 µm); the correlation with TSS could be caused by the fraction of colloidal organic matter in the range of 0.7 and 1 µm, which is retained in the filter during the measurement. Consequently, the variables selected for empirical models were $\Delta R_{20,(1.5,60)}$, CST, cCOD and SMP-CH.

Table 2.4. Kendall correlation coefficient (τ) and probability value (p) between raw sludge characteristics and optimal dosage of flux enhancer for filterability improvement (D_{opt}) including and excluding LiqOFMSW from the analysis. Significant correlation at levels 0.01 (**) and 0.05 (*).

Variable	Including LiqOFMSW in analysis		Excluding LiqOFMSW from analysis	
	τ	p	τ	p
$\Delta R_{20(1.5,60)}$	0.89**	0.0002	0.86**	0.002
CST	0.79**	0.006	0.71*	0.030
scCOD	0.43	0.179	0.33	0.381
cCOD	0.86**	0.002	0.81*	0.011
sCOD	0.57	0.061	0.43	0.239
TP	0.20	0.540	0.55	0.080
TON	0.44	0.119	0.43	0.179
NH_4-N	0.50	0.075	0.36	0.275
pH	0.31	0.304	0.11	0.810
Conductivity	0.55	0.080	0.39	0.300
TSS	0.56*	0.045	0.57	0.061
SMP-PR	0.62	0.069	0.62	0.069
SMP-HS	-0.08	0.839	-0.40	0.220
SMP-CH	0.61*	0.025	0.50	0.109
$D10$	0.22	0.477	0.57	0.061
$D50$	0.28	0.358	0.57	0.061
$D90$	0.17	0.612	0.29	0.399

2.3.5   Empirical models

The scatterplots, presented in Odriozola et al. (2021), suggest that the empirical model for $\Delta R_{20,(1.5,60)}$ was exponential: $D_{opt} = a \exp\left(b\,\Delta R_{20,(1.5,60)}\right)$, where a and b are parameters; whereas for CST, cCOD and SMP-CH linear models were adopted: $D_{opt} = a\,y + b$, where y represents CST, cCOD or SMP-CH variables.

Figure 2.11 displays the experimental data, the empirical models, and the prediction interval for new observations; on the left are the models calibrated including all the sludges and on the right the models calibrated excluding LiqOFMSW. Results shows that LiqOFMSW considerably influenced the calibration of the empirical models. Table 2.5 compares the predicted dosages with the models calibrated including and excluding LiqOFMSW.

The predictions using different empirical models slightly differed. However, all predicted optimal dosages are in the same order of magnitude as the measured D_{opt} and below the measured critical dosages D_{crit}. Therefore, all models showed their suitability for predicting the dosage required for filterability improvement of new sludge samples, especially as a reference dosage to avoid overdosing. Nevertheless, further research with sludges characterised by a poor filterability could improve the predictive value of the models.

2.3.6   Filtration of unbonded flux enhancer

Figure 2.12 shows that the two higher concentrations tested of Adifloc KD451, namely 0.5 and 1.0 g L⁻¹, significantly increased the filtration resistance R_T, whereas 0.1 g L⁻¹ had no effect on R_T. Compared with optimal dosages required for filterability improvement in the tested sludges (Table 2.3), the concentrations tested in this experiment (0.1, 0.5 and 1.0 g L⁻¹) are considerably high, and thus unexpected as unbonded polymer concentrations in AnMBRs. From the 10 samples tested only 4 had an optimal dosage above 0.1 g L⁻¹, as follows: LiqOFMSW (1.16 g L⁻¹), Food1 (0.38 g L⁻¹), Food3 (0.15 g L⁻¹), and Food3-II (0.23 g L⁻¹). Moreover, assuming that 5% of the polymer added to the sludge remains unbonded, which Iversen et al. (2008) have already argued as being an overestimation, then the concentration of unbonded polymer is below 0.1 g L⁻¹ even for the sludge with highest optimal dosage, which is LiqOFMSW. Therefore, the polymer can deteriorate the filtration performance when it remains unbonded in the bulk liquid, but only at high concentrations, which are unlikely to occur when in a polymer dosed AnMBR.

The COD measured in the permeate samples obtained in the AnDFCm installation, $c_{fe,P}$, is presented in Table 2.6. Results show that a fraction of the polymer passed through the membrane pores and contaminated the permeate, indicated by an increase of $c_{fe,P}$ with increasing polymer concentration in the bulk (c_{fe}); c_{fe} is the initial concentration of the polymer solution.

During Step 3 of the filtration test protocols (Figure 2.2), where the polymer solution was filtered in the AnDFCm installation, all the permeate produced was collected in a vessel; $c_{fe,P}$ represents the concentration in the produced permeate vessel. Thus, the permeate sample was diluted with the demineralised water, that remained in the permeate side inside the membrane

Table 2.5. Measured optimal (D_{opt}) and critical (D_{crit}) FE dosages for ΔR_{20} decrease, and predicted optimal dosages with empirical models calibrated using all sludge samples ($D_{\mathrm{opt}}^{m,i}$) and empirical models calibrated excluding LiqOFMSW ($D_{\mathrm{opt}}^{m*,i}$); where i are the input variable for the models: $\Delta R_{20(1.5,60)}$, cCOD, CST and SMP-CH. All values are in g L^{-1}.

Sludge name	Measured dosages		Predicted dosages with empirical models calibrated including LiqOFMSW				Predicted dosages with empirical models calibrated excluding LiqOFMSW			
	D_{opt}	D_{crit}	$D_{\mathrm{opt}}^{m,\Delta R_{20}}$	$D_{\mathrm{opt}}^{m,\mathrm{CST}}$	$D_{\mathrm{opt}}^{m,\mathrm{cCOD}}$	$D_{\mathrm{opt}}^{m,\mathrm{SMP-CH}}$	$D_{\mathrm{opt}}^{m*,\Delta R_{20}}$	$D_{\mathrm{opt}}^{m*,\mathrm{CST}}$	$D_{\mathrm{opt}}^{m*,\mathrm{cCOD}}$	$D_{\mathrm{opt}}^{m*,\mathrm{SMP-CH}}$
LiqOFMSW	1.16	2.5	1.13	1.14	1.16	1.18	0.67	1.00	1.15	2.24
BWa	0.06	NA [c]	0.08	NA [d]	0.12	0.09	0.12	NA [d]	0.12	0.06
BWb	0.03	NA [c]	0.03	0.03	0.05	0.06	0.06	0.04	0.05	0.01
BWc	0.03	0.12	0.02	0.03	0.03	0.10	0.04	0.04	0.03	0.10
BWc-II	0.02	0.10	0.02	0.03	0.02	0.10	0.04	0.04	0.02	0.09
Food1	0.38	0.68	0.49	0.45	NA [d]	0.25	0.39	0.40	NA [d]	0.38
Food2	0.03 [a]	0.10	0.02	0.07	0.01	0.09	0.04	0.08	0.01	0.08
Food2-II	NA [b]	NA [c]	0.01	0.07	0.02	0.09	0.03	0.08	0.02	0.08
Food3	0.15	1.0	0.09	0.13	0.18	0.11	0.13	0.13	0.18	0.10
Food3-II	0.23	NA [c]	0.11	0.16	0.15	0.11	0.15	0.15	0.15	0.11

Abbreviation: NA, not applicable.

[a] Optimal dosage determined using $\Delta R_{20} = \Delta R_{20(0.5,60)}$ instead of $\Delta R_{20} = \Delta R_{20(1.5,60)}$.

[b] Optimal dosage was not estimated because ΔR_{20} decrease was 100% immediately after the lower dosage tested.

[c] Critical dosage could not be estimated because no adverse effect was observed.

[d] The corresponding raw sludge characteristic was not determined.
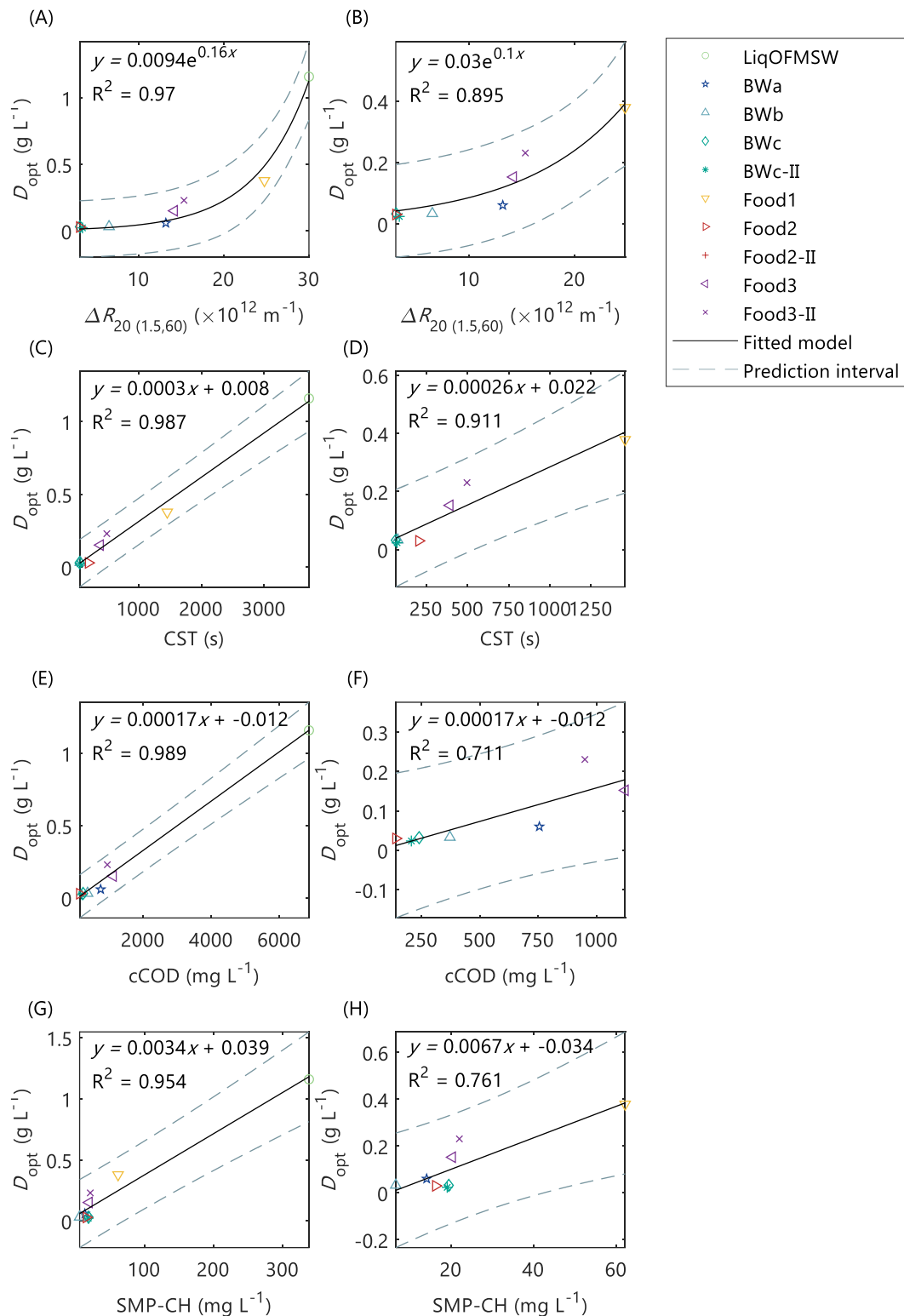
Figure 2.11. Experimental data and fitted model of the optimal FE dosage versus raw sludge characteristics including (left) and excluding (right) the sample LiqOFMSW during model calibration: (A, B) filterability expressed as $\Delta R_{20(1.5,60)}$, (C, D) capillary suction time, (E, F) concentration of colloidal organic matter, and (G, H) concentration of soluble carbohydrates. The grey-dashed lines represent the prediction interval for new observations; and R^2 is the coefficient of determination of the fitted model.

module when the filtration started. The volume of the permeate side of the membrane module was 0.208 L, which is comparable to the volumes of permeate collected (V_P), shown in Table 2.6. Consequently, the considerably smaller $c_{fe,P}$ compared to c_{fe} is partially due to the dilution during the filtration protocol step. Another cause for the reduced $c_{fe,P}$ can be that the polymer was retained inside the membrane or rejected by the membrane, further in the paper both processes are referred to as "retention by the membrane". The increasing R_T with c_{fe}, shown Figure 2.12, is an additional indication of the polymer interacting with the membrane, possibly being retained inside the membrane pores or in the membrane surface creating a cake-gel-type layer.

To estimate the amount of polymer that might have been retained by the membrane, the theoretical polymer concentration in the permeate vessel ($c_{fe,P,theo}$) was calculated assuming that all the polymer passed thorough the membrane. The permeate side of the membrane module was assumed to behave as a plug flow reactor (PFR) and the concentration drop in the membrane was considered negligible. The dynamic behaviour of a PFR with a step input in the inlet concentration is as follows: the concentration at the outlet, which is the permeate, is zero at times below the hydraulic retention time (HRT) and equal to the inlet concentration, which is c_{fe}, at time above or equal to HRT. Thus, the $c_{fe,perm,theo}$ was calculated as follows:

$$c_{fe,P,theo} = \frac{(t_F - \text{HRT})}{t_F} c_{fe} , \tag{2.4}$$

where t_F is the final filtration time. HRT was calculated with the volume of the permeate side of the membrane module, 0.208 L, and the flow rate through the membrane, this is the flux (60 L m^{-2} h^{-1}) multiplied by the membrane surface area ($A_m = 0.0239$ m^2); thus, HRT = 0.145 hours or 8.7 minutes.

The results in Table 2.6 show that the $c_{fe,P,theo}$ was significantly higher than $c_{fe,P}$, indicating that the membrane might have retained part of the polymer. The theoretical fraction of polymer retained by the membrane increased with c_{fe}, this might be caused by
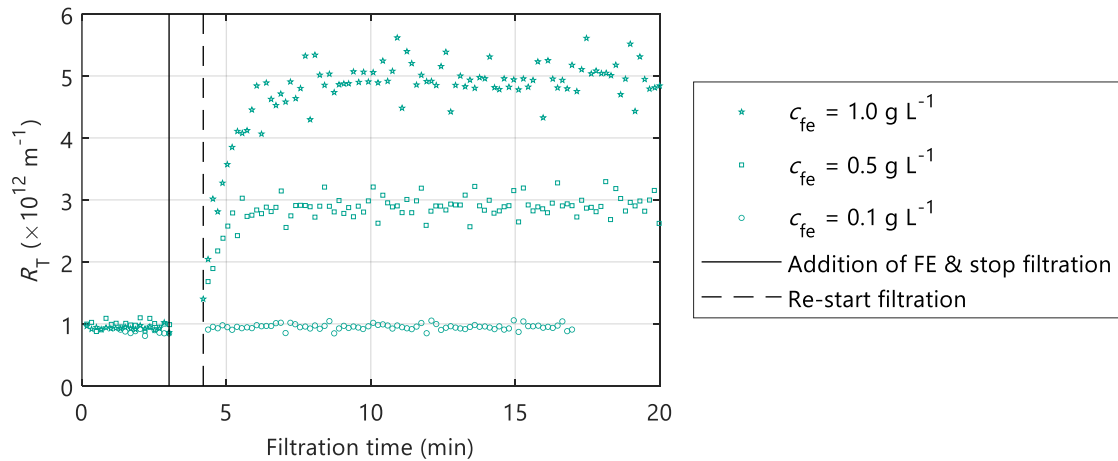
Figure 2.12. Total filtration resistance during filtration of flux enhancer (Adifloc KD451) solutions with different concentration (c_{fe}) in the AnDFCm installation at 60 L m^{-2} h^{-1} flux and 1.5 m s^{-1} crossflow velocity.

Table 2.6. Characteristics of permeate obtained while filtering flux enhancer solutions with different concentration (c_{fe}) in the AnDFCm installation, operated at 60 L m^{-2} h^{-1} flux and 1.5 m s^{-1} crossflow velocity.

c_{fe}		Permeate volume collected, V_P (L)	Permeate concentration (gCOD L^{-1}) [a]		Membrane retention (%) [b]
(g L^{-1})	(gCOD L^{-1})		$c_{fe,P}$	$c_{fe,P,theo}$	
0.1	0.1	0.33	0.018	0.037	50%
0.5	0.6	0.46	0.025	0.322	92%
1.0	1.1	0.47	0.046	0.670	93%

[a] COD concentration in the cumulative permeate collected during the filtration of Adifloc KD45 solution. $c_{fe,P}$ is the measured value with COD Kits, and $c_{fe,P,theo}$ is the value calculated assuming that the permeate side of the membrane module behaves as a plug flow reactor with an HRT of 8.7 min and without concentration polarization and polymer retention in the membrane.

[b] Theoretical fraction of polymer retained by the membrane, calculated as $(c_{fe,P,theo} - c_{fe,P})/c_{fe,P,theo}$.

charge repulsion between the membrane with adsorbed polymer and the polymer in the bulk liquid.

Therefore, a fraction of Adifloc KD451 was able to pass through the membrane pores and the concentration of the polymer in the permeate increases with c_{fe}. However, the retention in the membrane also increased with c_{fe}, and thus the concentration of polymer in the permeate remained relatively low.

2.4   DISCUSSION

This chapter analysed the effect of polymer dosage on the various sludge characteristics and water matrix parameters. The terminology 'optimal required dosage' or D_{opt} was introduced for the minimum required polymer dosage to exert a maximum improvement in sludge filterability; a dosage beyond D_{opt} had only a marginal additional effect. Moreover, a further increase in polymer dosage negatively impacted the sludge filterability. The dosage at which this occurred was defined as D_{crit} or the 'critical flux enhancer dosage'. The applied FE dosages exerted a different impact on the specific sludge characteristics and water matrix parameters of the various investigated sludges. As such, correlations were identified between D_{opt} and D_{crit} of the various sludges and some of these characteristics and parameters.

2.4.1   Effect of sludge characteristics on optimal FE dosage

2.4.1.1   Colloidal and soluble organic matter

The concentration of soluble and colloidal organic matter play a major role in fouling of membrane bioreactors (Christensen et al., 2018; Judd and Judd, 2011; Shi et al., 2018); high concentrations increase fouling by pore blocking, cake layer formation, and decrease in cake layer porosity. Electrostatic repulsion between the negatively charged colloidal particles prevents them from agglomerating, whereas the intermolecular attraction promotes bonding. Cationic polymers promote colloidal agglomeration by bridge flocculation, where polymer

segments are adsorbed onto the surface of different colloid particles linking them together. Alternatively, agglomeration is promoted by electrostatic patch mechanisms, where the polymer is adsorbed onto the particle surface creating positively charged patches that interact, upon collision, with the negative surface of other colloidal particles to form flocs. Moreover, excessive cationic polymer dosages can cause particle redispersion, also designated as deflocculation or restabilisation, by saturation of bridging sites or charge reversal due to complete surface coverage (Bratby, 2016).

Accordingly, in Figure 2.5A, csCOD decreased with increasing dosages of FE with a saturation behaviour which corresponds to complete colloidal surface coverage. The csCOD increased at dosages above D_{crit} due to redispersion of colloidal particles. The dosage at which complete coverage is attained depends on the colloidal surface area available. Regarding sludge filterability, D_{opt} was defined as the dosage at which the sludge filterability reaches saturation. Since the available colloidal surface is directly related to cCOD, D_{opt} was positively correlated with cCOD ($\tau = 0.86$, $p < 0.01$). Therefore, samples with higher concentrations of colloidal organic matter require higher FE dosages to mitigate fouling.

Soluble organic matter can be positively or negatively charged or can be neutral, namely: the overall charge of a protein depends on the pH and its isoelectric point; carbohydrates can be negatively charged (containing carboxylic groups or sulphuric ester groups), positively charged (with protonated free amino groups) or neutral; humic substances are negatively charged (containing carboxylic and phenolic groups). Therefore, the interaction with the cationic polymer is not straightforward, as it is for the exclusively colloidal organic matter. Consequently, sCOD did not correlate significantly with D_{opt} ($p > 0.05$).

A linear correlation between the optimum cationic polymer concentration and concentration of humic substances has been reported (Bratby, 2016). In this research, the SMP-HS was not significantly correlated with D_{opt} ($p > 0.05$), but the variation of SMP-HS between samples was small (Table 2.2), except for LiqOFMSW. The high optimal dosage required for LiqOFMSW was possibly due to the high concentration of SMP-HS that bind with the FE, thus decreasing the availability of FE to flocculate the colloidal material.

2.4.1.2   Supracolloidal organic matter concentration and size

Supracolloidal organic matter in sludge matrices, further referred to as flocs, usually present an overall negative surface charge (Braguglia et al., 2006; Jia et al., 1996). Thus, cationic FE may adsorb onto the flocs, thereby decreasing FE availability for flocculation of colloidal material. Consequently, bigger quantities of FE would be required at higher flocs concentrations. Nevertheless, colloidal material can be incorporated into flocs by interaction with the FE adsorbed or by entrapment between aggregated flocs. Therefore, flocs present opposite effects on the flocculation of colloidal material, and thus on filterability improvement. Consequently, no significant correlation was observed between scCOD and D_{opt}.

For suspensions with uniform particle size, higher optimal dosages are required for smaller particles due to its larger specific surface. Nevertheless, good flocculation

performance can be obtained at different dosages for samples with various particles sizes (Bratby, 2016). Therefore, the samples used in this research, which had flocs of a wide range of sizes (~1-1000 μm, Figure 2.3), had no significant correlation between the D_{opt} and the floc size distribution, represented by $D10$, $D50$ and $D90$ in Table 2.4.

2.4.1.3   pH and electrical conductivity

When using coagulants as FE, pH is a crucial variable. However, cationic polymers can be used within a wide pH range, without the need for pH adjustment. Research has shown an effect of pH on the optimal required dosage, which was mainly attributed to changes in the surface charge of the material to be flocculated (Bratby, 2016). Contrarily, relationship between pH and D_{opt} was observed; however, the pH range of the samples was narrow: 6.9 – 8.1 (Table 2.2). Similar pH values are observed in most membrane bioreactors where approximately neutral pH is required to favour biological processes. Therefore, pH is not expected to influence the required dosage of cationic polymer.

Electrical conductivity is correlated with ionic strength and it is a fast measurement to estimate the concentration of ions in solution. High ionic strength could positively influence aggregation of colloidal material by reducing the electrostatic repulsion of particles of the same charge. However, it might also harm flocculation by reducing the extension of the polymer chains; the size of polymer chains are very important for effectively bridging colloidal material (Bratby, 2016). Additionally, the adsorption of FE onto the negatively charged material can be reduced by polymer neutralisation by anions, or by decreased available adsorption sites due to adsorption of cations onto the colloidal material (Kasper, 1971). Therefore, ionic strength has opposite effects on flocculation of colloidal material. Accordingly, no correlation between conductivity and D_{opt} was observed.

2.4.2   Side effects of FE and the risk of overdosing

Dosages of FE above the D_{crit} caused an adverse effect on filterability, csCOD and sCOD in several sludges. Various researchers have observed this negative effect on different response variables (Braguglia et al., 2006; Collins et al., 2006; Díaz et al., 2014; Koseoglu et al., 2008; Wozniak, 2010; Zhang et al., 2017). Excessive FE dosage can impair filtration performance due to increased concentration of colloidal and soluble organic matter by deflocculation. Additionally, the interaction between the cationic FE, that remains unbonded in the bulk liquid, and the membrane may result in intense fouling, by FE adsorption over the membrane surface and inside the pores (Iversen et al., 2008). This was shown in Figure 2.6 by high $R_{T,water}$ after filtering sludge with excessive dosages of FE and in Figure 2.12 where the unbonded FE deteriorated the filtration performance, measured as an increase in R_T, upon contact with the membrane but only at high concentrations, which are unlikely to be present in AnMBRs dosed with FE.

The high $R_{T,water}$ measured after filtering sludge with excessive dosages of FE, suggests that the excess polymer caused irreversible fouling, which refers to the fouling that needs to

be removed by chemical cleaning. Irreversible fouling increases the frequency of chemical cleaning, decreasing the lifespan of the membranes. Therefore, it is crucial to avoid overdosing FE to the AnMBR.

Furthermore, Section 2.3.6 shows that a fraction of the unbonded Adifloc KD451 passed through the membrane and contaminated the permeate. Research had shown that polydiallyldimethylammonium chloride (polyDADMAC), which is the chemical compound in Adifloc KD451, can be a precursor of N-nitrosodimethylamine (NDMA), which is a suspected human carcinogen produced during chloramination or ozonation (Padhye et al., 2011; Tan et al., 2018). Therefore, determining the D_{opt} and D_{crit} for each sludge individually is crucial to avoid adverse effects on filterability and permeate contamination by unbonded FE.

2.4.3 Comparison of optimal and critical FE dosages determined with different response variables

The optimal and critical dosages determined in terms of filterability improvement (ΔR_{20} decrease) were compared with those obtained based on csCOD removal, sCOD removal and CST decrease. The CST showed the worst results: $D_{opt,CST}$ was most different from D_{opt}, and CST decrease proved unable to detect critical dosages ($D_{crit,CST}$). For most samples $D_{opt,CST}$ was higher than D_{opt}, probably because the FE increases scCOD which deteriorates dewaterability, here measured as CST, but does not have a direct effect on filterability. Thus, more FE is needed to compensate for the increased formation of scCOD increasing CST. Furthermore, during dead-end filtration, which is the principle of CST measurements, a sludge cake is deposited on top of the filter and can act as a first filtration step. At high FE dosages, exceeding saturation, this sludge cake might adsorb both the unbonded FE and the positively charged organic matter saturated with FE, and thereby protecting the filter. Such protective layer is not likely to be critical in crossflow filtration mode systems, such as in the AnDFCm installation and membrane bioreactors, due to the shearing effect of the cross flow. Therefore, high FE dosages caused a detrimental effect on filterability and not in CST. Consequently, required FE dosages which are assessed using CST measurements may lead to overdosing, with possible adverse effects in fouling and permeate quality.

Better results, compared to CST decrease, were obtained with sCOD removal as response variable: the difference with D_{opt} was lower and the adverse effect for determining $D_{crit,sCOD}$ was observed in several sludges. Nevertheless, the $D_{crit,sCOD}$ was only equal to D_{crit} in 3 samples (and differed in 5), and $D_{opt,sCOD}$ was generally higher than D_{opt}. This overestimation of the optimal required dosage might be attributed to possibility that part of the soluble material that is removed by the FE remains as colloidal material, which could have a similar adverse effect on filterability as the original soluble material. Similarly, Koseoglu et al. (2008) found that SMP removal, where SMP was measured as SMP-CH plus SMP-PR, and improvement in filtration performance do not always correlate.

The variable csCOD removal exhibited the best results in terms of optimal and critical dosages, likely because csCOD comprised both soluble and colloidal material, which

interacted with the FE and affect filterability. However, the difference between D_{opt} and $D_{opt,csCOD}$, which was on average 47%, remained significant.

Therefore, the use of crossflow filtration modes is recommended, such as the one applied in the AnDFCm installation, to determine the optimal dosage of FE. If such methods are not available, as is the case in most full-scale AnMBR and MBR plants, the use of csCOD removal as an alternative variable is recommended, instead of measurements based on dead-end filtration mode or based on soluble organic matter removal.

2.4.4 Guidelines for dosing FE in a continuous AnMBR

When using Adifloc KD451 as FE in a new sludge sample, D_{opt} can be estimated with the empirical models in Figure 2.11 by measuring any of the following sludge characteristics: $\Delta R_{20,(1.5,60)}$, CST, cCOD or SMP-CH. Furthermore, the estimated D_{opt}, further called $D_{opt,simulated}$, could be used to design an experiment to determine D_{opt} more precisely for each specific sludge. The following dosages should be used in the experiment: 0, 0.2, 0.4, 0.6, 0.8, 1, 1 ,1 ,1.5, 2 ,2.5 and 3-folds $D_{opt,simulated}$, where the triplicates at $D_{opt,simulated}$ are applied to estimate the variability of the test. After each dosage, the sludge filterability should be determined or, alternatively, the csCOD.

For the application of FE to a full-scale AnMBR, avoiding FE overdose is important since it can cause: i) reversible fouling increase caused by deteriorated sludge filterability, ii) irreversible fouling increase caused by the interaction of unbonded FE with the membrane, and iii) permeate contamination by part of the unbonded FE that can pass through the membrane. Thus, D_{crit} should be used as a limiting dosage, meaning that the concentration of FE in the reactor should be below D_{crit} during the entire operational period. Different dosing strategies can be applied, for example: continuously dosing FE to the reactor to sustain a concentration equal to D_{opt} while compensating for FE losses with the sludge wastage; or in a fed-batch mode, where the FE is dosed as a pulse to achieve D_{opt}, whenever the sludge has poor filterability, or high cCOD, CST or SMP-CH.

Moreover, the effectiveness of the FE can be largely affected by the degree of mixing during flocculation, which is governed by velocity gradients and time of flocculation (Bratby, 2016). Therefore, when applying FE to a full-scale AnMBR, special attention should be given to the mixing conditions.

The annual cost of dosing FE for fouling control in membrane bioreactors is subject to the volume of mixed liquor, price of FE, optimal required dosage, and frequency of dosage. As an example, the cost was estimated for the AnMBRs where the sludges with highest and lowest D_{opt} (i.e., LiqOFMSW and BWc-II) were collected. A dosing strategy where the frequency of dosage is adjusted to compensate for sludge wastage was assumed, resulting in a frequency of 1/SRT. The price of the Adifloc KD451 depends on the purchase amount and location. Nevertheless, the price used here was 6 € kg^{-1}, which was given by the supplier as a base price. The AnMBR where BWc-II was collected operated at 70 d SRT, 2.35 m^3 mixed liquor volume, and D_{opt} was 0.02 g L^{-1}, and thus the FE cost would be 1.5 € y^{-1} or 0.63 € m^{-3} y^{-1},

which is negligible. However, the AnMBR where LiqOFMSW was collected operated at 8 d SRT, 42 m^3 mixed liquor volume, and D_{opt} was 1.16 g L^{-1}, and thus the FE cost would be 13,337 € y^{-1} or 318 € m^{-3} y^{-1}. Therefore, the costs of FE dosing can vary considerable for different AnMBRs and should be considered in the economic evaluation of each treatment plant.

2.5 CONCLUSIONS

The main findings are summarised as follows:

- The optimal and critical dosages differed considerably between the various AnMBR sludge samples: D_{opt} ranged from 0.02 to 1.16 g L^{-1} and D_{crit} from 0.10 to 2.5 g L^{-1}.

- D_{opt} presented a linear relationship with CST ($R^2 = 0.975$), cCOD ($R^2 = 0.983$), and SMP-CH ($R^2 = 0.936$); and D_{opt} had an exponential relationship with ΔR_{20} ($R^2 = 0.950$), which is inversely related to sludge filterability. The empirical models derived can be potentially used to predict D_{opt} in new sludge samples, or as guidance for experimental design for D_{opt} determination.

- D_{opt} had non-significant correlations with supracolloidal COD (scCOD, above 1 μm), floc size, TP, TON, NH_4-N, SMP-PR and SMP-HS.

- Excessive FE dosages had an adverse effect on sludge filterability, increased irreversible fouling in the AnDFCm installation and possibly promoted permeate contamination by the unbonded FE. Therefore, overdosing must be avoided when applying FE to full-scale AnMBRs.

- The ΔR_{20}, measured following the AnDFCm protocol, was a reliable variable to determine the optimal and critical FE dosages. If the AnDFCm or an alternative crossflow filtration measurement is not available, csCOD removal could be used as an alternative variable to estimate the optimal FE dosage, since it provided better results than sCOD removal and CST decrease.

3

EFFECT OF FLUX ENHANCER DOSING ON METHANOGENIC ACTIVITY [*]

ABSTRACT

The application of cationic polymers to enhance membrane fluxes in anaerobic membrane bioreactors has been proposed by several authors. However, literature shows contradictory results on the influence of those chemicals on the biological activity. In this research, the effect of a cationic polymer on the production of methane from acetate by acetoclastic methanogens was studied. The effect of polymer concentration on the accumulated methane production (AMP) and the specific methanogenic activity (SMA) was assessed in batch tests. Batch tests results showed lower SMA values at higher concentrations of polymer and no effect on the final AMP. Different inhibition models were calibrated and compared to find the best fit and to hypothesize the prevailing inhibition mechanisms. The assessed inhibition models were: competitive (M1a), non-competitive (M2a), un-competitive (M3a), biocide-linear (M4a) and biocide-exponential (M5a). The parameters in the model related to the polymer characteristics were adjusted to fit the experimental data. M2a and M3a were the only models that fitted both experimental SMA and AMP. Although M1a and M4a adequately fitted the experimental SMA, M1a simulations slightly deviated from the experimental AMP, and M4a considerably underpredicted the AMP at concentrations of polymer above 0.23 gCOD L^{-1}. M5a did not adequately fit either experimental SMA and AMP results. Models a (M1a to M5a) were compared with models b (M1b to M5b), where moldes a consider the inhibition by the concentration of polymer in the bulk liquid, and models b consider the inhibition being caused by the total concentration of polymer in the reactor. Results showed that the difference between a and b models' simulations were negligible for all kinetic models considered (M1, M2, M3, M4 and M5). Therefore, the models that better predicted the experimental data were the non-competitive (M2a and M2b) and un-competitive (M3a and M3b) inhibition models, which are biostatic inhibition models. Consequently, the decreased methanogenic activity caused by polymer additions is presumably a reversible process.

3.1   INTRODUCTION

As shown in Chapter 1, cationic polymers composed of polydiallyldimethylammonium chloride (polyDADMAC), such as MPE50 and Adifloc KD451 and KD452, have been successfully used as flux enhancers (FE) in membrane bioreactors. However, scarce, and contradictory reports are published on the effect of these polymers on the microbial community. Consequently, prior to the application of a FE in an AnMBR, the possible effect on biomass activity needs to be studied.

Iversen et al. (2008) studied the biological inhibition of four polyDADMAC based FE on aerobic sludge. Their results showed no inhibitory effects on the endogenous oxygen uptake rate (OUR), however, two of the polymers had a 50-70% inhibitory effect on the exogenous OUR. In anaerobic digestion, to the authors' best knowledge, only two reports assessing the impact of polyDADMAC cationic polymers on the microbial activity are available. These reports showed no change on the COD removal (Díaz et al., 2014) and on the biogas production (Zhang et al., 2017) after polymer addition. However, in different research fields, polyDADMAC has been reported as an anti-microbial agent (Tran et al., 2017; Wang et al., 2017; Zhao et al., 2016) that can physically disrupt the prokaryotic cell wall.

The biochemical conversion processes of anaerobic digestion are hydrolysis, acidogenesis, acetogenesis and methanogenesis. These processes are carried out by complex microbial communities. Methanogenesis is carried out by acetoclastic and hydrogenotrophic methanogens. In a conventional mesophilic digester, the slow-growing acetoclastic methanogens are responsible for approximately 70 % of the methane produced, and are generally considered the most sensitive to the presence of inhibitors (Astals et al., 2015). Therefore, the classical approach to study the inhibitory effect of a specific compound on the biomass activity is by studying its effect on the acetoclastic methanogens.

Models are a powerful tool to reveal insight into the processes and interactions in a given system. The most common approach to model biological inhibition in anaerobic digestion, including weak acid/base, hydrogen, pH and cation inhibition, is the biostatic inhibition that considers the effect on growth and substrate uptake kinetics, and which is included in the Anaerobic Digestion Model No. 1 (Batstone et al., 2002). Furthermore, the disruption of the cells caused by a substance is considered a reactive irreversible toxicity and it is defined as biocidal inhibition (Batstone et al., 2002). Knowing the underlying inhibition mechanisms allows understanding of the long-term implications in a continuous reactor. For example, if the polymer exerts a biocidal effect on the microorganisms, then cell lysis will likely occur resulting in a release of soluble polymeric substances. The latter compounds are reported to deteriorate the sludge filterability (Krzeminski et al., 2012), leading to the need for more polymer addition to counteract the effect. A biocidal effect is irrecoverable, therefore continuously dosing of polymers can lead to severe biomass death and the need for re-inoculation. However, if the polymer will exert biostatic inhibition, it will not have a direct impact on filterability, and the effect on the biology will immediately recover when the polymer concentration decreases in the system. Additionally, depending on the dosage of the

polymer and the microbial growth rate, the overall microbial activity might be recovered by an increase in the biomass content.

This research assessed the effect of a cationic polymer concentration on the biological activity of anaerobic sludge. Modelling was used as a tool to study the inhibition mechanism of the polymer on the acetoclastic methanogenesis. This research compared biostatic and biocidal inhibition models based on their capacity to predict the dynamic methane production in batch experiments. The models were calibrated to fit the experimental data, namely the specific methanogenic activity (SMA) and the accumulated methane production (AMP) obtained in batch tests at different concentrations of polymer.

3.2   MATERIALS AND METHODS

3.2.1   Analytical methods

Chemical oxygen demand (COD) was measured using Hach Lange test kits, the total suspended solids (TSS) and volatile suspended solids (VSS) concentration following Standard Methods (APHA, 1999). Particle size distribution (PSD) was measured with a Microtrac Bluewave diffraction analyser (Malvern Instruments Ltd., UK), and reported as the 50th percentile of the volume-based particle size distribution, or median diameter, $D50$, which is the diameter at which 50 % of the sample's mass is comprised of particles with a diameter less than this value. All variables were measured in triplicate, immediately before and after the batch tests experiments. Reported results are averages of the triplicates.

3.2.2   Batch reactor tests

The effect of increasing polymer concentration on the SMA was assessed using Adifloc KD451 (Adipap, France). As explained in Chapter 2, the polymer was selected based on its capacity to significantly enhance the sludge filterability of municipal and industrial sludge samples when applied at very low concentrations, while no effect on pH was observed.

The inhibition tests were performed in 250 mL Schott glass bottles (200 mL filled with liquid and 50 mL as headspace) under mesophilic conditions using sodium acetate as carbon source. The inoculum was collected at an anaerobic digester of a near-by sewage treatment plant (Harnaschpolder, Den Hoorn, The Netherlands). The characteristics of the inoculum were as follows: 29.3 gTSS L^{-1}, 21.0 gVSS L^{-1} and $D50$ of 50 nm. The polymer was pre-mixed with the inoculum, in 1 L jars of a jar-test apparatus by mixing at 90 rpm during 30 minutes. Each SMA bottle was filled with 2.5 gCOD L^{-1} of sodium acetate, inoculum-polymer mixture, 0.6 mL L^{-1} micro and 6 mL L^{-1} macro nutrients solutions (Muñoz Sierra et al., 2018), 10 mM phosphate buffer solution at pH 7.0 (Spanjers and Vanrolleghem, 2016) and demineralised water, and then flushed the bottles with nitrogen gas for 1 min. The inoculum concentration in the bottles was 4 gVSS L^{-1} (corresponding to 6 gTSS L^{-1}), and the following concentrations of polymer were used: 0, 0.06, 0.11, 0.17, 0.23, 0.28, 0.34, 0.40 and 0.46 gCOD L^{-1}. The maximum concentration of polymer tested was approximately ten times the concentration of KD451 applied to a pilot AnMBR for fouling control in Chapter 4 (Odriozola et al., 2020), namely

0.05 gCOD L^{-1}. The SMA tests were performed in triplicate and placed the bottles inside an orbital shaker at 130 rpm with temperature control at 35 °C and over a 10-day period.

Methane production was measured using an "automated methane potential test system" (AMPTS from Bioprocess Control, Sweden). The AMPTS generates a digital pulse after a fixed volume of gas (~10 mL) has flowed through the gas cells, and measures the temperature and pressure in the water bath containing the gas cells. The AMPTS calculates and records the volume of gas under normal conditions (N-mL, 0 °C, 1 bar). The AMP, expressed in kgCOD kgVSS^{-1}, was calculated by dividing the data recorded in the AMPTS by the mass of VSS inoculated and by the stoichiometric methane production per kg COD, i.e., 3.5×10^5 N-mL kgCOD^{-1}. The SMA was calculated following Spanjers and Vanrolleghem (2016).

3.2.3   Mathematical models description

This research, compares the results from five different models, predicting the methane production from acetate in batch reactors in the presence of an inhibitory compound (the polymer). The first three models, M1a to M3a, describe the biostatic inhibition of acetate degradation by the concentration of inhibitor in the bulk liquid. The biostatic models assume that the inhibitor binds to the enzyme or the complex enzyme-substrate and does not allow the product formation. The kinetic models considered were as follows: competitive (M1a) where the inhibitor attaches to the enzyme in the same place as the substrate, non-competitive (M2a) where the inhibitor attaches to the enzyme in a different place changing the structure of the enzyme, and un-competitive (M3a) where the inhibitor attaches to the complex enzyme-substrate (Garcia Orozco, 2008). The fourth (M4a) and fifth (M5a) models describe the biocidal effect of the inhibitor concentration in the bulk liquid on the microbial decay. M4a was a linear model describing the decay rate change with the inhibitor concentration, and M5a an exponential model.

The model considered the following soluble components: total acetate (ac), methane gas (ch4), inorganic carbon (IC), carbon dioxide gas (co2), nitrogen gas (n2) and inhibitor (polymer) (I); and particulate components as follows: acetate degraders and adsorbed polymer. The model included the following processes: adsorption of the polymer (inhibitor) into the biomass, uptake of acetate by methanogens, liquid-gas transfer of nitrogen, carbon dioxide and methane, acid-base equilibria for inorganic carbon and biomass decay. The uptake of acetate was assumed to be performed by the dispersed biomass in the bulk liquid.

3.2.3.1   Polymer adsorption

Equilibrium conditions for polymer adsorption were assumed to be achieved after 30 minutes mixing the inoculum with the polymer, as shown by other authors for the absorption of polyDADMAC onto waste activated sludge (Zhao et al., 2016) and onto cellulosic fibres (Horvath et al., 2006). The Langmuir adsorption isotherm was used to describe the equilibrium conditions as follows:

$$X_{\text{fe},e} = q_{m,\text{ads}}\, c_{\text{X}} \frac{K_{L,\text{ads}}\, S_{\text{fe},e}}{1 + K_{L,\text{ads}}\, S_{\text{fe},e}}, \tag{3.1}$$

where $X_{\text{fe},e}$ (kgCOD m^{-3}) is the adsorbed polymer concentration after equilibrium, $q_{m,\text{ads}}$ (kgCOD kgTSS^{-1}) the maximum adsorption capacity corresponding to monolayer coverage, $K_{L,\text{ads}}$ (m^3 kgCOD^{-1}) the Langmuir affinity coefficient, c_{X} (kgTSS m^{-3}) the concentration of adsorbent (or total solid concentration) inside the reactor, $S_{\text{fe},e}$ (kgCOD m^{-3}) is the polymer concentration in the bulk liquid after equilibrium.

The mass balance of polymer inside the reactor was as follows:

$$S_{\text{fe},e} = \left(c_{\text{fe}} - X_{\text{fe},e} \right), \tag{3.2}$$

where c_{fe} (kgCOD m^{-3}) is the total concentration in the bulk liquid. Therefore, the equilibrium concentrations $S_{\text{fe},e}$ and $X_{\text{fe},e}$ were estimated by combining Equations (3.1) and (3.2). c_{fe} and c_{X} were determined experimentally and $q_{m,\text{ads}}$ and $K_{L,\text{ads}}$ were estimated by fitting the model to the experimental data. The concentration of polymer in the bulk liquid (S_{fe}, kgCOD m^{-3}) was assumed as equal to the equilibrium concentrations, namely $S_{\text{fe}} = S_{\text{fe},e}$.

3.2.3.2 Kinetic processes

The models included the conversion of acetate to methane and inorganic carbon by acetoclastic methanogenic archaea, and the biomass decay processes in the kinetic models, as summarised in Table 3.1. Models M1a, M2a and M3a considered the biostatic inhibition (competitive, non-competitive, and un-competitive) of the acetate degradation rate

Table 3.1. Description of kinetic process used in the evaluated models.

Model	Inhibition type	Uptake of acetate (ρ_1) [a]	Decay of acetate degraders (ρ_5) [b]
M0	No inhibition	$k_{m,\text{ac}} \dfrac{S_{\text{ac}}}{K_{s.\text{ac}} + S_{\text{ac}}} X_{\text{ac}}$	$b_{\text{ac}} X_{\text{ac}}$
M1a	Biostatic, competitive	$k_{m,\text{ac}} \dfrac{S_{\text{ac}}}{K_{s.\text{ac}}\left(1 + \dfrac{S_{\text{fe}}}{K_{I,\text{fe},\text{ac}}}\right) + S_{\text{ac}}} X_{\text{ac}}$	$b_{\text{ac}} X_{\text{ac}}$
M2a	Biostatic, non-competitive	$k_{m,\text{ac}} \dfrac{S_{\text{ac}}}{(K_{s.\text{ac}} + S_{\text{ac}})\left(1 + \dfrac{S_{\text{fe}}}{K_{I,\text{fe},\text{ac}}}\right)} X_{\text{ac}}$	$b_{\text{ac}} X_{\text{ac}}$
M3a	Biostatic, un-competitive	$k_{m,\text{ac}} \dfrac{S_{\text{ac}}}{K_{s.\text{ac}} + S_{\text{ac}}\left(1 + \dfrac{S_{\text{fe}}}{K_{I,\text{fe},\text{ac}}}\right)} X_{\text{ac}}$	$b_{\text{ac}} X_{\text{ac}}$
M4a	Biocide, linear	$k_{m,\text{ac}} \dfrac{S_{\text{ac}}}{K_{s.\text{ac}} + S_{\text{ac}}} X_{\text{ac}}$	$\dfrac{S_{\text{fe}}}{K_{I,\text{fe},\text{ac}}} b_{\text{ac}} X_{\text{ac}}$
M5a	Biocide, exponential	$k_{m,\text{ac}} \dfrac{S_{\text{ac}}}{K_{s.\text{ac}} + S_{\text{ac}}} X_{\text{ac}}$	$10^{S_{\text{fe}}/K_{I,\text{fe},\text{ac}}} b_{\text{ac}} X_{\text{ac}}$

[a] S_{ac} (kgCOD m^{-3}) is the total acetate concentration, X_{ac} (kgCOD m^{-3}) the concentration of acetate degraders, $K_{S,\text{ac}}$ the Monod half saturation constant (kgCOD m^{-3}), $k_{m,\text{ac}}$ (d^{-1}) the Monod maximum specific uptake rate and $K_{I,\text{fe},\text{ac}}$ (kgCOD m^{-3}) the concentration of inhibitor giving 50% inhibition.
[b] b_{ac} (d^{-1}) is the first order decay rate for acetate degraders.

(ρ_1, kgCOD m^{-3} d^{-1}) by the concentration of inhibitor in the bulk liquid.

The biomass decay rate (ρ_5, kgCOD m^3 d^{-1}) was described by first order kinetic in all models. Additionally, models M4a and M5a described the biocidal inhibition by relating the concentration of inhibitor with the first order decay rate. Therefore, as shown in Table 3.1, a simple linear model between the first order decay rate and the concentration of inhibitor in the bulk liquid S_{fe} was proposed in M4a, and an exponential term in M5a. The latter was analogous to the microbial inactivation kinetics by chemical compounds (Casolari, 1988).

3.2.3.3   Liquid-gas mass transfer

The specific liquid-gas mass transfer rates for methane (ρ_2, kgCOD m^{-3} d^{-1}), carbon dioxide (ρ_3 kmol m^{-3} d^{-1}) and nitrogen (ρ_4, kmol m^{-3} d^{-1}) was calculated as follows (Batstone et al., 2002):

$$\rho_2 = k_L a\left(S_{ch4} - K_{H,ch4}p_{ch4,G}\right), \tag{3.3}$$

$$\rho_3 = k_L a\left(S_{co2} - K_{H,co2}p_{co2,G}\right), \tag{3.4}$$

$$\rho_4 = k_L a\left(S_{n2} - K_{H,n2}p_{n2,G}\right), \tag{3.5}$$

where $k_L a$ is the dynamic gas–liquid transfer coefficient, $K_{H,n2}$ (kmol m^{-3} bar^{-1}), $K_{H,co2}$ (kmol m^{-3} bar^{-1}) and $K_{H,ch4}$ (kgCOD m^{-3} bar^{-1}) are the Henry's law coefficients, $p_{ch4,G}$, $p_{co2,G}$ and $p_{n2,G}$ (bar) the partial pressures of gases, and S_{ch4} (kgCOD m^{-3}), S_{co2} (kmol m^{-3}) and S_{n2} (kmol m^{-3}) the concentrations of methane, carbon dioxide and nitrogen in the liquid phase, respectively. The same $k_L a$ value was assumed for all gaseous components.

The gas phase composition was calculated assuming that gas-liquid equilibrium was reached for all gaseous components in accordance with Henry's law, and thus, $p_{i,G}$ was as follows:

$$p_{i,G} = p_G \frac{S_i/K_{H,i}}{\sum_i S_i/K_{H,i}}, \tag{3.6}$$

where p_G (bar) is the total gas pressure. S_{co2} was calculated from the concentration of inorganic carbon in the liquid phase (S_{IC}) using the acid-base equilibrium equation for inorganic carbon ($CO_{2,ac}/HCO_3^-$):

$$S_{co2} = S_{IC}\left(1 - \frac{K_{a,co2}}{K_{a,co2} + 10^{-pH}}\right), \tag{3.7}$$

where $K_{a,co2}$ is the acid-base equilibrium coefficient and pH (-) is the pH of the solution. Constant pH was assumed because a pH-buffer was added into the bottles in the batch-tests experiments.

Table 3.2. Stoichiometric coefficients ($v_{i,j}$).

Component $i \rightarrow$	1	2	3	4	5
j Process $\downarrow$	S_{ac}	S_{ch4}	S_{IC}	S_{n2}	X_{ac}
1 Uptake of acetate	-1	$1 - Y_{ac}$ [a]	$-\sum_{i\neq3} i_{C,i} v_{i,1}$ [b]		Y_{ac}
2 Liquid-gas transfer of ch4		-1			
3 Liquid-gas transfer of co2			-1		
4 Liquid-gas transfer of n2				-1	
5 Decay of X_{ac}					-1

[a] Y_{ac} is the yield coefficient.
[b] $i_{C,i}$ (kmole kgCOD[-1]) is the carbon content of component i.

3.2.3.4   Mass balances

The accumulated methane production, AMP (kgCOD kgVSS[-1]), was calculated with Equation (3.8) using the specific liquid-gas mass transfer rate for methane (ρ_2).

$$\frac{d\text{AMP}}{dt} = \frac{\rho_2}{t_{conv} c_{VSS}(0)}, \tag{3.8}$$

where $c_{VSS}(0)$ (kgVSS m[-3]) is the initial concentration of VSS in the reactor, experimentally determined, and t_{conv} (86,400 s d^{-1}) is a time conversion factor.

The mass balance equation for component i in the bulk liquid was as follows:

$$\frac{dc_i}{dt} = \frac{1}{t_{conv}} \sum_{j=[1-6]} v_{ij} \rho_j, \tag{3.9}$$

where c_i is the concentration of the soluble (S_i) or particulate (X_i) component i in the bulk liquid, t (s) the time, ρ_j (kgCOD m[-3] d^{-1} or kmol m[-3] d^{-1}) the rate of process j, and v_{ij} the stoichiometric coefficients of component i on process j, presented in Table 3.2.

3.2.4   Model implementation

3.2.4.1   Computational implementation

All computations were performed in Matlab® R2018a, and the built-in ordinary differential equations (ODE) solver *ode15s* was used to integrate the ordinary differential equations system. The initial conditions and parameters of the experiments needed for model resolution were: p_G, pH, c_X, c_{fe}, $S_i(0)$ and $X_{ac}(0)$.

    The modelled SMA (kgCOD kgVSS[-1] d^{-1}) was the maximum methane production rate calculated with Equation (3.10). The goodness of fit was assessed with the residual sum of squares in Equation (3.11), where $y_{e,i}$ is the experimental observation i and $y_{m,i}$ the corresponding model prediction.

$$\text{SMA prediction} = \max\left(\frac{\Delta \text{AMPT}}{\Delta t} t_{\text{conv}}\right), \tag{3.10}$$

$$\text{RSS}_k = \sum_i \left(y_{e,k,i} - y_{m,k,i}\right)^2, \tag{3.11}$$

where RSS_j is the residual sum of squares for the output variable k, $y_{e,k,i}$ the ith experimental value of the output variable k, $y_{m,k,i}$ the ith predicted value of the output variable k. RSS_{SMA} and RSS_{AMP} were calculated using SMA and AMP as the output variables, respectively. RSS_k was calculated for each polymer concentrations c_{fe} tested (shown in Section 3.2.2) by solving the models (M1a to M5a) individually for each c_{fe}.

As described in Section 3.2.2, the AMPTS generates a digital pulse after a fixed volume of gas has flowed through the gas cells; consequently, the time at which each data point was measured was different for each bottle, even for the triplicates of the same SMA test. Therefore, to estimate the RSS_{AMP}, the models needed to predict the methane production at the exact experimental time instant. To achieve this, the models were solved with a sufficiently small time-step (that is $\Delta t = 1000$ s), and the AMP prediction values were linearly interpolated at the exact experimental time instants for each SMA bottle.

3.2.4.2 Nominal values of parameters

The values of most parameters were obtained from literature and are summarised in Table 3.3. The values of parameters related to the polymer characteristics, namely $q_{m,\text{ads}}$, $K_{L,\text{ads}}$ and $K_{I,\text{fe,ac}}$, were selected based on specific assumptions, and the most influential ones estimated to fit the experimental data.

There are several commercial cationic polymers with similar compositions but each of them with different charges and molecular weights. To the authors' best knowledge, there were no specific values for the parameters related to the polymer characteristics reported in literature. The Langmuir adsorption model parameters, $q_{m,\text{ads}}$ and $K_{L,\text{ads}}$, are conditioned to the type of adsorbent and adsorbate. The values of $q_{m,\text{ads}}$ and $K_{L,\text{ads}}$ were estimated using experimental data for the adsorption of polyDADMAC onto different adsorbents from previous reports. The estimated values of $q_{m,\text{ads}}$ were 0.032, 0.450 and 0.035 kg kg^{-1} for adsorption onto silica gel of 6 nm pore size (Hubbe et al., 2011), activated sludge (Zhao et al., 2016) and cellulosic fibers (Horvath et al., 2006), respectively, and those for $K_{L,\text{ads}}$ were 2.0, 7.6 and 1960 m^3 kg^{-1}, respectively. $q_{m,\text{ads}}$ and $K_{L,\text{ads}}$ results were highly dispersed; therefore, the values proposed for adsorption onto activated sludge were used as an initial guess.

The $K_{I,\text{fe,ac}}$ was assumed equal to the S_{fe} calculated using Equations (3.1) and (3.2) by substituting for the values for $q_{m,\text{ads}}$ and $K_{L,\text{ads}}$ from activated sludge and for the value for c_{fe} equal to the experimental concentration of polymer at which the SMA value was 50% smaller than the SMA without polymer. Therefore, the $K_{I,\text{fe,ac}}$ was 0.014 kgCOD m^{-3}.

Table 3.3. Nominal parameter values at 35 °C

Component $i \rightarrow$		1	2	3	4	5	Reference
Parameter	Units	S_{ac}	S_{ch4}	S_{IC}	S_{n2}	X_{ac}	
$K_{H,i}$	kmol m^{-3} bar^{-1} [a]		0.108	0.027[b]	5.5×10^{-4}		Sander (2015)
$K_{a,co2}$	×10^{-7}			4.94			Batstone et al. (2002)
$i_{C,i}$	kmol kgCOD^{-1}	0.0313	0.0156		0	0.0313	Batstone et al. (2002)
$k_{m,ac}$	d^{-1}	8					Batstone et al. (2002)
$K_{s,ac}$	kgCOD m^{-3}	0.15					Batstone et al. (2002)
Y_{ac}	-	0.05					Batstone et al. (2002)
b_{ac}	d^{-1}	0.1					Batstone et al. (2004)
$k_{L}a$	d^{-1}		178	178[b]	178		Metcalf et al. (2002)

[a] $K_{H,i}$ units for methane: kgCOD m^{-3} bar^{-1}
[b] for CO_2

3.2.4.3 Initial conditions and experimental parameters

The solids concentration inside the reactor, c_X, was the initial concentration of TSS in the reactor, which was experimentally determined. c_{fe} was the concentration of polymer added to the SMA bottles.

The total gas pressure p_G was assumed constant and equal to the mean experimentally measured pressure, which was 1.01 bar. The ratio between partial pressure and total gas pressure at time zero was introduced as an initial condition in each model, and the soluble components concentrations ($S_{ch4}(0)$, $S_{IC}(0)$ and $S_{co2}(0)$) was estimated using Equations (3.6) and (3.7), assuming that the system starts at gas-liquid equilibrium. Since the bottles were initially flushed with nitrogen gas, the initial $p_{i,G}/p_G$ were 0, 0 and 1 for methane, carbon dioxide and nitrogen, respectively.

The initial concentration of acetate degraders was calculated as follows $X_{ac}(0) = i_{Xac,VSS,0} \, VSS(0)$, where $i_{Xac,VSS,0}$ (kgCOD kgVSS^{-1}) is the initial content of acetate degraders in the VSS. $i_{Xac,VSS,0}$ to was estimated fit the model M0 to the experimental AMP when no polymer was added to the SMA bottles. Here, the adsorption model was not included since no polymer was present in the reactor. The initial guess for $i_{Xac,VSS,0}$ was estimated with Equation (3.12) which assumes that all the methane produced from acetate left the bottles and $S_{ac} \gg K_{s,ac}$.

$$i_{Xac,VSS,0} = \frac{SMA}{k_{m,ac}(1 - Y_{ac})}. \tag{3.12}$$

3.2.5 Model calibration

As described in Sections 3.2.4, the parameters $q_{m,ads}$, $K_{L,ads}$, $K_{I,fe,ac}$ and $i_{Xac,VSS,0}$ were estimated to fit the experimental data. The AMP without polymer addition was used as the

model output (y) to estimate $i_{\text{Xac,VSS,0}}$; and for the remaining parameters, SMA for different total polymer concentrations c_{fe} was used as model output.

The model calibration procedure was as follows: (1) identification of a parameter subset (θ) containing only the influential parameters based on the standardised regression coefficients (β_i) from the linear regression model built using the MC simulations; (2) definition of the boundaries for the parameters based on the behaviour of the RSS with respect to uncertain model parameters; (3) parameter estimation (PE) with θ and evaluation of the quality of the estimators; (4) (when needed) identification of the θ that can be reliably estimated from the given experimental data, by modification of the model structure, identifiability analysis or both; and (5) PE with new θ and model. Additionally, model prediction uncertainty analysis (UA) was performed using the MC method with the parameter uncertainty obtained from PE.

3.2.5.1 Monte Carlo and linear regression

Global sensitivity analysis was performed to identify the effect of the parameters on the model output. The analysis was implemented based on linear regression models built from MC simulations. Input uncertainty was a uniform distribution with 99.9 % variability, 99.9 % instead of 100 % was used to avoid null values; zero values for some parameters would cause numerical problems, for example, if $K_{H,i}$ is zero (for any i) then there is a division by zero in Equation (3.6). Consequently, the minimum and maximum value of the distributions were $0.001\theta°$ and $1.999\theta°$, respectively, where $\theta°$ is the initial/nominal parameter vector. The notation $\theta \sim U(0.001\theta°, 1.999\theta°)$ is further used in this document. The θ included all parameters in each model. Latin hypercube sampling (Iman and Conover, 1982) with 500 samples (Sin et al., 2009) was used; β_i was computed using the mean-centred sigma-scaling (Helton and Davis, 2003), and β_i was estimated using the constrained linear least square minimisation function *lsqlin* with -1 and 1 as lower and upper bound, respectively. The estimation of β_i requires a scalar input; therefore, β_i was computed individually for each c_{fe} in M1a to M5a and for each time (t) in M0. The coefficient of determination (R^2) was applied to evaluate the quality of the regression model, that is: the model was considered sufficiently linear when $R^2 \geq 0.7$ (Sin et al., 2011). The mean, minimum and maximum R^2 were calculated with the β_i obtained for each parameter in the range of c_{fe} or t were $R^2 \geq 0.7$. The parameters with a mean abs(β_i) ≥ 0.10 were considered influential (Sin et al., 2011).

3.2.5.2 Parameter estimation

The behaviour of RSS_k with the parameter values in the subset θ varying in a wide range was studied to research the existence of local minimums and determine the boundaries and initial guess for the PE. MC simulations were performed with Latin hypercube sampling with 500 samples, using a uniform distribution with 99.9% variability for the parameter subset defined in Section 3.2.5.1, and RSS_k was calculated for each simulation. The range of the parameters based on the behaviour of RSS_k with respect to uncertain model parameters.

Subsequently, the parameters were estimated using the non-linear least squares solver *lsqnonlin* in Matlab® R2018a, with the trust region reflective algorithm and applying the lower and upper bounds previously identified. The input function for the *lsqnonlin* solver was an array with the residuals, where Residuals $= y_e - y_m$. Afterwards, the solver found the optimal value ($\hat{\theta}$) that minimises the sum of squares of the input function, consequently, it minimises the RSS_k in Equation (3.11). The standard deviation (σ_θ) and 95 % confidence interval (CI) of the estimators were calculated in accordance to Sin and Gernaey (2016).

The normality of the residuals needs to be evaluated since it is an underlying hypothesis for the implementation of least square method for parameter estimation. The distribution of the residuals was assessed graphically and Shapiro-Wilk test was applied to test the hypothesis of normality using the function *swtest* © (BenSaïda, 2009). When the null hypothesis of normality was rejected at a significance level 0.05, the parameters were estimated using bootstrap method, implemented as described in Sin and Gernaey (2016).

The quality of the estimators was assessed based on the uncertainty of the estimators and the pairwise linear correlation between the parameters and considered a good estimation when the relative error, namely $\sigma_\theta/\hat{\theta}$, was below 10 % and a poor estimation when it was above 50 % (Sin and Gernaey, 2016). Additionally, if the correlation coefficient between any pair of parameters was above 0.5, then the PE problem was considered ill conditioned. Then, identifiability analysis was used to select the parameter subset that can be identified uniquely from the experimental data. The collinearity index of the parameter subset k (γ^k) were calculated in accordance with Sin and Gernaey (2016). The threshold to select a uniquely parameter subset is reported between 5 and 15 (Sin and Gernaey, 2016); the parameter subset with γ^k below 10 was selected for the PE.

3.2.6 Modelling scenarios

Two different scenarios were studied. The first scenario (models a: M1a, M2a, M3a, M4a and M5a), considered that the inhibition is caused by the polymer (inhibitor) present in the bulk liquid. As described in Section 3.2.3.1, when a polymer is added to a sludge sample a fraction of the polymer is adsorbed onto the sludge and a fraction remains in the bulk liquid. The concentration of polymer in the bulk liquid after the adsorption reaching equilibrium is $S_{\text{fe},e}$, which was considered as the concentration of polymer responsible for the inhibition in the first scenario, namely $S_{\text{fe}} = S_{\text{fe},e}$.

In the second scenario (models b: M1b, M2b, M3b, M4b and M5b), the inhibition was assumed to be caused by the total amount of polymer added to the SMA bottles. The inhibition is caused by both the fraction of polymer adsorbed onto the sludge and the fraction remaining in the bulk liquid. Consequently, the adsorption model was not needed to describe the inhibition and it was removed from the model structure in models b and S_{fe} was set equal to the total concentration of polymer added to the SMA bottles (c_{fe}), namely $S_{\text{fe}} = c_{\text{fe}}$.

3.2.7 Model prediction uncertainty

The most suitable models were selected based on the model capacity to predict the experimental data (goodness of fit), which was assessed graphically and with the RSS_{SMA} and RSS_{AMP}. For the selected models, the model prediction uncertainty caused by the uncertainty in the estimators was studied using the MC method with Latin hypercube sampling. The uncertainty in the parameters was defined using the results from the PE, as a normal distribution with mean $\hat{\theta}$ and standard deviation σ_θ, namely $\theta \sim N(\hat{\theta}, \sigma_\theta{}^2)$, and represented the uncertainty propagation graphically.

3.3 RESULTS

3.3.1 Experimental results

Figure 3.1 shows that the polymer presented an inhibitory effect on the SMA. The SMA inhibition were 24, 27, 40, 44, 53, 54, 65, and 69 % at 0.06, 0.11, 0.17, 0.23, 0.29, 0.34, 0.40, and 0.46 gCOD L^{-1} of polymer concentration, respectively. A 50 % SMA inhibition was obtained at 0.27 gCOD L^{-1} of polymer, the value was obtained by linear interpolation between the experimental results at 0.23 and 0.29 gCOD L^{-1}.

The one-way ANOVA test was used to study if there is a difference in the final AMP between batch tests performed at different polymer concentrations. The batch tests performed at concentrations of 0.40 and 0.46 g L^{-1} were not considered in the test because the methane was still being produced when the experiment were stopped (Odriozola et al., 2019). The F-test was 2.10 with a probability value (p) of 0.114; thus, p was above the α-level of 0.05. Therefore, the difference between the AMP final values is not statistically significant. Therefore, no significant effect of the polymer was observed in the AMP achieved at the end of the tests.
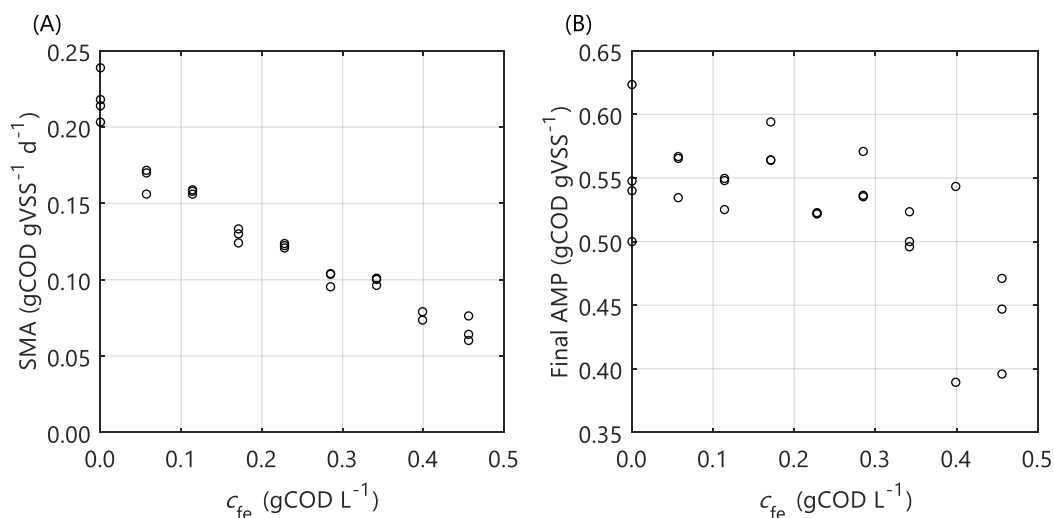
Figure 3.1. Specific methanogenic activity (SMA) and final accumulated methane production (AMP) obtained from batch test experiments using different concentrations of polymer (c_{fe}).

3.3.2 Modelling AMP without polymer addition (M0)

The linear regression models built using the MC simulations of M0 resulted in R^2 above 0.7 between 2 and 79 hours. The mean, minimum and maximum β_i values for the range with $R^2 > 0.70$ are presented in Table 3.4. The RSS_{AMP} was calculated for each MC simulation and the results are presented in Figure 3.2A-C. The behaviour of the RSS_{AMP} with $i_{\text{Xac,VSS,0}}$ for uncertainty only in $i_{\text{Xac,VSS,0}}$ is shown in Figure 3.2C.

The initial guess for $i_{\text{Xac,VSS,0}}$ estimation was 0.02, and the lower and upper bounds were 0.01 and 0.03, respectively. The PE results were as follows: 0.0198 kgCOD kgVSS^{-1} optimal value ($\hat{\theta}$), 1.9×10^{-4} standard deviation (σ_θ), 3.8×10^{-4} 95 % confidence interval (CI) and relative error $\sigma_\theta/\hat{\theta}$ of 1 %. PE varying the initial guess was performed and the same results were obtained. The null hypothesis of normality was rejected at a significance level 0.05 using the Shapiro-Wilky test with a p of 2×10^{-7}. The optimal value obtained using Bootstrap was equal
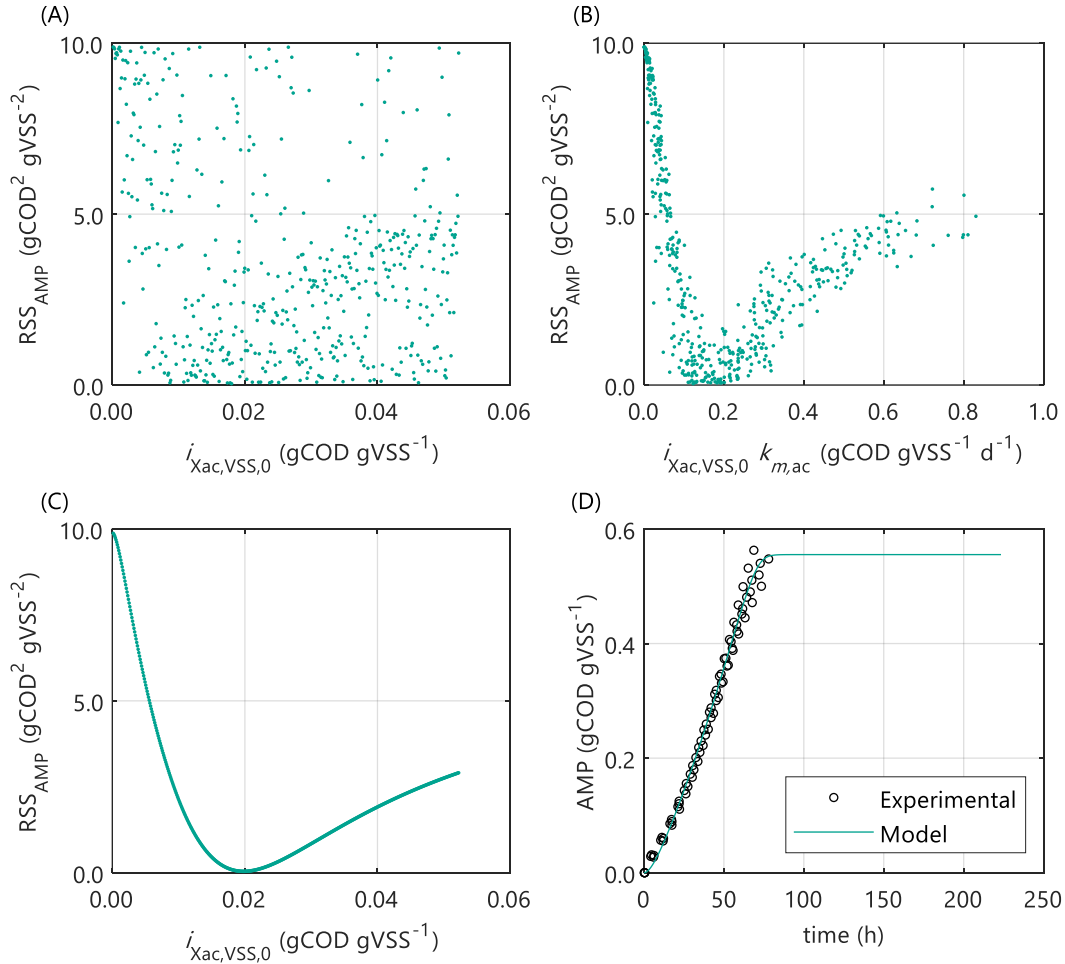
Figure 3.2. GSA and simulation results for batch model in the absence of polymer (M0). Correlations between the residual sum of squares for AMP as output variable (RSS_{AMP}) and uncertain parameters with $\theta \sim U(0.001\theta°, 1.999\theta°)$: (A) correlation of RSS_{AMP} with $i_{\text{Xac,VSS,0}}$ and (B) RSS_{AMP} with $i_{\text{Xac,VSS,0}} \, k_{m,\text{ac}}$, using MC simulations performed with uncertainty in all parameters; (C) correlation of RSS_{AMP} with $i_{\text{Xac,VSS,0}}$ using MC simulations performed with uncertainty only in the $i_{\text{Xac,VSS,0}}$. (D) Experimental and simulated AMP performed with the optimum value obtained from parameter estimation, namely $i_{\text{Xac,VSS,0}}$ = 0.0198 kgCOD kgVSS^{-1}.

Table 3.4. Sensitivity analysis results for M0: mean, minimum and maximum of the standardised regression coefficients (β_i) of linear models with $R^2 > 0.7$ of AMP as a function of time.

Parameter	M0 (mean R^2 = 0.81)		
	mean	minimum	maximum
$i_{Xac,VSS,0}$	0.52	0.43	0.60
$k_{m,ac}$	0.71	0.56	0.75
$K_{S,ac}$	-0.05	-0.06	0.01
Y_{ac}	0.05	-0.05	0.07
b_{ac}	-0.03	-0.05	-0.02
$k_L a$	0.03	0.02	0.10
$K_{H,ch4}$	-0.09	-0.30	-0.07
$K_{H,co2}$	0.00	-0.02	0.02
$K_{H,n2}$	0.03	0.02	0.04
$K_{a,co2}$	0.02	-0.04	0.06
$i_{C,Xac}$	-0.01	-0.02	0.01

to the one obtained with least squares method, namely 0.0198 kgCOD kgVSS^{-1}. Figure 3.2D displays the experimental AMP and the model predictions at the optimal values obtained with estimated parameters. Although the experimental data was collected over a 10-day period, not enough biogas to generate a new pulse in the AMPTS was produced in the bottles after 80 hours, the volume of the AMPTS cells was ~10 mL.

3.3.3   Modelling methanogenesis inhibition by polymer

The results from the linear models performed with the MC simulations with parameter uncertainty $\theta \sim U(0.001\theta°, 1.999\theta°)$ are summarised in Table 3.5. From the parameters present in the initial subsets θ, the ones with mean $\beta_i \geq 0.10$ were: $\{K_{I,fe,ac}, K_{L,ads}, q_{m,ads}\}$ in M1a to M4a and $\{K_{I,fe,ac}, K_{L,ads}\}$ in M5a.

The results from the PE in M1a to M5a are shown in Table 3.6. Figure 3.3 shows the comparison between the best-fit results of the five models and the experimental data. The correlation coefficients and collinearity index for all the possible combinations of parameters are summarised in Table 3.7. Based on the results, a new parameter subset was defined containing only $K_{I,fe,ac}$, and the values of $K_{L,ads}$ and $q_{m,ads}$ were set at their nominal values (defined in Section 3.2.4.2). Figure 3.4A and Figure 3.4B display the behaviour of the RSS$_{SMA}$ with $K_{I,fe,ac} \sim U(0.001\theta°, 1.999\theta°)$ for models a (M1a, M2a, M3a, M4a and M5a) and b (M1b, M2b, M3b, M4b and M5b), respectively. The results from the PE estimation are summarised in Table 3.8. Figure 3.5 compare between the best-fit results of the models with the experimental data.

Table 3.5. Sensitivity analysis results for M1a to M5a: mean of the standardised regression coefficients (β_i) and mean R^2 ($\overline{R^2}$) of linear models with $R^2 > 0.7$ of the SMA with different concentrations of polymer.

Parameter↓		M1a	M2a	M3a	M4a	M5a
	$\overline{R^2} \rightarrow$	0.80	0.80	0.80	0.83	0.80
$K_{I,\text{fe,ac}}$		0.17	0.19	0.20	0.18	0.15
$K_{L,\text{ads}}$		0.12	0.15	0.17	0.11	0.10
$q_{m,\text{ads}}$		0.13	0.17	0.20	0.16	0.08
$k_{m,\text{ac}}$		0.76	0.78	0.69	0.77	0.79
$K_{s,\text{ac}}$		-0.24	-0.14	-0.14	-0.15	-0.13
Y_{ac}		0.28	0.30	0.30	0.31	0.32
b_{ac}		-0.09	-0.11	-0.08	-0.12	-0.12
$k_L a$		0.02	0.03	0.00	-0.02	-0.01
$K_{H,\text{ch4}}$		-0.01	0.00	-0.01	-0.05	-0.02
$K_{H,\text{co2}}$		0.01	-0.01	0.00	-0.01	0.01
$K_{H,\text{n2}}$		-0.01	0.01	-0.02	-0.03	0.02
$K_{a,\text{co2}}$		0.00	-0.01	0.05	-0.01	-0.02
$i_{\text{C,Xac}}$		0.03	0.02	0.01	0.01	0.00

Table 3.6. Parameter estimation results for the SMA inhibition for M1a to M4a with parameter subset $\theta = \{K_{I,\text{fe,ac}}, K_{L,\text{ads}}, q_{m,\text{ads}}\}$ and M5a with $\theta = \{K_{I,\text{fe,ac}}, K_{L,\text{ads}}\}$: optimal values ($\hat{\theta}$), standard deviation ($\sigma_\theta$) and 95% confidence intervals (CI); and sum of square errors for SMA (RSS_{SMA}) and AMP (RSS_{AMP}) of the models.

Parameter	Model	$\hat{\theta}$	σ_θ	95% CI	$\sigma_\theta/\hat{\theta} \times 100$	RSS_{SMA}	RSS_{AMP}
$K_{I,\text{fe,ac}}$	1	0.001	0.029	0.060	2529 %	0.0021	0.67
	2	0.014	0.031	0.065	231 %	0.0027	0.48
	3	0.014	0.021	0.044	152 %	0.0027	0.57
	4	0.005	0.076	0.158	1400 %	0.0122	7.26
	5	0.016	0.112	0.231	689 %	0.0101	7.81
$K_{L,\text{ads}}$	1	11.1	12.2	24.0	110 %		
	2	152.6	1025.6	2014.9	672 %		
	3	61.9	383.6	753.7	620 %		
	4	2.0	4.2	8.3	211 %		
	5	6.4	22.6	44.4	351 %		
$q_{m,\text{ads}}$	1	0.17	0.05	0.10	29 %		
	2	0.24	0.03	0.06	13 %		
	3	0.24	0.04	0.08	18 %		
	4	0.45	0.47	0.92	104 %		

Table 3.7. Correlation and collinearity index for M1a to M5a for different parameter combinations k.

Subset $k \rightarrow$ Model↓	$\{K_{I,\text{fe,ac}}, K_{L,\text{ads}}\}$	$\{K_{I,\text{fe,ac}}, q_{m,\text{ads}}\}$	$\{K_{L,\text{ads}}, q_{m,\text{ads}}\}$	$\{K_{I,\text{fe,ac}}, K_{L,\text{ads}}, q_{m,\text{ads}}\}$
Collinearity index (γ^k)				
1	93	15	13	1828
2	135	18	16	2143
3	134	19	16	2139
4	116	19	16	2131
5	283	36	32	7631
Correlation coefficient				
1	-0.9999	-0.99	0.98	NA
2	-0.92	0.35	-0.70	NA
3	-0.74	-0.98	0.60	NA
4	-0.98	-0.94	0.87	NA
5	-0.99	-0.64	0.55	NA

Table 3.8. Parameter estimation results for the SMA inhibition process with parameter subset θ for M1a to M5a (with $S_{\text{fe}} = S_{\text{fe},e}$) and M1b to M5b (with $S_{\text{fe}} = c_{\text{fe}}$).

Model	θ	$\hat{\theta}$	σ_θ	95% CI	$\sigma_\theta/\hat{\theta} \times 100$	RSS_{SMA}	RSS_{AMP}
1	$\{K_{I,\text{fe,ac}}\}$	0.0017	4.4×10^{-5}	0.0001	2.6 %	0.0024	0.73
1b	$\{K_{I,\text{fe,ac}}\}$	0.0338	$9.8\ 10^{-4}$	0.0019	2.9 %	0.0030	0.83
2	$\{K_{I,\text{fe,ac}}\}$	0.0168	$3.6 10^{-4}$	0.0007	2.2 %	0.0025	0.53
2b	$\{K_{I,\text{fe,ac}}\}$	0.3341	7.5×10^{-3}	0.0149	2.2 %	0.0028	0.63
3	$\{K_{I,\text{fe,ac}}\}$	0.0143	3.1×10^{-4}	0.0006	2.1 %	0.0026	0.61
3b	$\{K_{I,\text{fe,ac}}\}$	0.2840	6.1×10^{-3}	0.0122	2.2 %	0.0028	0.69
4	$\{K_{I,\text{fe,ac}}\}$	0.0016	7.3×10^{-5}	0.0001	4.5 %	0.0106	6.91
4b	$\{K_{I,\text{fe,ac}}\}$	0.0321	1.5×10^{-3}	0.0030	4.7 %	0.0109	6.60
5	$\{K_{I,\text{fe,ac}}\}$	0.0165	4.4×10^{-4}	0.0009	2.7 %	0.0090	7.69
5b	$\{K_{I,\text{fe,ac}}\}$	0.3234	7.9×10^{-3}	0.0158	2.4 %	0.0076	7.36
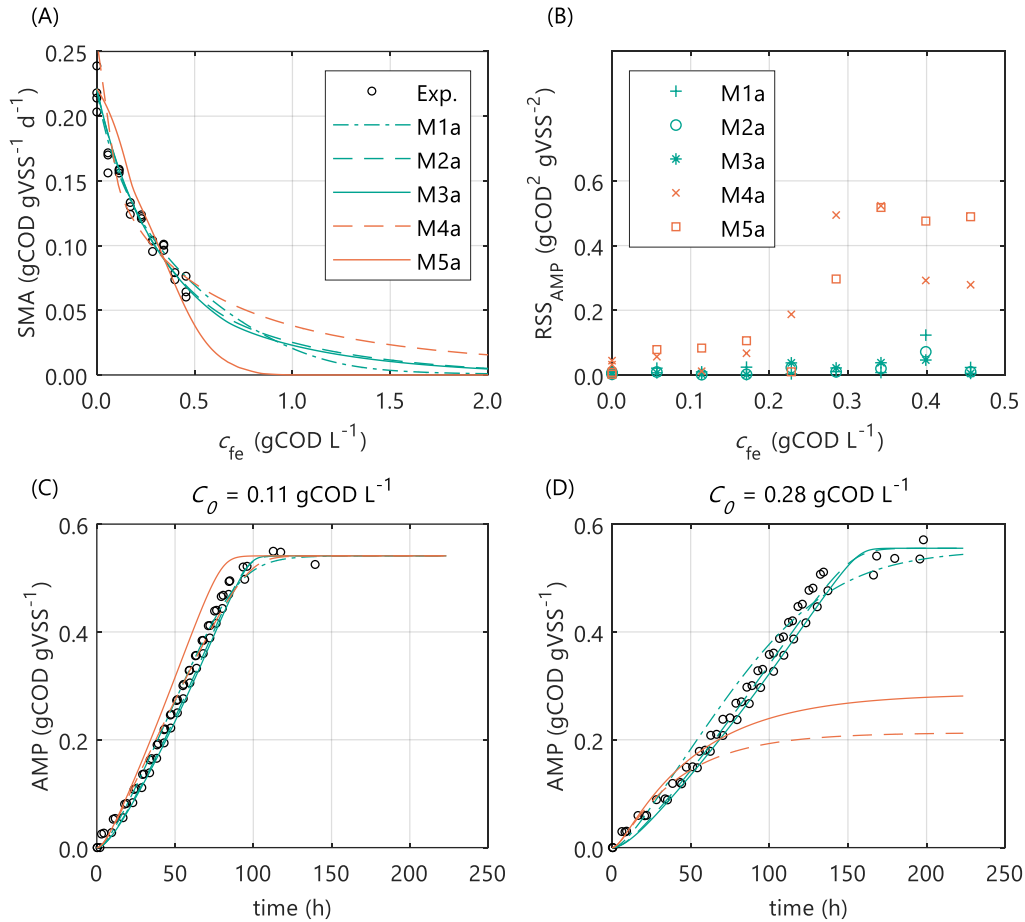
Figure 3.3. Simulations with parameter estimation results for the SMA inhibition for M1a to M4a with parameter subset $\theta = \{K_{I,\text{fe,ac}}, K_{L,\text{ads}}, q_{m,\text{ads}}\}$ and M5a with parameter subset $\theta = \{K_{I,\text{fe,ac}}, K_{L,\text{ads}}\}$: (A) experimental and simulated SMA, (B) RSS_{AMP}, (C) experimental and simulated AMP at 0.11 gCOD L^{-1} of polymer and (D) experimental and simulated AMP at 0.28 gCOD L^{-1}.
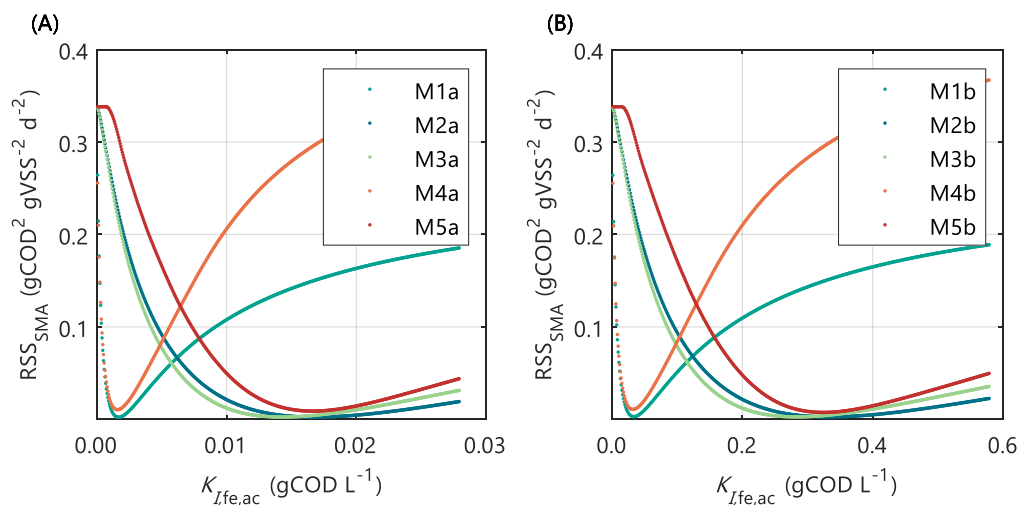
Figure 3.4. Correlations between the RSS_{SMA} and uncertain parameters using MC simulations with uncertainty $\theta \sim U(0.001\theta°, 1.999\theta°)$ only in $K_I K_{I,\text{fe,ac}}$. Results using (A) M1a to M5a and (B) M1b to M5b.
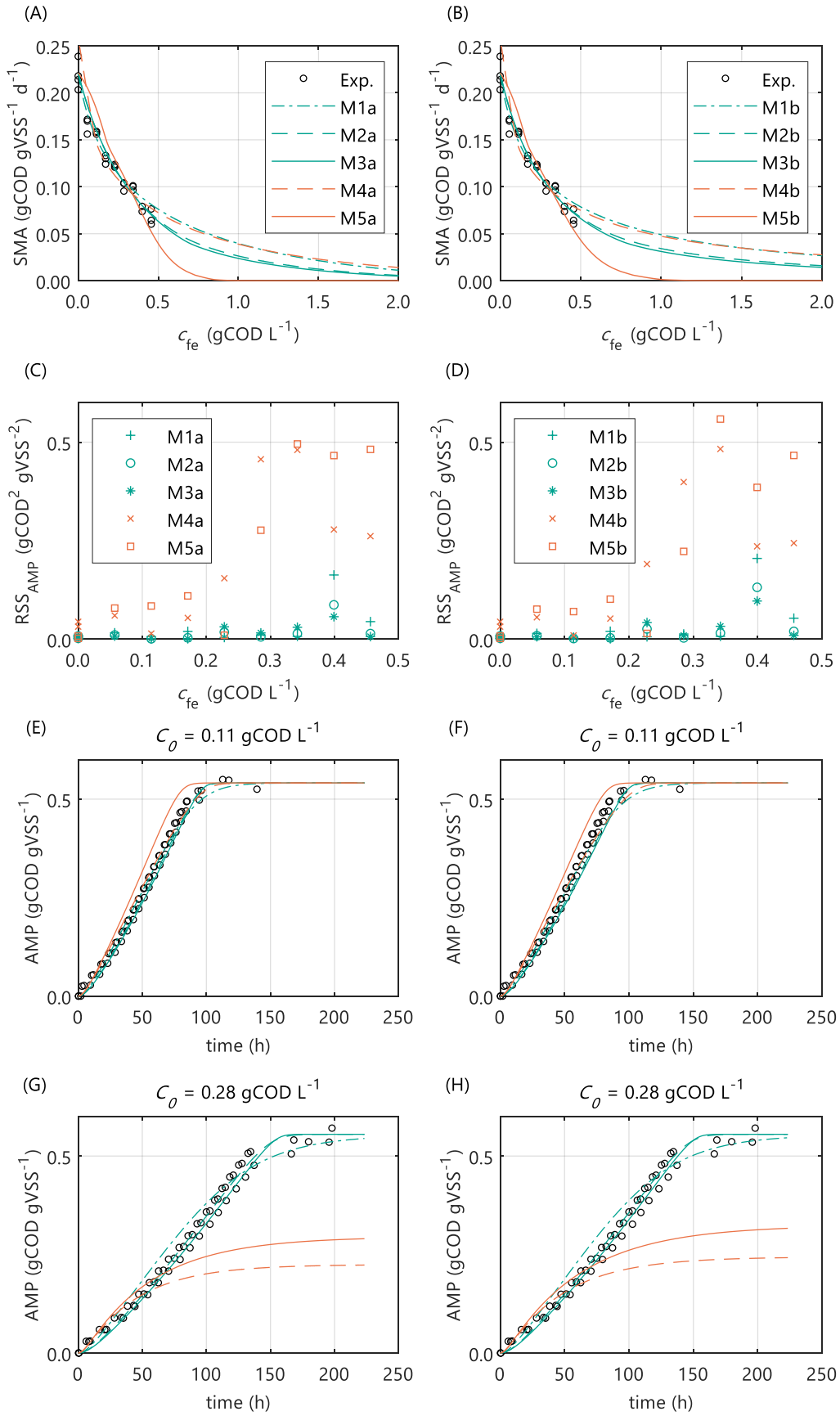
Figure 3.5. Simulations with parameter estimation results for the SMA inhibition, with parameter subset $\theta = \{K_{I,\mathrm{fe,ac}}\}$: experimental and simulated SMA for (A) M1a to M5a and (B) M1b to M5b, $\mathrm{RSS_{AMP}}$ for (C) M1a to M5a and (D) M1b to M5b, experimental and simulated AMP at 0.11 gCOD L^{-1} of polymer for (E) M1a to M5a and (F) M1b to M5b and experimental and simulated AMP at 0.28 gCOD L^{-1} for (G) M1a to M5a and (H) M1b to M5b.

3.3.4 Model prediction uncertainty

The uncertainty in the M2a and M2b predictions caused by the uncertainty in $K_{I,\mathrm{fe,ac}}$, with $\theta \sim N(\hat{\theta}, \sigma_\theta{}^2)$, are compared with the experimental data in Figure 3.6.
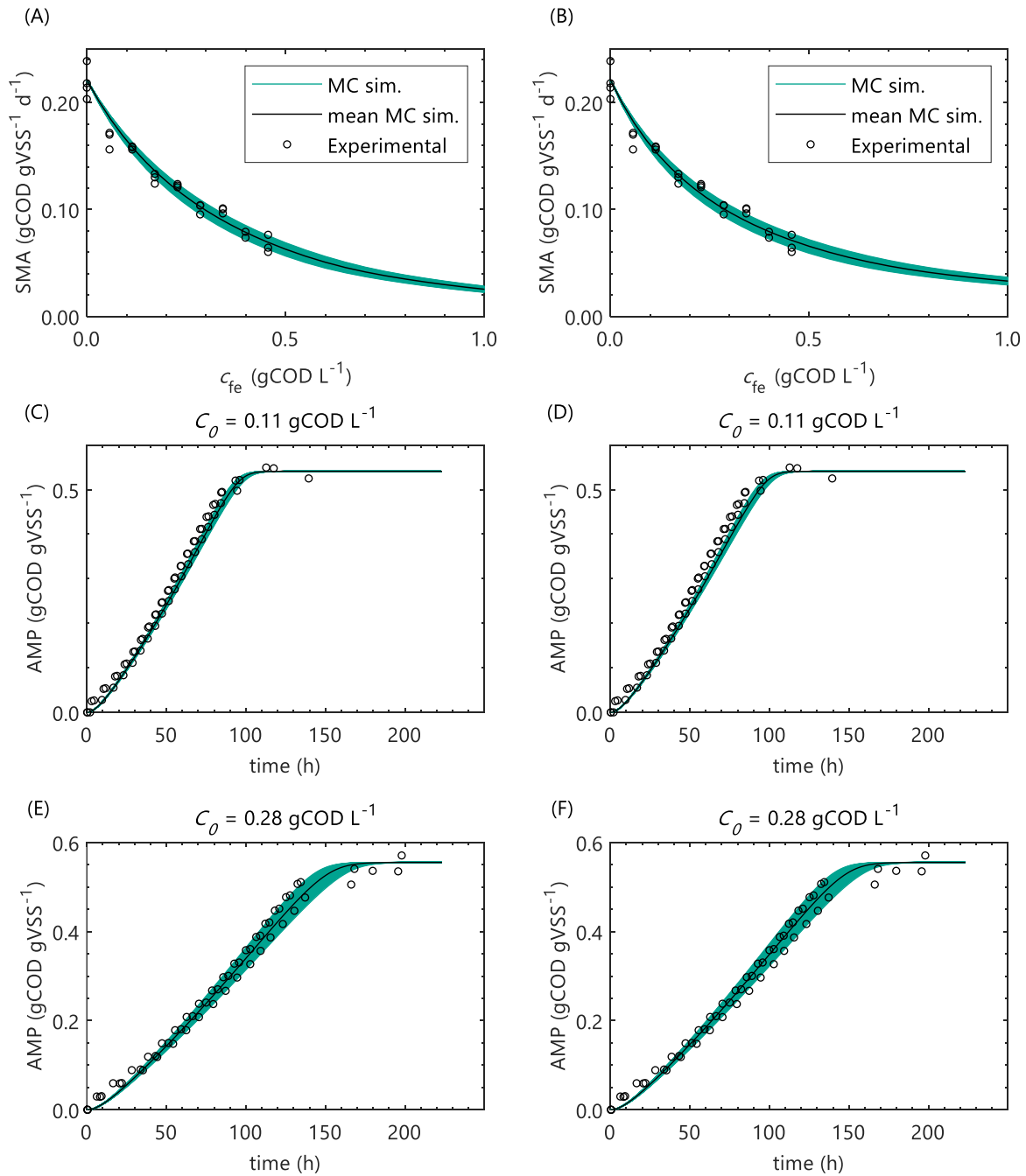
Figure 3.6. Monte Carlo simulations with uncertainty $\theta \sim N(\hat{\theta}, \sigma_\theta{}^2)$ and subset $\theta = \{K_{I,\mathrm{fe,ac}}\}$ for M2a and M2b. Experimental data, MC simulations (MC sim.) and mean MC simulations for: SMA for (A) M2a and (B) M2b, AMP at 0.11 gCOD L^{-1} of polymer for (C) M2a and (D) M2b and AMP at 0.28 gCOD L^{-1} for (E) M2a and (F) M2b

3.4   DISCUSSION

This research assessed the inhibition of SMA and AMP caused by cationic polymer addition to anaerobic sludge. The results showed that the polymer inhibited the SMA but did not influence the final AMP achieved.

   To the authors best knowledge, two reports are available that use Adipap polymers for fouling control in membrane bioreactors. Significant fouling decrease was achieved by adding 0.05 gCOD L⁻¹ of Adifloc KD451 to a pilot AnMBR (Odriozola et al., 2020) and 70 mg L⁻¹ (0.077 gCOD L⁻¹) of Adifloc KD452 to a pilot MBR (Iversen et al., 2009b). These concentrations are considerably below the 50 % SMA inhibition concentration, namely 0.27 gCOD L⁻¹. However, 24 and 27 % SMA inhibitions was obtained at 0.06 and 0.11 gCOD L⁻¹ of polymer concentration, respectively. Consequently, in a continuous AnMBR reactor, adding polymer might decrease the methane production rate, increase the acetate concentration, and decrease the organic matter removal when organic loading rates remain at the same level. The effect would start immediately after addition and it can be compensated by a decrease in the organic volumetric loading rate. Additionally, if the inhibition is reversible (biostatic) the overall conversion capacity of the bioreactor could be recovered by an increase in the biomass content. If the methanogenic microorganisms are in excess when adding the polymer to the AnMBR then the methane production, acetate concentration and organic matter removal might not be affected by small dosages of polymer.

3.4.1   Validity of nominal parameter values

The results from the global sensitivity analysis showed that a 99.9% variability on the gas-liquid transfer ($k_L a$, $K_{H,\mathrm{i}}$) and carbon content ($i_{C,\mathrm{Xac}}$) parameters had a negligible effect ($\beta_i <$ 0.10) on the SMA inhibition (Table 3.5) and on the AMP without polymer (Table 3.4). Consequently, for those parameters, the selection of the exact (true) parameter values was not crucial, and thus, the nominal parameter values from literature were used, presented in Section 3.2.4.2.

   Contrarily, the kinetic and stoichiometric parameters related to acetate degradation and biomass decay presented a significant effect on the model output. Particularly, the Monod maximum specific uptake rate $k_{m,\mathrm{ac}}$ was the most influential parameter in all considered models. The $i_{\mathrm{Xac,VSS,0}}$ was highly correlated with $k_{m,\mathrm{ac}}$, meaning that the optimal value for $i_{\mathrm{Xac,VSS,0}}$ is determined by the value of $k_{m,\mathrm{ac}}$ used (Figure 3.2B). Although, good model fits could be obtained with different combinations of $i_{\mathrm{Xac,VSS,0}}$ and $k_{m,\mathrm{ac}}$, this was outside the scope of this research. This chapter focused on modelling the SMA inhibition and comparing different inhibition models and not on the acetoclastic methanogenesis kinetics itself. Therefore, widely applied values for $k_{m,\mathrm{ac}}$, Y_{ac}, $K_{s,\mathrm{ac}}$ and b_{ac} were used, presented in Section 3.2.4.2.

3.4.2 Modelling AMP without polymer addition (M0)

The initial content of acetate degraders in the VSS ($i_{\mathrm{Xac,VSS,0}}$) showed a significant effect on the AMP model output (Table 3.4): 28 % ($\beta_i^2 \times 100$) of the output variability could be explained by the variability on $i_{\mathrm{Xac,VSS,0}}$. Therefore, $i_{\mathrm{Xac,VSS,0}}$ could be estimated to predict the methane production obtained experimentally. Results did not show a clear pattern of the behaviour of $\mathrm{RSS_{AMP}}$ with $i_{\mathrm{Xac,VSS,0}}$ with uncertainty in all parameters (Figure 3.2A). However, the $\mathrm{RSS_{AMP}}$ with $i_{\mathrm{Xac,VSS,0}}$ with uncertainty only in $i_{\mathrm{Xac,VSS,0}}$ (Figure 3.2C) showed a unique (global) minimum value at $i_{\mathrm{Xac,VSS,0}}$ around 0.02 gCOD gVSS^{-1}. Parameter estimation results showed that the quality of the estimator is good since the relative error was small and the model predictions fit the experimental data (Figure 3.2D).

3.4.3 Ill conditions SMA inhibition models

The influential unknown parameters, for PE, were identified using the results from the sensitivity analysis (Table 3.5). The subsets identified, with a threshold value of the mean β_i ≥ 0.10, are as follows: $\theta = \left\{K_{I,\mathrm{fe,ac}}, K_{L,\mathrm{ads}}, q_{m,\mathrm{ads}}\right\}$ in M1a to M4a and $\theta = \left\{K_{I,\mathrm{fe,ac}}, K_{L,\mathrm{ads}}\right\}$ in M5a.

The SMA simulations, at the optimal values obtained with PE, showed a good fit to the experimental data for the biostatic models (M1a, M2a and M3a) and the biocide-lineal model (M4a), as observed in Figure 3.3A. Accordingly, Figure 3.3C shows a good fit to the experimental AMP with M1a to M4a for a polymer concentration of 0.11 gCOD L^{-1}. However, for higher concentrations (Figure 3.3D) the M1a simulations slightly deviated from the experimental data, and the M4a simulations were considerably below the experimental data after 50 hours. The previous deviations are reflected by the $\mathrm{RSS_{AMP}}$ in Figure 3.3B. The accelerated biomass decay predicted in M4a caused a noticeably low concentration of microorganisms resulting in an extremely low methane production rate after 50 hours. Similarly, in M5a the AMP was underpredicted for high concentrations of polymer. Additionally, the biocide-exponential model (M5a) overpredicted and underpredicted the SMA at polymer concentrations c_{fe} below and above 0.3 gCOD L^{-1}, respectively.

Models a (M1a to M5a) considered the inhibition caused by the concentration of inhibitor in the bulk liquid S_{fe}, where S_{fe} as determined by the Langmuir isotherm adsorption model. Consequently, as expected, high pairwise correlation coefficients were obtained for all parameter combinations (Table 3.7). As a result, the relative errors obtained with PE were considerably high (Table 3.6). Therefore, although some of the models were able to predict the experimental data, the quality of the estimators was considered poor, namely the relative error was above 50 % (Sin and Gernaey, 2016).

From the collinearity indexes presented in Table 3.7, no combination of parameters could be used to achieve unique estimators from the experimental data, namely $\gamma^k > 10$ for all k. Therefore, a new PE was performed with a subset containing only one parameter. The inhibition coefficient $K_{I,\mathrm{fe,ac}}$ was selected for the PE because it presented a slightly higher effect on the simulated SMA (higher mean β_i, Table 3.5) compared to $q_{m,\mathrm{ads}}$ and $K_{L,\mathrm{ads}}$, and

the nominal $q_{m,\text{ads}}$ and $K_{L,\text{ads}}$ values were used. The simulation results with the optimal values obtained with PE (Figure 3.5, on the left) were very similar to the ones obtained at the optimal values from PE using $\theta = \{K_{I,\text{fe,ac}}, K_{L,\text{ads}}, q_{m,\text{ads}}\}$ (or $\theta = \{K_{I,\text{fe,ac}}, K_{L,\text{ads}}\}$ in M5a), Figure 3.3.

Additionally, a different inhibition approach was considered, where the inhibition was assumed to be caused by the total amount of polymer added to the SMA bottles, namely $S_{\text{fe}} = c_{\text{fe}}$. Therefore, the models b (M1b to M5b) were defined and compared with the original models a (M1a to M5a), where $S_{\text{fe}} = S_{\text{fe},e}$. In Figure 3.5 the simulation results for models a and b are displayed on the left and right graphs, respectively; the results are further discussed in Section 3.4.5.

3.4.4 Biostatic and biocidal SMA inhibition models

As discussed in Section 3.4.3, biocide models (M4a and M5a) underpredicted the experimental methane production at high polymer concentrations due to the accelerated biomass decay. Therefore, the biocide models M4a and M5a were not appropriate models to describe the inhibition of methanogenesis by the polymer. Contrarily, predictions with biostatic models (M1a, M2a and M3a) showed satisfactory fit to the experimental SMA and AMP (Figure 3.5). Therefore, it is likely that the polymer inhibition on the SMA is a reversible process (biostatic inhibition), instead of a reactive irreversible toxicity (biocidal inhibition). Consequently, in a continuous reactor, the inhibitory effect will be eliminated when the polymer concentration decreases. Additionally, based on the dosage of the polymer and the microbial growth rate, the overall microbial activity could be recovered by an increase in the biomass content.

Figure 3.5A shows that the simulations using the un-competitive (M3) and non-competitive (M2) inhibition models successfully fitted all the experimental SMA, while the competitive inhibition model (M1a) simulations slightly deviate from the SMA at the higher concentrations of polymer tested, namely 0.40 and 0.46 gCOD L^{-1}. Additionally, Figure 3.5G shows that the M5a overpredicted the AMP between 40 and 100 hours at 0.28 gCOD L^{-1}, while the M2a and M3a model simulations fitted the AMP remarkably well.

Therefore, although the M1a fitted the experimental data significantly well, the process was better described by M2a and M3a. Additionally, as a competitive inhibition model (M1) considers that the inhibitor binds to the same place as the substrate (Garcia Orozco, 2008), and because the polymer (inhibitor) and the acetate (substrate) are different molecules, the latter result was not unexpected.

The difference between the un-competitive and non-competitive models could only be observed in the AMP predictions at high concentration of polymer (**Figure 3.5**G). Based on the RSS presented in Table 3.8 the M2a seems to predict slightly better the experimental data. However, the difference was not considered sufficient to select one model over the other and both models were considered appropriate to describe the methanogenesis inhibition process.

3.4.5 Bulk liquid vs total polymer concentration inhibition

The behaviour of the RSS_{SMA} with $K_{I,\text{fe,ac}}$ revealed a unique (global) minimum for all models. Figure 3.4 displays the RSS_{SMA} as a function of $K_{I,\text{fe,ac}}$ for models with inhibition by the concentrations of polymer in the bulk liquid (Figure 3.4A) and by the total amount of polymer added to the system (Figure 3.4B). Results presented a similar behaviour for both inhibition models, however, the $K_{I,\text{fe,ac}}$ values that minimise the RSS_{SMA} are 20 times larger for the models with $S_{\text{fe}} = c_{\text{fe}}$, which corresponds to the ratio between the c_{fe} and $S_{\text{fe},e}$ obtained by applying the adsorption model with the nominal parameter values and experimental conditions.

Parameter estimation results showed that the models a (with $S_{\text{fe}} = S_{\text{fe},e}$) presented a slightly smaller RSS_{SMA} and RSS_{AMP} for each biostatic inhibition model considered with respect to the models b (with $S_{\text{fe}} = c_{\text{fe}}$), as shown in Table 3.8. However, the difference in the simulations with the models a (left plots) and models b (right plots) was negligible for each kinetic inhibition model used, as observed in Figure 3.5. The similarity between models a and b was due to the approximately linear relationship between c_{fe} and $S_{\text{fe},e}$ obtained using the polymer adsorption model (results not shown). This approximately linear behaviour was obtained using the experimental conditions tested (c_{fe} and c_{X}) and with the Langmuir parameter values obtained by parameter estimation ($K_{L,\text{ads}}$ and $q_{m,\text{ads}}$).

Therefore, both modelling approaches (bulk liquid or total polymer concentration inhibition) were considered appropriate to describe the methanogenesis inhibition caused by the polymer in the range of concentrations studied. Additionally, the uncertainty in the estimated parameters did not cause a considerable uncertainty on the model prediction for M2a and M2b, Figure 3.6.

3.5   CONCLUSIONS

The cationic polymer showed a negative effect on the biological activity of the anaerobic sludge. A 50 % SMA inhibition was obtained at 0.27 gCOD L^{-1} of polymer whereas no significant effect on the final AMP was observed.

Different models were presented and calibrated to fit the experimental data. The Monte Carlo method was successfully applied to study the sensitivity of the model outputs to the parameters and identify the parameter subsets for parameter estimation. The collinearity indexes and pairwise correlation coefficients showed that the parameters $K_{L,ads}$, $q_{m,ads}$ and $K_{I,fe,ac}$ are all highly correlated. Based on the Monte Carlo results and collinearity indexes the parameter subsets selected for parameter estimation was $\theta = \{K_{I,fe,ac}\}$ for all the models considered.

An alternative modelling approach was studied, that is models M1b to M5b, where the inhibition was caused by the total amount of polymer added to the reactor ($S_{fe} = c_{fe}$), and not by the concentration that remains in the bulk liquid after adsorption ($S_{fe} = S_{fe,e}$, M1a to M5a). The difference in the models' simulations with both approaches, namely $S_{fe} = S_{fe,e}$ and $S_{fe} = c_{fe}$, was negligible for each kinetic inhibition model used.

The simulated AMP values obtained with the biocide models, namely M4a and M5a, were below the experimental AMP at high concentrations of polymer, which was caused by a rapid decay of the acetate degraders simulated. The only models that adequately fitted the experimental SMA and AMP were the non-competitive (M2a and M2b) and un-competitive (M3a and M3b) inhibition models. Therefore, it is likely that the polymer inhibition on the SMA is reversible, instead of toxic and irreversible.

The concentrations of polymer (inhibitor) in the bulk liquid giving 50 % inhibition were 0.014 and 0.017 gCOD L^{-1} for M2a and M3a, respectively; and the total concentrations of inhibitor in the reactor giving 50 % inhibition were 0.334 and 0.284 gCOD L^{-1} for M2b and M3b, respectively.

The simulated SMA obtained with M1a and M4a adequately fitted the experimental SMA. However, the simulated AMP was below the experimental AMP for those models. Therefore, it is crucial to analyse both outputs, SMA and AMP, during model calibration.

4

FOULING MITIGATION BY FLUX ENHANCER DOSING INTO A PILOT-SCALE ANAEROBIC MEMBRANE BIOREACTOR FED WITH BLACKWATER [*]

ABSTRACT

Cationic polymers have proven to be suitable flux enhancers (FEs) in large-scale aerobic membrane bioreactors (MBRs), whereas in anaerobic membrane bioreactors (AnMBRs) research is scarce, and so far, only done at lab-scale. Results from MBRs cannot be directly translated to AnMBRs because the extent and nature of membrane fouling under anaerobic and aerobic conditions are different. This research focused on the long-term effect of dosing the cationic polymer Adifloc KD451 to a pilot AnMBR, fed with source-separated domestic blackwater. A single dosage of Adifloc KD451 at 50 mg L^{-1} significantly enhanced the filtration performance in the AnMBR, revealed by a decrease in both fouling rate and total filtration resistance. Nevertheless, FE addition had an immediate negative effect on the specific methanogenic activity (SMA), but this was a reversible process that had no adverse effect on permeate quality or chemical oxygen demand (COD) removal in the AnMBR. Moreover, the FE had a long-term positive effect on AnMBR filtration performance and sludge filterability. These findings indicate that dosing Adifloc KD451 is a suitable strategy for fouling mitigation in AnMBRs because it led to a long-term improvement in filtration performance, while having no significant adverse effects on permeate quality or COD removal.

4.1   INTRODUCTION

Researchers have emphasized the need for more research on flux enhancer (FE) dosing to membrane bioreactors in long-term and large-scale trials (Iversen, 2010; Iversen et al., 2009b; Koseoglu et al., 2008; Kulesha et al., 2018; Ozgun et al., 2013). As presented in Chapter 1, cationic polymers have proven to be suitable FE in large-scale MBRs, whereas in AnMBRs research is scarce, and so far, only done at lab-scale. Results from MBRs cannot be directly translated to AnMBRs because the extent and nature of membrane fouling under anaerobic and aerobic conditions are different.

Various researchers suggested the possible application of the online measurement of sludge filtration characteristics for automatic FE dosing control in membrane bioreactors (Brauns et al., 2011; Iversen, 2010). However, this has not been further studied or tested.

The aim of this research is to analyse the long-term effect of dosing the cationic polymer Adifloc KD451 to a pilot AnMBR fed with source-separated domestic blackwater. This work studies the effects on permeate quality, sludge characteristics, biological activity (i.e., COD removal and specific methanogenic activity, SMA) and AnMBR filtration performance (i.e., fouling rate and filtration resistance). Additionally, the applicability of in-situ measurements of sludge filterability as an input variable in a feedback control tool for FE dosage was determined.

4.2   MATERIALS AND METHODS

4.2.1   Pilot AnMBR plant description

The pilot AnMBR plant was located at the Business Centre Porto do Molle, Nigrán, Pontevedra, Spain. The reactor was fed with blackwater collected in segregated pipes in the main office building, where approximately 200 persons worked. The toilets in the building were conventional gravity flush toilets (3.0–4.5 L of water per flush).

Figure 4.1 shows the scheme of the pilot plant, including the AnDFCm installation connected to the AnMBR. The blackwater was stored in a 3–4 m^3 septic tank followed by a 1 m^3 equalisation tank. The AnMBR was composed of a 2.8 m^3 anaerobic stirred reactor connected to a 1.0 m^3 membrane tank. The membrane tank had one submerged ultrafiltration flat-sheet membrane module (Martins System, Berlin, Germany), made of polyethersulfone, with a 6.25 m^2 surface area and a 35 nm nominal pore size.

The pilot plant was coupled with a supervisory control and data acquisition (SCADA) system and several sensors. The following variables were measured and recorded once per minute by the SCADA: TMP, permeate flow rate, operational phase (i.e., filtration, relaxation or stand-by), accumulated permeate volume, motor frequency of B-1, P-2 and P-4, gas pressure in the headspace in the anaerobic reactor, liquid levels in the equalization tank, anaerobic reactor and membrane tank, and the temperature, pH and redox potential of the sludge in the anaerobic reactor. The lower detection limit of the biogas discharge flowmeter was usually higher than the flow, and thus the biogas discharge flow could not be detected accurately by
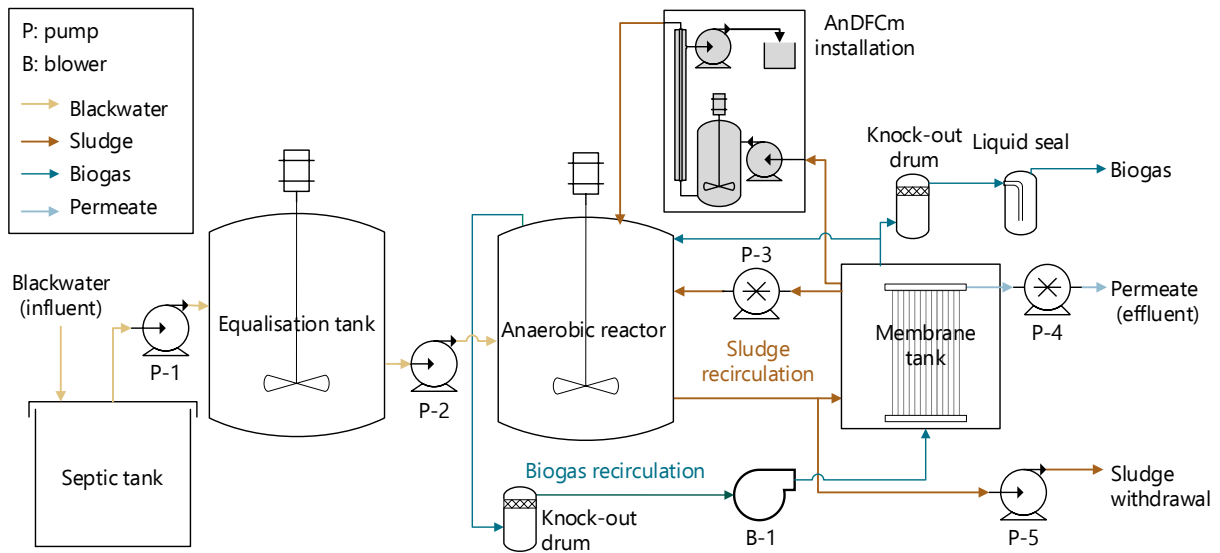
Figure 4.1. Scheme of the pilot AnMBR plant including the AnDFCm installation connected in bypass for in situ sludge filterability measurements.

the instrument. Moreover, the biogas recirculation flow rate (Q_G) was not measured online but manually recorded by the operators with a rotameter placed after B-1. These data were used to derive and calibrate an empirical model to calculate the specific gas demand (SGD_m), based on the liquid level in the membrane tank (H_{MT}) and the motor frequency of the blower (v_B); further details are given in Section 2.2.

Blackwater was homogenised in the equalization tank and pumped into the anaerobic reactor. The sludge was continuously recirculated through the anaerobic reactor and membrane tank, where the permeate was extracted under suction with a peristaltic pump (P-4). The blower and all pumps operated at constant motor input frequencies fixed by the operator. Under normal operational conditions, the membrane presented filtration and relaxation cycles of 300 and 90 s, respectively. The total liquid volume was ~2.8 m³ (membrane tank + anaerobic reactor), the hydraulic retention time (HRT) was ~2 days, the periodic sludge wastage was negligible (only sampling) and the reactor operated at room temperature. The headspace biogas was sparged below the membrane module at a Q_G of 6–8 Nm³ h⁻¹, which corresponds with an SGD_m of 0.96–1.28 Nm³ h⁻¹ m⁻², to provide suitable shear on the membrane surface.

4.2.2 Specific gas demand (SGD_m) model

In addition to the use of FE, research has proven that biogas or air sparging substantially affects fouling (Judd and Judd, 2011; Meng et al., 2017). Therefore, in this research, quantifying SGD_m continuously was important to account for the effect of biogas sparging on fouling, both before and after FE addition. SGD_m is calculated by dividing Q_G by the membrane surface area (A_m, m²). However, as above-mentioned, Q_G was not measured online, but manually recorded by the operators with a rotameter placed after the blower B-1.

The experimental SGD_m, which was calculated with the manually recorded Q_G, was used to derive and calibrate an empirical model to calculate SGD_m continuously, as in Equation (4.1, with the following online monitored variables: H_{MT} and v_B.

$$SGD_m = \frac{\gamma_0 + \gamma_1\,H_{MT} + \gamma_2\,v_B}{A_m}, \tag{4.1}$$

where γ_0 (Nm³ h⁻¹), γ_1 (Nm³ h⁻¹ m⁻¹), and γ_2 (Nm³ h⁻¹ Hz⁻¹) are the model parameters. These parameters were estimated to fit the experimental SGD_m, using the linear least squares optimisation function *lsqlin* in Matlab® R2019b.

4.2.3 Flux enhancer dosing

As explained in Chapter 2, the cationic polymer Adifloc KD451 (Adipap SA, France) was used as FE. A single dose of FE, i.e., pulse-dosage, was added to the AnMBR on day 16.. A 138.5 g pulse input of Adifloc KD451 was introduced to the bypass line of the AnMBR with an injection time of 45 min. This bypass line was also use for the AnDFCm installation (see Figure 1). The dosed mass was added to achieve a final concentration of Adifloc KD451 in the mixed liquor of 50 mg L⁻¹. This concentration was based on Table 2.3, and was an intermediate dosage between the optimal dosages for sludge filterability improvement and for csCOD removal of the sludge that was collected from the pilot-scale AnMBR fed with source-separated blackwater before the reactor was spiked with FE.

4.2.4 Monitoring phases

The AnMBR was inoculated with 500 L of sludge from the mesophilic anaerobic digester of the Guillarei municipal wastewater treatment plant and was operated for a 5-month acclimation period before Phase I, which is defined below. The AnMBR membrane was chemically cleaned with sodium hypochlorite prior to Phase I, and no further chemical cleanings were performed. On day 123, 0.84 m³ of sludge were withdrawn from the AnMBR because of a too-high accumulation of solids, and the removed volume was replaced with blackwater.

The three operational phases, relevant for this work, were defined as follows: Phase I (Period: 0–16 d) is the control phase before FE addition; Phase II (Period: 16–123 d) is the period following FE addition and before sludge withdrawal; and Phase III (Period: 123–154 d) is the period after sludge withdrawal.

To study the effect of biogas sparging on filtration performance, the AnMBR was operated with a reduced Q_G of 2–4 Nm³ h⁻¹, that is, an SGD_m of 0.32–0.64 Nm³ h⁻¹ m⁻², by decreasing the v_B over 2 days (Period: 37–39 d).

4.2.5 Physicochemical characterization

Hach Lange test kits were used to measure chemical oxygen demand (COD), ammonium–nitrogen (NH₄-N), total nitrogen (TN), and total phosphorous (TP). The organic matter was

measured as COD in different fractions, as described in Section 2.2.3, Chapter 2 — total COD (tCOD), supracolloidal COD (scCOD, above 1 μm) and colloidal + soluble COD, named submicron COD (csCOD, below 1 μm).

Total suspended solids (TSS), volatile suspended solids (VSS), fixed suspended solids (FSS), total solids (TS), volatile solids (VS) and fixed solids (FS) were measured following the Standard Methods (APHA, 1999). Alkalinity was measured using potentiometric titration to the end-point pH of 3.7 (APHA, 1999). Particle size distribution (PSD) was measured with a Microtrac Bluewave diffraction analyser (Malvern Instruments Ltd., UK), and reported as the 50th percentile of the volume-based particle size distribution, or median diameter, $D50$. PSD was assumed to represent floc size, as explained in Section 2.2.3, Chapter 2.

Grab Samples of Sludge, Blackwater and Permeate Were Taken from the AnMBR for Characterization. Suspended Solids, csCOD, Alkalinity, pH and PSD Were Measured in the Sludge; tCOD, TP, TN and NH$_4$-N in Both the Blackwater and the Permeate, and csCOD, scCOD, Alkalinity, pH and Total Solids in the Blackwater.

Sludge filterability was measured with short-term crossflow filtration tests, employing the anaerobic Delft filtration characterization method (AnDFCm) installation, connected in bypass to the AnMBR, as shown in Figure 1. During the in-situ filterability measurements, sludge flowed continuously from the membrane tank to the anaerobic reactor, passing through the AnDFCm installation, which contained an X-Flow membrane (Pentair, Enschede, the Netherlands), and had the following characteristics: tubular, 30 nm pore size, 8 mm internal diameter, and 95 cm length. The AnDFCm measured the additional resistance obtained when 20 L of permeate per m^2 of membrane surface area are produced, denominated as the ΔR_{20}; the sludge filterability is inversely related to ΔR_{20}. ΔR_{20} was measured by applying a flux of 60 L m^{-2} h^{-1} and a crossflow velocity of 1.5 m s^{-1}. The scheme of the AnDFCm installation in Figure 1 is simplified, and a more detailed representation of the installation and a description of the measuring protocol is presented in Section 2.2.4, Chapter 2.

4.2.6 Specific methanogenic activity (SMA)

The SMA was measured in Schott glass bottles with 400 mL liquid and 208 mL headspace, under mesophilic conditions using sodium acetate as carbon source and sludge samples from the AnMBR as inoculum. The sludge samples were placed at 4 ℃ before the SMA test, and thus a pre-activation period was included.

For the pre-activation period, all the SMA bottles, including blanks, were filled with 1.0 gCOD L^{-1} of sodium acetate, 2 gVSS L^{-1} of inoculum, 0.6 mL L^{-1} micro and 6 mL L^{-1} macro nutrients solutions (Muñoz Sierra et al., 2018), 10 mM phosphate buffer solution at pH 7.0 (Spanjers and Vanrolleghem, 2016) and demineralised water. The bottles were flushed with nitrogen gas for 1 min and placed inside an orbital shaker at 130 rpm with temperature set at 34 ℃.

For the SMA determination, after all the substrate was converted into methane, a new addition of sodium acetate, to reach 2 gCOD L^{-1}, was performed for all the bottles except the

blanks. The SMA was calculated from the methane production rate after the second addition of sodium acetate and following the protocol of Spanjers and Vanrolleghem (Spanjers and Vanrolleghem, 2016). The methane production rate was measured with an "automated methane potential test system" (AMPTS, Bioprocess Control, Sweden).

To study the adaptability of the biomass to the FE, SMA was measured in two sludge samples taken from the AnMBR as inoculums: one collected during Phase I immediately before FE addition, on day 16, and the other during Phase II, 3 weeks after FE addition, on day 37. The concentration of sludge (inoculum) in the SMA bottles was 2 gVSS L^{-1}, and no extra Adifloc KD451 was added to these bottles. Furthermore, with the sludge collected on day 16, an additional SMA test was performed by pre-mixing the sludge with Adifloc KD451, in 1 L jars at 90 rpm for 30 min and using the mix as inoculum. In the additional SMA test, the concentrations of sludge and Adifloc KD451 in the SMA bottles were 2 gVSS L^{-1} and 50 mg L^{-1}, respectively.

4.2.7 AnMBR filtration performance indices

The AnMBR filtration performance indices were total filtration resistance (R_T, m^{-1}) and fouling rate (FR, Pa s^{-1}). R_T was calculated with Darcy's law, as follows:

$$R_T = \frac{TMP}{\mu J}, \tag{4.2}$$

where μ is the dynamic viscosity of the permeate (Pa s), and J is the transmembrane flux (m s^{-1}), which is calculated by dividing the online monitored permeate flow by the membrane surface area. The permeate viscosity was assumed to be equal to pure water viscosity, and was calculated at the measured temperature (T, K) with the following empirical relationship (Janssen and Warmoeskerken, 1997):

$$\mu = 0.001 \, exp(0.580 - 2.520 \, \theta + 0.909 \, \theta^2 - 0.264 \, \theta^3),$$
$$with \, \theta = \frac{3.661 \, (T - 273.1)}{273.1}. \tag{4.3}$$

Fouling rate, FR, was measured as the change in TMP over time during each filtration cycle ($dTMP/dt$, Pa s^{-1}), and calculated it with the linear regression equation presented in Equation (4.4).

$$FR = \frac{dTMP}{dt} \approx \frac{n \sum_{i=1}^{n}(TMP_i \, t_i) - \sum_{i=1}^{n} TMP_i \, \sum_{i=1}^{n} t_i}{n \sum_{i=1}^{n} t_i^2 - \left(\sum_{i=1}^{n} t_i\right)^2}, \tag{4.4}$$

where t_i and TMP$_i$ are the times and corresponding TMP during one filtration cycle, and n is the number of observations.

4.2.8   Statistical analysis

The mean values from the SMA tests were compared using a Student's independent t-test assuming equal variances and parametric data. The p was calculated with the *ttest2* function in Matlab® R2019b.

The correlations between sludge characteristics, membrane performance indices and sludge filterability were studied. For the membrane performance indices, averaged values from a 2-hour period around the sludge sampling time were calculated.

Research has proven that biogas or air sparging substantially affects fouling (Judd and Judd, 2011; Meng et al., 2017). Thus, to eliminate the influence of biogas sparging on membrane performance, only the values of the membrane performance indices when the AnMBR operated under normal biogas sparging were used, that is, when the modelled SGD_m, as calculated with Equation (4.1), was between 0.96 and 1.28 $Nm^3\,h^{-1}\,m^{-2}$.

Since the data were not independent for most of the measured variables, the independence of the time-series was tested using a Ljung–Box test, with the function *lbqtest* in Matlab® R2019b (results are not shown). Independence is one of the assumptions of parametric tests; therefore, the non-parametric test Spearman's rank coefficient (r_s) was used. The statistical significance was assessed by comparing the probability values (p) with a 0.01 level of significance. r_s and p were computed with the *corr* function in Matlab® R2019b using "complete" rows, this is only rows of the input with no missing values.

4.3   RESULTS

4.3.1   Blackwater and permeate characteristics

Figure 4.2 compares the characteristics of the blackwater and the permeate during all the operational phases; Figure 4.3 displays the remaining blackwater characterization.

The organic matter concentration in the blackwater, measured as tCOD, was highly variable, ranging from 0.7 to 3.3 g L^{-1}, and tCOD decreased over time. Because the toilets in the building were conventional gravity flush toilets, as opposed to vacuum toilets, the blackwater tCOD concentration was lower than in other research studies, which reported tCOD values of 8.7 ± 4.0 g L^{-1} (Wendland et al., 2007), 9.8 ± 2.6 and 7.7 ± 2.2 g L^{-1} (De Graaff et al., 2010). High COD removal efficiencies between 89% and 98% were achieved during the entire operational period.

The blackwater characteristics, presented in Figure 4.2 and Figure 4.3, were highly variable throughout the operational period. This variation may be caused by the small and diverse group of persons generating the blackwater and the lack of external mixing in the septic tank. Approximately 200 persons worked in the building, however the number and specific persons that attended the office varied throughout the week due to the co-working spaces and new companies being installed. Furthermore, the characteristics of the blackwater that was being pumped into the equalization tank were likely affected by the time-of-day and

time-of-week that the pumping occurred. For example, the blackwater characteristics may have been different if the equalization tank was filled during office hours, when blackwater was entering the septic tank and thus promoting mixing, as opposed to out-of-office hours, when the septic tank was not mixed and sedimentation was likely to take place.

The concentrations of TN, TP and NH_4-N in the permeate were similar to those of the blackwater during most of the operational period, because these nutrients are not removed in anaerobic digestion, except for the fraction that is used for biomass growth. Moreover, owing to organic matter mineralization, the NH_4-N and ortho-phosphate concentrations may even increase in the AnMBR. Nevertheless, during the period of 51 to 72 days, the nutrient concentrations in the permeate were considerably below those of the blackwater, which was possibly caused by increased biomass growth and/or precipitate formation, such as of struvite and calcium phosphate species ($Ca_x(PO_4)_y$). The increase in blackwater tCOD load in the mentioned period might have led to increased biomass growth, agreeing with the observed increase in VSS concentration of the sludge shown in Figure 4.4E. The concomitant nutrient requirements for biomass growth would then result in decreased $NH4-N$ and TP concentrations in the permeate, as was shown in Figure 4.2. The estimated requirements of nitrogen and phosphorous for biomass growth when the blackwater tCOD increased to
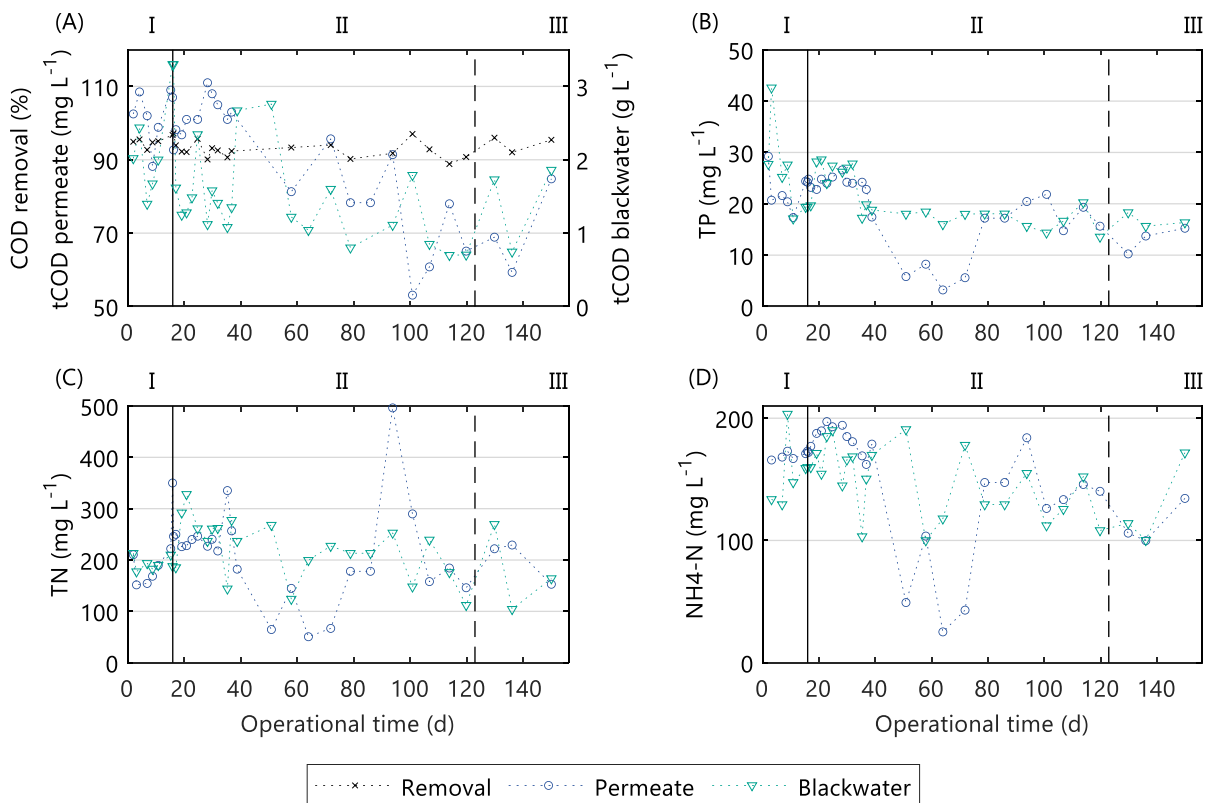
Figure 4.2. Blackwater and permeate characteristics during the operational period of pilot AnMBR dosed with flux enhancer: (A) total COD concentration and COD removal, (B) total phosphorous concentration, (C) total nitrogen concentration, and (D) ammonium−nitrogen concentration. A pulse-dosage of Adifloc KD451 achieving 50 mg L^{-1} was performed on day 16 (black continuous line), and sludge was withdrawn on day 123 (black dotted line). I, II and III are the operational phases described as follows: (I) control phase, (II) period following FE addition, and (III) period following sludge withdrawal.

2.7 gCOD L^{-1} were 14–19 mgN and 1–4 mgP per liter of influent, respectively. These values were calculated assuming a biomass yield of 0.10, a COD conversion of 92%, a biomass COD to VSS conversion of 1.42 gCOD gVSS^{-1}, and a nitrogen and phosphorous requirement based on the elemental composition of biomass, namely 80.8-108.8 mgN gVSS^{-1} and 4.3-23.8 mgP gVSS^{-1} (Hendriks et al., 2018). However, the observed decrease in NH$_4$–N and TP from blackwater to permeate largely exceeded the calculated biomass growth-related values, and amounted to 92–142 mgN L^{-1} and 10–13 mgP L^{-1}, respectively. Therefore, the decreased NH$_4$–N and TP concentrations in the permeate were likely caused by precipitate formation, which is influenced by the environmental conditions in the reactor, such as pH and the concentrations of different ions. Particularly, the precipitation of Ca$_x$(PO$_4$)$_y$ has been observed in reactors treating blackwater (Cunha et al., 2018; Tervahauta et al., 2014).

During the 10-day periods before and after FE addition, the mean COD removals were 94.8% and 94.2%, and the mean permeate tCOD values were 94.8 and 94.2 mg L^{-1}, respectively. Therefore, COD removal and permeate tCOD were seemingly not affected by dosing FE. Furthermore, around the moment of FE addition, the TN, TP and NH$_4$–N levels were
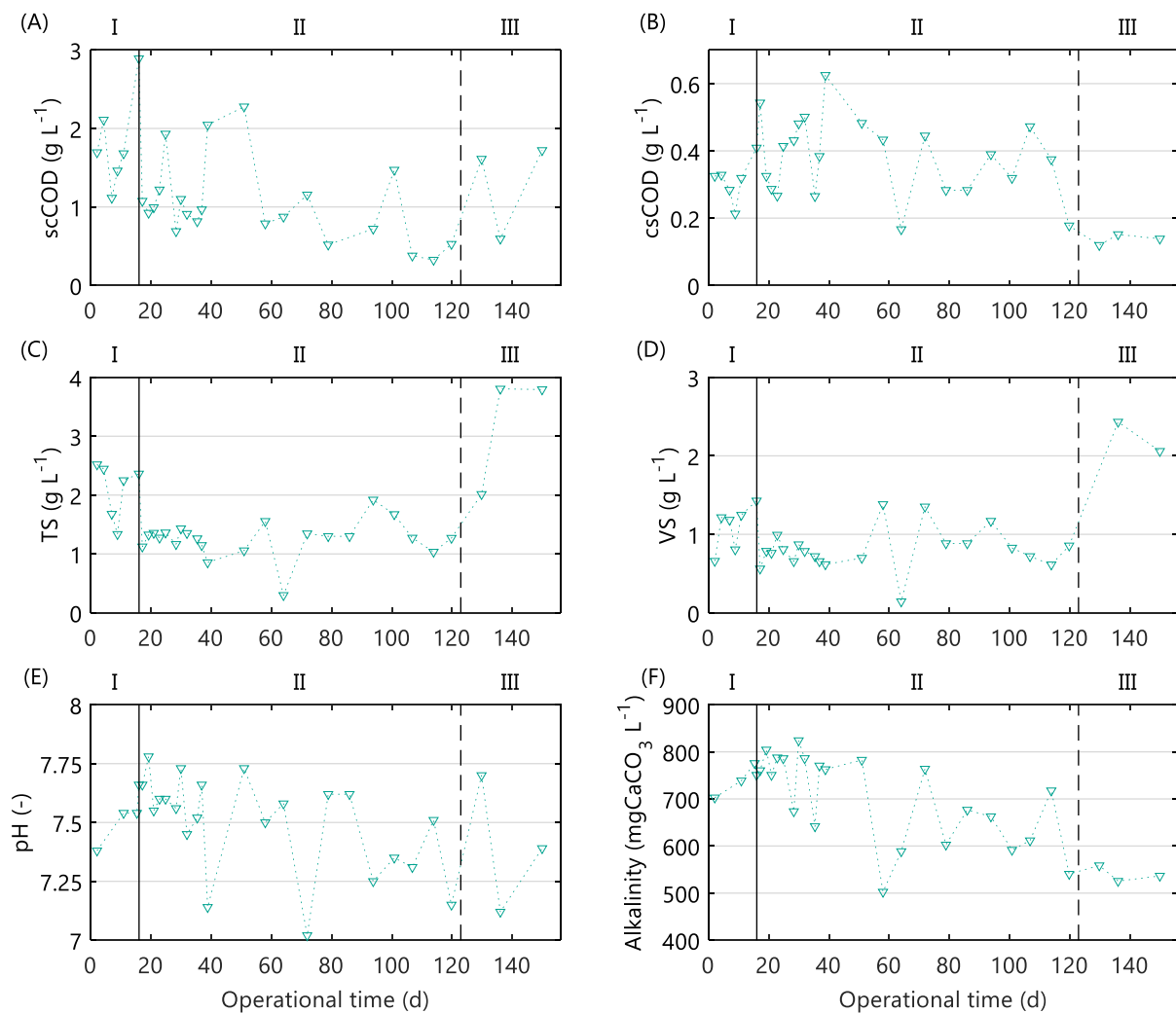

Figure 4.3. Blackwater characteristics during operational period of pilot AnMBR plant dosed with flux enhancer: (A) supracolloidal COD, (B) submicron COD, (C) total solids, (D) volatile solids, (E) pH, and (F) alkalinity.

increasing in the blackwater, and consequently in the permeate, because these nutrients are not removed during anaerobic digestion. Therefore, the increased concentrations in the permeate were very likely caused by their increase in blackwater, and not by FE addition.

On day 123, the VSS concentration in the mixed liquor dropped by 64% due to a considerable sludge withdrawal. However, this huge drop in VSS concentration did not impact COD removal or permeate quality in terms of COD concentration. Apparently, the potential organic loading or volumetric conversion capacity of the AnMBR was not fully utilised.

4.3.2   Sludge characteristics

Figure 4.4 shows the sludge characteristics during the operational period. During days 13 to 18, the sludge recirculation pump (P-3 in Figure 4.1) malfunctioned and caused an accumulation of solids in the membrane tank, shown by the increased TSS and VSS. The pump was repaired on day 18, and the TSS returned to its original value.

Furthermore, as explained in Section 4.3.1, a rapid increase in VSS was observed from days 39 to 51, which was attributed to an increased blackwater tCOD that promoted biomass growth and the accumulation of un-degraded particulate organic matter. Figure 4.4E shows a similar rapid VSS increase on day 94; however, on this occasion, the sudden increase cannot be explained by a high blackwater tCOD. Instead, the increased VSS was possibly caused by the accumulation of un-degraded particulate or colloidal organic matter from the blackwater, as a result of a change in blackwater composition, which was not notice when using the applied physicochemical characterization. Additionally, the lower temperature, shown in Figure 4.4I, could have reduced the hydrolysis rate, concomitantly explaining the slight decrease in COD removal efficiency observed in Figure 4.2A.

During the 10-day periods before and after FE addition, the mean ΔR_{20} values were 16.7×10^{12} and 7.8×10^{12} m^{-1}, the mean $D50$ values were 20.2 and 35.7 μm and the mean csCOD values were 740 and 391 mg L^{-1}, respectively. Therefore, on average, FE addition decreased the ΔR_{20} value by 53% (i.e., improved sludge filterability), increased $D50$ by 77% and decreased csCOD by 47%.

During Phase II, the effect of FE on filterability decreased slowly — the ΔR_{20} value increased on average 0.1×10^{12} m^{-1} per day. The filterability stayed below the lowest registered value in Phase I (i.e., 10.8×10^{12} m^{-1}) for a 50-day period, and achieved values similar to the mean ΔR_{20} in Phase I (i.e., 14.2×10^{12} m^{-1}) after 85 days. Furthermore, the increase in ΔR_{20} was simultaneous with the csCOD increase and $D50$ decrease.

The sludge withdrawal from the AnMBR, whereby 31% of the liquid volume was removed on day 123, caused a 62% decrease in TSS and only a 7% decrease in csCOD, and a 4% decrease in ΔR_{20}. The high decrease in TSS and low decrease in csCOD likely can be attributed to the fact that the purge was done from the bottom of the membrane tank, where particulate material is deposited by sedimentation, while colloidal material remains suspended.
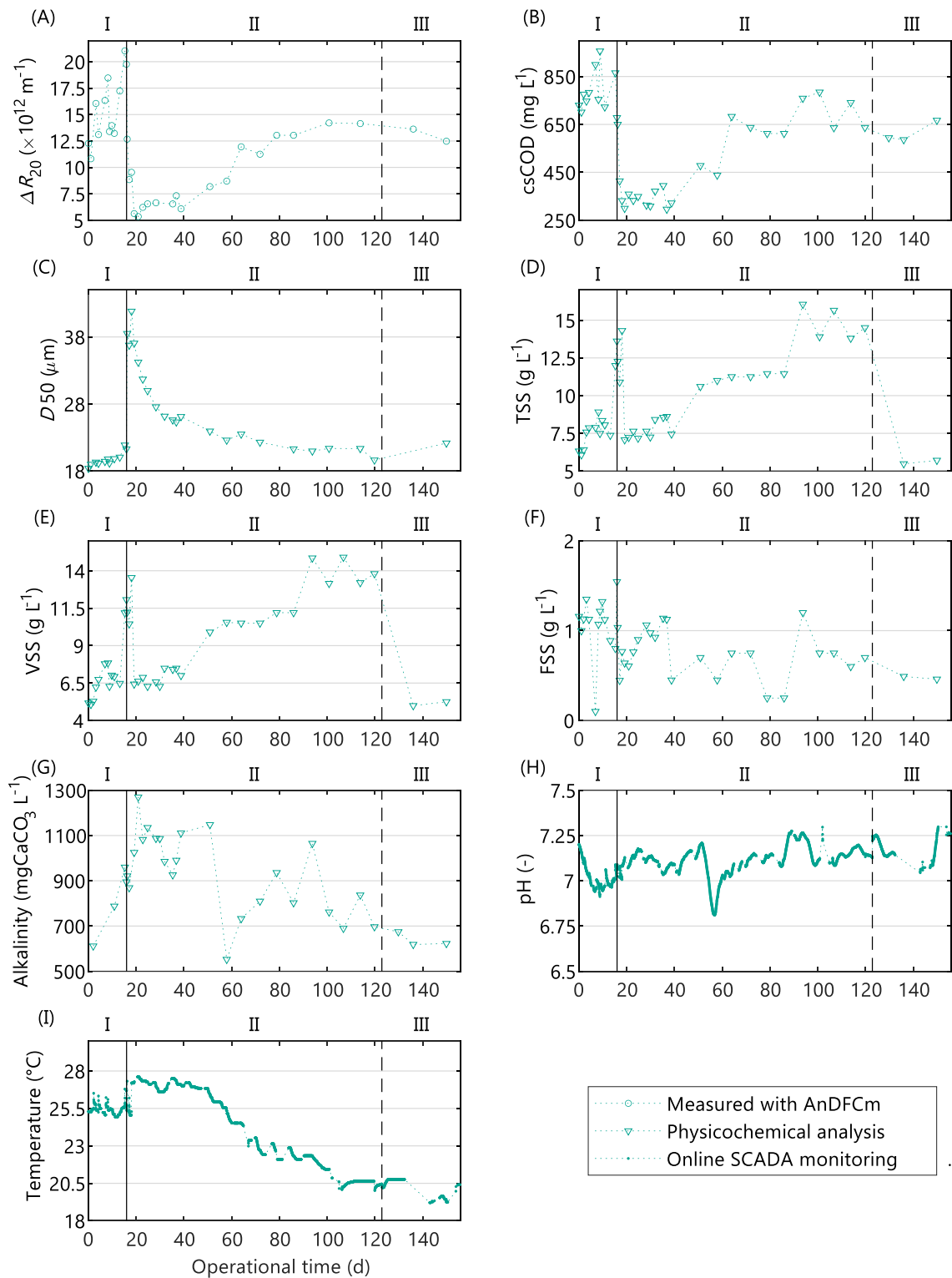
Figure 4.4. Sludge characteristics during operational period of pilot AnMBR plant dosed with flux enhancer: (A) sludge filterability expressed as ΔR_{20} (which is inversely related with filterability), (B) submicron COD, (C) floc size expressed as 50th percentiles of volume-based particle size distribution, (D) total suspended solids, (E) volatile suspended solids, (F) fixed suspended solids, (G) alkalinity, (H) pH, and (I) temperature.

4.3.3 Specific methanogenic activity

The effect of Adifloc KD451 on the biological activity was assessed with SMA tests, and the results are summarised in Figure 4.5. For Inoculum I, the mean SMA with 50 mg L^{-1} of Adifloc KD451 added to the bottle was 18% lower than the SMA without FE addition; this difference was statistically significant, with $p = 0.012$. Moreover, the mean SMA of Inoculum II did not present a statistically significant difference, $p = 0.76$, from the mean SMA of Inoculum I.
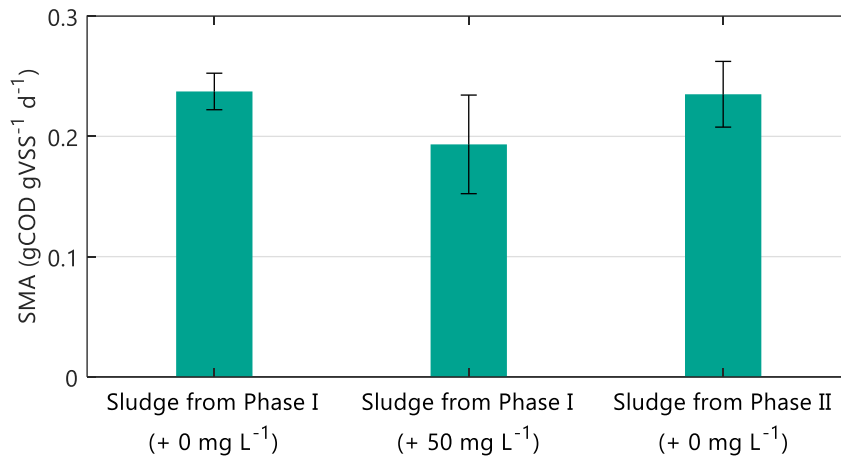
Figure 4.5. Specific methanogenic activity (SMA) of sludge samples collected from the pilot AnMBR immediately before (Phase I) and 3 weeks after (Phase II) FE addition. The values between brackets are the concentrations of Adifloc KD451 added to the SMA bottles, pre-mixed with inoculum. The error bars are the 95% confidence intervals.

4.3.4 SGD_m model calibration

The estimated parameters of the SGD$_m$ model in Equation (4.1), to evaluate the required gas sparging demand, were as follows: γ_0=-3.43 Nm^3 h^{-1}; γ_1=-14.57 Nm^3 h^{-1} m^{-1}; and γ_2=0.52 Nm^3 h^{-1} Hz^{-1}. Figure 4.6 shows the experimental and simulated SGD$_m$. The Pearson correlation coefficient between the experimental and simulated results was 0.906. Thus, the proposed model satisfactorily predicted SGD$_m$, and therefore, the simulated SGD$_m$ could be used as a continuous estimation of SGD$_m$ in the pilot AnMBR.

As described in Section 4.2.2, the continuous simulated SGD$_m$ was used to eliminate the influence of biogas sparging on membrane fouling when studying the correlation between sludge characteristics, membrane performance indices and sludge filterability.
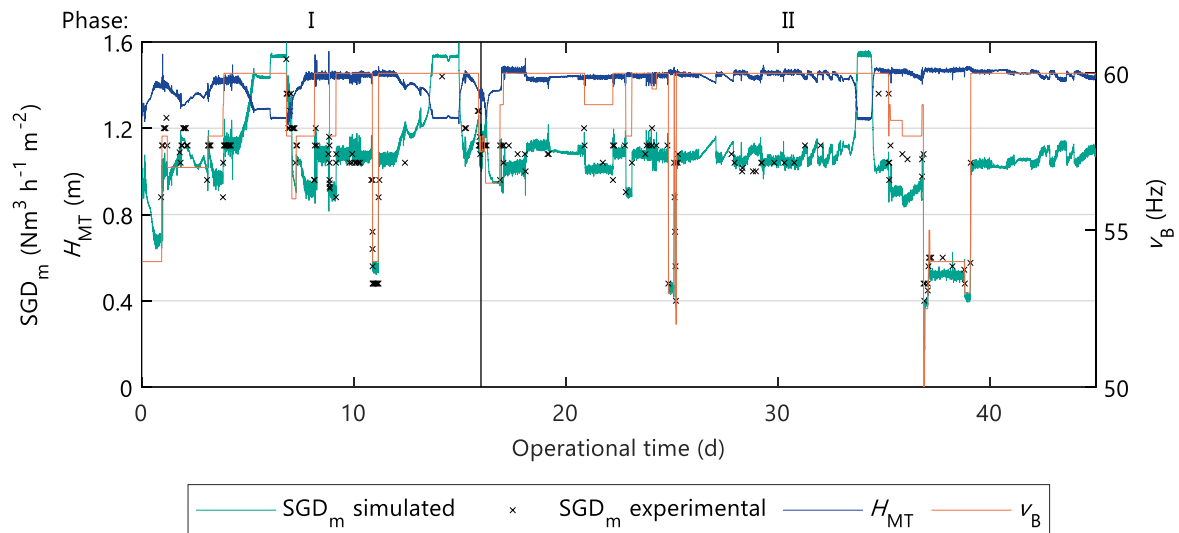
Figure 4.6. Simulated and experimental specific gas demand (SGD$_m$), level of liquid in the membrane tank (H_{MT}) and motor frequency of the blower (v_B) during the operational period of the AnMBR dosed with flux enhancer.

4.3.5 AnMBR filtration performance

The filtration performance of the AnMBR was assessed based on FR and R_T, as shown in Figure 4.7. The TMP could not be measured after day 58 due to technical difficulties with the online measurement of permeate pressure, that could not be resolved; thus the R_T and FR could not be calculated after day 58.

During the 10-day periods before and after FE addition, the mean R_T values were 6.6×10^{12} and 1.2×10^{12} m^{-1} and the mean FR values were 15.3 and 1.7 mbar min^{-1}, respectively. Therefore, FE addition improved the filtration performance of the AnMBR, clearly indicated by an 82% mean R_T decrease and an 89% mean FE decrease. Furthermore, during the 42-day
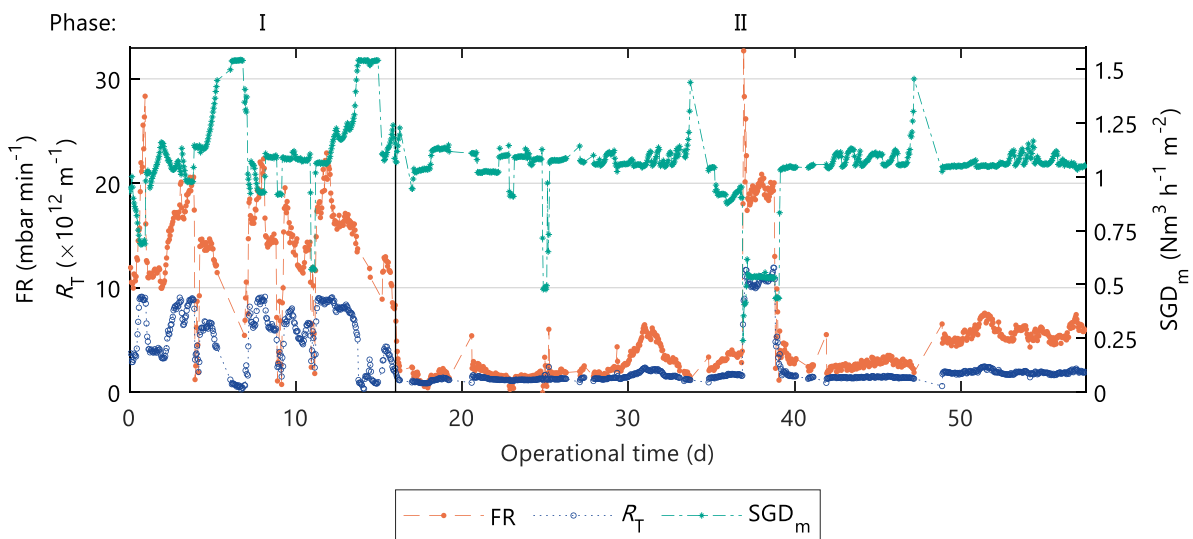
Figure 4.7. Pilot AnMBR mean hourly membrane performance state variables during operational period of pilot AnMBR plant dosed with flux enhancer: (A) mean TMP during one filtration cycle, and (B) transmembrane flux.

period recorded by the SCADA in Phase II, the FR and R_{T} values remained below the ones registered during Phase I.

The biogas blower did not have an automatic control, but instead was operated at a fixed motor frequency set by the operator. Thus, the SGD_{m} varied with the pressure in the membrane tank, which was determined by H_{MT}. Since the AnMBR was fed with blackwater generated in an office building, mostly empty outside working hours, there were weekends when there was less blackwater production (mainly during Phase I) and the reactor was not fed, resulting in decreased H_{MT} and increased SGD_{m}, as seen in Figure 4.6. Consequently, during these periods of low H_{MT}, the resulting FR and R_{T} values were low. Accordingly, FR and R_{T} considerably increased with decreasing SGD_{m} in Phase II (Period: 37–39 d). Therefore, as expected, the filtration performance on the AnMBR improved (in the short-term) with the higher biogas sparging rate, and conversely, it deteriorated with the low sparging rate.

4.3.6 Correlation analysis

Table 4.1 shows that the csCOD and $D50$ had statistically significant correlations with the ΔR_{20}, R_{T} and FR. The correlation coefficients were negative for $D50$ and positive for csCOD, suggesting that a sludge with a higher $D50$ and lower csCOD had better filterability and created less fouling. The results show that the $D50$ and csCOD were statistically significantly correlated.

Table 4.1. Spearman correlation half matrix between sludge characteristics, total filtration resistance (R_{T}), fouling rate (FR) and sludge filterability (expressed as ΔR_{20}). Significant correlation at level 0.01 (*); probability value (p) given between brackets.

Variable	R_{T}	FR	ΔR_{20}	csCOD	$D50$
R_{T}	1				
FR	0.96^* (8×10^{-12})	1			
ΔR_{20}	0.64^* (8×10^{-5})	0.75^* (8×10^{-5})	1		
csCOD	0.75^* (9×10^{-5})	0.82^* (5×10^{-6})	0.82^* (5×10^{-6})	1	
$D50$	-0.89^* (8×10^{-8})	-0.84^* (2×10^{-6})	-0.58^* (6×10^{-3})	-0.74^* (1×10^{-4})	1

4.4 DISCUSSION

4.4.1 Potential foulants and the role of flux enhancers

4.4.1.1 Soluble and colloidal organic matter

When added to a sludge sample, cationic polymers such as Adifloc KD451 are adsorbed onto the negatively charged surface of the suspended organic matter, such as colloidal material and flocs, promoting their agglomeration upon collision, consequently decreasing the concentration of colloidal material and increasing particle size. Moreover, colloidal and soluble material could be incorporated into the flocs by interaction with the cationic polymer adsorbed, or by entrapment between aggregated flocs. Accordingly, the addition of Adifloc KD451 to the AnMBR considerably decreased csCOD, which comprises colloidal and soluble material, and increased floc size.

The correlation analysis, in Section 4.3.6, showed that although both csCOD and $D50$ correlated with ΔR_{20}, FR and R_T, it was not possible to elucidate the individual effect of $D50$ and csCOD on fouling and filterability. Nevertheless, in Chapter 2, ΔR_{20} statistically significantly correlated with csCOD, cCOD and sCOD, but not with $D50$. Accordingly, in Iversen (2010), four of the tested FEs had no significant effect on mean floc size, while they decreased SMP and improved critical flux. Zhang et al. (2017) dosed 100 mg L^{-1} polyaluminium chloride or 400 mg L^{-1} PAC-SAE-Super, which reduced the TMP in a cross-flow filtration cell, while the mean floc size did not change significantly, and both colloidal and soluble organic matter decreased. Therefore, the results from previous research suggest that colloidal and soluble organic matter removal might have a higher impact on fouling mitigation than increasing floc size. Accordingly, researchers have consistently identified colloidal material as a major factor in reversible fouling in membrane bioreactors (Christensen et al., 2018; Gil et al., 2011; Huang et al., 2017; Judd and Judd, 2011; Lim et al., 2020; Remy, 2012). High colloidal concentrations increase the fouling rate by cake layer formation, pore blocking, and decreasing cake layer porosity.

4.4.1.2 Floc size

The addition of Adifloc KD451 to the AnMBR considerably increased median floc size, measured as $D50$. The effect of floc size on fouling has been addressed by several authors. Larger flocs can form more porous cakes, reduce the adhesion of the flocs to the membrane, increase the back-transport of flocs from the membrane surface to the bulk liquid, and reduce cake layer thickness by surface erosion or increased shear near the membrane surface (Belfort et al., 1994; Christensen et al., 2018; Hamedi et al., 2019; Shen et al., 2015), consequently decreasing membrane fouling.

Accordingly, the correlation analysis suggested that a higher $D50$ increased the sludge filterability and created less fouling. However, in Figure 4.4, the changes in $D50$ were simultaneous with, and opposite to, the changes in csCOD. Similarly, different researchers observed a decrease in fouling rate when simultaneously increasing the mean floc size and

decreasing the SMP or the concentration of submicron particles (De Temmerman et al., 2015; Huyskens et al., 2011b; Iversen, 2010; Koseoglu et al., 2012; Krzeminski et al., 2012; Wu et al., 2006; Zhang et al., 2010). To the authors' best knowledge, Zhang et al. (2017) is the only study wherein the fouling rate decreases with an increasing floc size, while no removal, or even a slight increase, of colloidal particles or SMP was observed. Therefore, from these studies and the results in this research, it is challenging to elucidate to what extent, if any, floc size affected fouling, or if the fouling improvement was simply caused by soluble and colloidal organic matter removal. Furthermore, some studies suggest that floc size had no effect on fouling mitigation, or even had a negative effect, which the author attributed to a decrease in the extracellular polymeric substances (EPS) (Chae et al., 2006) and to changes in the structure of the flocs (Remy, 2012). Nevertheless, the Carman–Kozeny equation and thermodynamic approaches suggest that floc size directly affects membrane fouling, and that small flocs have a stronger effect than large flocs (Belfort et al., 1994; Hamedi et al., 2019). Therefore, floc size might have a significant effect on membrane fouling for small flocs, whereas further increasing the size of already large particles might have a negligible effect on fouling mitigation.

The stronger correlation between $D50$ and filtration performance in the AnMBR (i.e., FR and R_T) than between $D50$ and filterability (Table 4.1) might be due to the different membrane configuration and operational conditions in the AnMBR compared to the AnDFCm installation, such as hydrodynamic conditions, membrane type, filtration and relaxation cycles, and mechanical cleaning (gas sparging vs. liquid cross-flow). Particularly, the AnMBR operates with filtration and relaxation cycles, whereas the AnDFCm installation operates with continuous filtration during filterability measurements. A recent study has demonstrated that under laminar conditions and without applying a membrane flux, large particles tend to move in larger numbers to the membrane than smaller particles, and with a membrane flux, large and small particles move in similar numbers (Naessens, 2018). Considering this, during relaxation in the AnMBR, the migration of larger particles to the membrane could create a cake layer with a high number of large particles, contributing to a highly permeable cake that can act as a protective layer during the filtration phase. Contrarily, the AnDFCm installation worked continuously in the filtration mode, and consequently this hypothetical protective cake layer formed by large particles was not formed, and thus the size of the large particles was less relevant.

4.4.2 Extent of flux enhancer effect

The flux enhancer had a long-term effect on sludge filterability and filtration performance; nevertheless, those effects slowly deteriorated over time, as shown by the ΔR_{20} returning to similar values as in Phase I, 85 days after FE addition. Similarly, after a pulse-dosage of MPE50 to a pilot MBR, R11 in Table 1.1, the MBR operated with a higher flux and a slightly lower TMP compared to the control phase during a 30-day period, after which sludge was withdrawn and the filtration performance deteriorated (Yoon and Collins, 2006). Moreover, Diaz et al. (2014) achieved a higher flux during a 4-week operating period compared to the

control phase, after dosing MPE50 to a lab-scale AnMBR fed with synthetic wastewater. During this period, no sludge was withdrawn.

Therefore, despite operating without sludge wastage, the effect of the FE can be lost over time due to several reasons, such as the following: biomass and colloidal material accumulation in the reactor due to microbial growth, floc breakage or the detachment of particulate material from flocs caused by shear; the loss of FE in the permeate or by FE biodegradation; and changes in sludge characteristics caused by fluctuations in the operational conditions or substrate characteristics.

4.4.3 Flux enhancer effect on permeate quality

When FE is added to sludge, a fraction of FE can remain unbonded in the bulk liquid, depending on the relevant physicochemical equilibria. Chapter 2 showed that Adifloc KD451 can pass through the membrane pores of the AnDFCm and contaminate the permeate. The membrane in the AnMBR had similar nominal pore size to the AnDFCm installation, that is, 35 and 30 nm, respectively. Thus, if the FE remains unbonded it can contaminate the AnMBR permeate. The AnMBR was dosed with 50 mg L^{-1} of Adifloc KD451, and thus assuming that 5% of the added FE remained unbonded (Iversen et al., 2008) and reached the permeate, that is 2.5 mg L^{-1} or 2.8 mgCOD L^{-1}. If this had been the case in the experiment in this research, and considering that the AnMBR permeate COD was between 90 and 110 mg L^{-1}, the contribution of FE to the permeate COD would have been negligible. Accordingly, the results in Section 3.1 show that the permeate COD was not affected by FE addition.

Furthermore, the permeate nutrient concentrations, namely TP, TN and NH_4–N, were apparently not affected by FE addition. Therefore, the addition of Adifloc KD451 to the AnMBR had seemingly no effect on permeate quality. Accordingly, MPE50 had no detrimental effect, or even slightly improved the permeate quality and nutrient removal (Alkmim et al., 2016; Iversen et al., 2009b; Wozniak, 2010; Yoon and Collins, 2006). Therefore, dosing FE, particularly cationic polymers, to MBRs and AnMBRs has no significant adverse effect on permeate quality.

4.4.4 Flux enhancer effect on biological activity

Under anaerobic conditions, results showed that Adifloc KD451 had an immediate inhibitory effect on the biological activity in the SMA test, which was in accordance with previous observations (Odriozola et al., 2019). Contrarily, under aerobic conditions, different cationic polymers, including Adifloc KD451, had no or slightly detrimental effect on the endogenous oxygen uptake rate (Iversen et al., 2009a; Yoon et al., 2005).

The SMA of sludge collected 3 weeks after FE addition to the AnMBR did not present a statistically significant difference from the sludge collected immediately before FE addition. Therefore, as proposed in previous research (Odriozola et al., 2019), although Adifloc KD451 had an immediate inhibitory effect on SMA, this was regarded as a reversible process. Moreover, the applied organic sludge loading rates to the AnMBR were relatively low, i.e., 0.01-0.18 gCOD gVSS^{-1} d^{-1}, meaning that a reduction of 18% in SMA does not harm the

process. It should be noted that in addition to the observed effect on SMA, FE may also irreversibly bind organic matter, reducing the biomethane potential of the substrate (Kooijman et al., 2017a) and thus the overall biogas production rate. Unfortunately, the daily biogas production could not be measured in the pilot experiment.

The results clearly show that FE addition had no adverse effect on COD removal in the AnMBR, as presented in Section 4.3.1, which is in accordance with previous research performed with MPE50 (Alkmim et al., 2016; Díaz et al., 2014). Therefore, this research suggests that dosing FE, particularly cationic polymers, has no significant adverse effect on COD removal efficiencies.

4.4.5 Sludge withdrawal as an alternative strategy for fouling control

As shown in Section 4.3.2, the sludge withdrawal performed on day 123 caused a high decrease in TSS (62% decrease), while it only slightly decreased csCOD (7% decrease), which was likely attributable to the location of the purge (in the bottom of the membrane tank) and the amount of withdrawn reactor broth. The low decrease in csCOD caused a small improvement in sludge filterability (ΔR_{20} decreased 4%). The results indicate that sludge withdrawal is not a very effective fouling control strategy, as the major part of csCOD remains suspended in the bulk of the liquid. Likely, only very large volume exchange ratios will impact the bulk liquid csCOD concentrations and thus the total membrane resistance. No further experiments were performed to prove this hypothesis since it was outside the scope of this research.

4.4.6 Filterability as input variable for fouling control and flux enhancer dosing

Under the normal operational biogas sparging conditions defined in Section 4.2.1, i.e., $SGD_m = 0.96-1.28 \ Nm^3 \ h^{-1} \ m^{-2}$, the sludge filterability was statistically correlated with the AnMBR filtration performance indices (i.e., FR and R_T), and thus the observed improvement in AnMBR filtration performance was possibly due to the improved sludge filterability. However, during the period of 37–39 days, the AnMBR filtration performance deteriorated, while sludge filterability slightly improved, and conversely, the AnMBR filtration performance improved while sludge filterability deteriorated during the periods of day 6–7 and day 13–14. These behaviours were attributed to changes in SGD_m; see Section 3.5. Therefore, relating sludge filterability to AnMBR filtration performance indices allowed us to identify the cause of filtration performance deterioration or improvement in the AnMBR.

Consequently, a fouling control tool that uses sludge filterability and AnMBR filtration performance indices as input variables could help decide on the appropriate intervention (Kraume et al., 2009), that is, manipulate either the sludge characteristics, for example by dosing FE, or the membrane operational conditions, for example by decreasing flux or increasing biogas sparging. Furthermore, the AnDFCm takes 20 min to determine filterability, and this time is negligible compared to the rate of change of filtration performance and sludge filterability observed in membrane bioreactors, as shown in Section 4.4.2. This means that the

dynamic of the measuring sensor is considerably faster than the dynamics in the process parameters, which is an indispensable property in a successful control tool. Therefore, in-situ filterability measurements with the AnDFCm proved to be an appropriate input variable for manipulating FE dosage for fouling control in AnMBRs.

4.5   CONCLUSIONS

This research evaluated the long-term effect on filtration performance, sludge characteristics, biological activity and permeate quality following a pulse-dosage of Adifloc KD451 as FE to a concentration of 50 mg L^{-1} in a pilot AnMBR. The main findings can be summarised as follows:

- FE addition improved the filtration performance of the AnMBR, as indicated by the 82% R_T and 89% FR reductions, without significantly affecting COD removal and permeate quality. The improvement was sustained in the long term—the FR and R_T values stayed below the ones registered during the control phase (i.e., Phase I) for at least 42 days, and after this period the SCADA system failed to measure FR and R_T.

- The improved filtration performance was attributed to increased floc size and reduced csCOD (i.e., colloidal + soluble organic matter concentration), thereby improving sludge filterability. The filterability returned to similar values as in the control phase 85 days after FE addition.

- The SMA values of the sludge samples collected immediately before and 3 weeks after FE addition were statistically similar; however, in batch tests, 50 mg L^{-1} of Adifloc KD451 caused an 18% SMA inhibition. Thus, the FE had a modest immediate effect on the SMA, which, however, had no significant impact on the AnMBR performance. Moreover, the drop in SMA was reversible.

- Relating in-situ measurements of sludge filterability with AnMBR filtration performance indices, i.e., FR and R_T, allowed us to identify the prevailing gas sparging rate as being the cause of filtration performance deterioration or improvement in the AnMBR.

- In-situ measurements of sludge filterability with the AnDFCm proved an appropriate input variable for manipulating FE dosage for fouling control in AnMBRs.

5

MODELLING A PILOT-SCALE ANAEROBIC MEMBRANE BIOREACTOR DOSED WITH FLUX ENHANCER AND COMPARISON OF CONTROL TOOLS FOR FLUX ENHANCER DOSING [**]

ABSTRACT

Flux enhancers (FE) have been successfully applied for fouling mitigation in membrane bioreactors. However, more research is needed to compare and optimise different dosing strategies to improve the filtration performance, while minimising the use of FE and preventing overdosing. Therefore, the goal of this research is to develop a simulation environment with an integrated comprehensive model that predicts the effect of FE dosing on sludge filterability and membrane fouling rate; and to use the developed simulation environment to compare five control tools to manipulate the FE dosing to an AnMBR. The integrated model coupled filtration, flocculation, and biochemical processes. The biochemical model was the ADM1 modified to include FE and colloidal material. We developed an empirical model for the FE induced flocculation of colloidal material. Various alternate filtration models from literature and empirical models proposed in this research were implemented, calibrated, validated, and compared. The best integrated model was successfully applied in the simulation environment to compare three feedback and two feedforward control tools to manipulate FE dosing to an AnMBR. The most appropriate control tool was a feedback sludge filterability controller that dosed FE continuously. This controller achieved more stable sludge filterability and fouling rate under specific disturbances than the other control tools. The simulation environment developed in this research provides a tool to test strategies for dosing flux enhancer dosing strategies into AnMBRs.

5.1 INTRODUCTION

Flux enhancer dosage to membrane bioreactors has been mostly done using an initial pulse-dosage, followed by periodic FE dosing to compensate for the FE loss by biodegradation and sludge withdrawal. However, this dosing strategy does not consider possible disturbances and is based on assumptions that might lead to FE underdose or overdose. Therefore, more research is needed that compares and optimises different dosing strategies to improve the filtration performance while minimising the use of FE and avoiding overdosing.

Comparing various FE dosing strategies using experiments, independent of the scale, is expensive and time-consuming. Additionally, dosing strategies should ideally be compared under identical operational conditions, which is challenging to achieve in different reactors in parallel or in the same reactor at different moments. A simulation environment is regarded as an effective tool to test various FE dosing strategies for fouling control, provided the model structure is commonly accepted. The simulation environment should have a comprehensive model able to predict the effect of FE dosing on membrane fouling rate and sludge filterability. However, thus far, such a comprehensive model has never been presented in the literature. Nevertheless, multiple models with diverse complexity have been discussed for the different processes involved in membrane bioreactors, including filtration, biochemical, hydrodynamic, and flocculation models (Naessens et al., 2012a, 2012b; Robles et al., 2018). These models can be adapted and coupled into a comprehensive integrated model that describes an AnMBR under FE dosage. The first step towards developing such an integrated model is to identify the variables that are affected by FE dosage and influence the filtration performance.

Colloidal material has been consistently identified as a major factor affecting sludge filterability (Odriozola et al., 2021) and reversible fouling in membrane bioreactors (Christensen et al., 2018; Gil et al., 2011; Huang et al., 2017; Judd and Judd, 2011; Lim et al., 2020; Odriozola et al., 2020; Remy, 2012). Colloidal material deposited in the cake layer can decrease cake porosity by filling the void space of the cake. The concentration of colloidal material decreases after dosing cationic polymers as FE, while the floc size increases, as discussed in Chapters 2 and 4. Regarding floc size, larger flocs can form more porous cakes, reduce the adhesion of the flocs to the membrane, increase the back-transport of flocs from the membrane surface to the bulk liquid, and reduce cake layer thickness by surface erosion (Belfort et al., 1994; Christensen et al., 2018; Hamedi et al., 2019; Shen et al., 2015), thus decreasing membrane fouling. However, as discussed in Chapter 4, the effect of floc size on membrane fouling is controversial. Floc size can have a substantial effect on membrane fouling for small flocs, whereas further increasing the size of already large particles might have a negligible effect on fouling mitigation. Considering the above, the colloidal material concentration is likely an appropriate state variable to describe the effect of FE dosing on the membrane fouling rate and sludge filterability, whereas floc size may not be an appropriate variable. The concentration of particulate material is a poor indicator of sludge fouling propensity by itself (Judd and Judd, 2011). However, it is a crucial input variable in filtration models because it affects cake layer formation by particle deposition over the membrane surface and may play a role in scavenging colloidal material (Lousada-Ferreira et al., 2015).

The concentration of particulate material is affected by biochemical processes (such as bioconversion, biomass growth and decay), influent characteristics, and flocculation of colloidal material. Therefore, to predict the effect of FE dosing on membrane fouling rate and sludge filterability, an integrated model including filtration with colloidal material deposition, (FE induced) flocculation, and biochemical processes is needed.

The IWA anaerobic digestion model No. 1 (ADM1) (Batstone et al., 2002) has been widely applied to simulate the biochemical processes occurring in anaerobic reactors (Batstone et al., 2015; Donoso-Bravo et al., 2011; Robles et al., 2018), including AnMBRs. Other biochemical models applied in AnMBR include the biological nutrient removal model No. 2 (BNRM2) (Barat et al., 2013) and the simple anaerobic model AM2b that incorporates the kinetics of soluble microbial products (SMP) (Benyahia et al., 2013). Although anaerobic digestion modelling is a relatively mature field, the kinetics of colloidal material has not yet been incorporated. Moreover, the FE could have a detrimental effect on the biological activity (Chapter 3). Therefore, to model a FE dosed AnMBR, the biochemical models should be extended to incorporate colloidal material and FE.

The filtration process in membrane bioreactors mostly has been modelled with grey box models, particularly by applying the resistance-in-series model, Darcy's Law, drag and lift forces, and the Carman-Kozeny equation to predict the membrane performance (such as fouling rate, transmembrane pressure, flux) based on sludge characteristics and operating conditions (Naessens et al., 2012a, 2012b; Robles et al., 2018). Researchers have modelled the reduction in cake layer porosity, and consequently the increase in the specific cake resistance (SCR), caused by the entrapment of colloidal material (Wu et al., 2012), extracellular polymeric substances (EPS) (Cho et al., 2005), SMP (Charfi et al., 2017; Zarragoitia-González et al., 2008) and submicron material (Zuthi et al., 2013). This could be an appropriate approach to incorporate the effect of FE dosing on membrane fouling and sludge filterability through changes in the concentration of colloidal material.

To model the flocculation process, population balance models (PBM) have been widely applied in chemical engineering to predict the particle size distribution (Jeldres et al., 2018). PBM divide the particles into populations each with a different particle size, and describe the dynamic of the number of particles present in each population. To incorporate PBM in an AnMBR integrated model, the equations describing the filtration and biochemical processes, for example, must be applied to each population, resulting in an extremely complex model with many state variables. Alternatively, a simpler flocculation model that describes the dynamics of floc size (i.e., mean particle size) can be useful and sufficient to assess the necessity of floc size as a linking variable between biochemical-flocculation models and filtration models.

The objective of this research is to develop and validate a comprehensive integrated model to be use as simulation environment and to test five control tools to manipulate the FE dosing to an AnMBR. The integrated model included flocculation, filtration, and biochemical processes to predict the effect of FE dosing on sludge filterability (as measured with the AnDFCm) and membrane fouling rate in an AnMBR. The tested control tools were: two feedback sludge filterability controllers, and two feedforward and one feedback FE

concentration controllers.

5.2 MATERIALS AND METHODS

5.2.1 Experimental data

5.2.1.1 Physicochemical characterization

Total suspended solids (TSS) and alkalinity were measured following the Standard Methods (APHA, 1999), using potentiometric titration to end-point pH of 3.7 for alkalinity. Particle size distribution (PSD) was measured with a Microtrac Bluewave diffraction analyser (Malvern Instruments Ltd., UK), and incorporated in the model as the geometric mean diameter (d_p) calculated as follows (Merkus, 2009):

$$d_p = exp\left(\sum_i \left(P_i \, ln \, d_{p,i}\right)\middle/\sum_i P_i\right),$$
(5.1)

where P_i is the volume fraction and $d_{p,i}$ is the diameter of the i-th particle.

Chemical oxygen demand (COD) and ammonium-nitrogen (NH4-N) were measured with Hach Lange test kits. The total COD (tCOD) was measured in the unfiltered sample, and the submicron COD (csCOD) in the fraction below 1 μm (Odriozola et al., 2021). The permeate COD (pCOD) was measured in the permeate collected from the pilot AnMBR.

5.2.1.2 Sludge filterability with the AnDFCm

Sludge filterability was measured with the anaerobic Delft filtration characterisation method (AnDFCm), described in short as follow, further detailed in Chapter 2. During filterability measurements, sludge flows continuously in crossflow mode, at 1.5 m s^{-1} velocity, through an X-Flow membrane (Pentair, the Netherlands) while permeate is extracted at 60 L m^{-2} h^{-1} flux. The membrane characteristics are as follows: ultrafiltration, tubular, 30 nm pore size, 8 mm internal diameter, 95 cm length, and 0.0239 m^2 surface area.

The output of the AnDFCm is the additional resistance obtained when 20 L of permeate per m^2 of membrane surface area are produced, denominated as ΔR_{20}; the sludge filterability is inversely proportional to ΔR_{20}.

5.2.1.3 Pilot AnMBR description and monitoring

The models were partially calibrated and validated using monitoring data from a pilot AnMBR plant treating blackwater from the main office building of the Business Centre Porto do Molle, Nigrán, Pontevedra, Spain. The AnMBR consisted of an anaerobic stirred reactor connected to a membrane tank with one submerged ultrafiltration flat-sheet membrane module (Martins System, Germany). The reactor was operated under alternating filtration-relaxation cycles, at room temperature, and with biogas sparging below the membrane module. The pilot plant was coupled with a supervisory control and data acquisition (SCADA) system and various

sensors. Table A1 summarises the characteristics and operational conditions of the pilot AnMBR plant. Further details of the pilot AnMBR are described in Chapter 4.

Grab samples of sludge, blackwater and permeate were regularly taken from the AnMBR for characterisation. Table A2 and Figure A1 show the physicochemical characteristics used for calibration of the biochemical-flocculation model. During days 13 to 18, TSS accumulated in the membrane tank due to malfunctioning of the sludge recirculation pump, this period was not included in the calibration of the biochemical-flocculation model.

The fouling rate (FR) in the pilot AnMBR was measured as the change in transmembrane pressure (TMP) over time during each filtration cycle ($d\text{TMP}/dt$), calculated with the following linear regression equation:

$$FR = \frac{d\text{TMP}}{dt} \approx \frac{n \sum_{i=1}^{n}(\text{TMP}_i\, t_i) - \sum_{i=1}^{n} \text{TMP}_i \sum_{i=1}^{n} t_i}{n \sum_{i=1}^{n} t_i^{\,2} - \left(\sum_{i=1}^{n} t_i\right)^2}, \tag{5.2}$$

where t_i and TMP_i are the time and corresponding TMP during one filtration cycle, and n is the number of observations. The fouling rate measured in the pilot AnMBR, displayed in Figure A2A, was used as model output during calibration and validation of the AnMBR filtration models (described in Section 5.2.4). The sludge characteristics, c_C, c_X, T and d_p shown in Figure A1, and gas sparging intensity (Figure A2B) were used as inputs during model calibration and validation. The total concentration of colloidal and particulate material in the mixed liquor expressed as suspended solids, c_C and c_X, respectively, were calculated as follows:

$$c_C = \frac{\text{csCOD} - \text{pCOD}}{i_{\text{COD,CI}}}, \tag{5.3}$$

$$c_X = \text{TSS} - c_C, \tag{5.4}$$

where $i_{\text{COD,CI}}$ the theoretical COD of inert colloidal material, which was considered equal to the theoretical COD of biomass, that is 1.42 gCOD g^{-1} (Mara et al., 2003). The values for csCOD, pCOD and TSS are the linearly interpolated values between measured values of each variable.

During the operation of the pilot, filterability was measured in-situ by connecting the AnDFCm installation in bypass to the pilot AnMBR, details are given in Chapter 4. The ΔR_{20} ranged from 5×10^{12} m^{-1} to 21×10^{12} m^{-1} during the operational period, with a mean value of 12×10^{12} m^{-1}, Figure A3. The ΔR_{20} was the output of the AnDFCm filtration models (described in Section 5.2.6), and the sludge characteristics shown in Figure A1 were used as inputs during model calibration.

Flux enhancer was added to the pilot as follows: 138.5 g pulse input (M_{fe} = 0.1385 kgCOD) of the cationic polymer Adifloc KD451 (Adipap SA, France), was introduced to the bypass line

of the pilot AnMBR on day 16 (t_{fe0} = 1,379,754 s) with an injection time (Δt_{fe}) of 2,700 s. Therefore, in the model, the FE mass flow rate ($\dot{m}_{\text{fe}}$) was as follows:

$$\dot{m}_{\text{fe}} = \begin{cases} 0, & t < t_{\text{fe0}} \\ \dfrac{M_{\text{fe}}}{\Delta t_{\text{fe}}}, & t_{\text{fe0}} \leq t \leq t_{\text{fe0}} + \Delta t_{\text{fe}} \\ 0, & t > t_{\text{fe0}} + \Delta t_{\text{fe}} \end{cases} . \tag{5.5}$$

5.2.1.4 Flux enhancer dosage-step experiments

Flocculation stoichiometry was assessed with FE dosage-step experiments using grab sludge samples from different AnMBRs. The relevant characteristics of the samples are summarised in Table A3. The dosage-step test consisted of consecutive stepwise increasing additions of Adifloc KD451 into a 40 L grab sludge sample. The experimental procedure and sample description are detailed in Chapter 2. The PSD, ΔR_{20}, and csCOD were measured 30 minutes after each dosage; the sludge was mixed throughout the experiment with an external stirrer.

5.2.2 General model description and approach

The proposed modelling approach is outlined in Figure 5.1. The main outputs of the integrated model are the AnMBR membrane fouling rate and the sludge filterability expressed as ΔR_{20}. The integrated model couples a biochemical-flocculation model with two filtration models: one for the AnMBR membrane module and one for AnDFCm installation membrane. The biochemical-flocculation model predicts the sludge characteristics that are used as input in both filtration models. For the AnMBR and AnDFCm filtration models, several alternate models were compared to select the best-fitting ones.

The AnMBR filtration process was modelled using two alternate approaches: (1) FR_RIS model and (2) empirical FR model. In the FR_RIS model the fouling rate (FR) is calculated as the change in TMP over time during each filtration cycle ($d\text{TMP}/dt$). The TMP is calculated by combining three submodels: resistance-in-series (RIS), Deposition and SCR. Deposition submodel is an ordinary differential equation system to describe the deposition of colloidal and particulate material onto the membrane, SCR submodel is an equation to calculate the SCR based on the amount and characteristics of the material deposited onto the membrane. All possible combinations between four alternate deposition submodels (Section 5.2.4.3), seven alternate SCR submodels (Section 5.2.4.2), and one RIS submodel (Section 5.2.4.1) resulted in 28 alternate FR_RIS models, which were compared. The empirical FR model is an algebraic equation to calculate FR directly from the operational variables and mixed liquor properties, this research proposed six alternate empirical FR models (Section 5.2.5). Therefore, 34 alternate AnMBR filtration models were compared, this is 28 FR_RIS and 6 empirical FR models.

In the AnDFCm filtration model the ΔR_{20} is the resistance of the cake layer (R_c) after 1,200 s of continuous filtration under the operational conditions of the AnDFCm. R_c is calculated by combining Deposition and SCR submodels. Twenty-one alternate AnDFCm

models (Section 5.2.6) were compared, that result from combinations of three Deposition and seven SCR alternate submodels.
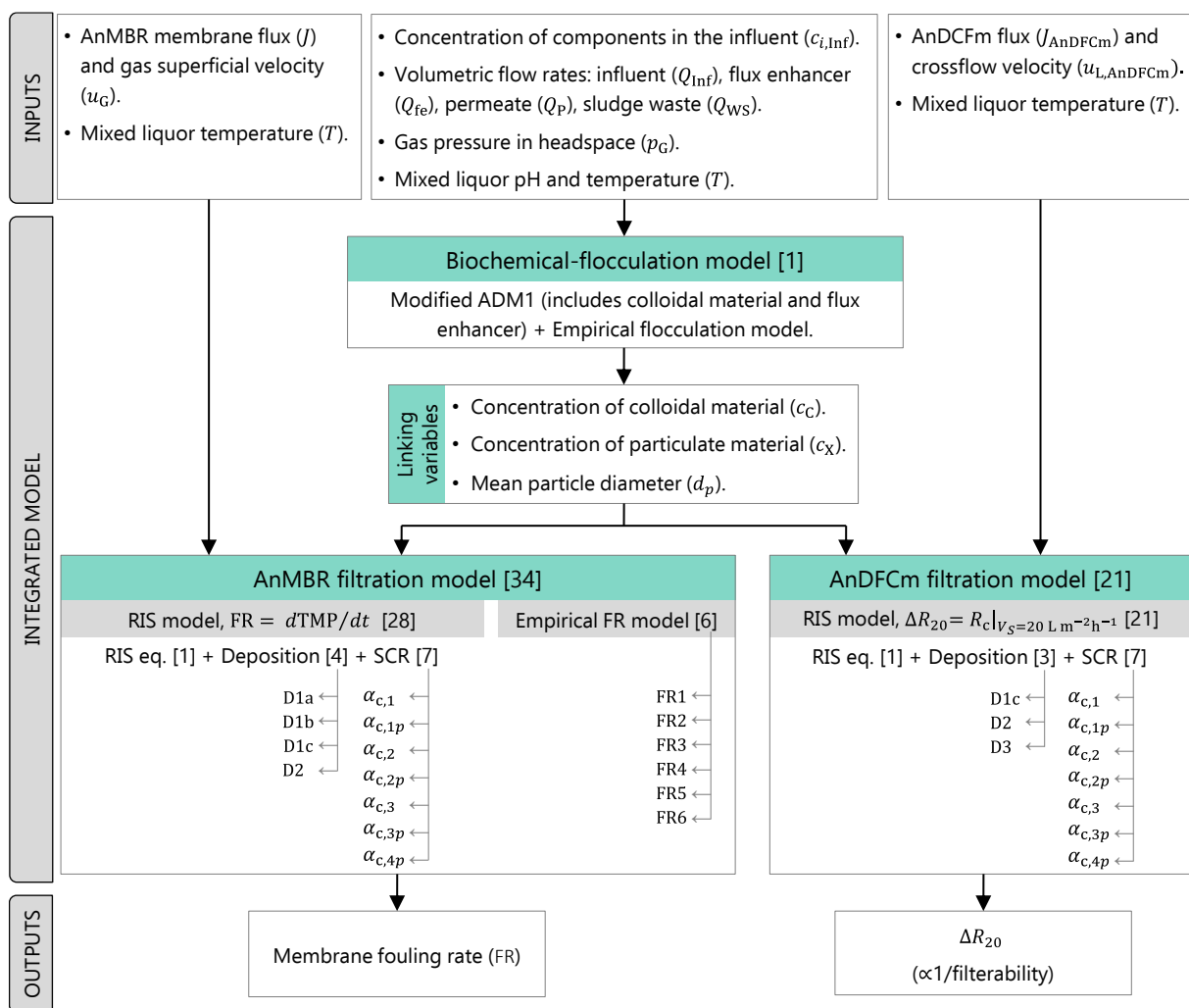
Figure 5.1. Modelling approach scheme. Between square brackets is the number of alternate models compared to select the most appropriate model. Abbreviations: ADM1, anaerobic digestion model No. 1; AnDFCm, anaerobic Delft filtration characterization method; RIS, resistance-in-series; SCR, specific cake resistance; TMP, transmembrane pressure. D1a, D1b, D1c, D2 and D3 are alternate deposition submodels; $\alpha_{c,1}$, $\alpha_{c,1p}$, $\alpha_{c,2}$, $\alpha_{c,2p}$, $\alpha_{c,3}$, $\alpha_{c,3p}$ and $\alpha_{c,4}$ are alternate SCR submodels; and FR1 to FR6 are alternate empirical FR models.
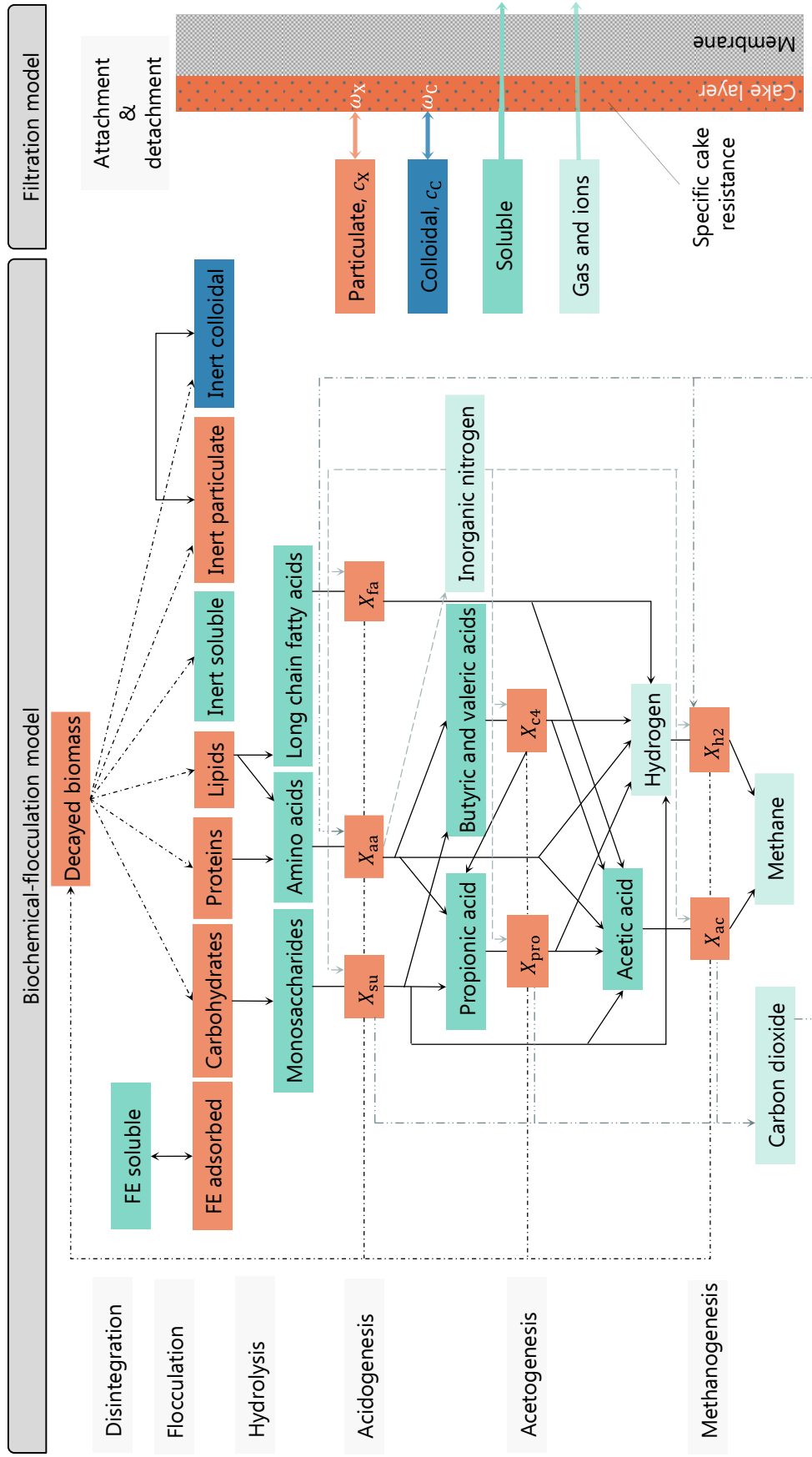
Figure 5.2. Scheme of the modified ADM1, extended to include processes caused by the addition of flux enhancer (FE), coupled with filtration model. X_i is the degrader of component i; c_X and c_C are the total concentration of particulate and colloidal materials in the bulk liquid, respectively; and ω_X and ω_C are the mass of particulate and colloidal materials deposited in the membrane, respectively.

5.2.3 Biochemical-flocculation model

The biochemical-flocculation model is an amended ADM1 (Batstone et al., 2002), modified to include the following processes caused by FE dosing: adsorption of FE onto particulate material, flocculation of colloidal material, and change in mean particle size as a result of flocculation. The model includes three new components as follows: inert colloidal material (C_I), FE in the bulk liquid (soluble, S_{fe}) and adsorbed FE (X_{fe}). Figure 5.2 displays the scheme of the modified ADM1 and Table 5.1 shows the stoichiometric (Petersen) matrix for the new processes. Section A2 in Appendix A displays the full stoichiometric matrix and process rate equations.

The modelled FE is a cationic polymer that interacts with the negatively charged surface of particulate and colloidal material. The adsorption of FE onto particulate material is described with the pseudo-first order model (El-Naas and Alhaija, 2011) in Equation (5.6), the FE adsorption onto particulate material promoted the flocculation of colloidal material as described in Equation (5.7).

$$\rho_{23} = k_{ads}\left(X_{fe,e} - X_{fe}\right), \tag{5.6}$$

$$\rho_{24} = Y_{fe,C}\, k_{ads}\left(X_{fe,e} - X_{fe}\right)\frac{C_I/i_{COD,CI}}{c_X + c_C}\frac{X_I}{X_I + 1 \times 10^{-6}}, \tag{5.7}$$

where k_{ads} is the adsorption rate coefficient, $X_{fe,e}$ the adsorbed concentration of FE after equilibrium, X_{fe} the concentration of FE adsorbed onto particulate material, $Y_{fe,C}$ the yield of colloidal material flocculated per unit of FE adsorbed onto the particulate material, C_I the concentration of colloidal inert, X_I the concentration of particulate inert, $i_{COD,CI}$ the theoretical chemical oxygen demand for C_I, and c_C and c_X are the total concentration of colloidal and particulate material, respectively, expressed as suspended solids, and calculated as follows:

$$c_C = \sum_i C_i/i_{COD,i}, \tag{5.8}$$

$$c_X = \sum_i X_i/i_{COD,i}, \tag{5.9}$$

where $i_{COD,i}$ is the theoretical chemical oxygen demand for component i. Through Equation (5.7) the model considers the deflocculation of X_I into C_I when the concentration of FE decreased, and thus the last term in Equation (5.7) was introduced to avoid negative C_I values when X_I approaches zero and there is no material to be deflocculated.

To calculate $X_{fe,e}$, the Langmuir adsorption isotherm in Equation (5.10), which describes the equilibrium conditions, is combined with Equation (5.11), which is the mass balance of FE inside the reactor at equilibrium conditions.

Table 5.1. Stoichiometric coefficients ($v_{i,j}$) for the flocculation processes caused by addition of flux enhancer (FE), for modified ADM1.

Component $i \rightarrow$	13	24	25	26
Process $j \downarrow$	S_{fe}: soluble FE	X_{I}: particulate inerts	C_{I}: colloidal inerts	X_{fe}: adsorbed FE
23 Adsorption of FE onto particulate material	-1			1
24 Flocculation of colloidal material		1	-1	

$$X_{\text{fe},e} = q_{m,\text{ads}}\, c_{\text{X}} \frac{K_{L,\text{ads}}\, S_{\text{fe},e}}{1 + K_{L,\text{ads}}\, S_{\text{fe},e}} \tag{5.10}$$

$$S_{\text{fe},e} = \left(c_{\text{fe}} - X_{\text{fe},e}\right) \tag{5.11}$$

where $q_{\text{m,ads}}$ is the maximum adsorption capacity corresponding to monolayer coverage, $K_{L,\text{ads}}$ the Langmuir affinity coefficient, $S_{\text{fe},e}$ the concentration of FE in the bulk liquid after equilibrium, and c_{fe} is the total concentration of FE inside the reactor.

Hydrolysis of decayed biomass has been reported as the slowest process in anaerobic digestion (Tugtas et al., 2006). Thus, the ADM1 approach was modified by decoupling the degradation rates of the decayed biomass and of the particulate material of the influent. For this, the model incorporates the disintegration of decayed biomass as the rate limiting process in biomass degradation, whereas the particulate material of the influent directly hydrolyses (without disintegration).

The following additional modifications and assumptions in the ADM1 were mage: (1) removal of ammoniacal nitrogen inhibition of acetoclastic methanogenesis, because it is negligible in the pH range 7.0 - 7.5 and at total nitrogen concentrations in the permeate of 80 – 200 mgN L^{-1}, as measured in the pilot AnMBR (Astals et al., 2018); (2) inclusion of a non-competitive inhibition of acetoclastic methanogenesis by FE ($I_{\text{fe,ac}}$) (Odriozola et al., 2019); and (3) inclusion of pH as an input of the model instead of performing the ion balance because pH was measured online by the SCADA.

Our model assumes that all soluble components pass through the membrane and reach the permeate, whereas the colloidal and particulate components are retained by the membrane and remain inside the reactor. Equation (5.12) gives the mass balances of component i in the liquid phase, and Equation (5.13) the mass balances of component i in the gas phases.

$$\frac{dc_i}{dt} = E_i - f_{i,\text{WS}} \frac{c_i Q_{\text{WS}}}{V_{\text{L}}} - f_{i,\text{P}} \frac{c_i Q_{\text{P}}}{V_{\text{L}}} + \frac{1}{t_{\text{conv}}} \sum_{j=[1-23]} v_{i,j} \rho_j \tag{5.12}$$

$$\frac{dc_{i,G}}{dt} = -\frac{c_{i,G} Q_G}{V_G} + \frac{V_L}{t_{conv} V_G} \sum_{j=[19-21]} v_{i,j} \rho_j \qquad (5.13)$$

where E_i is the input function of component i, $f_{i,P}$ the fraction of component i that passes through the membrane and reaches the permeate ($f_{i,P} = 0$ for colloidal and particulate components, and $f_{i,P} = 1$ for soluble components), $f_{i,WS}$ the fraction of component i that leaves the reactor with the sludge waste ($f_{i,WS} = 1$ for all components), $v_{i,j}$ the stoichiometric coefficient of component i in process j, ρ_j the rate of process j, t_{conv} the time conversion factor (86,400 s d^{-1}), $c_{i,G}$ the concentration of component i in the gas phase, and V_G the volume of the gas phase in the reactor. E_i was calculated with the concentration of component i in the influent ($c_{i,Inf}$), Equation (5.14). The FE was added to the reactor in a separate flow, which increased the concentration of FE in bulk liquid ($S_{fe} \equiv S_{13}$).

$$E_i = \begin{cases} \dfrac{c_{i,Inf} Q_{Inf}}{V_L}, & i = [1,12] \cup [14,26] \\[2mm] \dfrac{\dot{m}_{fe}}{V_L}, & i = 13 \end{cases} \qquad (5.14)$$

In the pilot AnMBR described in Section 5.2.1.3, the mean particle diameter (d_p) was almost constant throughout the operational period without dosing FE. This mean size was referred as the mean particle diameter at stable operation ($d_{p,St}$). Moreover, immediately after dosing FE to the pilot, d_p increased and then it decreased continuously until it reached $d_{p,St}$. Therefore, the empirical model in Equation (5.15) was proposed to describe the d_p dynamic in the pilot AnMBR.

$$\frac{dd_p}{dt} = \frac{1}{t_{conv}} \left(k_{floc,fe} \frac{dX_{fe}}{dt} + (d_{p,St} - d_p) k_{floc} \right) \qquad (5.15)$$

where k_{floc} is the empirical flocculation-deflocculation rate that represents aggregation and breakage, and $k_{floc,fe}$ the FE induced flocculation yield. The first term represents the immediate increase after FE dosing, where d_p changes linearly with the adsorbed FE concentration, as experimentally observed in the dosage-step tests with grab sludge samples described in Section 5.2.1.4. The second term of the equation represents the tendency of d_p to reach $d_{p,St}$ in the pilot AnMBR.

5.2.4   AnMBR filtration: alternate FR_RIS models

The AnMBR FR_RIS filtration models predict the cake layer formation by attachment and detachment of particulate material onto the membrane, and the SCR (α_c) by entrapment of colloidal material in the cake layer. The model output is fouling rate (FR) calculated with Equation (5.2) using the simulated TMP.

5.2.4.1 Resistance-in-series (RIS) submodel

The TMP was calculated by Darcy's law, as follows:

$$TMP = J\mu R_t, \tag{5.16}$$

where R_t is the total filtration resistance, μ is the dynamic viscosity of the permeate, and J is the transmembrane flux. The permeate viscosity was assumed equal to pure water viscosity and calculated at the measured temperature (T, K) with the following empirical relationship (Janssen and Warmoeskerken, 1997):

$$\mu = 0.001\, exp(0.580 - 2.520\,\theta + 0.909\,\theta^2 - 0.264\,\theta^3),$$
$$with\ \theta = \frac{3.661\,(T - 273.1)}{273.1}. \tag{5.17}$$

Although no chemical cleaning was performed in the pilot AnMBR during 2 years of operation, no irreversible fouling was observed. Therefore, the irreversible fouling resistance was neglected, and R_t was calculated with the following RIS submodel:

$$R_t = R_m + R_c, \tag{5.18}$$

where R_m is the intrinsic resistance of the membrane and R_c is the resistance of the cake layer. R_c was the product between the mass of particulate material deposited per membrane area (ω_X) and the SCR (α_c), as follows:

$$R_c = \omega_X \alpha_c. \tag{5.19}$$

5.2.4.2 Alternate specific cake resistance (SCR) submodels

Seven alternate SCR submodels were compared. In the first submodel, referred to as $\alpha_{c,1}$, the SCR was calculated with Equation (5.20) which combines the Carman-Kozeny equation for flow through a bed of spheres (Carman, 1997) with Darcy's Law and the thickness of the cake layer as $\delta_c = \omega_X / (\rho_X (1 - \varepsilon_c))$.

$$\alpha_{c,1} = \frac{k_{CK}\,(1 - \varepsilon_c)}{\rho_X\,d_p^2\,\varepsilon_c{}^3}, \tag{5.20}$$

where k_{CK} is the proportionality Carman-Kozeny coefficient (which includes the shape factor), ε_c the cake layer porosity, ρ_X the density of particulate material deposited onto the membrane, and d_p the mean diameter of the deposited particles which was assumed equal to the mean diameter of the particles in the bulk liquid. The latter assumption neglects the selectivity towards the deposition of smaller particles, which has been previously described (Naessens, 2018). However, this assumption was regarded as sufficient in this first modelling approach to assess the necessity of incorporating floc size as a linking variable between biochemical-flocculation and filtration models. The effect of the smaller particles deposited onto the membrane was accounted for by incorporating colloidal material as a state variable.

The colloidal material entrapped in the cake layer decreases the cake layer porosity (ε_c) as follows (Wu et al., 2012):

$$\varepsilon_c = \varepsilon_{c0} - (1 - \varepsilon_{c0})\frac{\omega_C\,\rho_X}{\rho_C\,\omega_X}, \tag{5.21}$$

where ρ_C and ω_C are the density and mass per unit of area of colloidal material deposited on the membrane, respectively.

Several authors reported the compression of the cake layer caused by TMP, which might cause deformation of soft sludge flocs and structural rearrangement of particles (Boyle-Gotla et al., 2014; Bugge et al., 2012; Jørgensen et al., 2014; Robles et al., 2013b; Sørensen and Sørensen, 1997). Therefore, the SCR submodels $\alpha_{c,1p}$ were defined as the extended versions of $\alpha_{c,1}$ that includes cake compression. The SCR of the compressed cake layer at the operating pressure ($\alpha_{c,1p}$) is calculated using the SCR at zero pressure ($\alpha_{c,1}$), the pressure drop over the cake (ΔP_c), and the pressure needed to double the specific resistance (P_a), as follows:

$$\alpha_{c,p} = \alpha_c\left(1 + \frac{\Delta P_c}{P_a}\right). \tag{5.22}$$

By Darcy's law $\Delta P_c = J\mu\omega_X\alpha_{c,p}$, and thus, combining Darcy's law with Equation (5.22) the following equation was derived:

$$\alpha_{c,1p} = \frac{\alpha_{c,1}}{\left(1 - \dfrac{J\mu\omega_X\alpha_{c,1}}{P_a}\right)}. \tag{5.23}$$

The SCR submodel $\alpha_{c,2}$, was the model proposed by Wu et al. (2012), presented in Equation (5.24), which does not include the dependency of d_p. Analogous to $\alpha_{c,1}$, $\alpha_{c,2}$ was extended into $\alpha_{c,2p}$, as shown in Table 5.2.

$$\alpha_{c,2} = \frac{k_c\,(1 - \varepsilon_c)^2}{\rho_X\,\varepsilon_c{}^3(1 - \varepsilon_{c0})}, \tag{5.24}$$

where k_c is a cake resistant coefficient, and ε_{c0} the cake layer porosity without colloidal material.

Moreover, Cho et al. (2005) developed an empirical equation to calculate SCR based the concentration of extracellular polymeric substances, total suspended solids, and TMP. Several researchers had successfully applied this equation or slightly modified versions in aerobic MBRs (Mannina et al., 2011; Suh et al., 2013; Zarragoitia-González et al., 2008; Zuthi et al., 2013). Furthermore, Mannina, Suh and collaborators (Mannina et al., 2011; Suh et al., 2013) modified Cho's model to exclude the TMP dependency by using the TMP coefficient P_b. The following three SCR submodels based on Cho's equation were included: $\alpha_{c,3}$, $\alpha_{c,3p}$ and $\alpha_{c,4p}$. The former, $\alpha_{c,3}$, corresponds to the equation presented by Mannina, Suh and collaborators, Equation (5.25); and $\alpha_{c,3p}$ is the compressible version of $\alpha_{c,3}$, presented in Table 5.2. Then, $\alpha_{c,4p}$ is an adapted version of Cho's original equation, where the ratio EPS/TSS was

Table 5.2. Specific cake resistance (SCR, α_c) submodels and the effects accounted for in each submodel.

SCR submodel	Equation	Effects considered		
		Colloidal material	Particle size	Compression, TMP
$\alpha_{c,1}$	$\dfrac{k_{CK}\,(1-\varepsilon_c)}{\rho_X\,d_p^2\,\varepsilon_c^{\;3}}$	X	X	
$\alpha_{c,1p}$	$\dfrac{\alpha_{c,1}}{\left(1-\dfrac{J\mu\omega_X\alpha_{c,1}}{P_a}\right)}$	X	X	X
$\alpha_{c,2}$	$\dfrac{k_c\,(1-\varepsilon_c)^2}{\rho_X\varepsilon_c^{\;3}(1-\varepsilon_{c0})}$	X		
$\alpha_{c,2p}$	$\dfrac{\alpha_{c,2}}{\left(1-\dfrac{J\mu\omega_X\alpha_{c,2}}{P_a}\right)}$	X		X
$\alpha_{c,3}$	$\dfrac{P_b}{\mu^2}\left(\zeta_1+\zeta_2\left(1-\exp\left(-\zeta_3\dfrac{\omega_C}{\omega_X}\right)\right)^{\zeta_4}\right)$	X		
$\alpha_{c,3p}$	$\dfrac{\alpha_{c,3}}{\left(1-\dfrac{J\mu\omega_X\alpha_{c,3}}{P_a}\right)}$	X		X
$\alpha_{c,4p}$	$R_m\left(\dfrac{\mu}{J\left(\zeta_1+\zeta_2\left(1-\exp\left(-\zeta_3\dfrac{\omega_C}{\omega_X}\right)\right)^{\zeta_4}\right)}-\omega_X\right)^{-1}$	X		X

substituted by ω_C/ω_X, presented in Equation (5.26). The model $\alpha_{c,4p}$ already includes cake compression because it is TMP dependent.

$$\alpha_{c,3}=\frac{P_b}{\mu^2}\left(\zeta_1+\zeta_2\left(1-\exp\left(-\zeta_3\frac{\omega_C}{\omega_X}\right)\right)^{\zeta_4}\right),\tag{5.25}$$

$$\alpha_{c,4p}=\frac{TMP}{\mu^2}\left(\zeta_1+\zeta_2\left(1-\exp\left(-\zeta_3\frac{\omega_C}{\omega_X}\right)\right)^{\zeta_4}\right),\tag{5.26}$$

where ζ_1, ζ_2, ζ_3 and ζ_4 are empirical coefficients. In $\alpha_{c,4p}$ the SCR was calculated combining equations (5.16), (5.18), (5.19) and (5.26), as follows:

$$\alpha_{c,4p}=R_m\left(\frac{\mu}{J\left(\zeta_1+\zeta_2\left(1-\exp\left(-\zeta_3\frac{\omega_C}{\omega_X}\right)\right)^{\zeta_4}\right)}-\omega_X\right)^{-1}.\tag{5.27}$$

5.2.4.3   Alternate deposition submodels

Two modelling approaches were compared to describe the cake layer formation by deposition of particulate material on the membrane surface. The first approach, further called "Deposition submodel 1 (D1)", was developed by Robles et al. (2013) to describe the filtration process in a submerged AnMBR. The second approach, "Deposition submodel 2 (D2)", was developed by Li and Wang (2006) and applied by different researchers in aerobic MBRs (Boyle-Gotla et al., 2014; Mannina et al., 2011; Nam et al., 2021; Suh et al., 2013; Wu et al., 2012; Zarragoitia-González et al., 2008). The deposition of colloidal material in the cake layer was based on the approach of Wu et al. (2012). Table 5.3 shows the stoichiometric coefficients and the kinetic expressions for both deposition submodels, and the extensions for colloidal material deposition.

Deposition submodel 1 (D1) includes two processes related to particulate material, Process 1 is the attachment of particulate material onto the membrane promoted by the flow of permeate and as a function of the concentration of particulate material in the bulk liquid (c_X), Equation (5.28). Process 2 is the detachment of particulate material promoted by the shear stress caused near the membrane surface by biogas sparging in the membrane tank, Equation (5.30). Robles et al. (2013) also included the particulate material detachment during back-flushing which was not included in the model since the pilot AnMBR did not operate with back-flush.

Robles et al. (2013) modelled Process 2 (detachment of particulate material) as a half-saturation switching function, Equation (5.30), where $q_{m,MS}$ is the maximum membrane scouring velocity and $K_{S,c}$ the half-saturation coefficient for cake mass during membrane scouring. Furthermore, based on experimental observation, they included a sigmoid inhibition function (I_{MS}) to account for the impact of filtering at conditions above and below critical levels, Equation (5.36) in Table 5.4, where K_F is an adjustable parameter representing the fouling rate when J_{20} approaches zero, and γ_0, γ_1 and γ_2 are parameters representing the influence of filtering capacity, biogas sparging and particulate material on the fouling rate, respectively.

Different equations to calculate I_{MS} were developed, summarised in Table 5.4, to be include in Deposition submodel D1. The submodel D1a is the original model by Robles et al. (2013), D1b is an extension to account for the influence of colloidal material with the parameter γ_3. D1c is a simplified submodel that eliminates the impact of filtering at conditions above and below critical levels (i.e., $I_{MS} = 1$).

Robles' model was extended to incorporate the deposition of colloidal material in the membrane surface. Analogous to the attachment of particulate material, the attachment of colloidal material to the membrane (Process 3) was promoted by the permeate flow and the concentration of colloidal material in the bulk liquid (c_C), Equation (5.32). The detachment of colloidal material from the membrane (Process 4), Equation (5.34), was caused by the detachment of the particulate material weighed by the ratio of colloidal to total material deposited.

Table 5.3. Stoichiometric coefficients and kinetic expressions for material deposition onto the membrane in alternate deposition submodels (D1 and D2).

Component $i \rightarrow$ Process $j \downarrow$	ω_X Deposited particulate	ω_C Deposited colloidal	c_X Particulate in bulk liquid	c_C Colloidal in bulk liquid	Deposition submodel 1 (D1) (Drag forces)		Deposition submodel 2 (D2) (Drag and lift forces)	
1 Attachment of particulate material	1		-1		$J_{20} c_X$	(5.28)	$\dfrac{24 J}{24 J + C_d d_p G} J c_X$	(5.29)
2 Detachment of particulate material by biogas sparging	-1		1		$q_{m,\mathrm{MS}} \dfrac{\omega_X}{K_{S,c}/A_\mathrm{m} + \omega_X} I_\mathrm{MS} \dfrac{u_G}{H_\mathrm{MT}} \omega_X$	(5.30)	$\dfrac{\beta_\mathrm{ST} G \omega_X}{\gamma V_\mathrm{F} + \omega_X} \omega_X$	(5.31)
3 Attachment of colloidal material		1		-1	$J_{20} c_C$	(5.32)	$f_{C,c} J c_C$	(5.33)
4 Detachment of colloidal material by biogas sparging		-1		1	$q_{m,\mathrm{MS}} \dfrac{\omega_X}{K_{S,c}/A_\mathrm{m} + \omega_X} I_\mathrm{MS} \dfrac{u_G}{H_\mathrm{MT}} \omega_C$	(5.34)	$\dfrac{\beta_\mathrm{ST} G \omega_X}{\gamma V_\mathrm{F} + \omega_X} \omega_C$	(5.35)

Table 5.4. Sigmoid inhibition function (I_{MS}) equations for alternate deposition submodels (D1a, D1b and D1c).

Deposition submodel	I_{MS} equation	
D1a	$I_{MS} = (1 + FR)^{-1}$ with $FR = K_F e^{J_{20}\left(\gamma_0 - \gamma_1 \frac{u_G}{H_{MT}} + \gamma_2 c_X\right)}$	(5.36)
D1b	$I_{MS} = (1 + FR)^{-1}$ with $FR = K_F e^{J_{20}\left(\gamma_0 - \gamma_1 \frac{u_G}{H_{MT}} + \gamma_2 c_X + \gamma_3 c_C\right)}$	(5.37)
D1c	$I_{MS} = 1$	(5.38)

Deposition submodel 2 (D2) describes the attachment of particulate material (Process 1) based on two competing forces, namely the attraction drag from the permeate flow and lifting force caused by the shear stress near the membrane surface. The kinetic expression of Process 1 is in Equation (5.29), where C_d is the drag coefficient and G the apparent shear rate. The detachment of particulate material, Process 2, was calculated with Equation (5.31), where γ is the compression coefficient, V_F the volume of permeate produced within the filtration time t_F with $V_F = J t_F$, and β_{ST} is a lumped parameter with $\beta_{ST} = \beta(1 - K_{ST})$ where β is the erosion rate coefficient of the cake layer and K_{ST} the stickiness coefficient.

The apparent shear rate (G) was calculated based on the gas superficial velocity (u_G), and the density (ρ_L) and dynamic viscosity (μ_L) of the mixed liquor, as follows:

$$G = \sqrt{\frac{\rho_L\, g\, u_G}{\mu_L}}.$$

(5.39)

The density ρ_L was assumed equal to the density of water (ρ_W) at the operational temperature T (K), The parameters of the quadratic function in Equation (5.40) were optimised to fit the ρ_W versus T data (Perry and Green, 2008), with a coefficient of determination (R^2) of 0.9997.

$$\rho_W = -0.0033\, T^2 - 0.1048\, T + 1001.5\,.$$

(5.40)

The viscosity μ_L was a function of the concentration of solids in the bulk liquid (TSS) and the viscosity of water at T (Equation (5.17)), as follows (Krauth and Staab, 1993):

$$\mu_L = a\, \mu_W\, e^{b\, \text{TSS}}\,,$$

(5.41)

where a and b are parameters, with a = 1.05 and b = 0.08.

In Deposition submodel 2, the attachment and detachment of colloidal material to the membrane was modelled following Wu et al. (2012). The attachment (Process 3) was calculated with Equation (5.33), where $f_{C,c}$ is the fraction of colloidal material entrapped in the cake layer. The detachment (Process 4) was caused by detachment of the cake layer, calculated with Equation (5.35).

5.2.5   AnMBR filtration: alternate empirical FR models

The empirical FR models are algebraic equations to calculate FR directly from the operational variables and mixed liquor properties, summarised in Table 5.5. The first FR model, FR1, is the one proposed by Robles et al. (2013) for I_{MS} calculation and extended for colloidal material, presented in Equation (5.37). This model was further modified into FR2 by eliminating the effect of c_X because the concentration of particulate material is a poor indicator of biomass fouling propensity by itself (Judd and Judd, 2011).

Based on the gas-step experiments in the pilot AnMBR described in Section A1, Appendix A, the FR was proportional to $u_G^{-\gamma_G}$, where γ_G is a parameter, this was incorporated in FR3. The conversion factor f_{conv} was introduced to achieve similar FR values as the model FR2 as follows: $f_{conv} = \overline{u_G}^{\gamma_G}$, where $\overline{u_G}$ is the mean gas velocity in the pilot AnMBR, $\overline{u_G} = 0.003$ m s^{-1}.

As discussed in Chapter 4, it is not clear if the floc size influences membrane fouling. Therefore, FR models including and excluding mean particle size, d_p, as an input variable were compared. The empirical models FR1, FR2 and FR3 were extended into FR4, FR5 and FR6, respectively, that include d_p.

Table 5.5. Alternate empirical FR models.

FR model	I_{MS} equation	
1	$FR = K_F e^{J_{20}\left(\gamma_0 - \gamma_1 \frac{u_G}{H_{MT}} + \gamma_2 c_X + \gamma_3 c_C\right)}$	(5.37)
2	$FR = K_F e^{J_{20}\left(\gamma_0 - \gamma_1 \frac{u_G}{H_{MT}} + \gamma_3 c_C\right)}$	(5.42)
3	$FR = f_{conv} K_F u_G^{-\gamma_G} e^{J_{20}\left(\gamma_0 + \gamma_3 c_C\right)}$	(5.43)
4	$FR = K_F e^{J_{20}\left(\gamma_0 - \gamma_1 \frac{u_G}{H_{MT}} + \gamma_2 c_X + \gamma_3 c_C - \gamma_4 d_p\right)}$	(5.44)
5	$FR = K_F e^{J_{20}\left(\gamma_0 - \gamma_1 \frac{u_G}{H_{MT}} + \gamma_3 c_C - \gamma_4 d_p\right)}$	(5.45)
6	$FR = f_{conv} K_F u_G^{-\gamma_G} e^{J_{20}\left(\gamma_0 + \gamma_3 c_C - \gamma_4 d_p\right)}$	(5.46)

5.2.6   AnDFCm filtration: alternate models

The ΔR_{20}, which is inversely related with sludge filterability, is the additional resistance obtained when a specific permeate volume (V_F) of 20 L per m^2 of membrane area is produced in the AnDFCm installation. The ΔR_{20} was measured at 60 L m^{-2} h^{-1} (1.67×10^{-5} m^3 m^{-2} s^{-1}) flux (J_{AnDFCm}) and 1.5 m s^{-1} crossflow velocity ($u_{L,AnDFCm}$). At 60 L m^{-2} h^{-1} flux the final filtration time to obtain 20 L m^{-2} of permeate is 1,200 s. Therefore, the AnDFCm filtration models predicted ΔR_{20} as R_c after 1,200 s of continuous filtration under the operational conditions of the AnDFCm starting with a clean membrane, meaning the initial conditions are $w_C = 0$ and $w_X = 0$, thereby initial $R_c = 0$.

The cake layer resistance, R_C, was calculated with Equation (5.19), and combining the alternate SCR submodels described in Section 5.2.4.2 and the alternate deposition submodels in Section 5.2.4.3, with the following modifications:

- the gas superficial velocity in the AnMBR membrane tank (u_G) was replaced by the crossflow velocity in the AnDFCm membrane tube ($u_{L,AnDFCm}$=1.5 m s^{-1});

- the transmembrane flux was J=J_{AnDFCm} (1.67$\times$10^{-5} m^3 m^{-2} s^{-1}) and J_{20}=J_{AnDFCm} μ/μ_{20};

- there were no relaxation cycles (continuous filtration);

- the parameters of the mixed liquor viscosity model, a and b in Equation (5.41), were estimated based on the viscosity measurement performed in the AnDFCm installation with sludge samples with different TSS, presented in Section A1, Appendix A;

- the deposition submodels D1a and D1b were not used because they were equal to D1c for the AnDFCm installations; the superficial velocity in the AnDFCm installation ($u_{L,AnDFCm}$=1.5 m s^{-1}) was three orders of magnitude higher than in the AnMBR (0.5$\times$10^{-3} < u_G < 5.7$\times$10^{-3} m s^{-1}), and thus $I_{MS} \cong 1$ in equations (5.36) and (5.37).

The AnDFCm installation operates in continuous filtration mode and at fixed flux and crossflow velocity. Thus, in addition to D2 and D1c, a simplified deposition submodel was proposed, referred to as "Deposition submodel 3" (D3), as follows:

$$\omega_X = f_{X,c} \, V_F \, c_X \,, \tag{5.47}$$

$$\omega_C = f_{C,c} \, V_F \, c_C \,, \tag{5.48}$$

where $f_{X,c}$ and $f_{C,c}$ are the fractions of particulate and colloidal materials deposited onto the membrane, respectively. These fractions represent the balance between the different forces acting over the particles. When $f_{X,c}$ and $f_{C,c}$ both equal one, all the material is deposited in the membrane, analogous to dead-end filtration. Deposition submodel 3 consisted of algebraic equations instead of ordinary differential equations (ODE), which simplified the resolution and computational cost considerably. The deposition submodels D1c, D2 and D3 were coupled with the 7 alternate SCR submodels in Table 5.2, obtaining 21 alternate AnDFCm models to compare.

5.2.7   Model implementation and parameter values

5.2.7.1   Biochemical-flocculation model

The ODE of the biochemical-flocculation model was solved with the built-in ODE solver *ode15s* in Matlab® R2019b, using a time-step of 0.01 d (864 s). Most parameter values were taken from literature. Most parameter values were taken from literature, the values used for the non-adjustable parameters are described in Section A3, Appendix A.

Disintegration and hydrolysis are the rate limiting steps in anaerobic digestion and have a high variability and sensitivity (Batstone et al., 2002). Thus, the biomass disintegration ($k_{dis,bio}$) and hydrolysis rate coefficients were included in the model calibration. To simplify

Table 5.6. Nominal values and range for global sensitivity analysis (GSA) of the adjustable parameters in the biochemical-flocculation model.

Parameter	Units	Nominal value	Lower bound	Upper bound
$i_{C,CXI,bio}$	kgCOD kgCOD^{-1}	0.10	0	1
$i_{CI,CSInf}$	kgCOD kgCOD^{-1}	0.03	0	1
$i_{Saa,SInf}$	kgCOD kgCOD^{-1}	0.18	0	1
$i_{Sfa,SInf}$	kgCOD kgCOD^{-1}	0.20	0	1
$i_{SI,SInf}$	kgCOD kgCOD^{-1}	0.15	0	1
$i_{Ssu,SInf}$	kgCOD kgCOD^{-1}	0.10	0	1
$i_{Svfa,SInf}$	kgCOD kgCOD^{-1}	0.37	0	1
$i_{Xch,XInf}$	kgCOD kgCOD^{-1}	0.17	0	1
$i_{XI,XInf}$	kgCOD kgCOD^{-1}	0.19	0	1
$i_{Xli,XInf}$	kgCOD kgCOD^{-1}	0.42	0	1
$i_{Xpr,XInf}$	kgCOD kgCOD^{-1}	0.22	0	1
k_{ads}	d^{-1}	48	16	144
$k_{dis,bio}$	d^{-1}	0.15	0.0096	4.5
k_{floc}	d^{-1}	0.02	0.01	0.05
$k_{floc,fe}$	m kgCOD^{-1} m^3	4.2×10^{-4}	1.6×10^{-5}	1.0×10^{-3}
k_{hyd}	d^{-1}	0.50	0.0096	4.5
$K_{L,ads}$	m^3 kg^{-1}	7.6	2	1960
$q_{m,ads}$	kgCOD kg^{-1}	0.45	0.032	0.45
$Y_{fe,C}$	kg kg^{-1}	363	0.3	815

the calibration, a unique hydrolysis rate coefficient (k_{hyd}) was considered for all hydrolysis processes, which seems to be warranted considering the low loading rates applied to the pilot AnMBR (Guo et al., 2021). Previous research reported rate limiting values for primary sludge or blackwater ranging from 0.0096 to 4.5 d^{-1} (Batstone et al., 2002; Elmitwalli et al., 2006; Feng, 2004; Wendland, 2008). Therefore, the range for global sensitivity analysis (GSA) was set from 0.0096 to 4.5 for k_{hyd} and $k_{dis,bio}$, as shown in Table 5.6. The nominal value for k_{hyd} was the value for disintegration in the ADM1 which is rate limiting compared to the proposed hydrolysis rates. For $k_{dis,bio}$ the nominal value was the limiting rate for biomass degradation and hydrolysis (Tugtas et al., 2006).

The yield of product p on substrate i ($f_{p,i}$), except $f_{p,bio}$, were given the values suggested in the ADM1 (not shown). The yield of product p on biomass ($f_{p,bio}$) during biomass decay were assumed as follows: 0.104 carbohydrates, 0.664 protein, 0.032 lipids, 0.1 soluble inert and

0.1 suspended inert (Tugtas et al., 2006). The suspended inert material was composed of particulate and colloidal material individually calculate as follow:

$$f_{\text{CI,bio}} = i_{\text{C,CXI,bio}}\left(1 - f_{\text{SI,bio}} - f_{\text{Xch,bio}} - f_{\text{Xpr,bio}} - f_{\text{Xli,bio}}\right), \tag{5.49}$$

$$f_{\text{XI,bio}} = \left(1 - i_{\text{C,CXI,bio}}\right)\left(1 - f_{\text{SI,bio}} - f_{\text{Xch,bio}} - f_{\text{Xpr,bio}} - f_{\text{Xli,bio}}\right), \tag{5.50}$$

where $i_{\text{C,CXI,bio}}$ is the colloidal fraction of the biomass suspended inert material, which was an adjustable parameter between 0 and 1, with an initial estimation of 0.1, that is: 10% of the suspended inter material release during biomass decay is colloidal and 90% is particulate.

The exact composition of the blackwater that was used as influent in the biochemical-flocculation model was unknown. Therefore, the composition was estimated based on the blackwater characterisation in Table A2, literature values and adjustable parameters. The total concentration of soluble ($c_{\text{S,Inf}}$), colloidal ($c_{\text{C,Inf}}$) and particulate ($c_{\text{X,Inf}}$) materials in the influent were calculated as follows:

$$c_{\text{S,Inf}} = \text{csCOD}_{\text{BW}}\left(1 - i_{\text{C,CSInf}}\right), \tag{5.51}$$

$$c_{\text{C,Inf}} = \text{csCOD}_{\text{BW}}\, i_{\text{C,CSInf}}, \tag{5.52}$$

$$c_{\text{X,Inf}} = \text{csCOD}_{\text{BW}} - \text{tCOD}_{\text{BW}}, \tag{5.53}$$

where $i_{\text{C,CSInf}}$ is the content of colloidal material in the submicron material of the influent, which was an adjustable parameter between 0 and 1. The concentrations of hydrogen, methane, FE and biomass were assumed negligible in the influent. The concentration of each component i in the influent ($c_{i,\text{Inf}}$) was calculated as follows:

$$c_{i,\text{Inf}} = \begin{cases} i_{i,\text{SInf}}\, c_{\text{S,Inf}} & , & i \in [1,2,3,4,5,6,7,12] \\ i_{i,\text{XInf}}\, c_{\text{X,Inf}} & , & i \in [14,15,16,24] \\ c_{\text{C,Inf}} & , & i = 25 \\ \text{Alk}_{\text{BW}}\big/50.044 & , & i = 10 \\ \text{NH4}_{\text{BW}} & , & i = 11 \\ 0 & , & i \in [8,9,13,26] \\ 0 & , & 17 \leq i \leq 23 \text{ (biomass)} \end{cases} \tag{5.54}$$

where $i_{i,\text{SInf}}$ and $i_{i,\text{XInf}}$ are the content of component i in the soluble and particulate fractions of the influent, respectively. The particulate fraction was composed of carbohydrates ($i_{\text{Xch,XInf}}$), proteins ($i_{\text{Xpr,XInf}}$), lipids ($i_{\text{Xli,XInf}}$) and interts ($i_{\text{XI,XInf}}$). The soluble fraction was composed of volatile fatty acids (VFA) ($i_{\text{Svfa,SInf}}$), monosaccharides ($i_{\text{Ssu,SInf}}$), amino acids ($i_{\text{Saa,SInf}}$), long chain fatty acids ($i_{\text{Sfa,SInf}}$) and interts ($i_{\text{SI,SInf}}$). These parameters were optimised during model calibration, the initial values were taken from literature (Gorini et al., 2011; Wendland, 2008) and the range for GSA was set between 0 and 1. To reduce the amount of adjustable parameters, the total VFA content in the soluble material of the influent ($i_{\text{Svfa,SInf}}$) was optimised instead of the four individual acids in the model. The content of the individual VFA was as follows:

$$i_{i,\text{SInf}} = i_{\text{Svfa,SInf}}\, i_{i,\text{Svfa}}\,, \tag{5.55}$$

where $i_{i,\text{Svfa}}$ is fraction of component i in the total VFA fraction; $i_{i,\text{Svfa}}$ was 0.05, 0.08, 0.24, 0.63 for acetic, propionic, butyric and valeric acid, respectively (Wendland, 2008). For mass conservation $\sum_i i_{i,\text{XInf}} = 1$ and $\sum_i i_{i,\text{SInf}} = 1$, therefore, the model included the following equation to avoid values higher than 1 during model calibration:

$$i_{i,\text{XInf}} = \frac{i_{i,\text{XInf}}}{\sum_i i_{i,\text{XInf}}}\,, \tag{5.56}$$

$$i_{i,\text{SInf}} = \frac{i_{i,\text{SInf}}}{\sum_i i_{i,\text{SInf}}}\,. \tag{5.57}$$

The flocculation related parameters were all adjustable parameters because they were first introduced in this research. The nominal values and ranges used for GSA are summarised in Table 5.6. As explained in Chapter 2, the nominal values and range for the Langmuir adsorption parameters, $q_{m,\text{ads}}$ and $K_{L,\text{ads}}$, were based on previously reported values for the adsorption of polydiallyldimethylammonium chloride (polyDADMAC) onto different adsorbents (Horvath et al., 2006; Hubbe et al., 2011; Zhao et al., 2016).

The nominal value of the empirical flocculation coefficient (k_{floc}) was the inverse of the 50 days needed for d_p to return to $d_{p,\text{St}}$ in the pilot AnMBR after being spiked with FE. The range was the inverse of the period when d_p approximates to $d_{p,\text{St}}$ after the spike, which was between 20 and 100 days. The FE adsorption rate coefficient (k_{ads}) was estimated with the batch flocculation kinetic experiments described in Section A1, Appendix A.

The yield of inert colloidal material flocculated per unit of FE adsorbed onto the particulate material ($Y_{\text{fe,C}}$) and the FE induced flocculation coefficient ($k_{\text{floc,fe}}$) were calculated based on the FE dosage-step experiments described in Section 5.2.1.4 as follows:

$$Y_{\text{fe,C}} = \frac{\text{csCOD} - \text{csCOD}_0}{c_{\text{fe}}} \frac{\text{TSS}}{\text{csCOD}}\,, \tag{5.58}$$

$$k_{\text{floc,fe}} = \frac{d_p - d_{p0}}{c_{\text{fe}}}\,, \tag{5.59}$$

where csCOD_0 and d_{p0} are the csCOD and d_p without FE (at the beginning of the experiment), respectively. $Y_{\text{fe,C}}$ and $k_{\text{floc,fe}}$ were calculated for each test and at each FE dosage; the mean, minimum and maximum values were used as nominal, lower and upper bounds, respectively.

5.2.7.2   AnMBR and AnDFCm filtration models

The ODE of the deposition submodels was solved using *ode45* in Matlab® R2019b to obtain ω_C and ω_X as a function of time. The time-step was set sufficiently low, 10 s, to capture the operational stages (filtration and relaxation) in the pilot AnMBR and avoid numerical problems. Subsequently, the SCR was calculated applying the equations in Table 5.2.

Table 5.7. Nominal values of the adjustable parameters in the AnMBR and AnDFCm filtration models.

Parameter	Units	Values	Reference
Deposition parameters			
C_d	-	0.40	(Wu et al., 2012)
$f_{C,c}$	-	0.25	(Wu et al., 2012)
$f_{X,c}$	-	0.25	This research [a]
K_F	Pa s^{-1}	5.6×10^{-4}	(Robles et al., 2013b)
$K_{S,c}$	kg	0.2	(Robles et al., 2013b)
$q_{m,MS}$	-	4.71	(Robles et al., 2014b)
β_{ST}	-	1.75×10^{-4}	(Li and Wang, 2006)
γ	kg m^{-3}	2.0×10^{-5}	(Li and Wang, 2006)
γ_0	s m^{-1}	2.81×10^{6}	(Robles et al., 2013b)
γ_1	s^2 m^{-1}	2.48×10^{8}	(Robles et al., 2013b)
γ_2	s m^{-2} kg^{-1}	5.1×10^{4}	(Robles et al., 2013b)
γ_3	s m^{-2} kg^{-1}	1.28×10^{6}	This research [b]
γ_4	s m^{-2}	1.75×10^{10}	This research [b]
γ_G	-	2.15	This research [c]
Specific cake resistance parameters			
k_c	m^{-2}	1.0×10^{17}	(Li and Wang, 2006)
k_{CK}	-	4.0×10^{7}	This research [d]
P_a	Pa	2.01×10^{4}	(Robles et al., 2014b)
P_b	Pa	4179.9	(Mannina et al., 2011)
ε_{c0}	-	0.66	(Wu et al., 2012)
ζ_1	-	1.16×10^{3}	(Zarragoitia-González et al., 2008)
ζ_2	-	1.36×10^{4}	(Zarragoitia-González et al., 2008)
ζ_3	-	172.4	(Zarragoitia-González et al., 2008)
ζ_4	-	150.9	(Zarragoitia-González et al., 2008)
ρ_C	kg m^{-3}	4.98×10^{3}	(Wu et al., 2012)
ρ_X	kg m^{-3}	1.24×10^{3}	(Wu et al., 2012)

[a] Assumed equal to $f_{C,c}$.

[b] Estimated to achieve similar weights to particulate matter on FR as follow: $\gamma_3 = \gamma_2\, \bar{c}_X/\bar{c}_C$ and $\gamma_4 = \gamma_2\, \bar{c}_X/\overline{d_p}$, where $\bar{c}_X$, $\bar{c}_C$ and $\overline{d_p}$ are the mean values in the pilot AnMBR for particulate material, colloidal material and floc size, respectively.

[c] Calculated with the experimental representative data iD6 and iD7 from the pilot AnMBR as follows: $\gamma_G = -\,(\log(\overline{FR}|_{iD6}) - \log(\overline{FR}|_{iD7}))/(\log(\overline{u_G}|_{iD6}) - \log(\overline{u_G}|_{iD7}))$, where $\overline{FR}|_{iD6}$ and $\overline{FR}|_{iD7}$ are the mean fouling rate and $\overline{u_G}|_{iD6}$ and $\overline{u_G}|_{iD7}$ the mean superficial gas velocity in the datasets iD6 and iD7, respectively.

[d] Estimated to obtain $\alpha_{c,1} \approx \alpha_{c,2}$ as follows: $k_{CK} = k_c d_p^2$, assuming floc size of 2×10^{-5} m.

The intrinsic resistance of the membrane in the AnDFCm installation was $5 \times 10^{11}\,\text{m}^{-1}$ which was the resistance when filtering water after performing chemical cleaning. This value was assumed as the R_m for both the AnMBR and the AnDFCm.

The nominal values for the adjustable parameters in the filtration models are summarised in Table 5.7. Most parameters were taken from literature, and $K_{S,G}$, γ_3, and k_{CK} were estimated based on experimental data and different assumptions.

5.2.8 Model calibration and validation

5.2.8.1 General calibration procedure

The biochemical-flocculation model, the 34 alternate AnMBR filtration models and the 21 alternate AnDFCm filtration models were calibrated separately. The calibration procedure was as follows: first, the subset containing only influential parameters (θ_I) was selected using global sensitivity analysis (GSA). The GSA was based on linear regression models built from Monte Carlo simulations using Latin hypercube sampling with N = 500, where N was selected by convergence analysis (Section A4, Appendix A). The input uncertainty was uniform. In the filtration modes, the variability was set to 20% around the initial or nominal parameter vector ($\theta°$), this is $\theta \sim U(0.8\theta°, 1.2\theta°)$. In the biochemical-flocculation model the upper and lower limits for GSA were selected from literature or proposed based on experimental observations, as presented in Section 5.2.7.1.

The standardised regression coefficients (SRC, β_k) for each parameter k were computed using the objective function ($f_{\text{objective}}$) in Equation (5.60) as output. When $R^2 \geq 0.7$, influential parameters with $|\beta_k| \geq 0.1$ (Sin and Gernaey, 2016) were selected.

$$f_{\text{objective}} = \sqrt{\sum_j w_j \frac{\sum_i \left(y_{e,j,i} - y_{m,j,i}\right)^2}{n_j}}, \qquad (5.60)$$

where w_j is the weight, $y_{e,j,i}$ the i-th experimental value, $y_{m,j,i}$ the i-th predicted value, and n_j the number of experimental observations of the output variable j. For a unique output variable, $w_j = 1$ and the objective function becomes the root-mean-square error (RMSE). For multiple output variables, $f_{\text{objective}}$ was calculated using normalised values by defining w_j as the inverse of the mean experimental value as follows: $w_j = \left(\sum_i y_{e,j,i}/n_j\right)^{-1}$.

Alternatively, if $R^2 < 0.7$, individual $\beta_k(t)$ were computed using the predicted values $y(t)$ as model output for each operational time; then calculated the mean $\overline{\beta_k}$ using the $\beta_k(t)$ values when $R^2 \geq 0.7$; then selected the influential parameters with $\left|\overline{\beta_k}\right| \geq 0.1$.

Subsequently, the parameters in θ_I were estimated using the nominal parameter values as initial guess ($\theta°$), and by minimising $f_{\text{objective}}$. Initially, an identifiability analysis from θ_I was used to select a new subset θ_{II} that can be reliably estimated from the given experimental data; and the parameters in θ_{II} were estimated. Then, θ_{III} was defined with the parameters contained in θ_I and not in θ_{II}, and the parameters in θ_{III} were estimated. The quality of the

estimators $\hat{\theta}$ was evaluated based on the relative error ($\sigma_\theta / \hat{\theta}$) as follows: below 0.1 good, above 0.5 poor (Sin and Gernaey, 2016), and between 0.1 and 0.5 moderate.

The identifiability analysis was performed by computing the collinearity index of the parameter subset k (γ_k) (Sin and Gernaey, 2016). The parameter subset with γ_k below 10 which contained the most influential parameter and had the highest number of parameters was selected.

5.2.8.2   Biochemical-flocculation model

The adjustable parameters of the biochemical-flocculation model are summarised in Table 5.6. Initially, the parameters related to the flocculation kinetic process in the biochemical-flocculation model, namely the subset $\theta = \{q_{m,\mathrm{ads}}, K_{L,\mathrm{ads}}, k_{\mathrm{ads}}, Y_{\mathrm{fe,C}}, k_{\mathrm{floc,fe}}\}$, were optimised with the csCOD and d_p measured in the dosage-step experiments described in Section 5.2.1.4. Calibration was done by using the samples from the reactor fed with blackwater, and validation with the remaining samples.

Subsequently, the remaining parameters in the biochemical-flocculation model were optimised using the long-term measurements of cCOD, TSS and d_p in the pilot AnMBR described in Section 5.2.1.3. The following experimentally measured variables were model inputs: Q_P, Q_WS, V_L, T, p_G, pH, $\dot{m}_\mathrm{fe}$, and blackwater characteristics (Alk$_\mathrm{BW}$, NH4$_\mathrm{BW}$, tCOD$_\mathrm{BW}$, and csCOD$_\mathrm{BW}$). The blackwater characteristics varied throughout the day and during the operation of the pilot, further explained in Chapter 4. The mean values, presented in Table A2, were used as model inputs for model implementation. The same dataset was used for calibration and validation of the long-term prediction, and thus the biochemical-flocculation model requires further validation with an independent dataset from a different operational period of the pilot or from another AnMBR.

5.2.8.3   AnMBR filtration model

The AnMBR filtration model was calibrated and validated using fouling rate data from the pilot AnMBR described in Section 5.2.1.3. The initial parameter subset is summarised in Table 5.7. The following experimentally measured variables were model inputs: J, u_G, T, c_C, c_X, and d_p.

The model was calibrated using eight datasets from the operation of the pilot AnMBR, shown in Figure A1 and Figure A2, whereby each dataset covered an 8-hour period. These 8 calibration datasets were selected to capture changes in the following operational conditions: gas sparging, mean particle size, and concentration of colloidal and particulate material. The model was validated by predicting the entire operational period of the pilot. However, the validation should be improved by applying the model to a different operational period of the pilot or to another AnMBR, but this data was not available during this research.

5.2.8.4   AnDFCm filtration model

The AnDFCm model was calibrated using in-situ ΔR_{20} measurement in the pilot AnMBR immediately after FE dosing and ex-situ ΔR_{20} measurement during the dosage-step tests BWa and BWb in Table A3 performed with grab samples from the pilot AnMBR. The model was validated using long-term in-situ measurements of ΔR_{20} measured in the pilot AnMBR. The initial parameter subset is shown in Table 5.7. The following experimentally measured variables were model inputs: $u_{L,AnDFCm}$, J_{AnDFCm}, T, c_C, c_X, and d_p.

5.2.9   Control tools for flux enhancer dosage

Several feedforward and feedback control tools to manipulate the FE mass flow rate fed to the reactor ($\dot{m}_{fe}$) were proposed and compared, as summarised in Table 5.8. The control tool FB_ΔR_{20}_10 is a feedback loop to control ΔR_{20} to a target setpoint ($\Delta R_{20,sp}$); $\Delta R_{20,sp}$ of $10\times10^{12}\,\text{m}^{-1}$ is an intermediate value between the pilot operation before and immediately after FE dosing (Figure A3). The control tool FB_ΔR_{20}_8-12 is similar to the latter, but ΔR_{20} is maintained inside a target range instead of to a specific value. FB_ΔR_{20}_8-12 starts dosing FE (on) when ΔR_{20} is above $12\times10^{12}\,\text{m}^{-1}$ and stops (off) when ΔR_{20} is below $8\times10^{12}\,\text{m}^{-1}$, thereby causing periodic FE pulses instead of a continuous dosage (as in FB_ΔR_{20}_10).

The feedforward control tool FF_Q_{WS} is analogous to the mostly applied FE dosing strategy reported in literature, that is: an initial FE pulse dosage that is followed by periodic additions to compensate for the loss of FE with sludge withdrawal and biodegradation (Chapter 4), with the objective to maintain a certain concentration of FE inside the reactor. The FE is not biodegradable in the proposed model, therefore, FF_Q_{WS} does not compensate for FE loss by biodegradation. Furthermore, an alternative dosing strategy used in literature is a step of FE on the influent (Dong et al., 2015, 2018), which was implemented in the control tool FF_Q_{Inf}.

The simulation without FE dosing, No_FE, was included to assess the improvement achieved when FE is added to the reactor by the control tools. Moreover, the feedback c_{fe} control tool FB_c_{fe} was included to compare with FF_Q_{WS} and FF_Q_{Inf}, whose controlled variable is also c_{fe}. Nevertheless, to apply FB_c_{fe} in practice a method to measure c_{fe} should be developed.

The feedback control tools were manually tuned to achieve a slow response (low $\dot{m}_{fe}$) to avoid overdosing. The FE concentration setpoint ($c_{fe,sp}$) was 8.7×10^{-3} kgCOD m^{-3}, which is equal to the concentration needed to achieve a ΔR_{20} of 10×10^{12} m^{-1} at the beginning of the simulated operational period. For FF_Q_{Inf}, the ratio of FE to influent flow ($Y_{fe,Inf}$) was 7.23×10^{-4} kgCOD m^{-3}, calculated as the ratio between the cumulative masses of FE and influent fed to the reactor during the first 100-day period simulated with FB_ΔR_{20}_10.

The control tools were implemented and tested in Simulink, Matlab® 2019b, by using the integrated model composed by the calibrated biochemical-flocculation model, and the best alternates of the calibrated AnMBR and AnDFCm filtration models. The implementation

Table 5.8. Control tools to manipulate the mass flow rate of flux enhancer ($\dot{m}_{fe}$) to an AnMBR.

Reference	Type of control	Measured variable	Controlled variable	$\dot{m}_{fe}$ calculation
FB_ΔR_{20}_10	Feedback, proportional	ΔR_{20}	ΔR_{20}	$1.6\times10^{-7}(\Delta R_{20} - \Delta R_{20,sp})$
FB_ΔR_{20}_8-12	Feedback, on-off	ΔR_{20}	ΔR_{20}	5×10^{-6}
FB_c_{fe}	Feedback, proportional	c_{fe}	c_{fe}	$1\times10^{-3}\left(c_{fe,sp} - c_{fe}\right)$
FF_Q_{WS}	Feedforward, pulse + proportional [a]	Q_{WS}	c_{fe}	$Q_{WS}\, f_{Xfe,WS}\, c_{fe,sp}$
FF_Q_{Inf}	Feedforward, proportional	Q_{Inf}	c_{fe}	$Y_{fe,Inf}\, Q_{Inf}$
No_FE	No control	NA	NA	0

[a] Initial pulse dosage to achieve the setpoint $c_{fe,sp}$ followed by continuous additions to compensate for the loss of flux enhancer with sludge withdrawal.

included a feedback TSS controller which manipulated Q_{WS} to sustain the TSS at a fixed setpoint (TSS_{sp}). A constant mixed liquor volume was assumed, whereby Q_{Inf} was calculated with the mass balance in Equation (A.5) with $\Delta V_L=0$; and $Q_{fe}=\dot{m}_{fe}/c_{fe,stock}$, where $c_{fe,stock}$ is the concentration of the stock solution fed to the reactor (30 kgCOD m^{-3}).

The model inputs T, pH, J_{20}, NH4$_{BW}$, Alk$_{BW}$, and u_G were assumed constant and equal to the mean values in the pilot AnMBR (Table A1 and Table A2). The total and submicron blackwater COD fluctuated inside the range of the pilot; the input shown in Figure A7 was generated with the "uniform random number" block from Simulink, with the minimum and maximum values from Table A2, seed of 30 days (the pattern is repeated every 30 days) and sample time of 12 min (changes every 12 minutes).

The fraction of component in the waste sludge, $f_{i,WS}$, were estimated based on the sludge withdrawal made on day 123, where 31% of the mixed liquor volume was removed causing a 62% decrease in TSS and 7% decrease in csCOD. Therefore, $f_{i,WS}$ was assumed as 2.0 for all particulate material ($f_{X,WS}$), and 0.22 for colloidal material ($f_{C,WS}$).
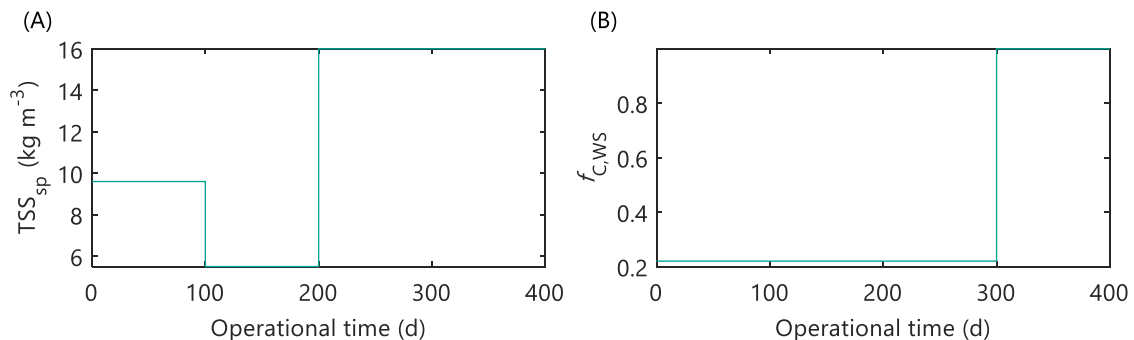
Figure 5.3. Applied disturbances to test the robustness of the control tools: (A) total suspended solids setpoint, and (B) fraction of colloidal material in the waste sludge.

Furthermore, the robustness of the control tools was tested by applying step disturbances in TSS_{sp} and $f_{C,WS}$, displayed in Figure 5.3. The TSS_{sp} were 9.6, 5.5 and 16.0 kg m^{-3} corresponding to the mean, minimum and maximum TSS in the pilot. The initial $f_{C,WS}$ was 0.22 and increased to 1 on day 300, owing to a better mix before wastage.

5.3   RESULTS AND DISCUSSION

5.3.1   Experimental data

The experimental results of the pilot AnMBR and batch tests are summarised in Section A1, Appendix A.

5.3.2   Biochemical-flocculation model

5.3.2.1   Calibration of fast processes

The influential parameters, selected with GSA, in the subset $\theta = \{q_{m,ads}, K_{L,ads}, k_{ads}, Y_{fe,C}, k_{floc,fe}\}$ were estimated to fit the experimental csCOD and d_p measured in the dosage-step experiments using sludge samples from a reactor fed with blackwater.

The linear models built using $f_{objective}$ had R^2 of 0.63 and 0.06 for the variables csCOD and d_p, respectively; and R^2 was 0.52 when both csCOD and d_p were used together in $f_{objective}$. Consequently, because R^2 were below 0.7, these models built with $f_{objective}$ were not used for sensitivity evaluation. Instead, as described in Section 5.2.8, the sensitivity was evaluated with the mean SRC $(\overline{\beta_k})$ of the linear models that had $R^2 > 0.7$, the models were built with the predicted csCOD or d_p at each operational time instant. The mean R^2 were 0.90 and 0.98 for csCOD and d_p, respectively. Results in Table A10 show that $Y_{fe,C}$ was the only

Figure 5.4. Short-term biochemical-flocculation model calibration. Sludge characteristics during flux enhancer dosage-step test with sludge samples from a pilot AnMBR fed with blackwater: (A) submicron COD, and (B) mean geometric particle diameter.

influential parameter (with $\left| \overline{\beta_k} \right| \geq 0.1$) on csCOD, and $k_{\text{floc,fe}}$ on d_p. Therefore, the parameters were estimated separately for each output variable as follows: $k_{\text{floc,fe}}$ was estimated to fit the experimental d_p, and $Y_{\text{fe,C}}$ to fit the experimental csCOD.

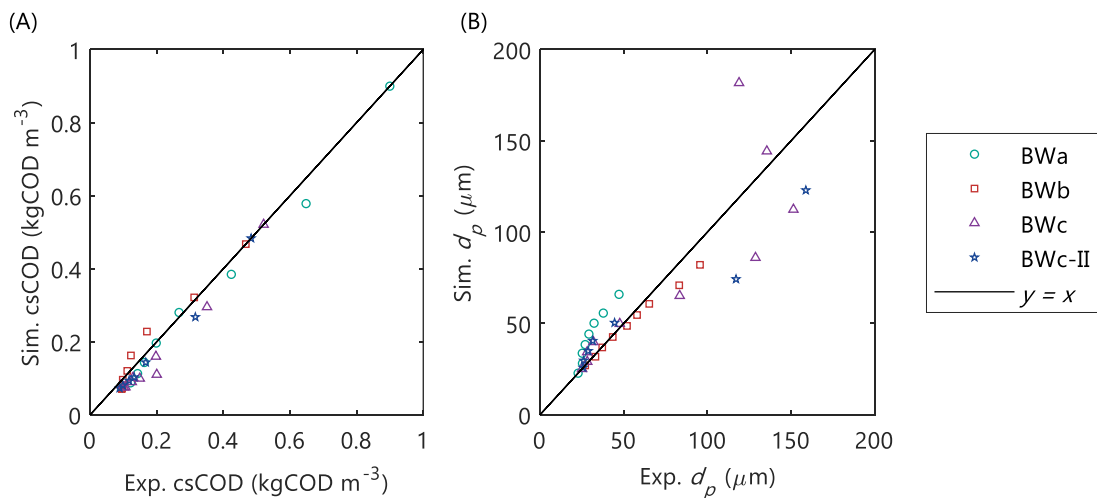Results in Table A10 show that the optimal values ($\hat{\theta}$) had good quality because the relative error, $\sigma_\theta / \hat{\theta}$, was below 0.1 (Sin and Gernaey, 2016). Figure 5.4 compares the experimental observations with the simulated values for the calibrated parameters. The model satisfactorily predicted the csCOD in the batch tests; however, the model overestimated or underestimated the floc size for a considerable number of observations. Therefore, the model in Equation (5.15) could be further developed to improve the prediction of floc size changes caused by FE dosing.

5.3.2.2 Calibration of slow processes

Table A11 summarises the SRC of the linear models built using $f_{\text{objective}}$ with different output variables. The linear model with TSS had an R^2 below 0.7, and thus the sensitivity on TSS was evaluated with the $\overline{\beta_k}$ of the linear models that had $R^2 > 0.7$, results in Table A11.

Based on the GSA results, k_{floc} was estimated with d_p as a unique output variable because k_{floc} was the only influential parameter on d_p and had a negligible influence on TSS and cCOD. Then, $i_{\text{CI,CSInf}}$ and $i_{\text{Xli,XInf}}$ were estimated with cCOD and TSS as output variables because they were the only influential parameter on cCOD and the most influential parameters on TSS. The subset $\{i_{\text{Xch,XInf}}, i_{\text{Xli,XInf}}, i_{\text{Xpr,XInf}}\}$ was also influential on TSS, however, the model did not improve further by optimising this subset with TSS as output variable, the optimal values were almost identical to the initial guess, thus, the initial (nominal) values were used for $i_{\text{Xch,XInf}}$, $i_{\text{Xli,XInf}}$ and $i_{\text{Xpr,XInf}}$. Table A12 summarises the estimated parameters. The parameters $i_{\text{CI,CSInf}}$ and $i_{\text{Xli,XInf}}$ had good quality, whereas k_{floc} had medium quality.

Figure 5.5 shows the experimental data and model predictions with the estimated parameters. The model predicted a sharp cCOD decrease and d_p increase caused by FE dosing on day 16. Then cCOD slowly increased over time due to the accumulation of colloidal inerts coming from the influent, decayed biomass, and deflocculation. The latter was caused by the loss of unbonded FE (S_{fe}) with the permeate flow that lowered the equilibrium concentration $X_{\text{fe},e}$ causing desorption of FE from the particulate material (i.e., $\rho_{23} < 0$), displayed in Figure A8B, and concomitantly deflocculation (i.e., $\rho_{24} < 0$).

The predicted d_p decrease, after the sharp increase on day 16, was overpronounced compared to the experimental observations. To improve the prediction capacity, Equation (5.15) was substituted with the modified Equation (5.61):

$$\frac{dd_p}{dt} = \frac{1}{t_{\text{conv}}} \left(k_{\text{floc,fe}} \frac{dX_{\text{fe}}}{dt} + \left(Y_{\text{floc,fe}} \left(\frac{c_{\text{fe}}}{c_{\text{X}} + c_{\text{C}}} \right) d_{p,\text{St}} - d_p \right) k_{\text{floc}} \right), \qquad (5.61)$$

where the stable mean particle size was proportional to the ratio between c_{fe} and the total concentration of suspended material ($c_X + c_C$) inside the reactor, with a proportionality parameter $Y_{floc,fe}$.

The parameters k_{floc} and $Y_{floc,fe}$ were optimised to fit the experimental floc size; the optimal values for k_{floc} and $Y_{floc,fe}$ were 0.34 d^{-1} and 46.9 kg kgCOD^{-1} with $\sigma_\theta/\hat{\theta}$ of 0.28 and 0.35, respectively. Figure 5.5A shows that the modified model in Equation (5.61) adjusted better to the experimental values than the original model in Equation (5.15).

The model predicted a continuous TSS increase, shown in Figure 5.5A, caused by the accumulation of inert material (Figure A8B) coming from the influent and decaying biomass because the reactor was operated without sludge wastage. Because the model considered constant influent composition, the fluctuations in TSS were caused by fluctuations of the influent flow rate and of the temperature and pH of the mixed liquor (which affect the conversion rates). However, in the pilot AnMBR the fluctuations in the solids content was affected by variations in the blackwater composition, which was highly variable throughout
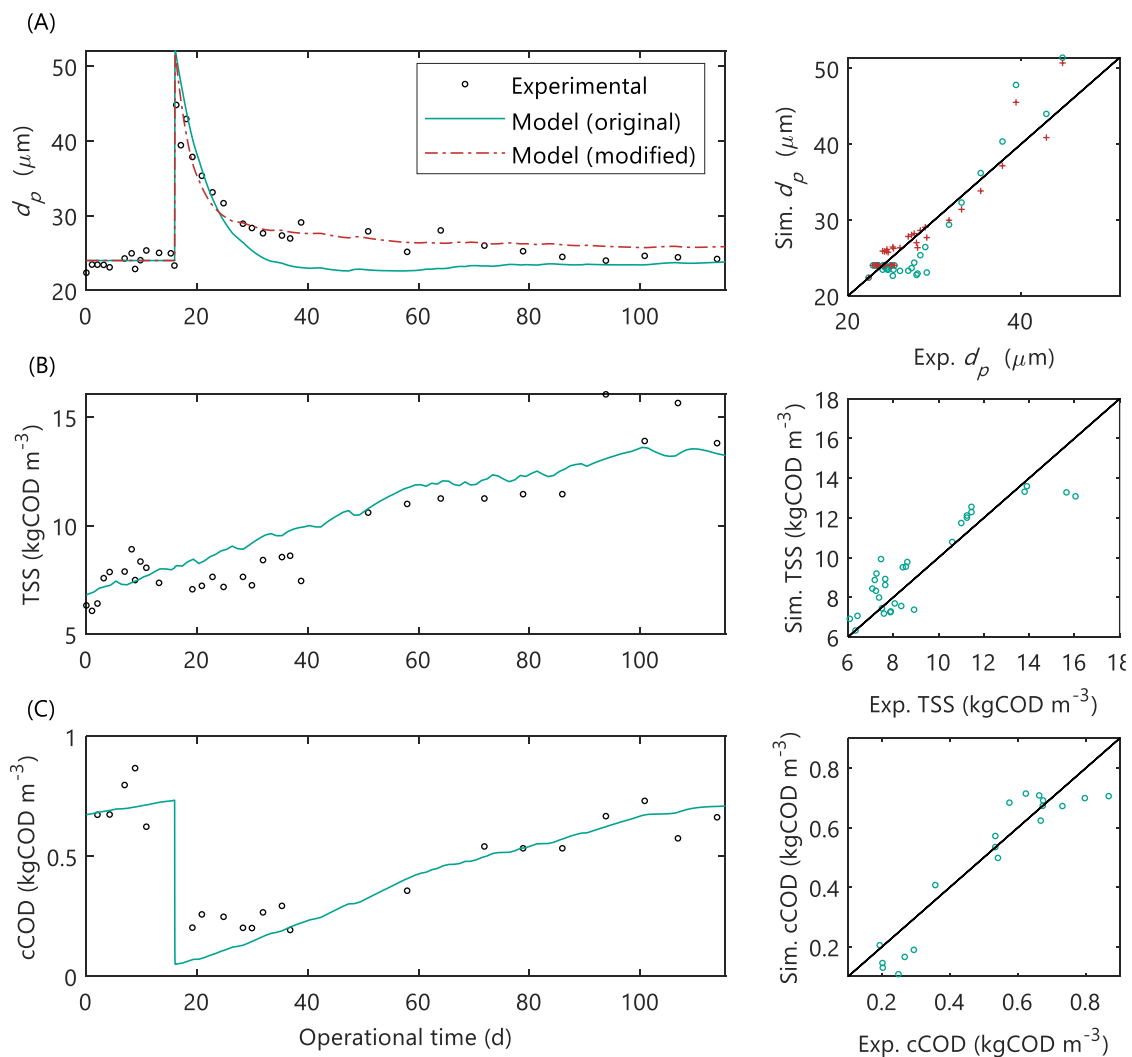

Figure 5.5. Long-term biochemical-flocculation model calibration. Sludge characteristics during operational period of pilot AnMBR plant dosed with flux enhancer on day 16: (A) mean particle diameter, (B) total suspended solids, and (C) colloidal COD.

the operational period (Chapter 4). Therefore, the predicted TSS deviated from the experimental values likely due to the lack of an exact characterisation of the influent. Additionally, the applied physicochemical characterization was not sufficient to detect all the fluctuations in the exact blackwater composition. Therefore, a more comprehensive and frequent blackwater characterization using flow-proportional sampling should be done to predict the exact TSS dynamics.

5.3.2.3   Interaction of flux enhancer with soluble microbial products

The sample LiqOFMSW had a substantially high concentration of humic substances (HS), 5.16 g L^{-1} (Table A3). Humic substances have negatively charged carboxylic and phenolic groups that bind to cationic polymers (Bratby, 2016). Particularly, polyDADMAC, which is the chemical compound in Adifloc KD451, has been used for titration of HS due to their high interaction (Ishiguro et al., 2007; Kam and Gregory, 2001; Tan et al., 2011). Therefore, the biochemical-flocculation model described in Section 5.2.3, which did not include FE-HS binding, was extended to include the interaction between FE and HS. The FE-HS binding was implemented as a linear model (Chianese et al., 2020) and assuming equilibrium conditions, meaning that the adsorption of FE onto HS was assumed considerably faster than the adsorption of FE onto particulate material. The concentration of FE bonded to HS ($c_{\text{fe,hs}}$) was calculated with Equation (5.62), where $K_{eq,\text{fe,hs}}$ is the equilibrium coefficient and S_{hs} the concentration of HS. The mass balance of FE in Equation (5.63) substituted Equation (5.11).

$$c_{\text{fe,hs}} = \frac{K_{eq,\text{fe,hs}}\, S_{\text{hs}}\, S_{\text{fe}}}{K_{eq,\text{fe,hs}}\, S_{\text{hs}} + 1}, \qquad (5.62)$$

$$S_{\text{fe},e} = c_{\text{fe}} - X_{\text{fe},e} - c_{\text{fe,hs}}. \qquad (5.63)$$

The equilibrium coefficient, $K_{eq,\text{fe,hs}}$, was optimised to fit the experimental csCOD and d_p measured in the dosage-step experiments using the samples from the reactor fed with blackwater and LiqOFMSW.

A similar approach could be followed for the interaction of the FE with carbohydrates and proteins. The overall charge of proteins is negative when the pH is above their isoelectric point (pI); and carbohydrates are negatively charged when they contain carboxylic groups or sulphuric ester groups. To incorporate the interaction of the FE with humic substances, proteins or carbohydrates the overall charge of these components should be measured, for example by titration, but this was outside the scope of this research. In Chapter 2, a strong correlation was found between the SMP-CH and the optimal FE dosage needed for filterability improvement. Thus, the model was further extended to incorporate FE-CH binding, with the equilibrium coefficient $K_{eq,\text{fe,ch}}$ and using the same modelling and calibration approach as for FE-HS binding.

Figure 5.6 and Figure 5.7 compare the experimental csCOD and d_p with the predicted values of models including and excluding FE binding to HS and CH. The predicted csCOD and d_p in LiqOFMSW with the models without FE binding (onto HS, CH and proteins) and

including only FE-CH binding greatly deviated from the experimental data, whereas the predictions with both models including FE-HS binding approximated the experimental data. Therefore, the models suggest that limited flocculation observed in LiqOFMSW was likely caused by the interaction of the FE with the humic substances in the sample. Furthermore, the models including only FE-HS deviated more in the remaining samples than the model that included both FE-CH and FE-HS binding. This suggested that the interaction between FE and carbohydrates might also limit flocculation.

The samples Food3 and Food3-II were collected from a reactor fed with whey and wash-water. Alpha-lactoglobulin (pI=4.2) and beta-lactoglobulin (pI=5.2) are the two major

Figure 5.6. Experimental and simulated submicron COD during flux enhancer dosage-step test with sludge samples from different sources. Comparison of predictions with models including and excluding the interaction of the flux enhancer (FE) with soluble humic substances (HS) and carbohydrates (CH).

whey proteins, which at the pH of the samples (pH=7.2) have an overall negative charge. Thus, in Food3 and Food3-II the overpredicted flocculation (Figure 5.6F,G and Figure 5.7F,G) could be caused by the limited availability of FE for colloidal flocculation due to its interaction with the negatively charged proteins in the samples.
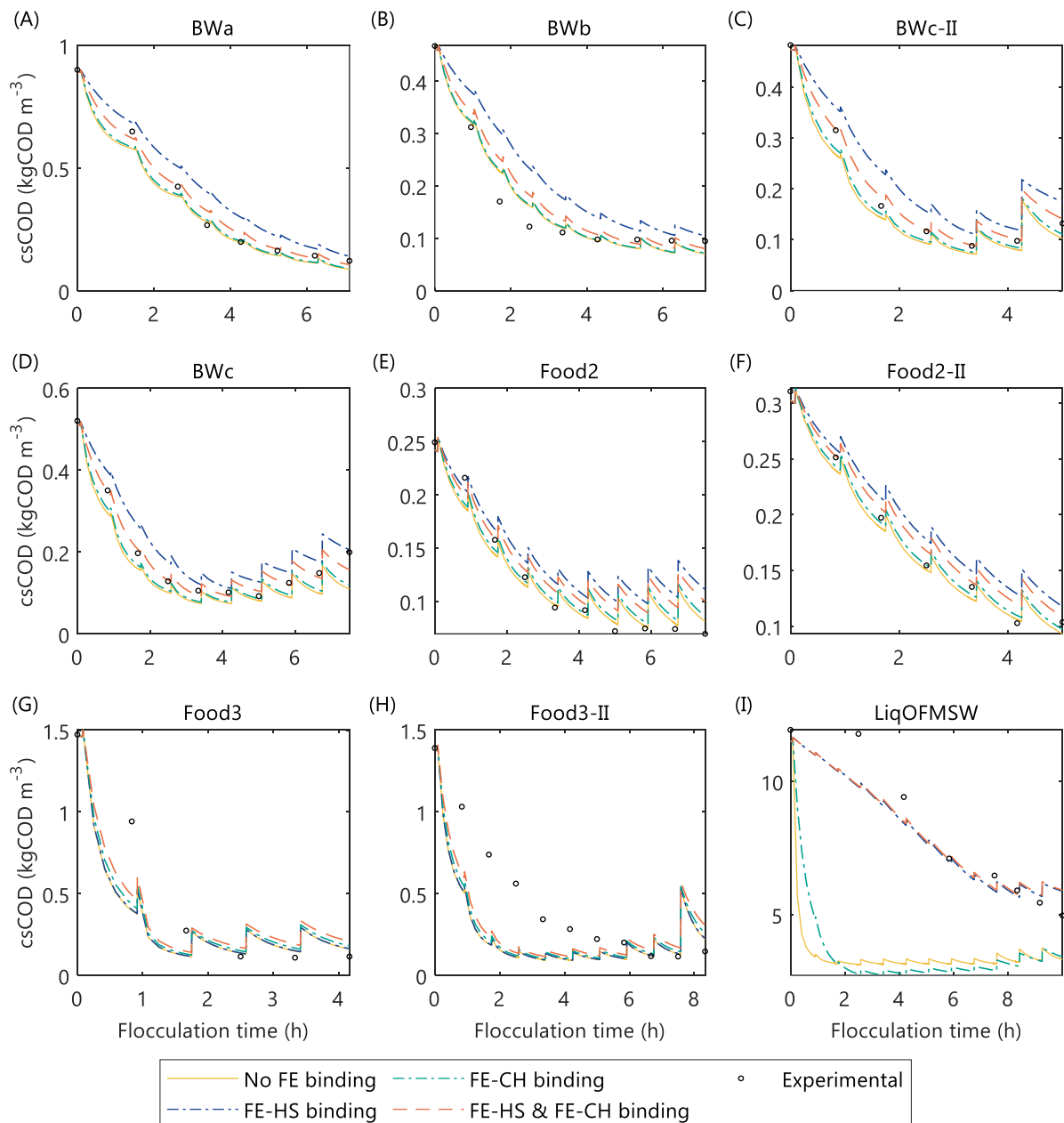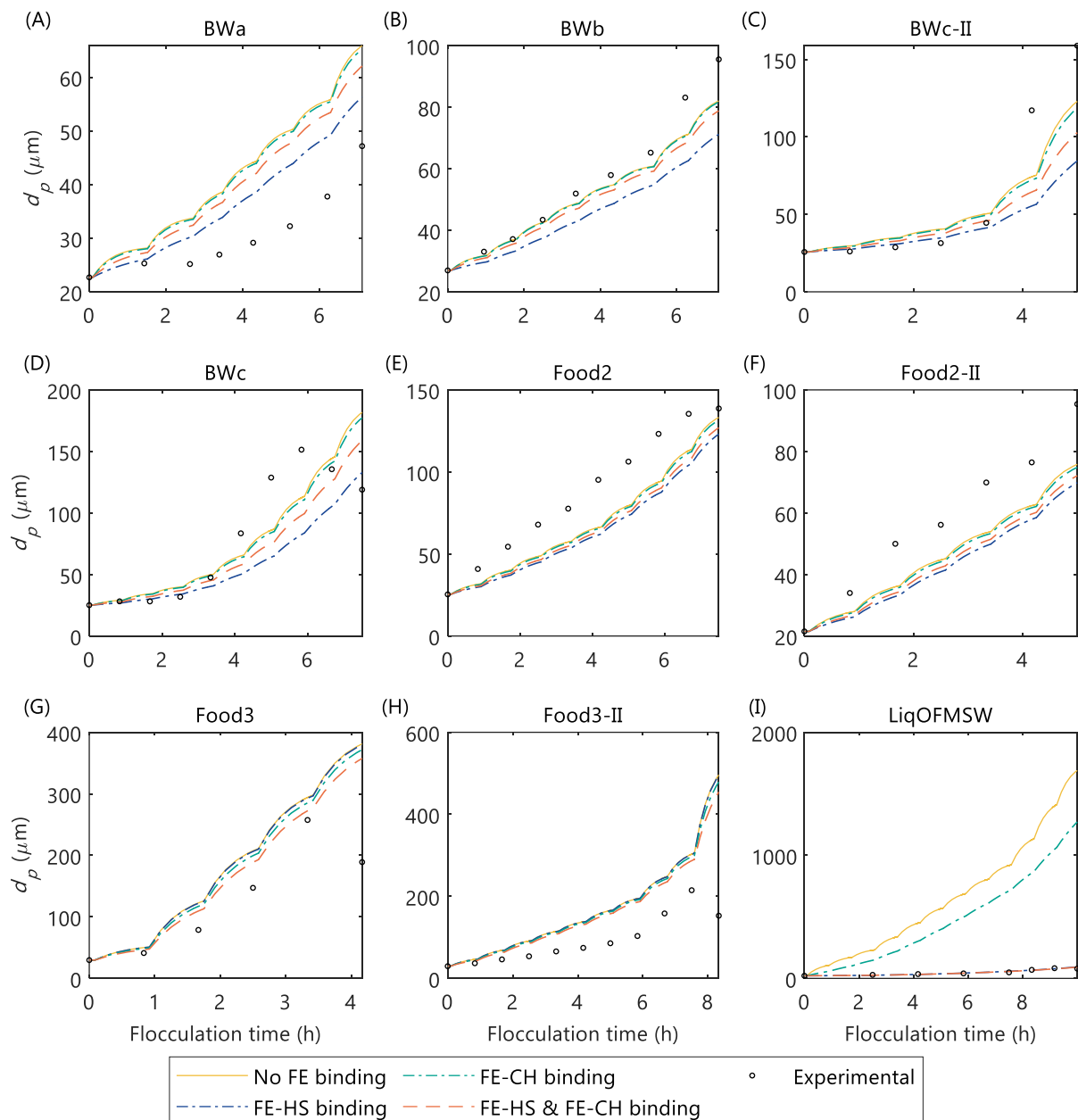

Figure 5.7. Experimental and simulated mean particle diameter during flux enhancer dosage-step test with sludge samples from different sources. Comparison of predictions with models including and excluding the interaction of the flux enhancer (FE) with soluble humic substances (HS) and carbohydrates (CH).

5.3.3 AnMBR filtration model

5.3.3.1 Calibration of alternate empirical FR models

The GSA results, in Table A13, showed that almost all parameters, except γ_G, were influential in the empirical FR models and were therefore optimised. The parameters were estimated using the representative dataset from the pilot AnMBR (shown in Figure A2A), the optimal values and quality of the estimators are summarised in Table A16. Figure A9 compares the experimental FR in the representative dataset with the predicted values using the optimised parameters for each empirical FR model. The calibrated models were unable to predict accurately each specific FR values, nevertheless, the FR trend was well predicted.

In Table A16, most estimators presented good ($\sigma_\theta/\hat{\theta} \leq 0.1$) or moderate ($0.1 < \sigma_\theta/\hat{\theta} \leq 0.5$) quality, except γ_2 which had poor quality ($\sigma_\theta/\hat{\theta} > 0.5$). The parameter γ_2 represents the influence of c_X on FR, and thus the high relative error of γ_2 agreed with previous research that reported that the concentration of particulate material is a poor indicator of biomass fouling propensity by itself (Judd and Judd, 2011). Accordingly, in Figure 5.8 the empirical models FR1 and FR2 had identical predictions during the entire operation of the pilot AnMBR; the only difference between these models is that FR1 included c_X and FR2 did not. Apparently, c_X had no influence on FR prediction in this research and could therefore be removed from the model. The same conclusion was derived after comparing FR4 and FR5.

5.3.3.2 Calibration of alternate FR_RIS models

Table A14 summarises the GSA results for the RIS AnMBR filtration models. The parameters C_d, β_{ST}, k_c, k_{CK}, ε_{c0}, ρ_X, and P_b were influential in all models, and γ_0, ζ_2 and ζ_3 were influential in most models; whereas $f_{C,c}$, γ, K_F, γ_3, and ρ_C were none-influential in all models, and $K_{S,c}$, $q_{m,MS}$, γ_1, γ_2, P_a, ζ_1, and ζ_4 were only influential in a few models. Particularly, ε_{c0} was the most influential parameter in all the models that included it, presenting SRC between 0.77 and 0.93.

The parameters were estimated using the representative dataset from the pilot AnMBR. The optimal values and quality of the estimators are summarised in Table A17. Figure A10 to Figure A13 compare the experimental FR with the predicted values using the optimised parameters for each model.

The majority of the models that included a SCR submodel based on the empirical equation by Cho et al. (2005), namely $\alpha_{c,3}$, $\alpha_{c,3p}$ and $\alpha_{c,4p}$, had at least one estimator with poor quality ($\sigma_\theta/\hat{\theta} > 0.50$). Additionally, these models were unable to predict the experimental FR in the representative dataset used for calibration. The models D1a $\alpha_{c,3p}$ and D1c $\alpha_{c,4}$ considerably underpredicted the FR when c_C was high (iD1 and iD2). The models D1b $\alpha_{c,3p}$ and D1c $\alpha_{c,3p}$ predicted FR well at high c_C but underpredicted the FR when c_C was low (iD4 to iD8). The remaining models had considerably poor FR predictions for all the representative datasets. Therefore, the models that included $\alpha_{c,3}$, $\alpha_{c,3p}$ or $\alpha_{c,4}$ could not be satisfactorily calibrated with the procedure described in Section 5.2.8.

Conversely, all the models that included a SCR submodel that is based on the Carman-Kozeny equation (i.e., $\alpha_{c,1}$, $\alpha_{c,1p}$, $\alpha_{c,2}$ and $\alpha_{c,2p}$) presented good estimators' quality ($\sigma_\theta/\hat{\theta} \leq 0.1$) and FR at high and low c_C in the representative dataset was well predicted. However, all these models considerably underpredicted FR when the reactor operated at low u_G (dataset iD6); and most models, except D1c $\alpha_{c,1}$ and D1c $\alpha_{c,2}$, slightly overpredicted FR when c_X was high (dataset iD3).

5.3.3.3 Long-term model validation

The prediction capacity of the calibrated models was assessed by analysing the prediction during the entire operation of the pilot AnMBR, shown in Figure 5.8 for the empirical FR models and in Figure 5.9 for the FR_RIS models that included Carman-Kozeny based SCR submodels. The y-axis was limited between 0-60 for better visualization and discussion; Figure A14 to Figure A22 display the individual plots for each model without imposed limits. The models that included the SCR submodels $\alpha_{c,3}$, $\alpha_{c,3p}$ or $\alpha_{c,4}$ were not further analysed because they could not be satisfactorily calibrated with the procedure described in Section 5.2.8, and thus were unable to predict the representative data used for calibration.

In general terms, all the FR_RIS models in Figure 5.9 and empirical FR models in Figure 5.8 predicted satisfactorily the effect of c_C on the fouling rate. During the period without FE (0-16 d) the experimental and predicted FR values were considerably higher than the FR after FE dosing (after day 16). Nevertheless, during the initial period (0-16 d), the empirical FR
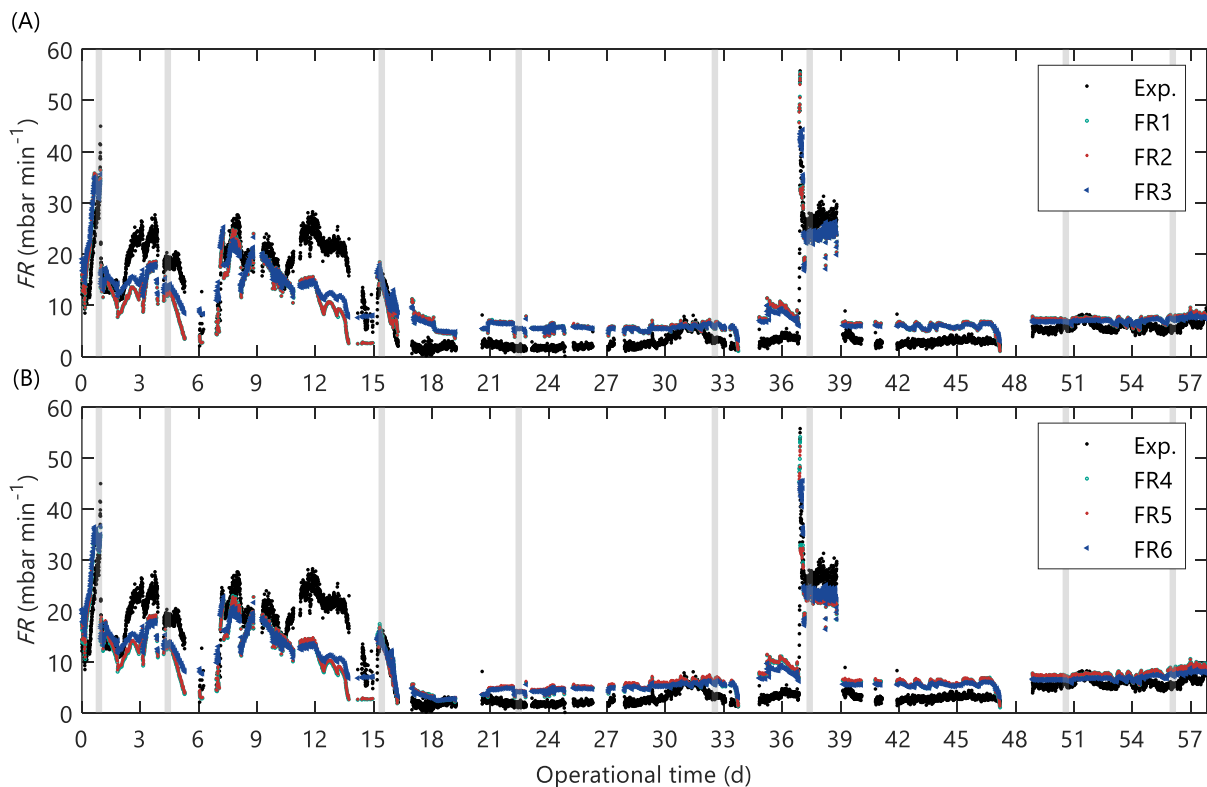
Figure 5.8. Validation of the AnMBR empirical fouling rate (FR) models which (A) exclude and (B) include floc size as input variable. The grey vertical areas represent the representative dataset (iD1 to iD8 from left to right) used for model calibration. Imposed limits between 0-60 in y-axis.
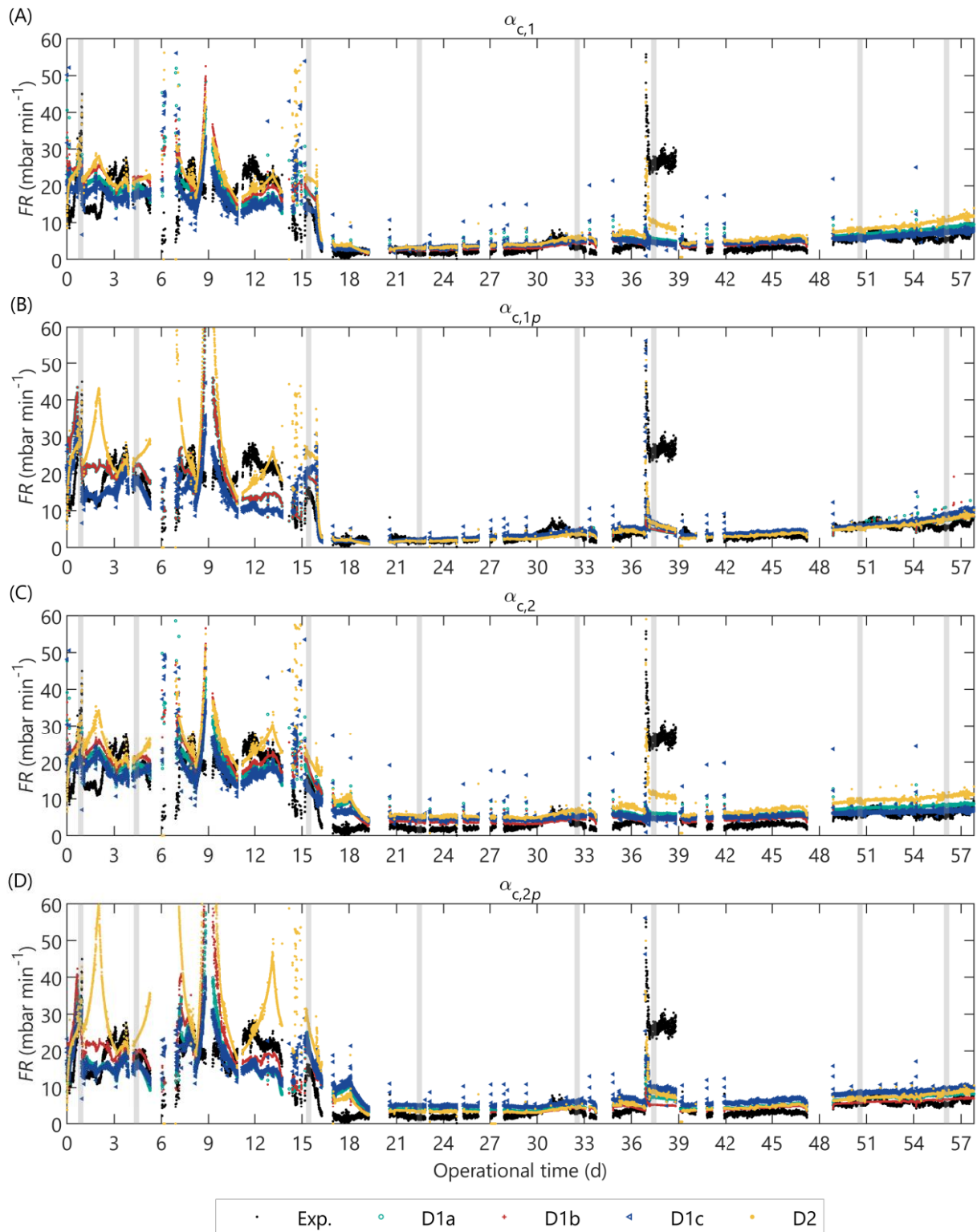
Figure 5.9. Validation of the alternate FR_RIS AnMBR filtration models combining the different deposition submodels (D1a, D1b, D1c and D2) with the Carman-Kozeny based specific cake resistance submodels: (A) $\alpha_{c,1}$, (B) $\alpha_{c,1p}$, (C) $\alpha_{c,2}$ and (D) $\alpha_{c,2p}$. The grey-vertical areas represent the representative dataset (iD1 to iD8 from left to right) used for model calibration. Imposed limits between 0-60 in y-axis

models considerably underpredicted the FR at high u_G (periods 4.5-7 and 12-15 days), this is further explained below. The deposition submodels based on Robles et al. (2013), that is D1a, D1b and D1c, presented similar behaviour, and D1b was slightly more sensitive to c_C than D1a and D1c because in D1b c_C affects the deposition of particulate material through I_{MS}.

The lack of online gas flow measurements was a limitation for model calibration and validation, especially for the empirical FR models that are highly sensitive to u_G. For example, the biggest deviation between the experimental data and the predicted values was between days 12 and 15 where the reactor operated at a low liquid level in the membrane tank (H_{MT}) causing a high simulated u_G, calculated with Equation (A.1). However, the simulated u_G during this period could not be confirmed with experimental data, therefore, it could not be confirmed that the input variable u_G was correct or if the actual values were lower, and the model could have predicted the FR accurately. Similarly, in the period 34.8-36.8 d the simulated u_G was 8 to 36% lower than the experimental (manually recorded) u_G which caused the overpredicted FR values. Therefore, to improve model calibration and validation the biogas should be monitored online to provide a reliable input variable.

Similarly, the use of grab samples for determining the as input variables for sludge characterization limited model calibration and validation. This was particularly true for the fluctuating sludge characteristics that were highly influential in the model, such as c_C, which was calculated as the difference between the measured csCOD and pCOD. The pCOD was relatively stable during the reactor operation, however, csCOD fluctuated considerably (particularly before FE dosing on day 16) and had only few datapoints. For model implementation, linear interpolation between measurements were applied resulting in c_C with sharp fluctuations and peaks that caused fluctuations in the simulated FR, but the true values of c_C between grab samples could not be confirmed, hampering proper model validation.

The FR_RIS models overpredicted the fouling rate at high c_C (> 0.5 kgCOD m^{-3}), and the overprediction was higher for D2. From the Robles et al. (2013) based FR_RIS models, D1c $\alpha_{c,1p}$ and D1c $\alpha_{c,1}$ had the lowest fouling rate overpredictions, and D1c $\alpha_{c,1p}$ was slightly better than D1c $\alpha_{c,1}$. The models that combined the submodel D2 with a Carman-Kozeny based SCR submodel (i.e., $\alpha_{c,1}$, $\alpha_{c,1p}$, $\alpha_{c,2}$ and $\alpha_{c,2p}$) presented instabilities or pronounced peaks at high c_C (shown in Figure A1D), which was attributed to the considerably low estimated ε_{c0} of 0.12 - 0.17 (Table A17). When colloidal material accumulated in the cake, the porosity (ε_c) was reduced below ε_{c0}, resulting in values close to zero causing an overpronounced increase in SCR because of the term: $\alpha_c \propto \varepsilon_c^{-3}$ (Table 5.2). The low ε_{c0} value in D2 was estimated because this deposition submodel predicted approximately 200 times less material deposition onto the membrane surface than the deposition submodels based on Robles et al. (2013), and thus the SCR increased (by decreasing the porosity) to reach similar R_c values. To elucidate which modelling approach was more accurate the amount of particulate and colloidal material deposited should be measured, which was unfortunately not possible in the current research.

The models that included floc size as input variable (Figure 5.8B, Figure 5.9A and Figure 5.9B) improved the FR prediction at large floc size (i.e., operational period 17-30 days) compared to the models that did not include floc size (Figure 5.8A, Figure 5.9C and Figure 5.9D). These results suggest that floc size had a direct impact on FR and should be included as state variable in a model that predicts the effect of FE on FR.

During days 37-39, the reactor was operated at considerably low u_G causing a sharp fouling rate increase despite the low c_C. The empirical FR models predicted this behaviour satisfactorily and only slightly underestimated the fouling rate. Additionally, the empirical FR models predicted adequately the fouling rate increase caused by the u_G decrease during the day 1 in which c_C was high. Contrarily, all FR_RIS models predicted only a slight or no increase in fouling rate during 37-39 d, thus substantially underestimating the fouling rate. Nevertheless, some FR_RIS models (namely the ones with $\alpha_{c,1p}$, $\alpha_{c,2p}$ or D2) could predict the fouling rate increase during day 1. The deposition submodel D2, that considered drag and lift forces, was slightly more sensitive to u_G than the submodels that considered only drag forces (D1a, D1b and D1c) because in D2 u_G affects the attachment and detachment of particulate material (through G), whereas in the other submodels only the detachment is affected by u_G. In summary, at high c_C, the effect of low u_G on fouling rate was satisfactorily predicted by all the empirical FR models and by the FR_RIS models that include either the SCR submodels with cake compression ($\alpha_{c,1p}$ and $\alpha_{c,2p}$) or the deposition submodel D2; whereas at low c_C, only the empirical FR models could predict the effect of low u_G on fouling rate.

The reactor was not intentionally operated at high u_G; however, during some periods H_{MT} decreased due to influent shortage which increased the simulated u_G calculated with Equation (A.1). However, the experimental u_G was measured few times during those periods: the experimental u_G on day 14 was 8% lower than the calculated value; on day 7 the calculated and experimental values were equal. Thus, the prediction at high u_G was analysed on day 7. All the empirical FR models and the FR_RIS models that combined the deposition submodels D1a, D1b or D1c with SCR submodels with cake compression ($\alpha_{c,1p}$ or $\alpha_{c,2p}$) predicted satisfactorily the fouling rate at high u_G, whereas the models that included SCR submodels without cake compression ($\alpha_{c,1}$ or $\alpha_{c,2}$) or the deposition submodel D2, overpredicted the fouling rate. Particularly for D2, the fouling rate was substantially high, because the c_C was elevated and caused instabilities in the model, as explained above.

5.3.4 AnDFCm filtration model

5.3.4.1 Calibration of alternate model

Table A4 summarises the GSA results for all alternate AnDFCm filtration models. Analogous to the GSA results for the alternate AnMBR filtration models, the parameters C_d, β_{ST}, k_c, k_{CK}, ε_{c0}, ρ_X, P_b, ζ_2 and ζ_3 were influential in all or most models; h_t, γ, ρ_C, ζ_1, and ζ_4 were none-influential in all or most models; and ε_{c0} was the most influential parameter in all the models. Opposite to the GSA results for the alternate AnMBR filtration models, $K_{S,c}$ and $q_{m,MS}$ (which are associated with the detachment processes) were only influential in some AnMBR

models, whereas they were influential in most AnDFCm models. This might be caused by the higher superficial velocity in the AnDFCm installation ($u_{L,AnDFCm}$=1.5 m s^{-1}) compared to the AnMBR ($0.5\times10^{-3} < u_G < 5.7\times10^{-3}$ m s^{-1}) which increases the detachment.

The influential parameters were estimated using in-situ ΔR_{20} measurement in the pilot AnMBR immediately after FE dosing and ex-situ ΔR_{20} measurement during the dosage-step tests BWa and BWb. Table A19 summarises the parameter estimation procedure and Table A20 the optimal values and quality of the estimators. The quality of the parameters was worse than for the AnMBR models, especially for the deposition related parameters, that is: 74% of the deposition related and 40% SCR related parameters had poor quality. This was partially caused by the high pairwise correlation between parameters (>0.50) producing an ill-conditioned optimisation problem (Sin and Gernaey, 2016). The parameter ε_{c0} was of good quality because it was estimated separately for most models, namely $\theta_{II} = \{\varepsilon_{c0}\}$, except for D2 $\alpha_{2,p}$ and D2 α_2 where $\theta_{II} = \{\varepsilon_{c0}, C_d\}$. ε_{c0} was estimated separately because it was the most influential parameter in each model and most subsets containing ε_{c0} had a collinearity index above the threshold of 10.

The calibration procedure can be improved by adding identifiability steps or improving the dataset used for calibration. For example, adding a second identifiability step with θ_{III}, decreased the parameters with poor quality from 74% to 38% for the deposition parameters and from 40% to 17% for the SCR parameters (results not shown) and identical or similar predictions of the validation data was obtained with one and two identifiability steps, Figure A27. The only models, of which predictions with one and two identifiability steps differed, were D1c $\alpha_{c,1}$, D2 $\alpha_{c,1}$, D3 $\alpha_{c,1}$, D3c $\alpha_{c,3}$, and D3c $\alpha_{c,3p}$; where for D1c $\alpha_{c,1}$ the prediction was considerably improved by adding a second identifiability analysis, whereas for the remaining models the prediction was only slightly worsen. Therefore, the calibration procedure was improved by adding a second identifiability step because it decreased the relative error of the parameters without deteriorating the model prediction capacity substantially or even improving it. Further adding extra identifiability steps was not analysed in this research.

Figure A24 and Figure A25 compare the experimental ΔR_{20} with the predicted values using the optimal parameters for each model, which were obtained with the original calibration procedure with one identifiability step. Most of the models that included a SCR submodel with cake compression ($\alpha_{c,jp}$) could not be calibrated to satisfactorily predict the experimental data. The exceptions were D1c $\alpha_{c,2p}$ and D3 with $\alpha_{c,1p}$, $\alpha_{c,2p}$, and $\alpha_{c,3p}$. Although D1c $\alpha_{c,2p}$ approximated the experimental ΔR_{20} used for calibration, the model failed at high c_X during model validation (Figure A26B). For models with D3, the predictions with the compression submodels $\alpha_{c,ip}$ were identical to the corresponding non-compressed submodel $\alpha_{c,i}$ for i = [1,2,3]. This was because the estimated $f_{X,c}$ was considerably low, causing negligible deposition of particulate material (ω_X), thereby the compressed SCR approximated the SCR without compression. Therefore, the models that coupled D3 with $\alpha_{c,1p}$, $\alpha_{c,2p}$, or $\alpha_{c,3p}$ in fact, did not describe a compressible cake.

Regarding the alternate AnDFCm models that included a non-compressible SCR submodel different observations were found. The models that included $\alpha_{c,1}$ predicted the experimental ΔR_{20} reasonably for the three datasets used during calibration, these models behaved similar for all deposition submodels (i.e., D1c, D2 and D3). For models including $\alpha_{c,2}$ or $\alpha_{c,3}$, D1c $\alpha_{c,2}$ and D3 $\alpha_{c,2}$ behaved similarly whereas D2 $\alpha_{c,2}$ differed; and analogous D1c $\alpha_{c,3}$ and D3 $\alpha_{c,3}$ behaved similarly and D2 $\alpha_{c,3}$ differed. D2 $\alpha_{c,2}$ predicted the experimental ΔR_{20} better than D1c $\alpha_{c,2}$ and D3 $\alpha_{c,2}$; whereas D2 $\alpha_{c,3}$ predicted the experimental ΔR_{20} worse for D1c $\alpha_{c,3}$ and D3 $\alpha_{c,3}$. The models are further discussed using the long-term predictions in the following section.

5.3.4.2 Long-term validation

Figure 5.10 compares the experimental and predicted long-term ΔR_{20} of the pilot AnMBR sludge for the alternate models without cake compression; and Figure A26 shows the predictions of the alternate models with cake compression.

Figure A26 suggested that the model with D3 could predict the experimental ΔR_{20} when combined with cake compresion SCR submodels. However, as explained above, the models combining D3 with $\alpha_{c,1p}$, $\alpha_{c,2p}$, or $\alpha_{c,3p}$, in fact did not describe a compressible cake. Therefore, all the models that included cake compression were unable to predict the experimental ΔR_{20}. Accordingly, the shape of the filtration curve obtained when filtering different anaerobic sludge samples in the AnDFCm installation suggested that the cake layer formed was mostly non-compressible. This is further discussed in Section A11, Appendix A.

The alternate AnDFCm filtration models without cake compression in Figure 5.10, satisfactorily predicted the filterability improvement (i.e., ΔR_{20} decrease) caused by dosing FE on day 16. During the period without FE (0-16 d) the experimental and predicted ΔR_{20} values were considerably higher than the ΔR_{20} after FE dosing (after day 16) for the models with $\alpha_{c,1}$ or $\alpha_{c,2}$. However, for the models with $\alpha_{c,3}$, the difference between these periods was less clear because the models predicted relatively high ΔR_{20} in the period 20-35 d, which was caused by small fluctuations in c_C and c_X.

Figure A28 illustrates the sensitivity of the models to c_X and c_C inside the operational range of the pilot. Sludge was withdrawn from the pilot on day 123 causing a drop in c_X from 14 to 5.5 kg m^{-3}, whereas c_C and ΔR_{20} were almost unaltered. Figure 5.10 shows that D3 $\alpha_{c,2}$ was the only model that accurately predicted this behaviour because it had only moderate sensitivity to c_X, as illustrated in Figure A28F. The models including $\alpha_{c,1}$, $\alpha_{c,3}$ or D2 overpredicted the ΔR_{20} drop after sludge withdrawal because models with $\alpha_{c,1}$ or D2 were too sensitive to c_X and with $\alpha_{c,3}$ too sensitive to c_C/c_X. The high sensitivity of $\alpha_{c,1}$ and D2 to c_X also caused the overprediction when c_X was high (85-125 d). Similarly, D1c $\alpha_{c,2}$ had an elevated sensitivity to c_X but with an opposite effect on ΔR_{20}, that is: a higher c_X caused a lower ΔR_{20}, consequently D1c $\alpha_{c,2}$ overpredicted ΔR_{20} at low c_X (after sludge withdrawal) and underpredicted ΔR_{20} at high c_X (85-125 d).

Opposite to the AnMBR filtration models, the incorporation of d_p as input variable in the AnDFCm filtration models worsened the ΔR_{20} prediction. During the operational period at large floc size (17-25 days) the models with $\alpha_{c,2}$ (without d_p) accurately predicted the experimental ΔR_{20} whereas the models with $\alpha_{c,1}$ (with d_p) underpredicted ΔR_{20}. Additionally, the models with $\alpha_{c,1}$ predicted peaks in ΔR_{20} around days 60, 94 and 120, caused by small d_p reductions, these ΔR_{20} peaks were not observed experimentally. These results suggested that floc size might not have a direct impact on sludge filterability and could be excluded as state variable in the AnDFCm filtration models for ΔR_{20} prediction. The negligible effect of floc size on sludge filterability might be caused by the absence of relaxation cycles in the AnDFCm as previously proposed in Section 4.4.1.2, Chapter 4.
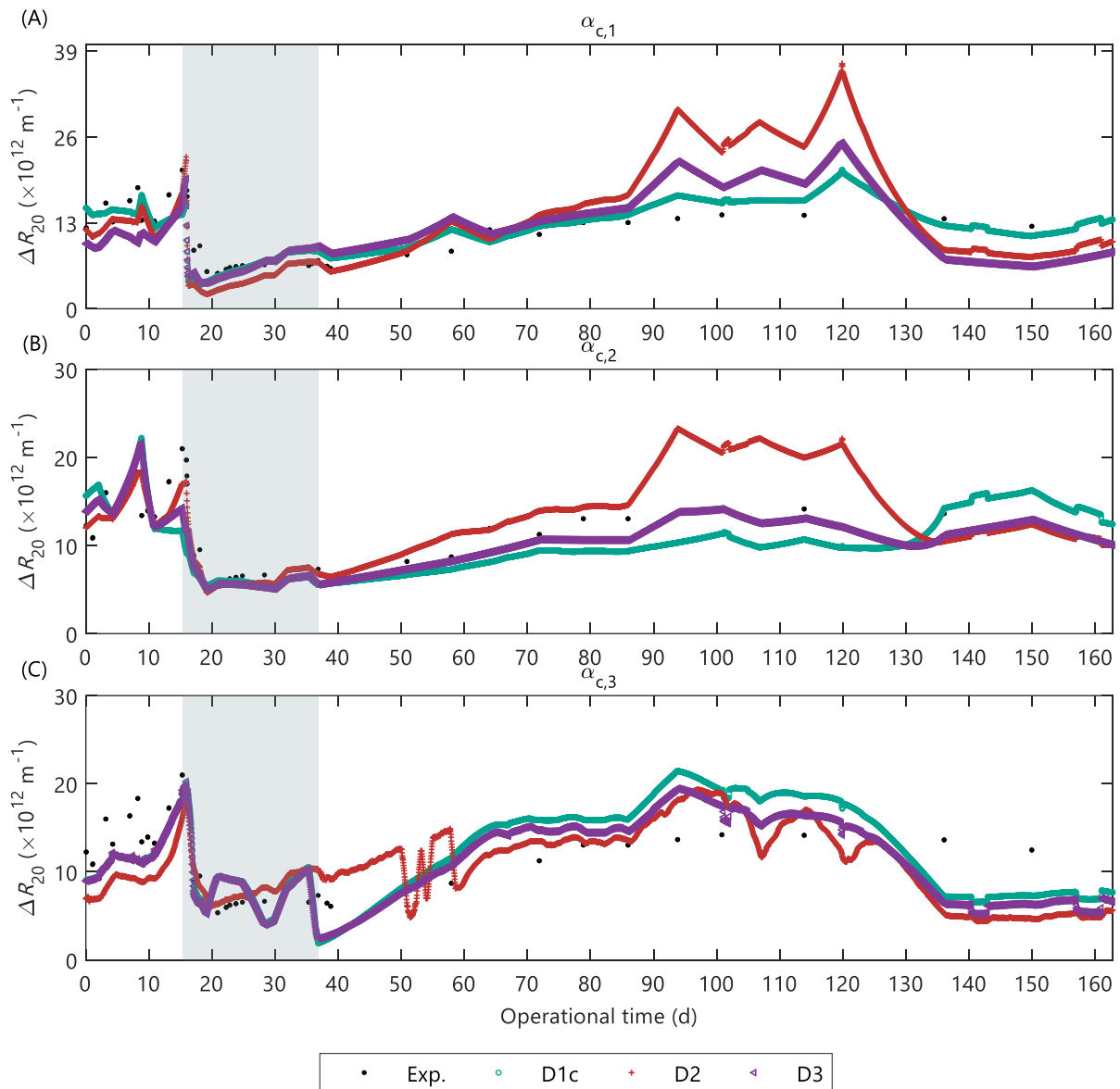

Figure 5.10. Validation of the alternate AnDFCm filtration models that combine the different deposition submodels (D1c, D2 and D3) with the non-compressible specific cake resistance submodels: (A) $\alpha_{c,1}$, (B) $\alpha_{c,2}$, and (C) $\alpha_{c,3}$. The grey area represent the in-situ data used for model calibration.

5.3.5   Model limitation, applicability and further development

The calibrated biochemical-flocculation model satisfactorily predicted the dynamics of d_p and cCOD in the pilot AnMBR dosed with FE. Nevertheless, a more frequent and comprehensive influent characterization is needed to improve model calibration and validation to accurately predict the fluctuations in TSS, c_X and c_C. Additionally, the same dataset was used for calibration and validation, and thus the model requires further validation with an independent dataset from a different operational period of the pilot or from another AnMBR.

The extended biochemical-flocculation model presented in Section 5.3.2.3, which incorporated the interaction of FE with soluble humic substances, carbohydrates and proteins, should be employed for reactors with high concentrations of any of these components.

The biochemical-flocculation model included only inert colloidal material, the model could be further extended to incorporate biodegradable colloidal components consisting of proteins, carbohydrates, lipids, humic substances, etc. Furthermore, particle size prediction could be improved, for example by incorporating a population balance model in the biochemical-flocculation model to predict the particle size distribution (Jeldres et al., 2018). This would increase the complexity of the model by increasing the amount of state variables and parameters, but it might also increase the accuracy of the model.

From the alternate AnMBR filtration models, the FR_RIS that included Carman-Kozeny based SCR submodels and all the proposed empirical FR models predicted satisfactorily the effect of c_C on fouling rate. Nevertheless, the empirical FR models might have underpredicted and the FR_RIS overpredicted FR at high c_C. Furthermore, all the empirical FR models and none of the FR_RIS models predicted the effect of the low u_G on the fouling rate when the reactor was operated at low c_C. Therefore, one empirical and one FR_RIS model were selected for the simulation environment to cover a predicted fouling rate range. Nevertheless, the calibration of the alternate AnMBR filtration models should be further improved by online gas monitoring and more intensive grab samples monitoring, particularly for csCOD which fluctuated and highly affected the model. Additionally, the validation should be improved by applying the alternate models to an independent dataset.

The empirical FR model FR6 was selected because it included d_p as input variable, which improved the prediction, and better predicted FR at high u_G compared with FR4 and FR5. From the FR_RIS models, D1c $\alpha_{c,1p}$ and D1c $\alpha_{c,1}$ had the lowest FR overpredictions at high c_C; and in Figure A23, D1c $\alpha_{c,1p}$ was more sensitive to u_G and less sensitive to c_X than D1c $\alpha_{c,1}$, as experimentally observed; therefore, the model D1c $\alpha_{c,1p}$ was selected for the simulation environment.

From the AnDFCm filtration models, the best alternate model to predict sludge filterability was D3 $\alpha_{c,2}$ because it had limited sensitivity to c_X as experimentally observed and predicted satisfactorily the experimental ΔR_{20}, including the ΔR_{20} decrease after FE dosing and the small change in ΔR_{20} value after sludge withdrawal.

5.3.6 Control tools for dosing flux enhancer

The integrated model was used as a simulation environment to test the various control tools presented in Table 5.8, for manipulating FE dosing to the pilot AnMBR. The simulation environment included the biochemical-flocculation model with no binding between FE and soluble humic substances, carbohydrates, and proteins because the reactor did not present high values of any of these variables. Therefore, the original biochemical-flocculation model described in Section 5.2.3 was used, but with the mean particle size dynamics from Equation (5.61). As previously explained, the sludge filterability was predicted as ΔR_{20} with the AnDFCm filtration model D3 $\alpha_{c,2}$; and the fouling rate was predicted with the empirical FR model FR6 and the FR_RIS model D1c $\alpha_{c,1p}$.

Results in Figure 5.11 show that all control tools substantially improved reactor performance by decreasing ΔR_{20} and membrane fouling compared to the reactor without FE dosing (No_FE). The decrease was caused by FE induced flocculation which reduced the concentration of colloidal material and increased the floc size.

The total mass of FE added in the 400-day simulated period varied between the different control tools, the lowest and highest amounts were 0.25 and 0.46 kg for FF_Q_{WS} and FB_ΔR_{20}_8-12, respectively. Considering the base FE price given by the supplier of Adifloc KD451 of 6 € kg^{-1}, the FE cost was between 1.37 and 2.50 € y^{-1}, or 0.49 and 0.89 € m^{-3} y^{-1}, which is negligible. Nevertheless, as discussed in Chapter 2, the costs of FE dosing can vary considerable for different AnMBRs.

The feedback ΔR_{20} control tool FB_ΔR_{20}_8-12 was the tool that required most FE due to the higher loss of FE with the permeate, shown in Figure 5.11I. This was because high amounts of FE were dosed in a short period, elevating the concentration of unbonded FE (S_{fe}) which passed through the membrane and left the reactor with the permeate flow. Additionally, as expected, FB_ΔR_{20}_8-12 caused less stable filterability and fouling rate than FB_ΔR_{20}_10. Accordingly, continuous dosing the FE MPE50 to a pilot MBR caused a more stable time-to-filter and used less FE than applying periodic pulses when the time-to-filter reached 200 s^{-1} (Alkmim et al., 2016), these strategies were analogous to FF_Q_{WS} and FB_ΔR_{20}_8-12, respectively.

The c_{fe} for FB_ΔR_{20}_10 in Figure 5.11G was assumed as the optimal FE dosage required to sustain an adequate and stable sludge filterability inside the reactor (D_{opt}). This dosage varied between 1 and 27 mgCOD L^{-1} during the simulated period due to changes in sludge characteristics. Consequently, the c_{fe} control tool (namely FB_c_{fe}, FF_Q_{WS}, and FF_Q_{Inf}), which targeted a specific $c_{fe,sp}$ of 8.7 mgCOD L^{-1}, under or overdosed FE during certain periods. For example, at high c_X (250-400 d) more FE was required to achieve similar c_C reductions because the FE was adsorbed onto the particulate material, thereby decreasing its availability for colloidal material flocculation. Here, the c_{fe} control tools underdosed FE causing an increased ΔR_{20} and fouling rate, compared to FB_ΔR_{20}_10. Conversely, at low c_X (100-200 d), the FE required was lowered, and the c_{fe} control tools overdosed FE increasing the FE concentration in the permeate and using unnecessary FE.
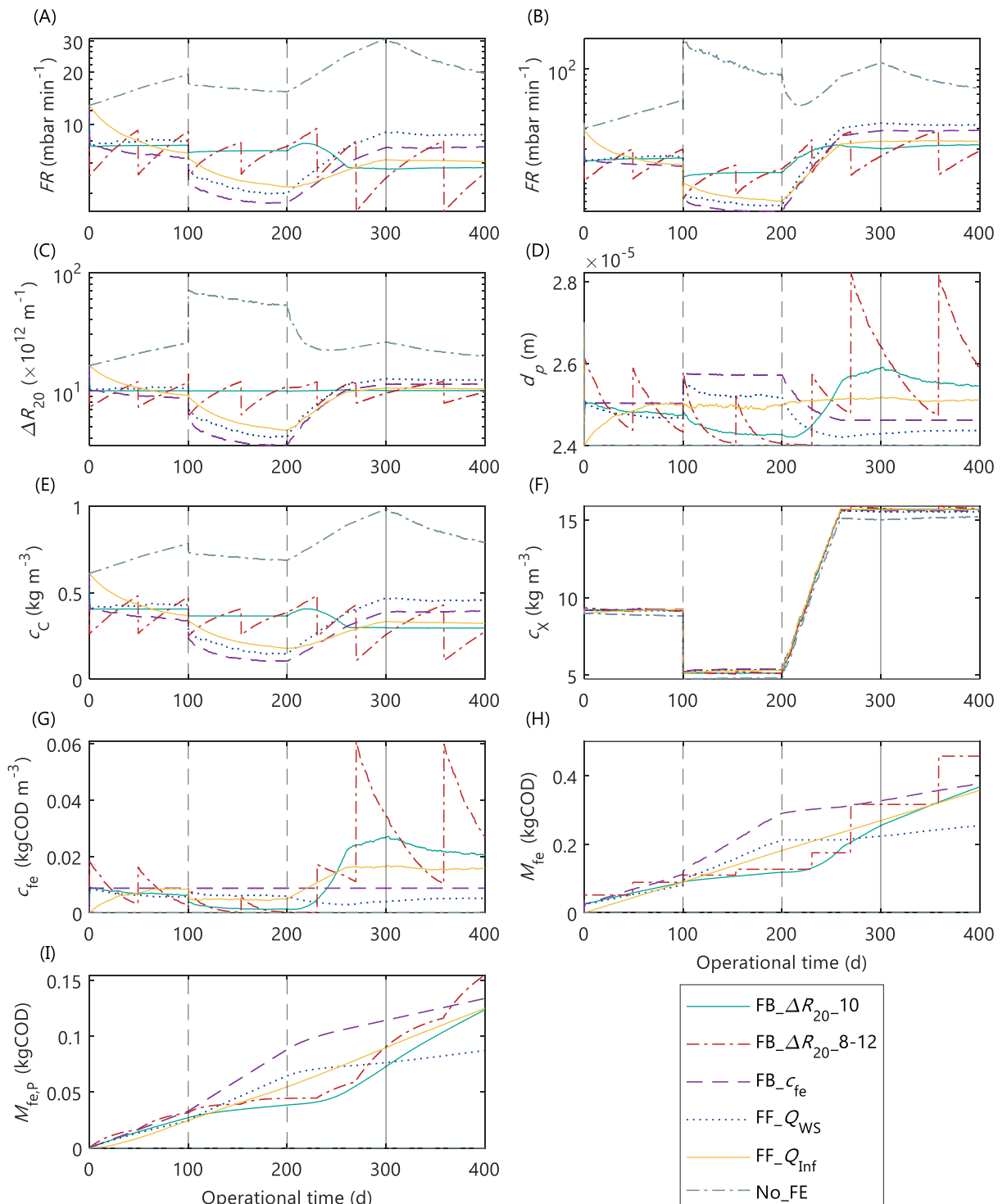
Figure 5.11. Simulated pilot AnMBR behaviour with different feedback (FB) and feedforward (FF) control tools for manipulating the flux enhancer (FE) dosage. Compared variables: (A) fouling rate with empirical model FR6, (B) fouling rate with RIS model D1c $\alpha_{c,1p}$, (C) sludge filterability expressed as ΔR_{20}, (D) mean particle diameter, (E) colloidal material concentration, (F) particulate material concentration, (G) total FE concentration inside the reactor, (H) cumulative mass of FE dosed, and (I) cumulative mass of FE removed with permeate flow. The vertical lines indicate applied disturbances on: TSS setpoint (dotted) and $f_{C,WS}$ (continuous).

5.4 CONCLUSIONS

The main findings are summarised as follows:

- The proposed biochemical-flocculation model predicted satisfactorily the dynamics of mean particle diameter and colloidal material concentration. Nevertheless, the long-term model prediction requires further validation.

- Soluble humic substances, carbohydrates and proteins might bind to the cationic polymer used as flux enhancer and reduce its availability for colloidal material flocculation.

- The concentration of colloidal material was an appropriate linking variable between biochemical-flocculation and filtration models for fouling rate and ΔR_{20} prediction. Whereas mean particle diameter was only appropriate for fouling rate prediction, but it worsen ΔR_{20} prediction.

- From the 34 alternate AnMBR filtration models tested, the 28 FR_RIS models, which predicted fouling rate based on TMP (FR=dTMP$/dt$), were unable to predict the effect of low gas superficial velocity on fouling rate when the concentration of colloidal material was low. Contrarily, the six empirical FR models proposed in this research succeeded on capturing this effect.

- The alternate AnDFCm filtration models without cake layer compression predicted ΔR_{20} better than the alternate models with compressible cake.

- For model calibration and validation, better and extra input data was required, particularly online gas flow measurements and intensive and comprehensive monitoring of sludge and blackwater characteristics.

- The integrated calibrated model was used as a simulation environment to test different control tools to manipulate the flux enhancer dosing to the pilot AnMBR. The feedback ΔR_{20} proportional control tool, referred to as ΔR_{20}_10, was the preferred controller.

- The simulated optimal dosage to control sludge filterability varied during the operational period due to changes in sludge characteristics.

- Compared to periodically dosing flux enhancer in the form of pulses, continuous flux enhancer dosing decreased permeate contamination by flux enhancer, required less flux enhancer, and achieved more stable sludge filterability and fouling rate.

6

CONCLUSIONS, RECOMMENDATIONS, AND OUTLOOK

Membrane fouling is a major challenge limiting economic feasibility and applicability of AnMBRs. This thesis studied the feasibility of implementing a fouling control tool for AnMBRs that manipulates the flux enhancer dosing based on sludge filterability measurements. This work focused on the use of cationic polymers as flux enhancers and used the cationic polymer Adifloc KD451 in all experimental phases. Chapters 2 to 4 analysed the feasibility of dosing flux enhancers in long-term and large-scale AnMBRs, the possible side effects of flux enhancers, the causes of variation in optimal dosage, and the feasibility of using in-situ sludge filterability measurements (such as ΔR_{20}) as an input variable in the fouling control tool. Furthermore, in Chapter 5 a simulation environment with an integrated model that predicts the effect of flux enhancer dosing on sludge filterability and membrane fouling rate was developed. This simulation environment was used to compare five control tools to manipulate the flux enhancer dosing to a pilot AnMBR.

This chapter summarises the conclusions obtained throughout this thesis. Moreover, this chapter provides recommendations for the application of flux enhancers for fouling mitigation in AnMBRs, and for using the simulation environment developed in this thesis.

6.1 CONCLUSIONS

Overall, it can be concluded that dosing cationic polymers (such as Adifloc KD451) as flux enhancers is a suitable strategy for fouling mitigation in large-scale AnMBR because it showed a long-term improvement of filtration performance and sludge filterability, while having no significant adverse effects on permeate quality and chemical oxygen demand removal efficiency. Nevertheless, determining the optimal dosage and using an appropriate dosing strategy is crucial to avoid overdosing that can cause adverse effects on filterability and permeate contamination by unbonded flux enhancer. The main additional conclusions of this thesis are summarised as follows:

The flux enhancer Adifloc KD451 significantly enhances the sludge filterability of municipal and industrial sludge samples when applied below the critical dosage. In Chapter 2, the cationic polymer Adifloc KD451 improved sludge filterability of all sludge samples tested which were collected from five large-scale AnMBRs treating industrial or municipal wastewater. Nevertheless, excessive flux enhancer dosages had an adverse effect on sludge filterability, increased irreversible fouling in the AnDFCm installation and promoted permeate contamination by the unbonded flux enhancer (Chapters 2 and 5). Therefore, overdosing must be avoided when applying flux enhancers to large-scale AnMBRs.

The optimal required dosage of flux enhancer varies due to changes in sludge characteristics. In large-scale membrane bioreactors, the sludge characteristics are constantly changing due to variations in the membrane and reactor operational conditions, these variations affect the required optimal dosage of flux enhancer. In Chapter 5, the simulated optimal flux enhancer dosage required to sustain an adequate and stable sludge filterability in a pilot AnMBR varied between 0.001 and 0.027 g L^{-1} during the simulated

400-day period. In Chapter 2, the optimal and critical dosages differed considerably between sludge samples from various AnMBRs, the optimal dosage ranged from 0.02 to 1.16 g L^{-1} and critical dosage from 0.10 to 2.5 g L^{-1}. The main factors affecting these dosages were the concentrations of colloidal material and soluble microbial products (carbohydrates, proteins and humic substances), capillary suction time and sludge filterability (Chapters 2 and 5).

Floc size has a significant effect on the AnMBR membrane fouling rate and a negligible effect on sludge filterability (measured as ΔR_{20} with the AnDFCm). In Chapter 4, the correlation between mean particle size (i.e., floc size) and the AnMBR filtration performance indices (i.e., fouling rate and total filtration resistance) was stronger than between floc size and sludge filterability (expressed as ΔR_{20}). Accordingly, in Chapter 5, the inclusion of floc size as input variable in the AnDFCm filtration models worsened the ΔR_{20} predictions whereas including floc size in the AnMBR filtration models improved the fouling rate predictions. The negligible effect of floc size on ΔR_{20} might be caused by the absence of relaxation cycles in the AnDFCm (Chapter 4).

The flux enhancer that remains unbonded in the bulk liquid can pass through the membrane pores and contaminate the permeate. When flux enhancer is added to sludge, a fraction of flux enhancer can remain unbonded in the bulk liquid, depending on the relevant physicochemical equilibria. Chapter 2 showed that a fraction of unbonded Adifloc KD451 can pass through the membrane pores and contaminate the permeate. The contribution of flux enhancer to the permeate COD is negligible (Chapter 4 and 5). However, polydiallyldimethylammonium chloride (polyDADMAC), the chemical compound in several cationic polymers used as flux enhancers, can be a precursor of N-nitrosodimethylamine, which is a suspected human carcinogen produced during chloramination or ozonation. Therefore, minimising permeate contamination by flux enhancer is crucial.

The flux enhancer Adifloc KD451 has a reversible inhibitory effect on the biological activity. In Chapter 3, batch tests showed that the cationic polymer Adifloc KD451 presented a significant inhibitory effect on the specific methanogenic activity of the sludge. This inhibition was successfully described by a reversible process using biostatic non-competitive and un-competitive inhibition models. Accordingly, in Chapter 4, dosing the cationic polymer to a pilot-scale AnMBR had a modest immediate inhibitory effect on the specific methanogenic activity, but this was a reversible process that had no adverse effect on permeate quality or chemical oxygen demand removal efficiency.

The costs of flux enhancer dosing varies considerably for different AnMBRs and should be considered in the economic evaluation of each treatment plant. The annual cost of dosing flux enhancer is subject to the volume of mixed liquor, price of flux enhancer, and required dosage. In Chapter 2 the annual cost varied from 1.5 € y^{-1} to 13,337 € y^{-1} for different AnMBRs.

In-situ sludge filterability measurement, performed with the AnDFCm, is a suitable input variable to manipulate flux enhancer dosing into an AnMBR. In Chapter 4, relating in-situ measurements of sludge filterability with AnMBR filtration performance indices (i.e., fouling rate and total filtration resistance) allowed to identify the cause of filtration performance deterioration and improvement in the AnMBR. Furthermore, the interval of change in filtration performance and sludge filterability observed in membrane bioreactors (~days) was negligible compared to the interval of sludge filterability measurements allowed by the AnDFCm (~20 minutes per measurement). Nevertheless, the AnDFCm installation requires further automation to become a stand-alone device able to operate automatically and in-situ. Chapter 5 shows, in a simulation environment, the applicability of the AnDFCm installation as a sensor in fouling control tools for AnMBRs.

Flux enhancer dosage is unsuitable as input variable to manipulate flux enhancer dosing into an AnMBR. The most applied flux enhancer dosing strategy in membrane bioreactors reported in literature targets to maintain a certain dosage of flux enhancer, i.e., a concentration of flux enhancer inside the reactor, by performing a single pulse-dosage or an initial pulse-dosage that is followed by periodic flux enhancer dosing to compensate for the loss by biodegradation and sludge withdrawal. However, in Chapter 5, the required flux enhancer dosage varied during the operational period of membrane bioreactors due to changes in sludge characteristics. Consequently, the control tools that target to maintain a certain flux enhancer concentration inside the reactor caused under and overdosing of flux enhancer during certain simulated periods.

Continuously dosing small quantities of flux enhancer is a preferred dosing strategy compared to periodically dosing higher quantities of flux enhancer in the form of pulses. In Chapter 5, two feedback filterability controllers to manipulate flux enhancer dosing to a pilot AnMBR were compared in a simulation environment. The first was a proportional controller that dosed flux enhancer continuously (referred to as FB_ΔR_{20}_10), and the second an on-off controller that dosed periodic pulses of flux enhancer (referred to as FB_ΔR_{20}_8-12). Compared to FB_ΔR_{20}_8-12, FB_ΔR_{20}_10 decreased permeate contamination by flux enhancer, required less flux enhancer, and achieved more stable sludge filterability and fouling rate.

6.2   RECOMMENDATIONS AND OUTLOOK

Following the conclusions of this thesis, when dosing flux enhancer to membrane bioreactors it is important to avoid flux enhancer overdosing. The following consequences can arise from flux enhancer overdosing: deteriorated sludge filterability resulting in increased reversible fouling, increased irreversible fouling caused by the interaction of unbonded flux enhancer with the membrane, and permeate contamination by part of the unbonded flux enhancer that passes through the membrane.

To avoid overdosing, the flux enhancer should be dosed in small quantities, the required dosage should be monitored, and the dosing should be corrected based on the required dosage. To implement this manually, the operators need to perform regular dosage-step tests to determine the required flux enhancer dosage, and adjust the dosing based on the results. This could be costly in terms of material and labour, and susceptible to human error. To overcome these disadvantages, an automatic control tool should be implemented. For example, using an online in-situ sludge fouling potential sensor (such as the AnDFCm installation) to manipulate the flux enhancer dosing. This control tool is more robust because the monitoring is continuous and does not require an operator.

The feedback ΔR_{20} proportional control tool proposed in this thesis, referred to as ΔR_{20}_10, should be further tested in a real AnMBR, since it was only tested in a simulation environment. The controller should be tested in a pilot-scale AnMBR by imposing defined disturbances, such as ramps and pulses. The control tool ΔR_{20}_10 was the preferred controller to manipulate flux enhancer dosing. Moreover, to implement this control tool in a real AnMBR, the AnDFCm installation requires further automation to become a stand-alone device able to operate automatically and online.

Calibration and validation of the integrated AnMBR model, developed in Chapter 5, should be further improved by gas monitoring and intensive and comprehensive monitoring of sludge and influent characteristics. Furthermore, model validation should be improved by using an independent dataset from a different operational period of the pilot AnMBR.

The simulation environment developed in this thesis provides a tool to test flux enhancer dosing strategies into AnMBRs. The integrated AnMBR model used in the simulation environment was developed, calibrated, and validated under specific conditions, that is using the flux enhancer Adifloc KD451 in the pilot AnMBR described in Chapter 5. To use the simulation environment under different conditions, the integrated model should be initially validated under those conditions.

For reactors with high concentrations of soluble microbial products, the extended biochemical-flocculation model presented in Section 5.3.2.3 should be used. This model incorporates the interaction of flux enhancer with soluble microbial products.

The biochemical-flocculation model includes only inert colloidal material, the model could be further extended to incorporate other colloidal components, such proteins, carbohydrates, lipids, humic substances, etc. This would increase the complexity of the model by increasing the amount of state variables and parameters, but it might also increase the accuracy of the model. Furthermore, particle size prediction should be improved, for example by incorporating a population balance model in the biochemical flocculation to predict the particle size distribution (Jeldres et al., 2018).

This thesis focuses on one flux enhancer (i.e., Adifloc KD451), and its dosing into one pilot-scale AnMBR and into grab sludge samples from a limited number (five) of AnMBRs. The methods applied in this thesis are nevertheless applicable to test other flux enhancers and other large-scale AnMBRs.

A

SUPPLEMENTARY MATERIAL
CHAPTER 5

A1. EXPERIMENTAL DATA

Pilot AnMBR supplementary experimental data

Table A1 summarises the characteristics and operational conditions of the pilot AnMBR plant. The gas superficial velocity in the membrane tank was calculated based on the specific gas demand model developed in Odriozola et al (2020), as follows:

$$u_G = \frac{-3.43 - 14.57\, H_{MT} + 0.52\, v_B}{3600\, A_{MT}},$$
(A.1)

where v_B is the motor frequency of the blower, H_{MT} the liquid level and A_{MT} the cross-sectional area of the membrane tank.

The 20℃-normalised transmembrane flux (J_{20}) was calculated with the motor frequency of the permeate pump (v_P), using Equation (A.2) based on a flux-step experiment performed in the pilot AnMBR.

$$J_{20} = \left.(0.154\, v_P + 0.733)\middle/ 3.6e6\right. .$$
(A.2)

The transmembrane flux (J) was calculated to reflect the permeate viscosity dependence on temperature with Equation (A.3), where μ_{20} is the permeate viscosity at 20℃ and μ the permeate viscosity at the operational temperature.

$$J = J_{20} \frac{\mu_{20}}{\mu}.$$
(A.3)

The flow rates of blackwater (Q_{Inf}) and permeate (Q_P), which were used in the biochemical-flocculation model (described in Section 5.2.3), were calculated with a time-step (Δt) of 864 s (0.01 days). Q_P was the ratio between the volume of permeate produced during one time-step (ΔV_P) and Δt, and Q_{Inf} is calculated applying a mass balance in the liquid phase of the pilot AnMBR, as follows:

$$Q_P = \frac{\Delta V_P}{\Delta t},$$
(A.4)

$$Q_{Inf} = Q_P + Q_{WS} - Q_{fe} + \frac{\Delta V_L}{\Delta t},$$
(A.5)

where Q_{WS} and Q_{fe} are the flow rates of wasted sludge and flux enhancer, respectively, and ΔV_L the difference in V_L between time-steps.

Table A1. Characteristics of the pilot AnMBR and operational conditions relevant for model calibration and validation.

Description	Nomenclature	Units	Mean value	Range
Cross-sectional area MT	A_{MT}	m^2	0.68	NA
Gas pressure in AR headspace	p_G	bar	1.03	[1.00, 1.06]
Gas superficial velocity in MT	u_G	$\times 10^{-3}$ m s^{-1}	3.0	[0.5, 5.7]
Liquid level in MT	H_{MT}	m	1.42	[1.22, 1.56]
Membrane surface area	A_m	m^2	6.25	NA
Mixed liquor pH	pH	-	7.1	[6.8, 7.5]
Mixed liquor temperature	T	K	296	[292, 301]
Motor frequency blower	v_B	s^{-1}	59	[50, 60]
Motor frequency permeate pump	v_P	s^{-1}	60	[30, 60]
Flow rate influent	Q_{Inf}	$\times 10^{-5}$ m^3 s^{-1}	2.0	[0.9, 38]
Flow rate permeate	Q_P	$\times 10^{-5}$ m^3 s^{-1}	2.0	[0.9, 2.6]
Flow rate wasted sludge [a]	Q_{WS}	$\times 10^{-5}$ m^3 s^{-1}	~ 0	[0, 38]
Total filtration time in one cycle	θ_F	s	300	NA
Total relaxation time in one cycle	θ_R	s	90	NA
Total mixed liquor volume	V_L	m^3	2.7	[2.0, 2.9]
Transmembrane flux, 20°C-normalised	J_{20}	$\times 10^{-6}$ m^3 m^2 s^{-1}	2.7	[1.5, 2.8]
Transmembrane flux	J	$\times 10^{-6}$ m^3 m^2 s^{-1}	3.2	[1.7, 3.3]
Transmembrane pressure	TMP	$\times 10^3$ Pa	0.82	[0, 2.8]

Abbreviations: AR: anaerobic reactor; COD: chemical oxygen demand; MT: membrane tank; NA: not applicable.

[a] Sludge waste negligible during normal operation, except for a one-time sludge withdrawal of 31% of the mixed liquor performed on day 123.

Table A2. Blackwater, permeate and mixed liquor characteristics during pilot AnMBR operation.

Sample	Parameter	Nomenclature (for model)	Units	Mean value	Range
Blackwater	Alkalinity	Alk_{BW}	kgCaCO$_3$ m^{-3}	0.69	[0.50, 0.82]
	Ammonium	$NH4_{BW}$	kgN m^{-3}	0.15	[0.10, 0.20]
	Submicron COD	$csCOD_{BW}$	kg m^{-3}	0.34	[0.12, 0.63]
	Total COD	$tCOD_{BW}$	kg m^{-3}	1.62	[0.7, 3.3]
Mixed liquor	Colloidal COD [a]	cCOD	kg m^{-3}	0.50	[0.20, 0.87]
	Mean particle diameter	d_p	$\times 10^5$ m	2.7	[2.1, 4.5]
	Submicron COD	csCOD	kg m^{-3}	0.59	[0.30, 0.96]
	Total suspended solids	TSS	kg m^{-3}	9.6	[5.5, 16.0]
Permeate	Total COD	pCOD	kg m^{-3}	0.09	[0.05, 0.11]

[a] Calculated as the difference between the mixed liquor csCOD and the total permeate COD.
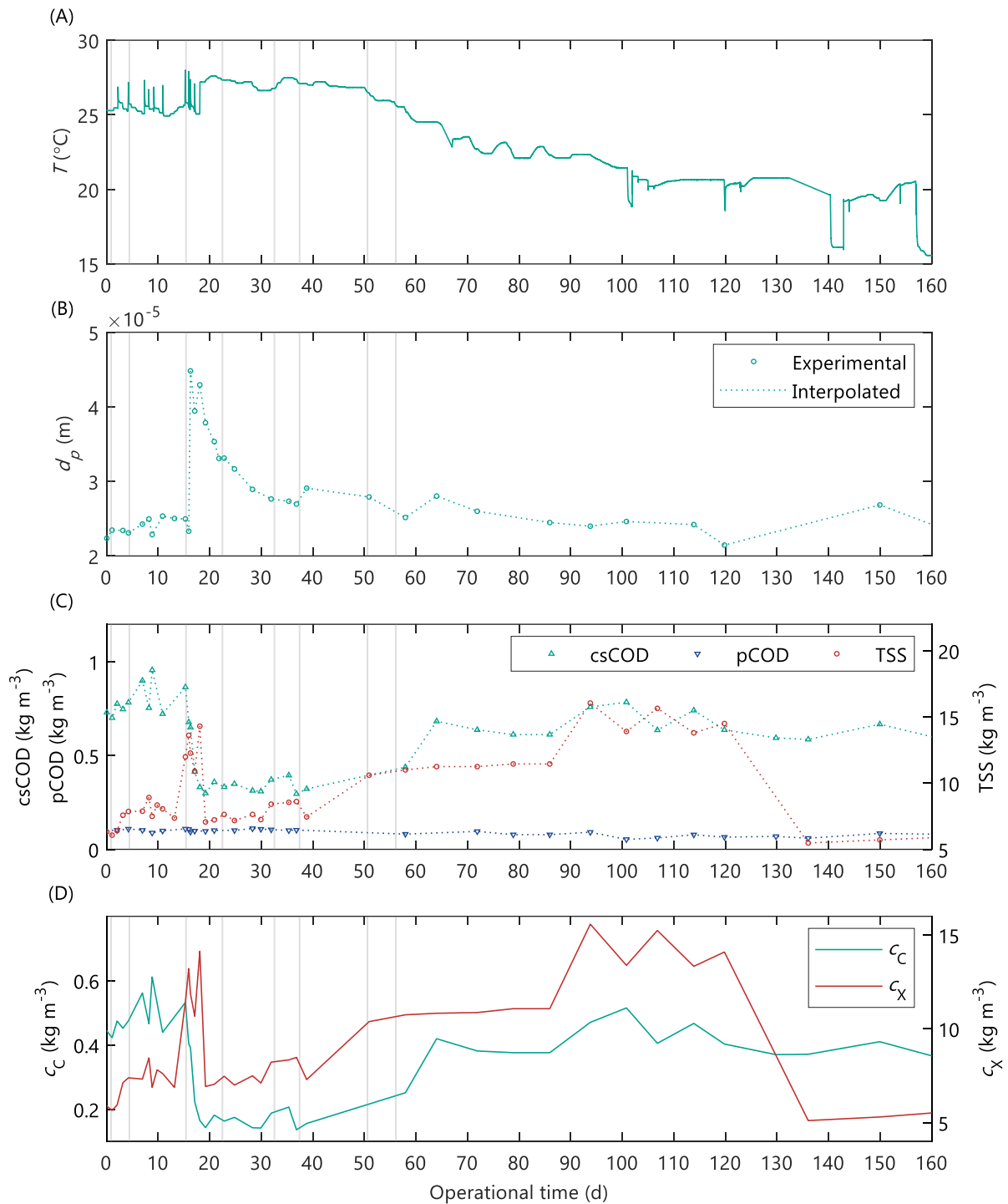
Figure A1. Pilot AnMBR mixed liquor characteristics used as inputs in the AnMBR and AnDFCm filtration models: (A) temperature measured by SCADA, (B) measured and interpolated mean particle diameter, (C) measured (markers) and interpolated (dotted lines) submicron COD, permeate COD and total suspended solids concentrations, and (D) calculated colloidal and particulate material concentrations. The grey-vertical areas represent the representative dataset, iD1 to iD8 from left to right, used for calibration of the filtration models.

(A)

(B)
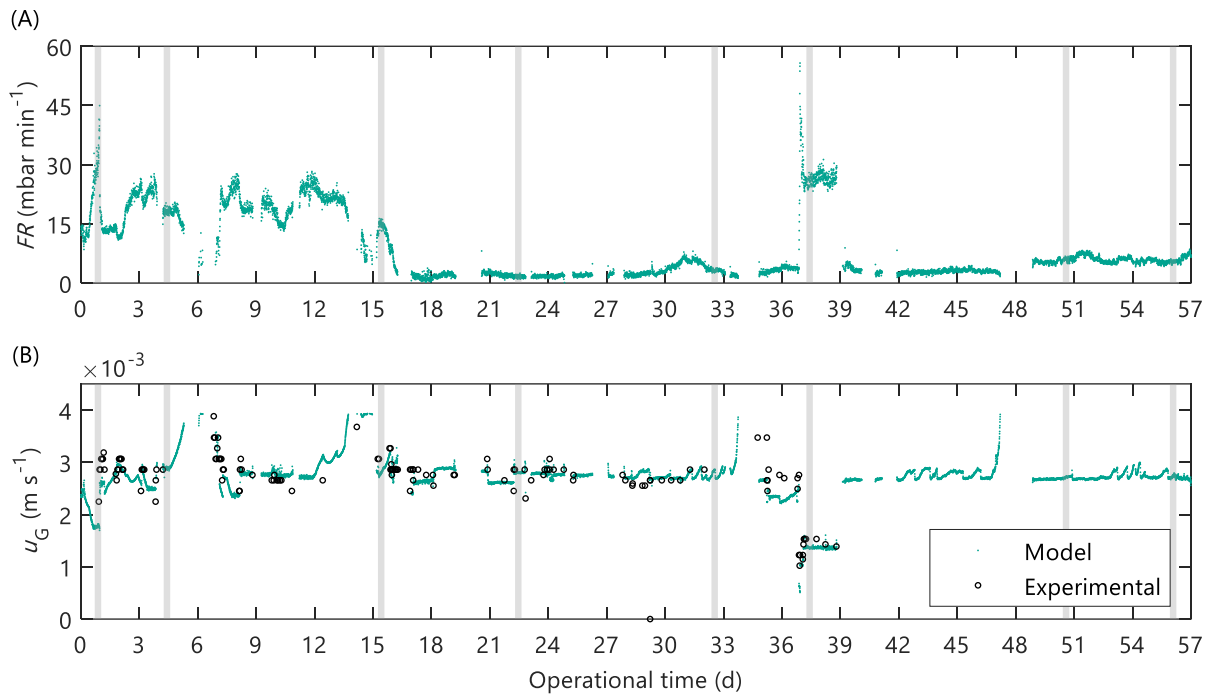
Figure A2. Pilot AnMBR operational variables used during AnMBR filtration model calibration and validation: (A) fouling rate, and (B) gas superficial velocity in the membrane tank. The grey-vertical areas represent the representative dataset, iD1 to iD8 from left to right, used for calibration of the AnMBR filtration models.
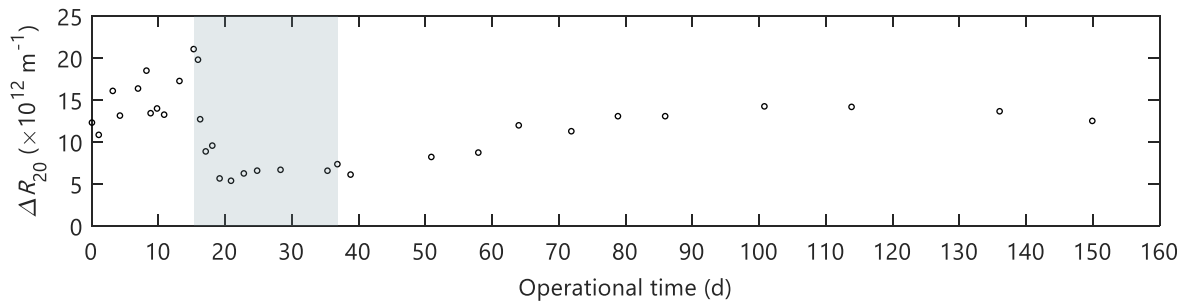
Figure A3. ΔR_{20} measured in-situ in the pilot AnMBR. The grey area represent the data used for AnDFCm filtration model calibration

Batch flocculation kinetic experiments

Flocculation kinetics were assessed in batch assays by intensive monitoring the PSD as a function of time after FE dosing into a grab sludge sample. The sludge samples were collected from a full-scale anaerobic digester treating primary and secondary sludge of a sewage treatment plant (Harnaschpolder, Den Hoorn, the Netherlands). The tests were performed in a jar-test apparatus with a mixing speed of 90 rpm and under dosing of 0.1, 0.2 and 0.3 g L^{-1} of Adifloc KD451, with two replicates per dosage. The sludge was premixed for 10 minutes to homogenise the sample before FE dosing.

The FE caused a rapid increase in the median particle size followed by a gradual decrease reaching a steady value, Figure A4. The time to reach steady values was higher at higher FE concentrations, varying from 10 to 90 minutes.

The FE adsorption rate coefficient (k_{ads}) was estimated as the inverse of the flocculation time, thus, k_{ads} was between 16 and 144 d-1, and a nominal value of 48 d-1 was assumed (equivalent to 30 minutes). Similarly, researchers achieved equilibrium conditions after mixing for 30 minutes for the absorption of polyDADMAC onto waste activated sludge (Zhao et al., 2016) and onto cellulosic fibres (Horvath et al., 2006).
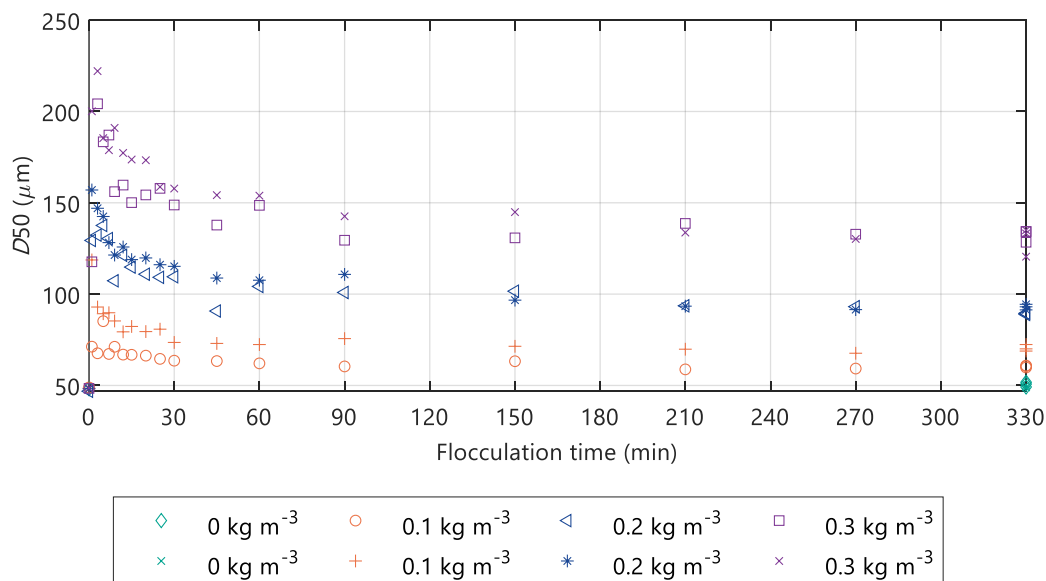
Figure A4. Median particle diameter immediately after flux enhancer addition at different concentrations into a sludge grab sample from full-scale digester. The experiments were performed in a jar test apparatus continuously mixed at 90 rpm. Duplicate measurements have the same colour.

Batch flux enhancer dosage-step supplementary data

Table A3. Grab sludge samples characteristics used in flocculation tests collected from four different large-scale AnMBRs.

AnMBR No.	AnMBR fed	Sample name	pH	TSS (g L^{-1})	SMP-HS (mg L^{-1})	SMP-PR (mg L^{-1})	SMP-CH (mg L^{-1})
1	Liquid fraction of OFMSW digestate [a]	LiqOFMSW	8.1	12.4	5,164	NA [b]	339
2	Source separated blackwater	BWa	7.2	8.6	80	50	14
		BWb	7.2	8.7	71	15	7
		BWc	7.5	4.2	89	74	19
		BWc-II	6.9	3.9	83	71	19
3	Confectionery factory wastewater	Food2	7.2	14.4	32	0	16
		Food2-II	7.2	17.8	33	0	16
4	Whey and wash-water	Food3	7.2	9.5	0	109	20
		Food3-II	7.2	10.7	0	117	22

[a] OFMSW, organic fraction municipal solid waste.

[b] SMP-PR could not be determined because SMP-HS was too high, and the sample had to be diluted 20 times.

Global sensitivity analysis results

Table A4. Sensitivity analysis of alternate AnDFCm filtration models: standardised regression coefficients (β_k) and mean of the standardised regression coefficients with $R^2 > 0.7$ ($\overline{\beta_k}$). Influential parameters with absolute β_k or $\overline{\beta_k}$ value above 0.10 (*).

Model	R^2	$\overline{R^2}$	C_d	$f_{C,c}$	$f_{X,c}$	h_t	$K_{S,c}$	$q_{m,MS}$	β_{ST}	γ
							β_k ($\overline{\beta_k}$)		
D1c $\alpha_{c,1}$	0.92	0.92					-0.09	0.10*		
D1c $\alpha_{c,1p}$	0.06	0.84					0.02 (0.12*)	0.004 (-0.12*)		
D1c $\alpha_{c,2}$	0.95	0.92					-0.11*	0.07		
D1c $\alpha_{c,2p}$	0.02	ND [a]					ND [a]	ND [a]		
D1c $\alpha_{c,3}$	0.98	0.98					-0.27*	0.25*		
D1c $\alpha_{c,3p}$	0.02	0.93					0.04 (0.27*)	-0.06 (-0.28*)		
D1c $\alpha_{c,4p}$	0.00	0.98					0.01 (0.40*)	-0.05 (-0.41*)		

[a] Cannot be determined because all $R^2 < 0.7$. The subset used for parameter estimation was the one from D1c $\alpha_{c,2}$.

Table A4 continued. Sensitivity analysis of alternate AnDFCm filtration models: standardised regression coefficients (β_k) and mean of the standardised regression coefficients with $R^2 > 0.7$ ($\overline{\beta_k}$). Influential parameters with absolute β_k or $\overline{\beta_k}$ value above 0.10 (*).

Model	R^2	$\overline{R^2}$	C_d	$f_{C,c}$	$f_{X,c}$	h_t	$K_{S,c}$	$q_{m,MS}$	β_{ST}	γ
					β_k ($\overline{\beta_k}$)				
D2 $\alpha_{c,1}$	0.90	0.91	0.14*	-0.03		-0.02			0.14*	0.01
D2 $\alpha_{c,1p}$	0.89	0.89	0.12*	-0.06		-0.02			0.18*	-0.01
D2 $\alpha_{c,2}$	0.90	0.90	0.13*	-0.06		-0.002			0.18*	-0.005
D2 $\alpha_{c,2p}$	0.89	0.90	0.12*	-0.05		0.04			0.23*	0.02
D2 $\alpha_{c,3}$	0.98	0.95	0.48*	-0.01		0.01			0.50*	0.0001
D2 $\alpha_{c,3p}$	0.97	0.95	0.49*	-0.01		-0.01			0.52*	0.01
D2 $\alpha_{c,4p}$	0.98	0.95	0.58*	-0.02		0.01			0.62*	0.01
D3 $\alpha_{c,1}$	0.93	0.91		0.004	-0.18*					
D3 $\alpha_{c,1p}$	0.93	0.91		-0.01	-0.19*					
D3 $\alpha_{c,2}$	0.11	0.92		0.02 (0.01)	0.08 (0.20*)					
D3 $\alpha_{c,2p}$	0.21	0.92		-0.06 (-0.01)	-0.03 (0.18*)					
D3 $\alpha_{c,3}$	0.97	0.96		-0.56*	0.09					
D3 $\alpha_{c,3p}$	0.97	0.96		-0.55*	0.10*					
D3 $\alpha_{c,4p}$	0.01	0.91		0.03 (0.12*)	0.06 (0.62*)					

Table A4 continued. Sensitivity analysis of alternate AnDFCm filtration models: standardised regression coefficients (β_k) and mean of the standardised regression coefficients with $R^2>0.7$ ($\overline{\beta_k}$). Influential parameters with absolute β_k or $\overline{\beta_k}$ value above 0.10 (*).

Model	β_k ($\overline{\beta_k}$)					
	k_c	k_{CK}	ε_{c0}	ρ_C	ρ_X	P_a
D1c $\alpha_{c,1}$		-0.19*	0.93*	0.01	0.18*	
D1c $\alpha_{c,1p}$		0.07 (0.19*)	-0.26* (-0.87*)	-0.001 (0.02)	0.03 (-0.20*)	0.01 (-0.03)
D1c $\alpha_{c,2}$	-0.18*		0.92*	0.03	0.19*	
D2 $\alpha_{c,1}$		-0.16*	0.88*	0.05	0.13*	
D2 $\alpha_{c,1p}$		-0.19*	0.87*	0.03	0.15*	
D2 $\alpha_{c,2}$	-0.18*		0.89*	0.04	0.14*	-0.18*
D2 $\alpha_{c,2p}$	-0.18*		0.89*	0.04	0.17*	-0.18*
D3 $\alpha_{c,1}$		-0.18*	0.92*	0.02	0.18*	
D3 $\alpha_{c,1p}$		-0.17*	0.90*	0.01	0.18*	-0.003
D3 $\alpha_{c,2}$	-0.01 (0.17*)		0.31* (-0.89*)	0.01 (-0.01)	-0.12* (-0.22*)	
D3 $\alpha_{c,2p}$	-0.05 (0.18*)		0.46* (-0.92*)	0.04 (0.005)	0.03 (-0.18*)	0.02 (0.01)

(continued)

Table A4 continued. Sensitivity analysis of alternate AnDFCm filtration models: standardised regression coefficients (β_k) and mean of the standardised regression coefficients with $R^2>0.7$ ($\overline{\beta_k}$). Influential parameters with absolute β_k or $\overline{\beta_k}$ value above 0.10 (*).

Model	β_k ($\overline{\beta_k}$)					
	P_a	P_b	ζ_1	ζ_2	ζ_3	ζ_4
D1c $\alpha_{c,3}$		-0.52*	-0.08	-0.44*	-0.61*	0.11*
D1c $\alpha_{c,3p}$	-0.07 (-0.04)	0.07 (0.54*)	-0.03 (0.50*)	0.12* (0.04)	-1×10^{-5} (0.23*)	0.01 (-0.07)
D1c $\alpha_{c,4p}$			-0.04 (0.64*)	-0.06 (0.15*)	0.01 (0.06)	-0.02 (-0.01)
D2 $\alpha_{c,3}$		-0.49*	-0.04	-0.46*	-0.01	0.004
D2 $\alpha_{c,3p}$	-0.003	-0.52*	-0.04	-0.48*	-0.003	-0.003
D2 $\alpha_{c,4p}$			-0.05	-0.56*	-0.01	-0.002
D3 $\alpha_{c,3}$		-0.48*	-0.08	-0.39*	-0.56*	0.10*
D3 $\alpha_{c,3p}$	-0.02	-0.44*	-0.06	-0.37*	-0.57*	0.11*
D3 $\alpha_{c,4p}$			-0.03 (0.08)	-0.07 (0.67*)	0.002 (0.11*)	0.06 (-0.03)

Gas-step test in the pilot AnMBR

The effect of gas sparging on the fouling rate was assessed with gas-step experiments in the pilot AnMBR. The gas superficial velocity in the membrane tank (u_G) was stepwise decreased at the beginning of each relaxation cycle. The step height was -0.4×10^{-3} m s^{-1}, the maximum and minimum u_G were 2.7×10^{-3} and 0.6×10^{-4} m s^{-1}, respectively. The duration of the filtration and relaxation were 15 minutes.

The FR models in Table 5.5 were optimised to fit the experimental fouling rate measured during the gas-step test in the pilot AnMBR. The gas-step test was performed at constant J_{20}, H_{MT}, c_X and c_C; therefore, Equation (5.37) becomes $FR = K_F e^{(a_0 - a_1 u_G)}$, where a_0 and a_1 are parameters, with $a_1 = -\gamma_1 J_{20}/H_{MT}$ and $a_0 = J_{20}(\gamma_0 + \gamma_2 c_X)$; and Equation (5.43) becomes $FR = a_0 u_G^{-\gamma_G}$ with $a_0 = f_{conv} K_F e^{J_{20}(\gamma_0 + \gamma_3 c_C)}$. The parameters were optimised to fit the experimental data using the function *fit* in Matlab®, the experimental and simulated results are displayed in Figure A5.
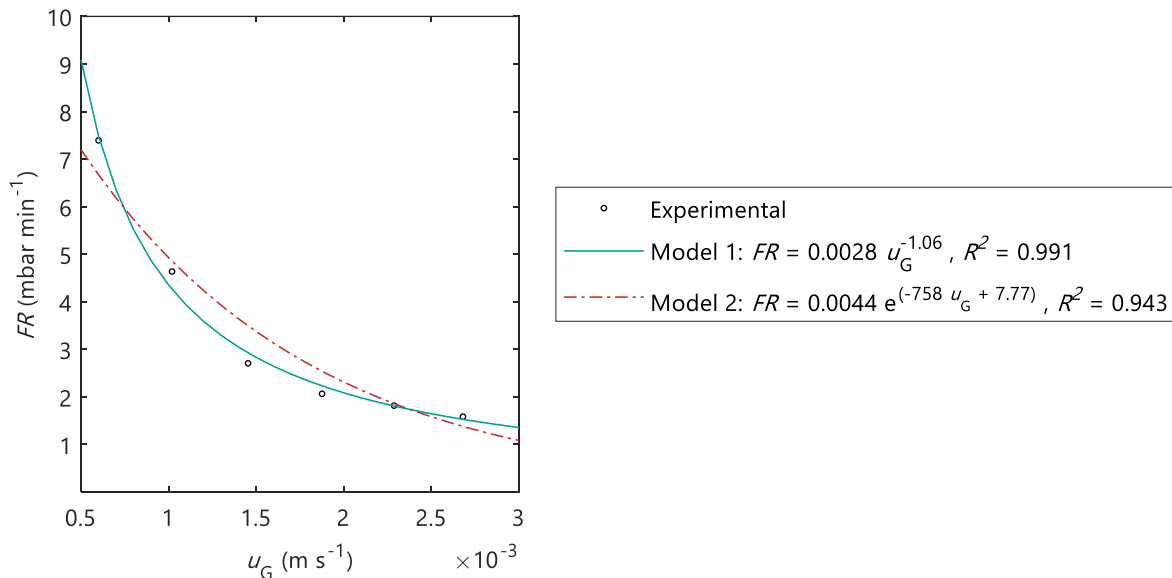
Figure A5. Experimental and simulated fouling rate during the gas-step experiment in the pilot AnMBR.

Sludge viscosity in the AnDFCm installation

The dynamic viscosity of sludge samples at different sludge concentrations was determined using the AnDFCm installation operated at 1.5 m s^{-1} crossflow velocity. Five sludge samples were collected from three different AnMBRs and one anerobic digester, the TSS of the samples ranged from 3 to 30 g L^{-1}.

The dynamic viscosity of the mixed liquor (μ_L) was calculated using the experimentally measured pressure drop along membrane in the AnDFCm installation (Δp) (Geilvoet, 2010; Moreau et al., 2009). μ_L was calculated with Equation (A.6) which combines Euler's and Darcy-Weisbach equations for energy loss in a pipe and the empirical formula that relates the Darcy-Weisbach friction factor with the Reynold's number (Re) for laminar flow (Re<2300).

$$\mu_L = \frac{D_m^2}{32 u_L}\left(-\rho_L\, g + \frac{\Delta p}{\Delta L}\right),$$
(A.6)

where D_m is the membrane internal diameter (0.008 m), u_L the fluid crossflow velocity (1.5 m s^{-1}), ρ_L the fluid density, g the gravitational acceleration, and ΔL the height difference (0.95 m, membrane length). The density ρ_L was assumed equal to the density of water (ρ_W) at the operational temperature T, calculated as follows:

$$\rho_W = -0.0033\, T^2 - 0.1048\, T + 1001.5\,.$$
(A.7)

The Re was calculated with Equation (A.8) to assess the rheological conditions, where laminar flow corresponds to Re <2300, and turbulent to Re > 4000.

$$Re = \frac{\rho_L u_L D_m}{\mu_L}\,.$$
(A.8)

The viscosity of sludge sample with different TSS was measured in the AnDFCm installation, results are show in Table A5. All sludges presented laminar flow (Re<2300), which was assumed during viscosity calculation in Equation (A.6).

The parameters of the mixed liquor viscosity model, a and b in Equation (5.41), were estimated with the function fit in Matlab®. The calibrated model was as follows:

$$\frac{\mu_L}{\mu_W} = 9.35\, e^{0.047\,\text{TSS}}\,.$$
(A.9)

The water viscosity (μ_W) was calculated at each sludge temperature with Equation (A.7). Figure A6 displays the experimental and simulated data.

Table A5. Sludge characteristics and viscosity calculations.

Sludge	TSS (g L^{-1})	T (°C)	Δp (Pa)	Re	μ_L (Pa s)
1	3	17.3	18,334	1,047	0.0113
2	5	21.5	17,902	1,104	0.0108
3	10	24.3	19,693	978	0.0127
4	15	30.2	22,198	728	0.0165
5	30	29.5	33,202	400	0.0305
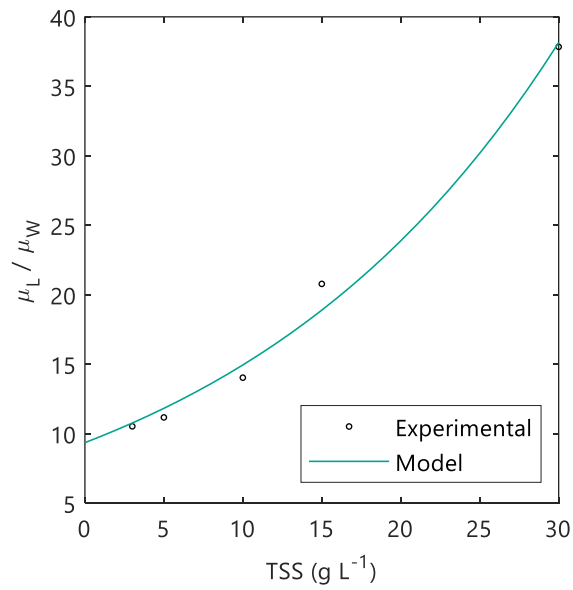
Figure A6. Model calibration of the mixed liquor apparent viscosity (μ_L), normalised by water viscosity (μ_W), in the AnDFCm installation for sludges with different concentrations of total suspended solids (TSS).

A2. PETERSEN MATRIX

Table A6. Process rate equations (ρ_j) of the biochemical-flocculation model.

j	Process ↓	Units	Rate ρ_j
1	Hydrolysis of carbohydrates	kgCOD m^{-3} d^{-1}	$k_{hyd,\text{ch}} X_{\text{ch}}$
2	Hydrolysis of proteins	kgCOD m^{-3} d^{-1}	$k_{hyd,\text{pr}} X_{\text{pr}}$
3	Hydrolysis of lipids	kgCOD m^{-3} d^{-1}	$k_{hyd,\text{li}} X_{\text{li}}$
4	Uptake of sugars	kgCOD m^{-3} d^{-1}	$k_{m,\text{su}} \dfrac{S_{\text{su}}}{K_{s,\text{su}}+S_{\text{su}}} X_{\text{su}} I_{1,\text{su}}$
5	Uptake of amino acids	kgCOD m^{-3} d^{-1}	$k_{m,\text{aa}} \dfrac{S_{\text{aa}}}{K_{s,\text{aa}}+S_{\text{aa}}} X_{\text{aa}} I_{1,\text{aa}}$
6	Uptake of LCFA	kgCOD m^{-3} d^{-1}	$k_{m,\text{fa}} \dfrac{S_{\text{fa}}}{K_{s,\text{fa}}+S_{\text{fa}}} X_{\text{fa}} I_{2,\text{fa}}$
7	Uptake of valerate	kgCOD m^{-3} d^{-1}	$k_{m,\text{c4}} \dfrac{S_{\text{va}}}{K_{s,\text{c4}}+S_{\text{va}}} X_{\text{c4}} \dfrac{1}{1+S_{\text{bu}}/S_{\text{va}}} I_{2,\text{c4}}$
8	Uptake of butyrate	kgCOD m^{-3} d^{-1}	$k_{m,\text{c4}} \dfrac{S_{\text{bu}}}{K_{s,\text{c4}}+S_{\text{bu}}} X_{\text{c4}} \dfrac{1}{1+S_{\text{va}}/S_{\text{bu}}} I_{2,\text{c4}}$
9	Uptake of propionate	kgCOD m^{-3} d^{-1}	$k_{m,\text{pro}} \dfrac{S_{\text{pro}}}{K_{s,\text{pro}}+S_{\text{pro}}} X_{\text{pro}} I_{2,\text{pro}}$
10	Uptake of acetate	kgCOD m^{-3} d^{-1}	$k_{m,\text{ac}} \dfrac{S_{\text{ac}}}{K_{s,\text{ac}}+S_{\text{ac}}} X_{\text{ac}} I_{3,\text{ac}}$
11	Uptake of hydrogen	kgCOD m^{-3} d^{-1}	$k_{m,\text{h2}} \dfrac{S_{\text{h2}}}{K_{s,\text{h2}}+S_{\text{h2}}} X_{\text{h2}} I_{1,\text{h2}}$
12	Decay of X_{su}	kgCOD m^{-3} d^{-1}	$b_{\text{su}} X_{\text{su}}$
13	Decay of X_{aa}	kgCOD m^{-3} d^{-1}	$b_{\text{aa}} X_{\text{aa}}$
14	Decay of X_{fa}	kgCOD m^{-3} d^{-1}	$b_{\text{fa}} X_{\text{fa}}$
15	Decay of X_{c4}	kgCOD m^{-3} d^{-1}	$b_{\text{c4}} X_{\text{c4}}$
16	Decay of X_{pro}	kgCOD m^{-3} d^{-1}	$b_{\text{pro}} X_{\text{pro}}$
17	Decay of X_{ac}	kgCOD m^{-3} d^{-1}	$b_{\text{ac}} X_{\text{ac}}$
18	Decay of X_{h2}	kgCOD m^{-3} d^{-1}	$b_{\text{h2}} X_{\text{h2}}$
19	Disintegration of biomass	kgCOD m^{-3} d^{-1}	$k_{\text{dis,bio}} X_{\text{bio}}$
20	Liquid-gas transfer of H$_2$	kmol m^{-3} d^{-1}	$k_L a\left(S_{\text{h2}} - K_{H,\text{h2}}\, c_{\text{h2,G}} RT\right)$
21	Liquid-gas transfer of CH$_4$	kmol m^{-3} d^{-1}	$k_L a\left(S_{\text{ch4}} - K_{H,\text{ch4}}\, c_{\text{ch4,G}} RT\right)$
22	Liquid-gas transfer of CO$_2$	kmol m^{-3} d^{-1}	$k_L a\left(S_{\text{co2}} - K_{H,\text{ch4}} c_{\text{co2,G}} RT\right)$
23	Adsorption of flux enhancer onto particulate material	kgCOD m^{-3} d^{-1}	$k_{\text{ads}}\left(X_{\text{fe},e} - X_{\text{fe}}\right)$
24	Flocculation of colloidal material	kgCOD m^{-3} d^{-1}	$Y_{\text{fe,C}}\, k_{\text{ads}}\left(X_{\text{fe},e} - X_{\text{fe}}\right) \dfrac{C_{\text{I}}/i_{\text{COD,CI}}}{c_{\text{X}} + c_{\text{C}}} \dfrac{X_{\text{I}}}{X_{\text{I}} + 1\times10^{-6}}$

Inhibition factors:

$I_{1,j} = I_{\text{ph},j}\, I_{\text{IN,lim}}$

$I_{2,j} = I_{\text{ph},j}\, I_{\text{IN,lim}}\, I_{\text{h2},j}$

$I_{3,j} = I_{\text{ph},j}\, I_{\text{IN,lim}}\, I_{\text{fe}}$

$$I_{\text{ph},j} = \frac{1 + 2\times10^{0.5(\text{pH}_{\text{LL},j}-\text{pH}_{\text{UL},j})}}{1 + 10^{(\text{pH}-\text{pH}_{\text{UL},j})} + 10^{(\text{pH}_{\text{LL},j}-\text{pH})}}$$

$$I_{\text{IN,lim}} = \frac{S_{\text{IN}}}{K_{s,\text{IN}}+S_{\text{IN}}}$$

$$I_{\text{h2},j} = \frac{1}{1 + S_{\text{h2}}/K_{I,\text{h2},j}}$$

$$I_{\text{fe}} = \frac{1}{1 + S_{\text{fe}}/K_{I,\text{fe}}}$$

Table A7. Stoichiometric coefficients ($v_{i,j}$) of the biochemical-flocculation model.

j	Component → i	1 S_{su}	2 S_{aa}	3 S_{fa}	4 S_{va}
	Process ↓	S_{su}	S_{aa}	S_{fa}	S_{va}
1	Hydrolysis of carbohydrates	1			
2	Hydrolysis of proteins		1		
3	Hydrolysis of lipids	$1 - f_{fa,li}$		$f_{fa,li}$	
4	Uptake of sugars	-1			
5	Uptake of amino acids		-1		$(1 - Y_{aa})f_{va,aa}$
6	Uptake of LCFA			-1	
7	Uptake of valerate				-1
8	Uptake of butyrate				
9	Uptake of propionate				
10	Uptake of acetate				
11	Uptake of hydrogen				
12	Decay of X_{su}				
13	Decay of X_{aa}				
14	Decay of X_{fa}				
15	Decay of X_{c4}				
16	Decay of X_{pro}				
17	Decay of X_{ac}				
18	Decay of X_{h2}				
19	Disintegration of biomass				
20	Liquid-gas transfer of H_2				
21	Liquid-gas transfer of CH_4				
22	Liquid-gas transfer of CO_2				
23	Adsorption of flux enhancer onto particulate material				
24	Flocculation of colloidal material				
	Component → ($kgCOD\ m^{-3}$)	Monosaccharides	Amino Acids	Long chain fatty acids (LCFA)	Total Valerate

(continued)

Table A7 continued. Stoichiometric coefficients ($v_{i,j}$) of the biochemical-flocculation model.

j \ i	5 S_{bu}	6 S_{pro}	7 S_{ac}	8 S_{h2}	9 S_{ch4}	10 S_{IC}
1						
2						
3						
4	$(1-Y_{su})f_{bu,su}$	$(1-Y_{su})f_{pro,su}$	$(1-Y_{su})f_{ac,su}$	$(1-Y_{su})f_{h2,su}$		$-\sum\limits_{i\neq 10} i_{C,i} v_{i,su}$
5	$(1-Y_{aa})f_{bu,aa}$	$(1-Y_{aa})f_{pro,aa}$	$(1-Y_{aa})f_{ac,aa}$	$(1-Y_{aa})f_{h2,aa}$		$-\sum\limits_{i\neq 10} i_{C,i} v_{i,aa}$
6			$(1-Y_{fa})0.7$	$(1-Y_{fa})0.3$		
7		$(1-Y_{c4})0.54$	$(1-Y_{c4})0.31$	$(1-Y_{c4})0.15$		
8	-1		$(1-Y_{c4})0.8$	$(1-Y_{c4})0.2$		
9		-1	$(1-Y_{pro})0.57$	$(1-Y_{pro})0.43$		$-\sum\limits_{i\neq 10} i_{C,i} v_{i,pro}$
10			-1		$1-Y_{ac}$	$-\sum\limits_{i\neq 10} i_{C,i} v_{i,ac}$
11				-1	$1-Y_{h2}$	$-\sum\limits_{i\neq 10} i_{C,i} v_{i,h2}$
12						
13						
14						
15						
16						
17						
18						
19						
20				-1		
21					-1	
22						-1
23						
24						
Component (kgCOD m⁻³)	Total Butyrate	Total Propionate	Total Acetate	Hydrogen gas	Methane gas	Inorganic Carbon (kmol m⁻³)

Table A7 continued. Stoichiometric coefficients ($v_{i,j}$) of the biochemical-flocculation model.

i / j	11 S_{IN}	12 S_I	13 S_{fe}	14 X_{ch}	15 X_{pr}	16 X_{li}
1				-1		
2					-1	
3						-1
4	$-Y_{su}i_{N,su}$					
5	$-Y_{aa}i_{N,aa}$					
6	$-Y_{fa}i_{N,fa}$					
7	$-Y_{c4}i_{N,c4}$					
8	$-Y_{c4}i_{N,c4}$					
9	$-Y_{pro}i_{N,pro}$					
10	$-Y_{ac}i_{N,ac}$					
11	$-Y_{h2}i_{N,h2}$					
12						
13						
14						
15						
16						
17						
18						
19		$f_{SI,bio}$		$f_{ch,bio}$	$f_{pr,bio}$	$f_{li,bio}$
20						
21						
22						
23			-1			
24						
Component (kgCOD m⁻³)	Inorganic Nitrogen (kmol m⁻³)	Soluble inerts	Flux enhancer (in bulk liquid)	Carbohydrates	Proteins	Lipids

(continued)

Table A7 continued. Stoichiometric coefficients ($v_{i,j}$) of the biochemical-flocculation model.

j \ i	17 X_{su}	18 X_{aa}	19 X_{fa}	20 X_{c4}	21 X_{pro}	22 X_{ac}	23 X_{h2}
1							
2							
3							
4	Y_{su}						
5		Y_{aa}					
6			Y_{fa}				
7				Y_{c4}			
8				Y_{c4}			
9					Y_{pro}		
10						Y_{ac}	
11							Y_{h2}
12	-1						
13		-1					
14			-1				
15				-1			
16					-1		
17						-1	
18							-1
19							
20							
21							
22							
23							
24							
Component (kgCOD m^{-3})	Sugar degraders	Amino acid degraders	LCFA degraders	Valerate and butyrate degraders	Propionate degraders	Acetate degraders	Hydrogen degraders

(continued)

Table A7 continued. Stoichiometric coefficients ($v_{i,j}$) of the biochemical-flocculation model.

i / j	24 X_I	25 C_I	26 X_{fe}	27 X_{bio}	28 $c_{h2,G}$	29 $c_{ch4,G}$	30 $c_{co2,G}$
1							
2							
3							
4							
5							
6							
7							
8							
9							
10							
11							
12				1			
13				1			
14				1			
15				1			
16				1			
17				1			
18				1			
19	$f_{XI,bio}$	$f_{CI,bio}$		-1			
20					1/16		
21						1/64	
22							1
23			1				
24	1	-1					
Component (kgCOD m^{-3})	Particulate inerts	Colloidal inerts	Flux enhancer (adsorbed)	Decayed biomass	Hydrogen in gas phase (kmol m^{-3})	Methane in gas phase (kmol m^{-3})	Carbon dioxide in gas phase (kmol m^{-3})

A3. PARAMETER VALUES

Most parameter values were taken from literature. The reaction rate for process j (k_j) was calculated at the operational temperature as follows (Durán, 2013):

$$k_j\big|_T = k_j\big|_{T_{\text{ref}}} \theta_j^{(T-T_{\text{ref}})} , \tag{A.10}$$

where θ_j is the temperature correction factor for k_j, and T_{ref} the reference temperature. The reaction rate k_j is: the first order reaction rate coefficient for hydrolysis ($k_{\text{hyd},j}$) for $j \in [1,3]$, the Monod maximum specific uptake rate ($k_{m,j}$) for $j \in [4,11]$, the first order decay rate of microorganism (b_j) for $j \in [12,18]$, and the first order reaction rate coefficient for biomass disintegration ($k_{\text{dis,bio}}$) for $j = 19$. Table A8 summarises the values for k_j at $T_{\text{ref}} = 308.15$ K and θ_j.

Table A8 shows the values of the following stoichiometric and inhibitions parameters: Monod half saturation coefficient for process j ($K_{S,j}$), Monod half saturation coefficient for inorganic nitrogen ($K_{S,\text{IN}}$), concentration of inhibitor i giving 50% inhibition on process j ($K_{I,i,j}$), empirical upper ($\text{pH}_{\text{UL},j}$) and lower ($\text{pH}_{\text{LL},j}$) pH inhibition coefficients, and yield coefficient of biomass on substrate for process j (Y_j).

Table A9 shows the carbon and nitrogen content in the different components and the theoretical chemical oxygen demand used to calculate the total concentration of particulate and colloidal material expressed as suspended solids.

The gas-liquid transfer coefficient ($k_L a$) for oxygen, 178 d^{-1} (Metcalf et al., 2002), was used for all gases. Henry's law coefficients were calculated at the operational temperature with Equation (A.11) using the values at T_{ref}. The $K_{H,i}$ at 308.15 K were 0.012 kgCOD m^{-3} bar^{-1}, 0.108 kgCOD m^{-3} bar^{-1}, and 0.027 kmol m^{-3} bar^{-1}, and $\theta_{H,i}$ were 525, 1744, 2405 for hydrogen, methane and carbon dioxide, respectively (Sander, 2015).

$$K_{H,i}\big|_T = K_{H,i}\big|_{T_{\text{ref}}} e^{\theta_{H,i}\left(\frac{1}{T}-\frac{1}{T_{\text{ref}}}\right)} . \tag{A.11}$$

Table A8. Kinetic and stoichiometric parameter values for biochemical reactions at 35°C.

j	k_j [a] (d^{-1})	θ_j (-)	$K_{S,j}$ (kgCOD m^{-3})	$K_{S,\mathrm{IN}}$ (M)	$K_{I,\mathrm{h2},j}$ (kgCOD m^{-3})	$K_{I,\mathrm{fe},j}$ (kgCOD m^{-3})	pH$_{\mathrm{UL},j}$ (-)	pH$_{\mathrm{LL},j}$ (-)	Y_j (-)
1	0.5 [b]	1.066							
2	0.5 [b]	1.066							
3	0.5 [b]	1.066							
4	30	1.033	0.5	1×10^{-4}			5.5	4	0.1
5	50	1.033	0.3	1×10^{-4}			5.5	4	0.08
6	6	1.033	0.4	1×10^{-4}	5×10^{-6}		5.5	4	0.06
7	20	1.043	0.2	1×10^{-4}	1×10^{-5}		5.5	4	0.06
8	20	1.043	0.2	1×10^{-4}	1×10^{-5}		5.5	4	0.06
9	13	1.043	0.1	1×10^{-4}	3.5×10^{-6}		5.5	4	0.04
10	8	1.031	0.15	1×10^{-4}		0.02	7	6	0.05
11	35	1.030	7×10^{-6}	1×10^{-4}			6	5	0.06
12-18	0.1	1.066							
19	0.15 [b]	1.066							

Note: most values are the ones suggested for mesophilic solids in the ADM1 (Batstone et al., 2002), except: b_j (Batstone et al., 2004), θ_j (Durán, 2013), $K_{I,\mathrm{fe}}$ (Odriozola et al., 2019) and $k_{\mathrm{dis,bio}}$ (Tugtas et al., 2006).

[a] k_j is $k_{\mathrm{hyd},j}$ for $j \in [1,3]$, $k_{m,j}$ for $j \in [4,11]$, b_j for $j \in [12,18]$, and $k_{\mathrm{dis,bio}}$ for $j = 19$.

[b] Initial guess for parameter estimation.

Table A9. Composition matrix: nitrogen content ($i_{N,i}$), carbon content ($i_{C,i}$) and theoretical chemical oxygen demand ($i_{COD,i}$) for the component i.

	Component i		$i_{N,i}$ (kmol kgCOD^{-1})	$i_{C,i}$ (kmol kgCOD^{-1})	$i_{COD,i}$ (kgCOD kg^{-1})
1	S_{su}	Monosaccharides	0	0.0313	
2	S_{aa}	Amino Acids	0.007	0.0054 [c]	
3	S_{fa}	Long chain fatty acids (LCFA)	0	0.0217	
4	S_{va}	Total Valerate	0	0.0240	
5	S_{bu}	Total Butyrate	0	0.0250	
6	S_{pro}	Total Propionate	0	0.0268	
7	S_{ac}	Total Acetate	0	0.0313	
8	S_{h2}	Hydrogen gas	0	0	
9	S_{ch4}	Methane gas	0	0.0156	
10	S_{IC}	Inorganic Carbon	0	1	
11	S_{IN}	Inorganic Nitrogen	1	0	
12	S_{I}	Soluble inerts [a]	0.00625	0.0313	
13	S_{fe}	Flux enhancer in bulk liquid	0.0045 [b]	0.0357 [b]	
14	X_{ch}	Carbohydrates	0	0.0313	1.19 [d]
15	X_{pr}	Proteins	0.007	0.0054 [c]	1.42 [d]
16	X_{li}	Lipids	0	0.0220	2.90 [d]
17	X_{su}	Sugar degraders	0.00625	0.0313	1.42 [e]
18	X_{aa}	Amino acid degraders	0.00625	0.0313	1.42 [e]
19	X_{fa}	LCFA degraders	0.00625	0.0313	1.42 [e]
20	X_{c4}	Valerate and butyrate degraders	0.00625	0.0313	1.42 [e]
21	X_{pro}	Propionate degraders	0.00625	0.0313	1.42 [e]
22	X_{ac}	Acetate degraders	0.00625	0.0313	1.42 [e]
23	X_{h2}	Hydrogen degraders	0.00625	0.0313	1.42 [e]
24	X_{I}	Particulate inerts [a]	0.00625	0.0313	1.42 [e]
25	C_{I}	Colloidal Inerts [a]	0.00625	0.0313	1.42 [e]
26	X_{fe}	Flux enhancer adsorbed	0.0045 [b]	0.0357 [b]	1.14 [f]
27	X_{bio}	Decayed biomass	0.00625	0.0313	1.42 [e]

Note: unless otherwise stated the reference is the ADM1 (Batstone et al., 2002).
[a] Biomass values assumed for inert material.
[b] Calculated from the chemical formula of polydiallyldimethylammonium chloride, $(C_8H_{16}NCl)_n$.
[c] Mean value of inorganic carbon content in different amino acids presented in the ADM1.
[d] Reference Lidholm and Ossiansson (2008).
[e] Reference Mara et al. (2003).
[f] Experimentally measured in Adifloc KD451.

A4. GSA CONVERGENCE ANALYSIS

The sample size, N, used for GSA was determined by convergence analysis based on the stability in parameter selection. The convergence analysis was as follows (Benedetti et al., 2011): 30 batches (k=30) of Monte Carlo simulations using Latin hypercube sampling with 100 samples (n=100) per batch were performed. The SRC were calculated after each batch with the cumulative number of output files, where $\beta_{i,k}$ was the SRC of the i-th parameter in the k-th batch. The convergence criterion was the stability in the parameter selection, with N=100k when the parameters with $\left|\beta_{i,k}\right| \geq 0.1$ in the k-th batch remain the same for five consecutive batches.

A5. SIMULATED INFLUENT CHARACTERISTICS

(A)

(B)
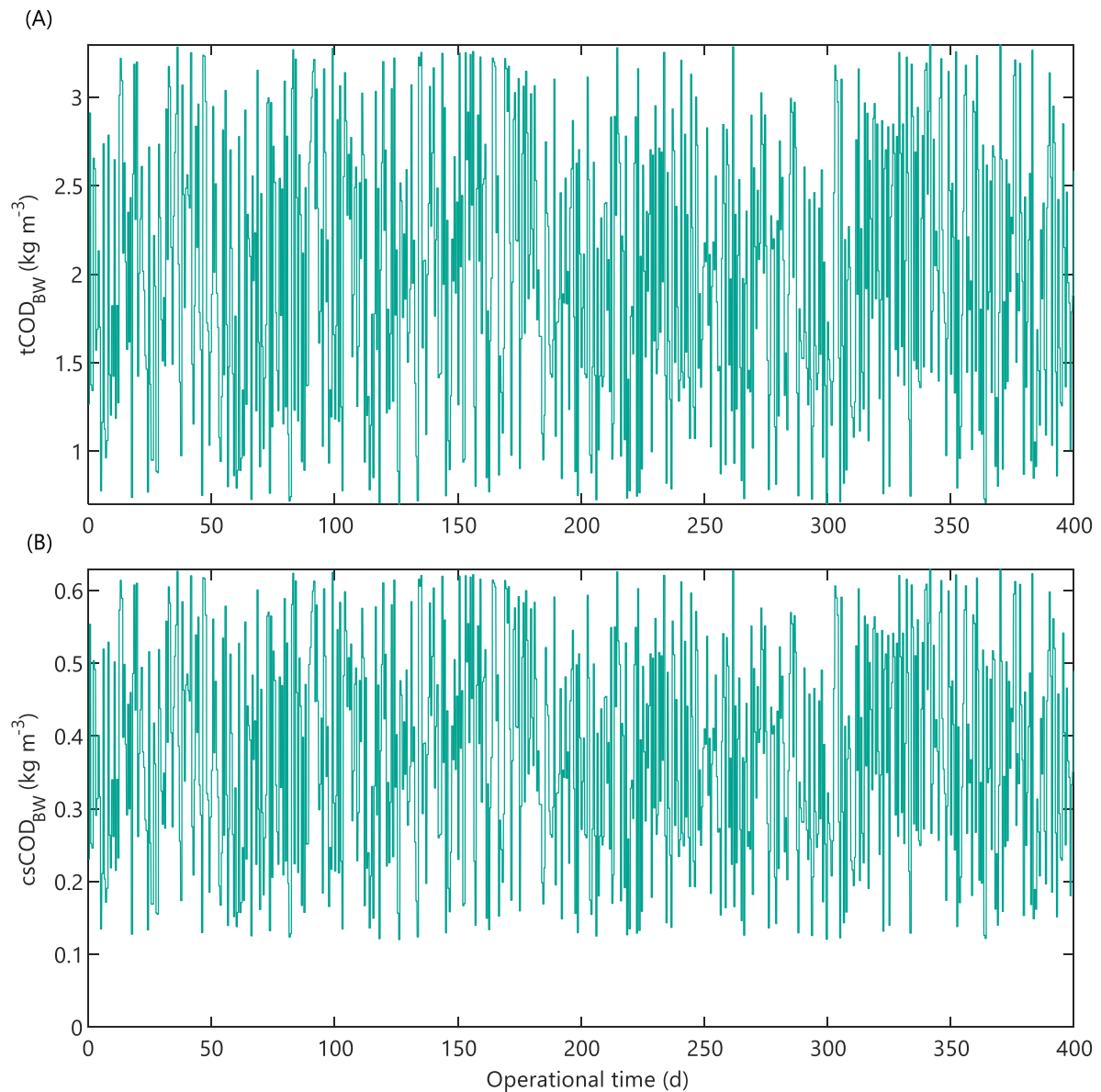
Figure A7. Simulated blackwater characteristics used in the simulation environment: (A) total COD, and (B) submicron COD.

A6. CALIBRATION AND VALIDATION OF BIOCHEMICAL-FLOCCULATION MODEL

Fast processes calibration results

Table A10. Flocculation model calibration results: mean of the standardised regression coefficients with $R^2 > 0.7$ $(\overline{\beta_k})$ for different output variables, and values $(\hat{\theta})$, standard deviation (σ_θ), and relative error $(\sigma_\theta / \hat{\theta})$ of the estimated parameters.

Parameter	Units	$\overline{\beta_k}$ for csCOD	$\overline{\beta_k}$ for d_p	$\hat{\theta}$	σ_θ	$\sigma_\theta / \hat{\theta}$
k_{ads}	d^{-1}	-0.07	0.07			
$k_{\text{floc,fe}}$	m kgCOD^{-1} m^3	-0.02	0.98	6.00×10^{-4}	0.43×10^{-4}	0.07
$K_{L,\text{ads}}$	m^3 kg^{-1}	-0.03	0.003			
$q_{m,\text{ads}}$	kgCOD kg^{-1}	-0.03	0.02			
$Y_{\text{fe,C}}$	kg kg^{-1}	-0.95	0.0004	649.8	0.34	0.001

Slow processes calibration results

Table A11. Sensitivity analysis of the biochemical-flocculation model: standardised regression coefficients (β_k) and mean of the standardised regression coefficients with $R^2 > 0.7$ $(\overline{\beta_k})$ for different output variables. Influential parameters with absolute value above 0.1 (*).

Parameter	Units	β_k for TSS, cCOD & d_p	β_k for TSS & cCOD	β_k for TSS	β_k for d_p	β_k for cCOD	$\overline{\beta_k}$ for TSS
	$R^2 \rightarrow$	0.97	0.97	0.45	0.95	0.97	$\overline{R^2} = 0.77$
$i_{\text{C,CXI,bio}}$	kgCOD kgCOD^{-1}	0.05	0.05	-0.01	-0.01	0.05	-0.01
$i_{\text{CI,CSInf}}$	kgCOD kgCOD^{-1}	0.96*	0.96*	0.32*	0.06	0.95*	0.46*
$i_{\text{Saa,SInf}}$	kgCOD kgCOD^{-1}	0.01	0.01	-0.05	-0.01	0.01	-0.02
$i_{\text{Sfa,SInf}}$	kgCOD kgCOD^{-1}	0.01	0.01	0.03	0.01	0.01	0.01
$i_{\text{SI,SInf}}$	kgCOD kgCOD^{-1}	-0.001	-0.001	0.002	-0.01	-0.001	-0.01
$i_{\text{Ssu,SInf}}$	kgCOD kgCOD^{-1}	-0.01	-0.01	0.01	-0.01	-0.01	-0.003
$i_{\text{Svfa,SInf}}$	kgCOD kgCOD^{-1}	-0.001	-0.001	-0.01	0.02	-0.0003	0.001
$i_{\text{Xch,XInf}}$	kgCOD kgCOD^{-1}	0.04	0.04	-0.25*	-0.05	0.06	-0.25*
$i_{\text{XI,XInf}}$	kgCOD kgCOD^{-1}	-0.17*	-0.17*	0.44*	0.09	-0.20*	0.62*
$i_{\text{Xli,XInf}}$	kgCOD kgCOD^{-1}	0.04	0.04	-0.22*	-0.05	0.06	-0.24*
$i_{\text{Xpr,XInf}}$	kgCOD kgCOD^{-1}	0.04	0.04	-0.15*	-0.02	0.05	-0.21*
$k_{\text{dis,bio}}$	d^{-1}	0.001	0.001	-0.01	-0.01	0.002	-0.003
k_{floc}	d^{-1}	-0.02	-0.01	0.00	-0.95*	-0.01	0.004
k_{hyd}	d^{-1}	0.002	0.002	-0.11*	-0.01	0.01	-0.05

Table A12. Parameter estimation of the biochemical-flocculation model: values ($\hat{\theta}$), standard deviation (σ_θ), and relative error ($\sigma_\theta/\hat{\theta}$) of the estimated parameters, and output variable used for parameter estimation.

Parameter	Units	$\hat{\theta}$	σ_θ	$\sigma_\theta/\hat{\theta}$	Output variable
$i_{CI,CSInf}$	kgCOD kgCOD^{-1}	0.0287	6×10^{-6}	2×10^{-4}	cCOD & TSS
$i_{XI,XInf}$	kgCOD kgCOD^{-1}	0.189	9×10^{-6}	5×10^{-5}	cCOD & TSS
k_{floc}	d^{-1}	0.16	0.02	0.128	d_p

Prediction with calibrated model
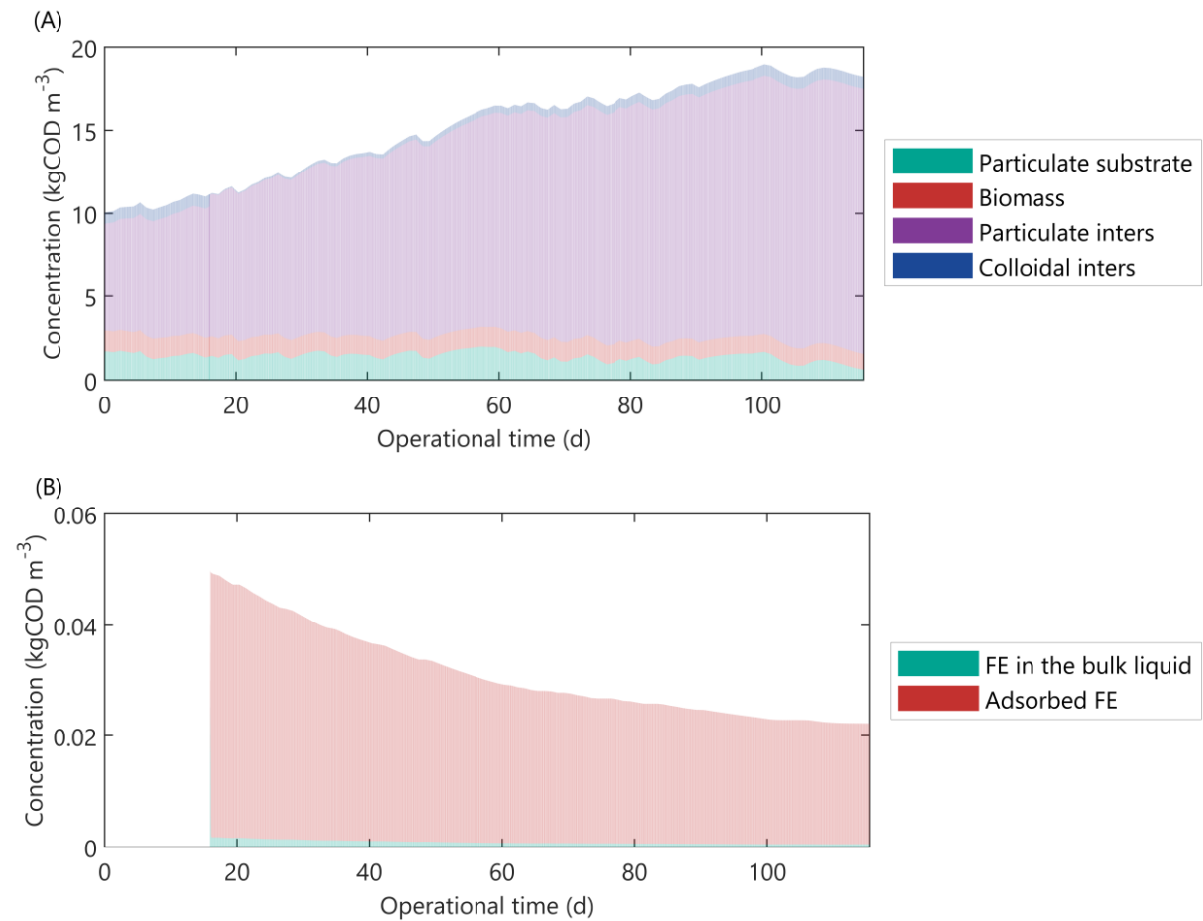
Figure A8. Simulated concentrations inside the reactor during operational period of pilot AnMBR dosed with flux enhancer (FE) on day 16: (A) particulate and colloidal materials, and (B) FE components.

A7. CALIBRATION AND VALIDATION OF ALTERNATE ANMBR FILTRATION MODELS

Global sensitivity analysis results

Table A13. Sensitivity analysis of the alternate AnMBR empirical fouling rate (FR) models: standardised regression coefficients (β_k) and mean of the standardised regression coefficients with $R^2 > 0.7$ ($\overline{\beta_k}$). Influential parameters with absolute β_k or $\overline{\beta_k}$ value above 0.10 (*).

Model	R^2	$\overline{R^2}$	β_k ($\overline{\beta_k}$)						
			K_F	γ_0	γ_1	γ_2	γ_3	γ_4	γ_G
FR1	0.13	0.81	0.05 (0.12*)	-0.28* (0.86*)	-0.10 (-0.14*)	0.15* (0.19*)	0.09 (0.15*)		
FR2	0.85	0.83	-0.13*	-0.88*	0.12*		-0.17*		
FR3	0.02	0.85	0.10 (0.15*)	0.04 (0.90*)			0.08 (0.13*)		0.07 (0.06)
FR4	0.88	0.81	-0.12*	-0.90*	0.11*	-0.13*	-0.14*	0.13*	
FR5	0.82	0.82	-0.15*	-0.84*	0.11*		-0.18*	0.16*	
FR6	0.88	0.83	-0.11*	-0.91*			-0.15*	0.17*	-0.10

Table A14. Sensitivity analysis of the alternate AnMBR filtration models: standardised regression coefficients (β_k) and mean of the standardised regression coefficients with $R^2 > 0.7$ ($\overline{\beta_k}$). Influential parameters with absolute β_k or $\overline{\beta_k}$ value above 0.10 (*).

Model	R^2	$\overline{R^2}$	β_k ($\overline{\beta_k}$)					
			C_d	$f_{C,c}$	$K_{S,c}$	$q_{m,MS}$	β_{ST}	γ
D1a $\alpha_{c,1}$	0.92	0.89			-0.01	0.02		
D1a $\alpha_{c,1p}$	0.03	0.80			-0.02 (0.001)	-0.09(-0.002)		
D1a $\alpha_{c,2}$	0.95	0.89			-0.01	-0.004		
D1a $\alpha_{c,2p}$	0.07	0.83			-0.02 (-0.03)	-0.09 (-0.02)		
D1a $\alpha_{c,3}$	0.98	0.92			0.003	0.001		
D1a $\alpha_{c,3p}$	0.96	0.88			-0.06	0.08		
D1a $\alpha_{c,4p}$	0.05	0.79			0.11* (0.06)	-0.03 (-0.05)		
D1b $\alpha_{c,1}$	0.94	0.91			-0.004	-0.01		
D1b $\alpha_{c,1p}$	0.04	0.79			0.04 (0.02)	0.05 (-0.03)		
D1b $\alpha_{c,2}$	0.97	0.91			0.01	-0.002		
D1b $\alpha_{c,2p}$	0.03	0.84			-0.02(-0.001)	-0.02 (-0.03)		
D1b $\alpha_{c,3}$	0.97	0.91			-0.01	0.01		
D1b $\alpha_{c,3p}$	0.96	0.88			-0.08	0.12*		
D1b $\alpha_{c,4p}$	0.03	0.87			-0.04 (0.04)	-0.10 (-0.08)		
D1c $\alpha_{c,1}$	0.93	0.92			-0.02	-0.01		
D1c $\alpha_{c,1p}$	0.84	0.85			0.01	0.03		
D1c $\alpha_{c,2}$	0.94	0.93			-0.02	0.02		
D1c $\alpha_{c,2p}$	0.74	0.73			-0.01	0.02		
D1c $\alpha_{c,3}$	0.99	0.92			-0.04	0.06		
D1c $\alpha_{c,3p}$	0.98	0.91			-0.07	0.10*		
D1c $\alpha_{c,4p}$	0.92	0.86			-0.27*	0.37*		
D2 $\alpha_{c,1}$	0.90	0.90	0.14*	-0.03			0.21*	0.01
D2 $\alpha_{c,1p}$	0.91	0.90	0.16*	0.01			0.20*	0.02
D2 $\alpha_{c,2}$	0.90	0.90	0.16*	-0.04			0.21*	-0.005
D2 $\alpha_{c,2p}$	0.89	0.89	0.14*	-0.02			0.17*	-0.01
D2 $\alpha_{c,3}$	0.98	0.97	0.39*	-0.07			0.56*	-0.01
D2 $\alpha_{c,3p}$	0.98	0.97	0.42*	-0.05			0.59*	0.003
D2 $\alpha_{c,4p}$	0.98	0.97	0.47*	-0.08			0.67*	-0.004

(continued)

Table A14 continued. Sensitivity analysis of the alternate AnMBR filtration models: standardised regression coefficients (β_k) and mean of the standardised regression coefficients with $R^2 > 0.7$ ($\overline{\beta_k}$). Influential parameters with absolute β_k or $\overline{\beta_k}$ value above 0.10 (*).

Model	β_k ($\overline{\beta_k}$)				
	K_F	γ_0	γ_1	γ_2	γ_3
D1a $\alpha_{c,1}$	-0.02	-0.32*	0.04	-0.03	
D1a $\alpha_{c,1p}$	0.02 (0.04)	-0.004 (0.28*)	-0.01 (-0.07)	0.03 (0.05)	
D1a $\alpha_{c,2}$	-0.04	-0.31*	0.03	-0.03	
D1a $\alpha_{c,2p}$	0.04 (0.03)	-0.02 (0.02)	-0.004 (-0.02)	0.06 (0.02)	
D1a $\alpha_{c,3}$	-0.09	-0.78*	0.11*	-0.11*	
D1a $\alpha_{c,3p}$	-0.10	-0.69*	0.10*	-0.09	
D1a $\alpha_{c,4p}$	-0.06 (0.05)	0.11* (0.48*)	-0.02 (-0.08)	0.11* (0.05)	
D1b $\alpha_{c,1}$	-0.03	-0.16*	0.02	-0.02	-0.03
D1b $\alpha_{c,1p}$	0.04 (0.02)	0.05 (0.23*)	-0.01 (-0.03)	0.04 (0.02)	0.06 (0.01)
D1b $\alpha_{c,2}$	-0.01	-0.14*	0.02	-0.03	-0.03
D1b $\alpha_{c,2p}$	0.06 (0.01)	0.01 (0.01)	-0.06 (-0.02)	-0.01 (-0.01)	-0.03 (0.005)
D1b $\alpha_{c,3}$	-0.07	-0.49*	0.09	-0.07	-0.10
D1b $\alpha_{c,3p}$	-0.03	-0.40*	0.07	-0.06	-0.08
D1b $\alpha_{c,4p}$	0.05 (0.07)	0.06 (0.51*)	-0.03 (-0.03)	-0.06 (0.05)	-0.02 (0.03)

(continued)

Table A14 continued. Sensitivity analysis of the alternate AnMBR filtration models: standardised regression coefficients (β_k) and mean of the standardised regression coefficients with $R^2 > 0.7$ ($\overline{\beta_k}$). Influential parameters with absolute β_k or $\overline{\beta_k}$ value above 0.10 (*).

Model	β_k ($\overline{\beta_k}$)					
	k_c	k_{CK}	ε_{c0}	ρ_C	ρ_X	P_a
D1a $\alpha_{c,1}$		-0.18*	0.85*	0.003	0.18*	
D1a $\alpha_{c,1p}$		0.04 (0.18*)	-0.07 (-0.77*)	-0.04 (0.01)	-0.08 (-0.18*)	-0.08 (-0.04)
D1a $\alpha_{c,2}$	-0.18*		0.89*	0.01	0.17*	
D1a $\alpha_{c,2p}$	0.09 (0.22*)		-0.2* (-0.86*)	0.005 (-0.03)	-0.1 (-0.21*)	-0.06 (-0.07)
D1b $\alpha_{c,1}$		-0.19*	0.91*	-0.001	0.18*	
D1b $\alpha_{c,1p}$		0.08 (0.2*)	-0.09 (-0.81*)	0.05 (0.02)	-0.05 (-0.18*)	-0.06 (-0.07)
D1b $\alpha_{c,2}$	-0.19*		0.93*	0.01	0.17*	
D1b $\alpha_{c,2p}$	-0.03 (0.2*)		-0.09 (-0.86*)	0.0004 (-0.03)	-0.08 (-0.18*)	-0.08 (-0.06)
D1c $\alpha_{c,1}$		-0.18*	0.91*	0.03	0.21*	
D1c $\alpha_{c,1p}$		-0.19*	0.87*	-0.01	0.17*	0.05
D1c $\alpha_{c,2}$	-0.20*		0.93*	0.01	0.19*	
D1c $\alpha_{c,2p}$	-0.18*		0.81*	0.02	0.19*	0.08
D2 $\alpha_{c,1}$		-0.17*	0.86*	0.02	0.16*	
D2 $\alpha_{c,1p}$		-0.17*	0.88*	0.04	0.17*	0.02
D2 $\alpha_{c,2}$	-0.16*		0.89*	0.03	0.17*	
D2 $\alpha_{c,2p}$	-0.18*		0.88*	-0.01	0.17*	-0.01

(continued)

Table A14 continued. Sensitivity analysis of the alternate AnMBR filtration models: standardised regression coefficients (β_k) and mean of the standardised regression coefficients with $R^2 > 0.7$ ($\overline{\beta_k}$). Influential parameters with absolute β_k or $\overline{\beta_k}$ value above 0.10 (*).

Model	$\beta_k\ (\overline{\beta_k})$					
	P_a	P_b	ζ_1	ζ_2	ζ_3	ζ_4
D1a $\alpha_{c,3}$		-0.43*	-0.07	-0.37*	-0.19*	0.04
D1a $\alpha_{c,3p}$	0.14*	-0.42*	-0.05	-0.38*	-0.15*	0.04
D1a $\alpha_{c,4p}$			0.02 (0.24*)	-0.03 (0.1)	-0.06 (0.57*)	-0.05 (-0.20*)
D1b $\alpha_{c,3}$		-0.64*	-0.08	-0.54*	-0.26*	0.04
D1b $\alpha_{c,3p}$	0.20*	-0.59*	-0.06	-0.52*	-0.2*	0.04
D1b $\alpha_{c,4p}$			-0.05 (0.49*)	0.05 (0.12*)	0.03 (0.35*)	0.06 (-0.13*)
D1c $\alpha_{c,3}$		-0.70*	-0.10*	-0.61*	-0.28*	0.06
D1c $\alpha_{c,3p}$	0.12*	-0.68*	-0.09	-0.60*	-0.25*	0.05
D1c $\alpha_{c,4p}$			-0.05	-0.81*	-0.31*	0.05
D2 $\alpha_{c,3}$		-0.48*	-0.04	-0.44*	-0.06	0.01
D2 $\alpha_{c,3p}$	-0.001	-0.50*	-0.04	-0.47*	-0.08	0.01
D2 $\alpha_{c,4p}$			-0.04	-0.52*	-0.08	0.01

Parameter estimation results

Table A15. Parameter estimation procedure for the alternate AnMBR filtration models. Parameters contained in subset θ_{II} and θ_{II}, number of pairwise correlations above 0.50 (nCorr) and root mean square error (RMSE) at optimal parameter values.

Mode	Subset θ_{II}			Subset θ_{III}		
	Parameters	nCorr	RMSE	Parameters	nCorr	RMSE
D1a $\alpha_{c,1}$	$\{\varepsilon_{c0}, \gamma_0\}$	0	10.3	$\{k_{CK}, \rho_X\}$	1	8.0
D1a $\alpha_{c,1p}$	$\{\varepsilon_{c0}, \gamma_0\}$	0	10.4	$\{k_{CK}, \rho_X\}$	0	8.4
D1a $\alpha_{c,2}$	$\{\varepsilon_{c0}, \gamma_0\}$	0	11.1	$\{k_c, \rho_X\}$	1	7.9
D1a $\alpha_{c,2p}$	$\{\varepsilon_{c0}\}$	NA	10.9	$\{k_c, \rho_X\}$	0	7.7
D1a $\alpha_{c,3}$	$\{\gamma_0, \zeta_2, \zeta_3, \gamma_2\}$	ND[a]	10.6	$\{\gamma_1, P_b\}$	ND[a]	10.6
D1a $\alpha_{c,3p}$	$\{\gamma_0, \zeta_3, P_a\}$	1	11.1	$\{\gamma_1, P_b, \zeta_2\}$	1	11.0
D1a $\alpha_{c,4p}$	$\{\gamma_0, \zeta_2, \zeta_1\}$	1	57.6	$\{\zeta_4\}$	NA	57.6
D1b $\alpha_{c,1}$	$\{\varepsilon_{c0}, \gamma_0\}$	0	10.1	$\{k_{CK}, \rho_X\}$	1	8.3
D1b $\alpha_{c,1p}$	$\{\varepsilon_{c0}, \gamma_0\}$	0	10.4	$\{k_{CK}, \rho_X\}$	0	8.4
D1b $\alpha_{c,2}$	$\{\varepsilon_{c0}, \gamma_0\}$	0	10.8	$\{k_c, \rho_X\}$	1	8.2
D1b $\alpha_{c,2p}$	$\{\varepsilon_{c0}\}$	NA	10.9	$\{k_c, \rho_X\}$	1	8.2
D1b $\alpha_{c,3}$	$\{\gamma_0, \zeta_3, P_b\}$	ND[a]	7.6	$\{\zeta_2\}$	NA	7.6
D1b $\alpha_{c,3p}$	$\{\gamma_0, \zeta_3, P_b, q_{m,MS}\}$	1	9.3	$\{P_a, \zeta_2\}$	ND[a]	9.3
D1b $\alpha_{c,4p}$	$\{\gamma_0, \zeta_1, \zeta_2, \zeta_3, \zeta_4\}$	6	157.3	NA	NA	NA
D1c $\alpha_{c,1}$	$\{\varepsilon_{c0}\}$	NA	10.9	$\{k_{CK}, \rho_X\}$	1	9.5
D1c $\alpha_{c,1p}$	$\{\varepsilon_{c0}\}$	NA	9.0	$\{k_{CK}, \rho_X\}$	1	7.7
D1c $\alpha_{c,2}$	$\{\varepsilon_{c0}\}$	NA	11.8	$\{k_c, \rho_X\}$	1	9.5
D1c $\alpha_{c,2p}$	$\{\varepsilon_{c0}\}$	NA	10.1	$\{k_c, \rho_X\}$	1	7.0
D1c $\alpha_{c,3}$	$\{\zeta_1, \zeta_2, P_b\}$	ND[a]	12.0	$\{\zeta_2\}$	NA	12.0
D1c $\alpha_{c,3p}$	$\{\zeta_2, P_b, P_a, q_{m,MS}\}$	3	10.5	$\{\zeta_2\}$	NA	10.5
D1c $\alpha_{c,4p}$	$\{\zeta_2, \zeta_3\}$	1	11.7	$\{q_{m,MS}, K_{S,c}\}$	0	11.7
D2 $\alpha_{c,1}$	$\{\varepsilon_{c0}, \beta_{ST}, C_d\}$	0	7.1	$\{k_{CK}, \rho_X\}$	0	7.1
D2 $\alpha_{c,1p}$	$\{\varepsilon_{c0}, \beta_{ST}, C_d\}$	1	8.1	$\{k_{CK}, \rho_X\}$	1	8.1
D2 $\alpha_{c,2}$	$\{\varepsilon_{c0}, \beta_{ST}, C_d\}$	0	7.0	$\{k_c, \rho_X\}$	1	7.0
D2 $\alpha_{c,2p}$	$\{\varepsilon_{c0}, \beta_{ST}, C_d\}$	0	7.8	$\{k_c, \rho_X\}$	1	7.8
D2 $\alpha_{c,3}$	$\{\beta_{ST}, C_d, P_b\}$	0	16.4	$\{\zeta_2\}$	NA	10.8
D2 $\alpha_{c,3p}$	$\{\beta_{ST}, C_d, P_b\}$	1	15.4	$\{\zeta_2\}$	NA	15.4
D2 $\alpha_{c,4p}$	$\{\beta_{ST}, C_d, \zeta_2\}$	1	15.6	NA	NA	NA
FR1	$\{\gamma_0, \gamma_1, \gamma_2, \gamma_3\}$	4	3.8	$\{K_F\}$	NA	3.8
FR2	$\{\gamma_0, \gamma_1, \gamma_3\}$	2	3.8	$\{K_F\}$	NA	3.8
FR3	$\{\gamma_0, \gamma_3\}$	1	3.5	$\{K_F\}$	NA	3.5
FR4	$\{\gamma_0, \gamma_1, \gamma_2, \gamma_3\}$	4	3.7	$\{K_F, \gamma_4\}$	1	3.7
FR5	$\{\gamma_0, \gamma_1, \gamma_3\}$	2	3.7	$\{K_F, \gamma_4\}$	1	3.7
FR6	$\{\gamma_0, \gamma_3\}$	1	3.4	$\{K_F, \gamma_4\}$	1	3.4

NA: not applicable

[a] Could not be determined due to numerical error: the Jacobian was zero for all values in at least one parameter resulting in division by zero when calculating the covariance matrix.

**Table A16**. Optimised parameter values ($\hat{\theta}$) for the alternate AnMBR empirical fouling rate (FR) models. Relative error $\sigma_\theta/\hat{\theta}$ shown between brackets. θ^o is the initial guess (nominal values).

↓Model	K_F	γ_0	γ_1	γ_2	γ_3	γ_4
Units→	$\times 10^{-4}$ Pa s^{-1}	$\times 10^6$ s m^{-1}	$\times 10^8$ s^2 m^{-1}	$\times 10^4$ s m^{-2} kg^{-1}	$\times 10^6$ s m^{-2} kg^{-1}	$\times 10^{10}$ s m^{-2}
$\theta^o \rightarrow$	5.6	2.81	2.48	5.1	1.28	1.75
FR1	5.60 [0.01]	4.19 [0.004]	5.44 [0.03]	3.92 [5.93]	1.10 [0.03]	
FR2	5.60 [0.01]	4.19 [0.003]	5.42 [0.02]		1.09 [0.03]	
FR3	5.60 [0.01]	3.08 [0.003]			1.12 [0.02]	
FR4	6.39 [0.11]	4.65 [0.004]	5.19 [0.03]	38.11 [0.60]	0.83 [0.04]	1.94 [0.08]
FR5	6.21 [0.11]	4.67 [0.003]	5.03 [0.02]		0.80 [0.04]	1.90 [0.08]
FR6	5.75 [0.10]	3.60 [0.002]			0.88 [0.02]	1.79 [0.08]

Table A17. Optimised parameter values ($\hat{\theta}$) for the alternate AnMBR filtration models. Relative error $\sigma_\theta/\hat{\theta}$ shown between brackets. θ^o is the initial guess (nominal values).

↓Model	C_d	$K_{S,c}$	$q_{m,\text{MS}}$	β_{ST}
Units→	-	kg	-	-
$\theta^o \rightarrow$	0.40	0.2	4.71	1.75×10^4
D1b $\alpha_{c,3p}$			1.4×10^4 [3×10^{-5}]	
D1c $\alpha_{c,3p}$			3.04 [1×10^{-5}]	
D1c $\alpha_{c,4p}$		0.32 [3×10^{-5}]	6.93 [2×10^{-5}]	
D2 $\alpha_{c,1}$	0.31 [7×10^{-7}]			2.28×10^{-4} [6×10^{-4}]
D2 $\alpha_{c,1p}$	0.40 [6×10^{-7}]			1.78×10^{-4} [0.001]
D2 $\alpha_{c,2}$	0.39 [4×10^{-7}]			2.37×10^{-4} [6×10^{-4}]
D2 $\alpha_{c,2p}$	0.47 [4×10^{-7}]			1.96×10^{-4} [9×10^{-4}]
D2 $\alpha_{c,3}$	0.33 [0.01]			0.505 [0.01]
D2 $\alpha_{c,3p}$	0.30 [1×10^{-4}]			4.5×10^{-7} [1.40]
D2 $\alpha_{c,4p}$	0.34 [1×10^{-5}]			2.3×10^{-6} [0.57]

(continued)

Table A17 continued. Optimised parameter values ($\hat{\theta}$) for the alternate AnMBR filtration models. Relative error $\sigma_\theta/\hat{\theta}$ shown between brackets. θ^o is the initial guess (nominal values).

↓Model		γ_0	γ_1	γ_2
	Units→	$\times 10^6$ s m^{-1}	$\times 10^8$ s^2 m^{-1}	s m^{-2} kg^{-1}
	$\theta^o \to$	2.81	2.48	5.1×10^4
D1a $\alpha_{c,1}$		2.52 [2×10^{-5}]		
D1a $\alpha_{c,1p}$		5.59 [1×10^{-8}]		
D1a $\alpha_{c,2}$		2.47 [2×10^{-5}]		
D1a $\alpha_{c,3}$		33.0 [∞^a]	2.47 [∞^a]	0.5 [∞^a]
D1a $\alpha_{c,3p}$		3.03 [4×10^{-5}]	3.59 [3×10^{-5}]	
D1a $\alpha_{c,4p}$		2.72 [8×10^{-8}]		
D1b $\alpha_{c,1}$		2.46 [3×10^{-5}]		
D1b $\alpha_{c,1p}$		5.27 [1×10^{-9}]		
D1b $\alpha_{c,2}$		2.26 [3×10^{-5}]		
D1b $\alpha_{c,3}$		33.8 [∞^a]		
D1b $\alpha_{c,3p}$		3.69 [3×10^{-5}]		
D1b $\alpha_{c,4p}$		2.85 [7×10^{-8}]		

[a] The Jacobian was zero for all values in at least one parameter resulting in division by zero when calculating the covariance matrix.   (continued)

Table A17 continued. Optimised parameter values ($\hat{\theta}$) for the alternate AnMBR filtration models. Relative error $\sigma_\theta/\hat{\theta}$ shown between brackets. θ^o is the initial guess (nominal values).

↓Model	k_c	k_{CK}	ε_{c0}	ρ_X	P_a
Units→	$\times 10^{17}\,\text{m}^{-2}$	$\times 10^7$	-	$\times 10^3\,\text{kg m}^{-3}$	$\times 10^4\,\text{Pa}$
$\theta^o \rightarrow$	1.0	4.0	0.66	1.24	2.01
D1a $\alpha_{c,1}$		21 [0.04]	0.38 [0.01]	18.4 [0.03]	
D1a $\alpha_{c,1p}$		35 [0.01]	0.57 [0.003]	20.6 [0.04]	
D1a $\alpha_{c,2}$	6.12 [0.04]		0.44 [0.01]	23.9 [0.03]	
D1a $\alpha_{c,2p}$	9.53 [0.01]		0.61 [0.003]	22.8 [0.02]	
D1a $\alpha_{c,3p}$				20.5 [0.04]	1.07 [0.03]
D1b $\alpha_{c,1}$		21 [0.04]	0.41 [0.01]	20.6 [0.04]	
D1b $\alpha_{c,1p}$		35 [0.01]	0.57 [0.003]	25.0 [0.03]	
D1b $\alpha_{c,2}$	5.60 [0.04]		0.46 [0.01]	25.0 [0.03]	
D1b $\alpha_{c,2p}$	9.33 [0.01]		0.63 [0.003]		
D1b $\alpha_{c,3p}$					7.8×10^{12}[0.06]
D1c $\alpha_{c,1}$		15.71 [0.04]	0.31 [0.01]	12.1 [0.05]	
D1c $\alpha_{c,1p}$		17.11 [0.02]	0.43 [0.002]	7.29 [0.04]	
D1c $\alpha_{c,2}$	4.73 [0.05]		0.37 [0.01]	16.8 [0.04]	
D1c $\alpha_{c,2p}$	5.94 [0.01]		0.49 [0.002]	10.6 [0.02]	
D1c $\alpha_{c,3p}$					0.69 [0.20]
D2 $\alpha_{c,1}$		4 [0.02]	0.12 [0.004]	1.24 [0.03]	
D2 $\alpha_{c,1p}$		4 [0.01]	0.16 [0.002]	1.23 [0.02]	
D2 $\alpha_{c,2}$	0.99 [0.02]		0.13 [0.004]	1.25 [0.02]	
D2 $\alpha_{c,2p}$	1.00 [0.01]		0.17 [0.002]	1.23 [0.02]	

(continued)

Table A17 continued. Optimised parameter values ($\hat{\theta}$) for the alternate AnMBR filtration models. Relative error $\sigma_\theta/\hat{\theta}$ shown between brackets. θ^o is the initial guess (nominal values).

↓Model	P_b	ζ_1	ζ_2	ζ_3	ζ_4
Units→	$\times 10^3$ Pa	$\times 10^3$	$\times 10^4$	-	-
$\theta^o \rightarrow$	4.1799	1.16	1.36	172.4	150.9
D1a $\alpha_{c,3}$	4.22 [∞ᵃ]		14.9 [∞ᵃ]	111 [∞ᵃ]	
D1a $\alpha_{c,3p}$	4.26 [1×10⁵]		1.4 [1×10⁵]	1037 [705]	
D1a $\alpha_{c,4p}$		1.17 [0.001]		177 [2×10⁻⁴]	150.9 [5×10⁻⁴]
D1b $\alpha_{c,3}$	137.6 [∞ᵃ]		1.36 [0.03]	66.7 [∞ᵃ]	
D1b $\alpha_{c,3p}$	58.1 [0.02]		2.34 [∞ᵃ]	106.2 [0.02]	
D1b $\alpha_{c,4p}$		1.13 [2.01]	1.38 [0.17]	173.5 [0.01]	156.9 [0.25]
D1c $\alpha_{c,3}$	58.7 [∞ᵃ]		1.36 [0.04]	1752 [∞ᵃ]	
D1c $\alpha_{c,3p}$	9.46 [0.18]		1.36 [0.005]	127.9 [0.01]	
D1c $\alpha_{c,4p}$			1.98 [0.01]	381.1 [0.01]	
D2 $\alpha_{c,3}$	7.23 [8×10⁴]		2.04×10⁶ [0.04]		
D2 $\alpha_{c,3p}$	8.1 [0.61]		1.36 [0.02]		
D2 $\alpha_{c,4p}$			2.52 [0.47]		

ᵃ The Jacobian was zero for all values in at least one parameter resulting in division by zero when calculating the covariance matrix.
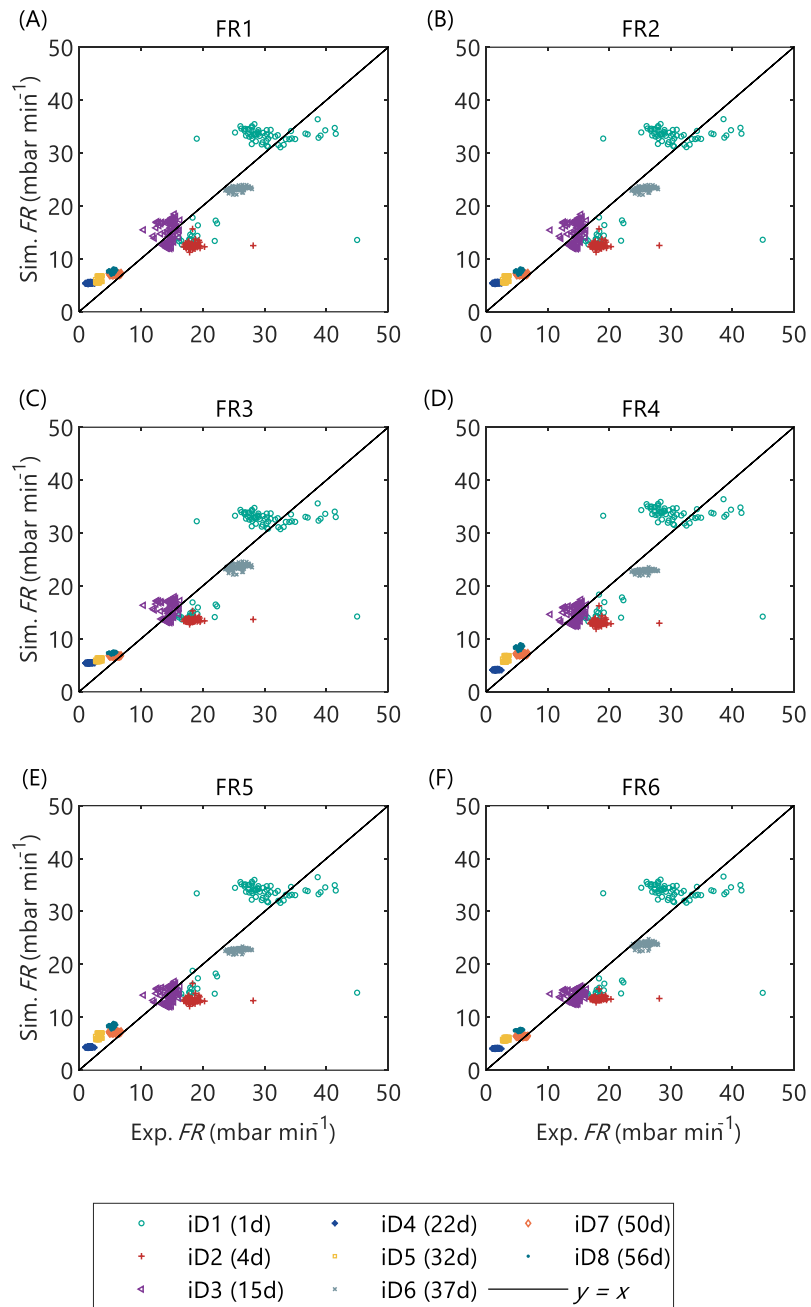
Figure A9. Calibration of the alternate AnMBR empirical fouling rate models, FR1 to FR6, using the representative dataset from the pilot AnMBR, iD1 to iD8.
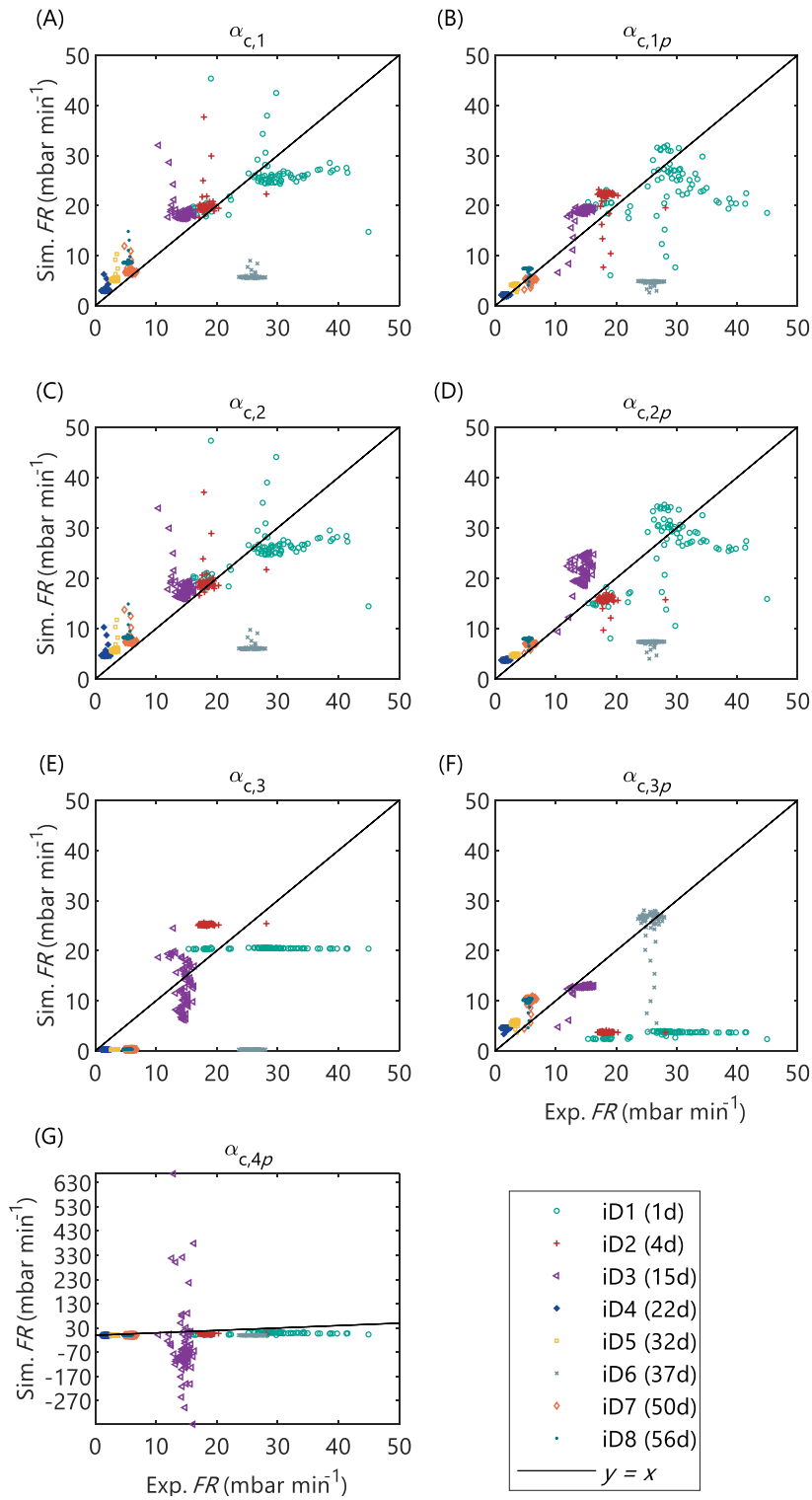
Figure A10. Calibration of the alternate AnMBR filtration models with deposition submodel D1a and different specific cake resistance submodels, $\alpha_{c,1}$ to $\alpha_{c,4p}$; using the representative dataset from the pilot AnMBR, iD1 to iD8.
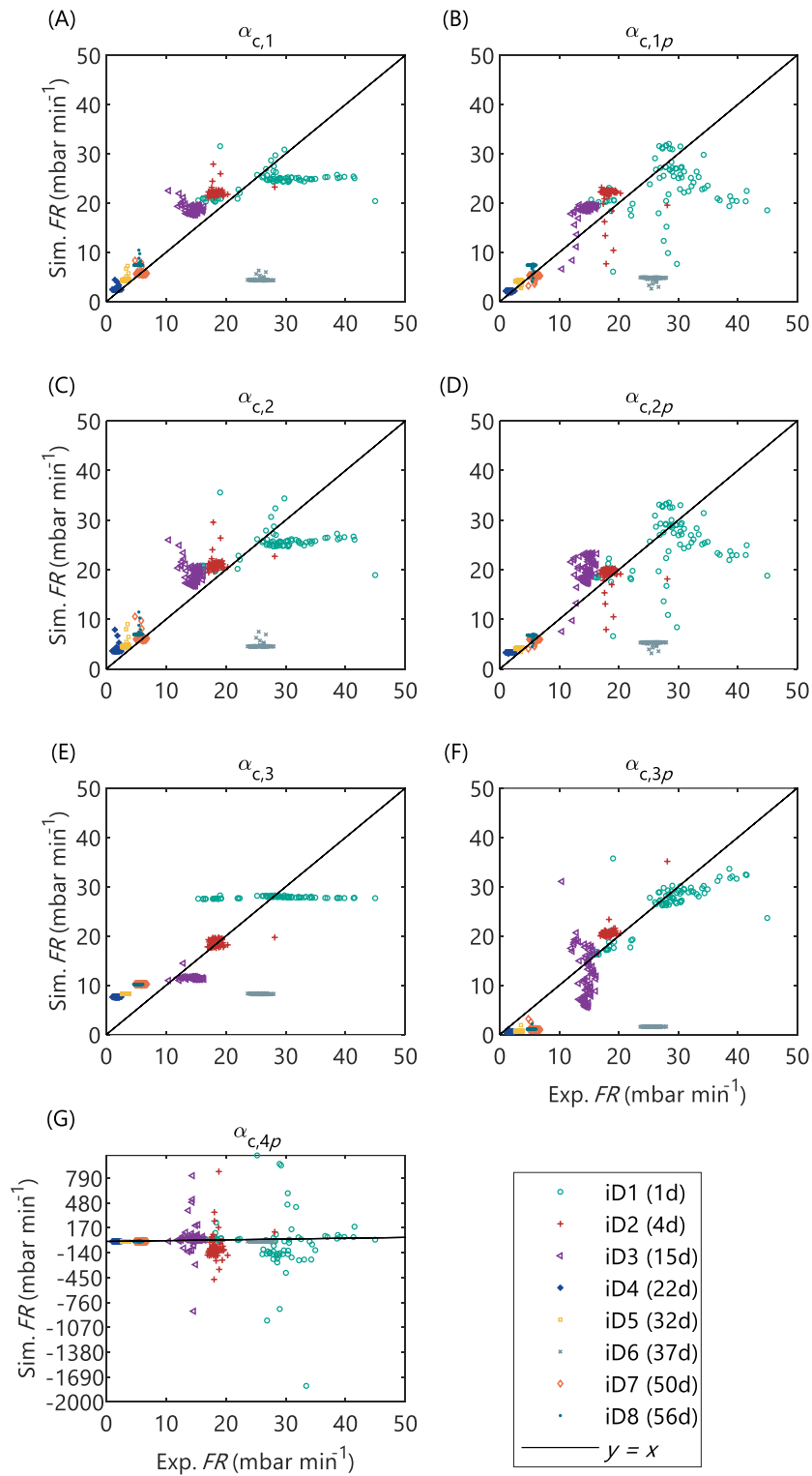
Figure A11. Calibration of the alternate AnMBR filtration models with deposition submodel D1b and different specific cake resistance submodels, $\alpha_{c,1}$ to $\alpha_{c,4p}$; using the representative dataset from the pilot AnMBR, iD1 to iD8..
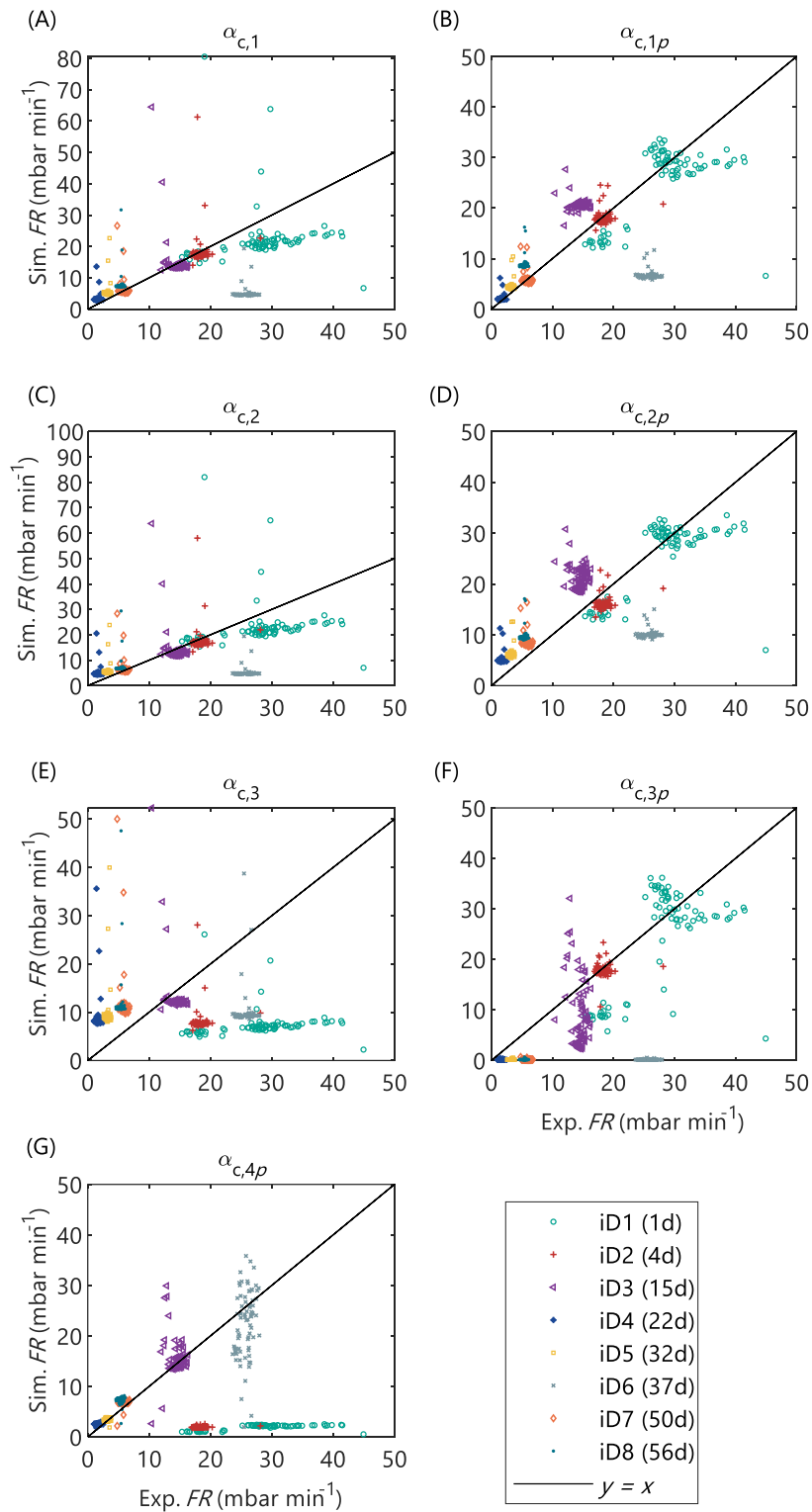
Figure A12. Calibration of the alternate AnMBR filtration models with deposition submodel D1c and different specific cake resistance submodels, $\alpha_{c,1}$ to $\alpha_{c,4p}$; using the representative dataset from the pilot AnMBR, iD1 to iD8..
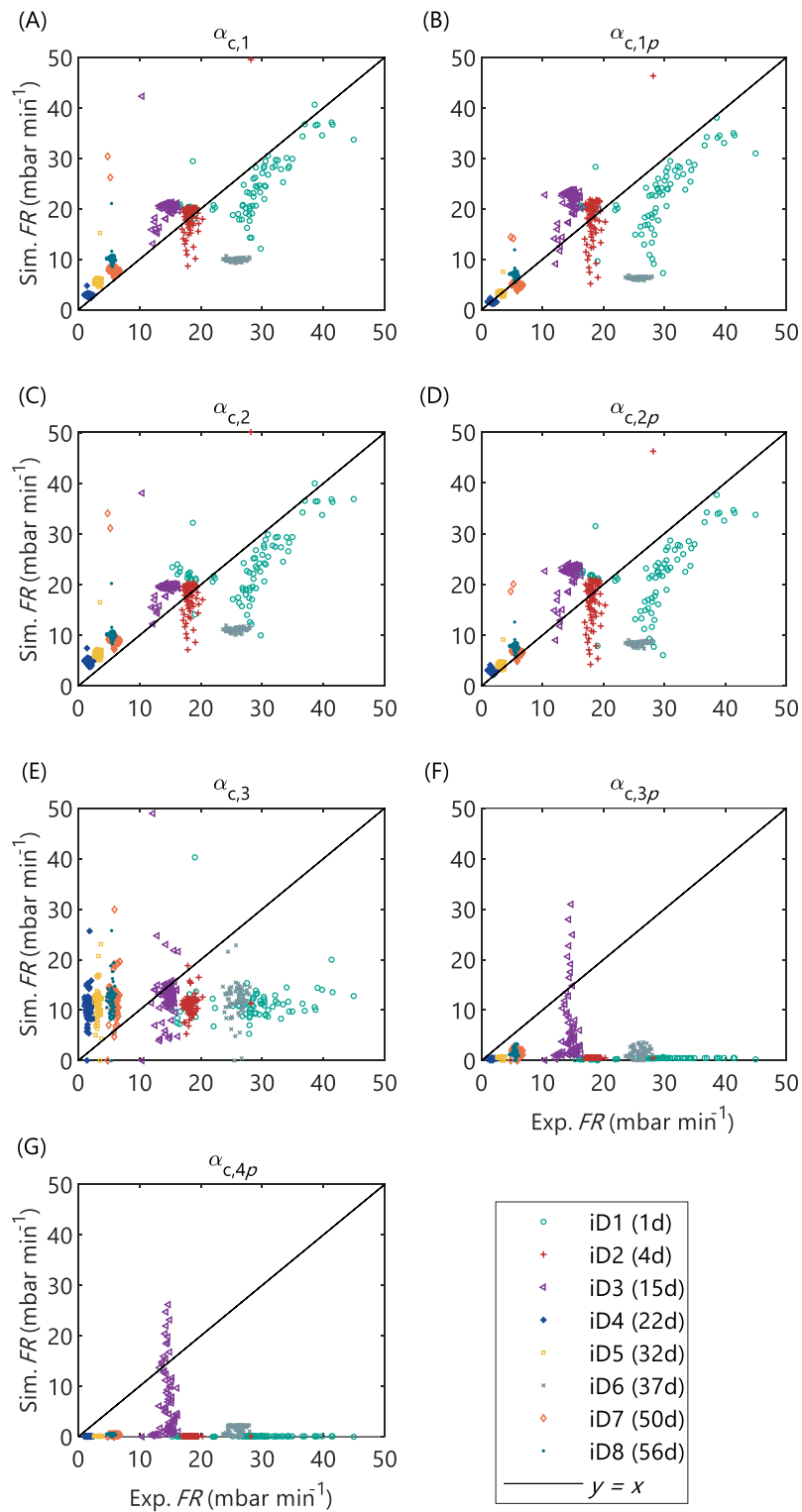
Figure A13. Calibration of the alternate AnMBR filtration models with deposition submodel D2 and different specific cake resistance submodels, $\alpha_{c,1}$ to $\alpha_{c,4p}$; using the representative dataset from the pilot AnMBR, iD1 to iD8.

Long-term prediction with calibrated model
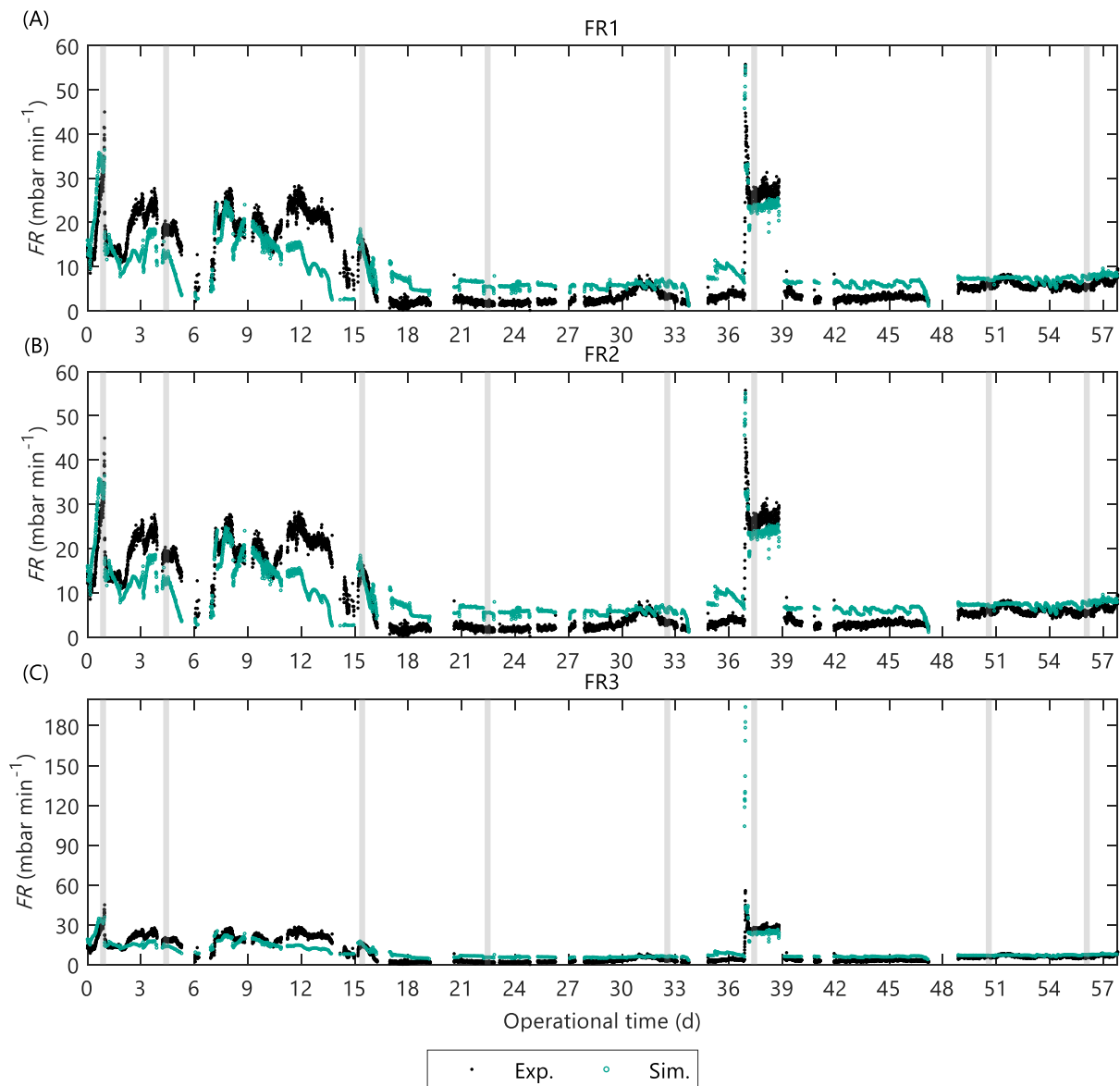
Figure A14. Validation of the alternate AnMBR empirical fouling rate (FR) models that excluded floc size as input variable: (A) FR1, (B) FR2, and (C) FR3. The grey vertical areas represent the representative dataset (iD1 to iD8 from left to right) used for model calibration.
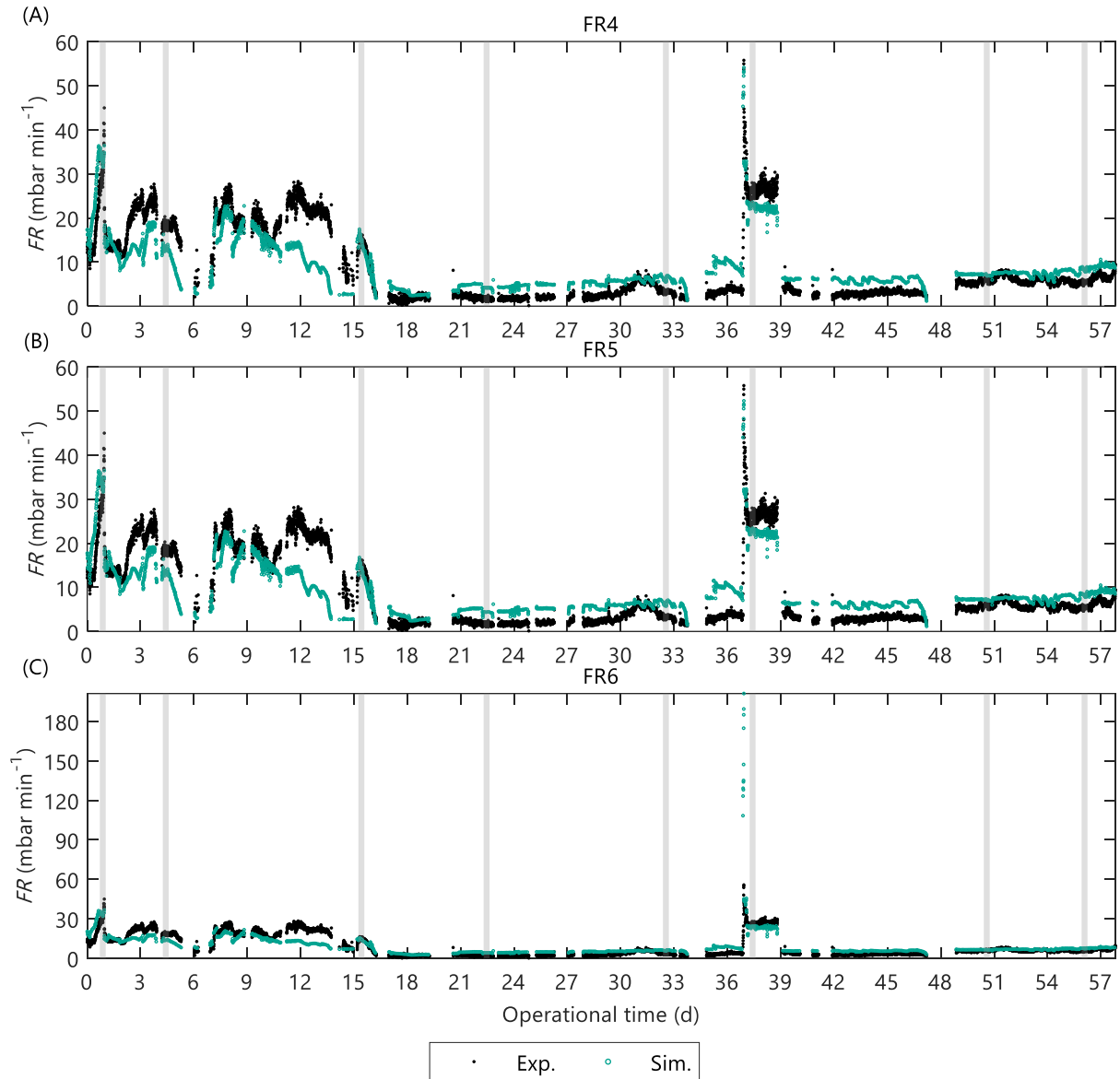
Figure A15. Validation of the alternate AnMBR empirical fouling rate (FR) models that included floc size as input variable: (A) FR4, (B) FR5, and (C) FR6.
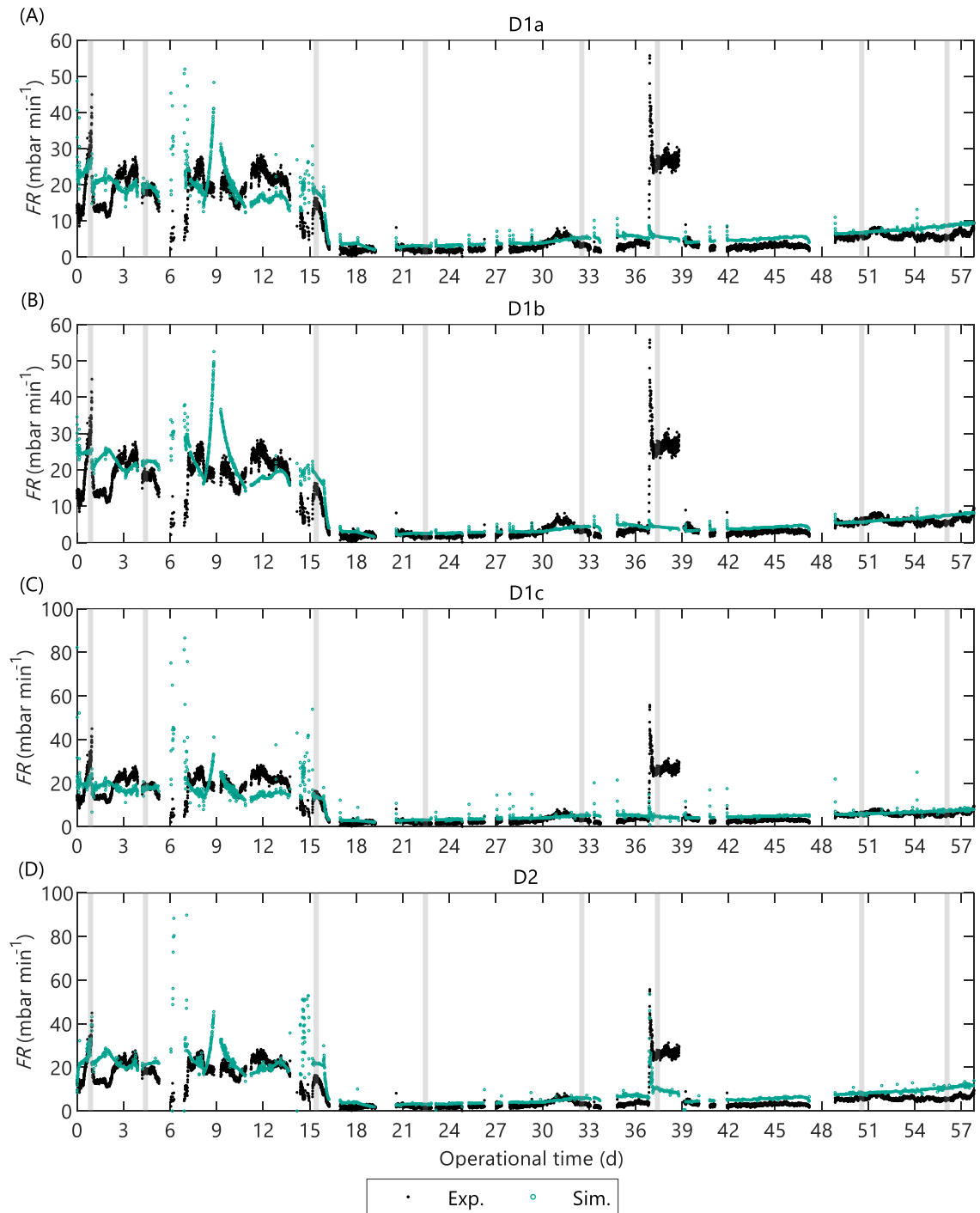
Figure A16. Validation of the alternate AnMBR filtration models that combine the specific cake resistance model $\alpha_{c,1}$ with the different deposition submodels: (A) D1a, (B) D1b, (C) D1c and (D) D2.
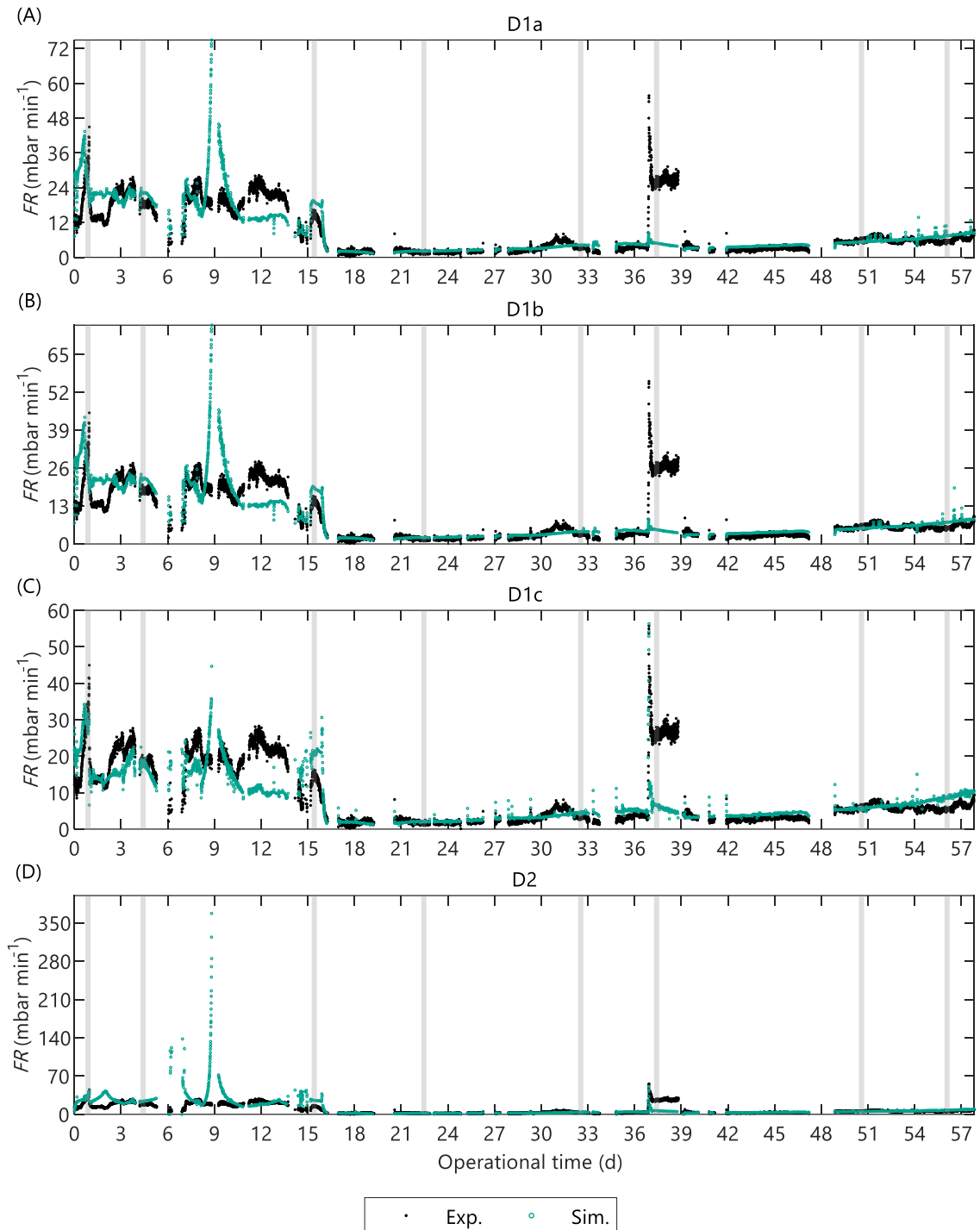
Figure A17. Validation of the alternate AnMBR filtration models that combine the specific cake resistance submodel $\alpha_{c,1p}$ with the different deposition submodels: (A) D1a, (B) D1b, (C) D1c and (D) D2.
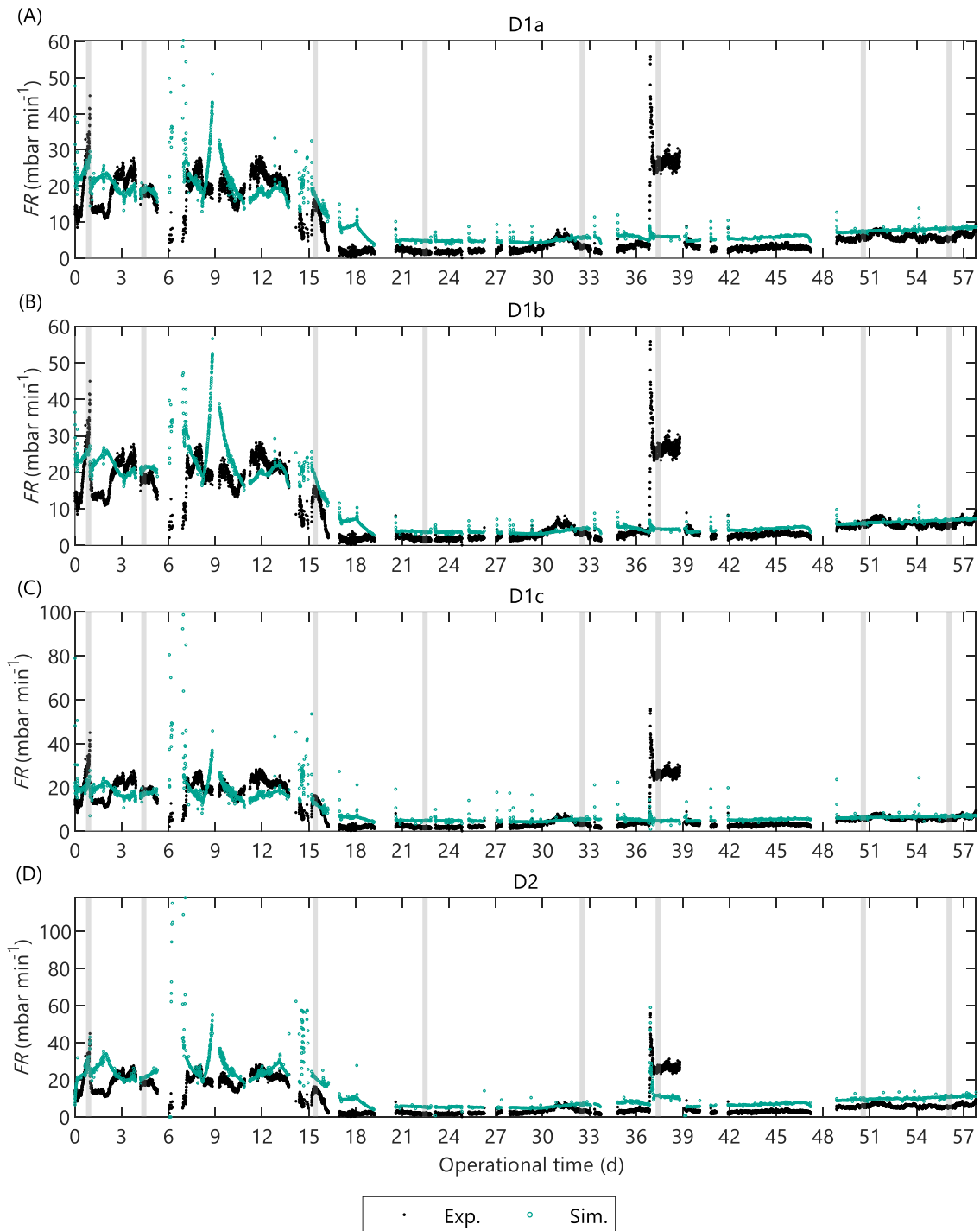
Figure A18. Validation of the alternate AnMBR filtration models that combine the specific cake resistance submodel $\alpha_{c,2}$ with the different deposition submodels: (A) D1a, (B) D1b, (C) D1c and (D) D2.
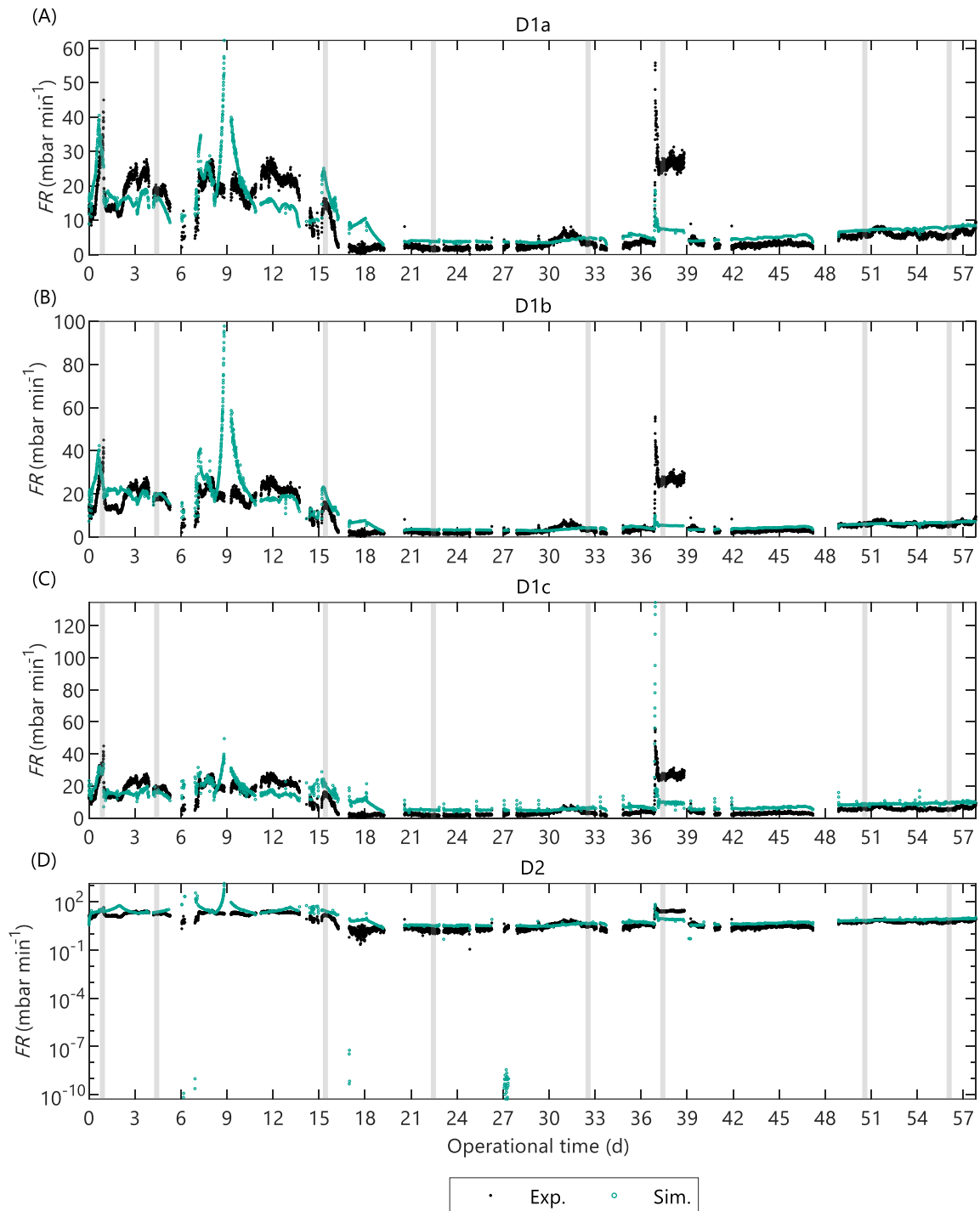
Figure A19. Validation of the alternate AnMBR filtration models that combine the specific cake resistance submodel $\alpha_{c,2p}$ with the different deposition submodels: (A) D1a, (B) D1b, (C) D1c and (D) D2.
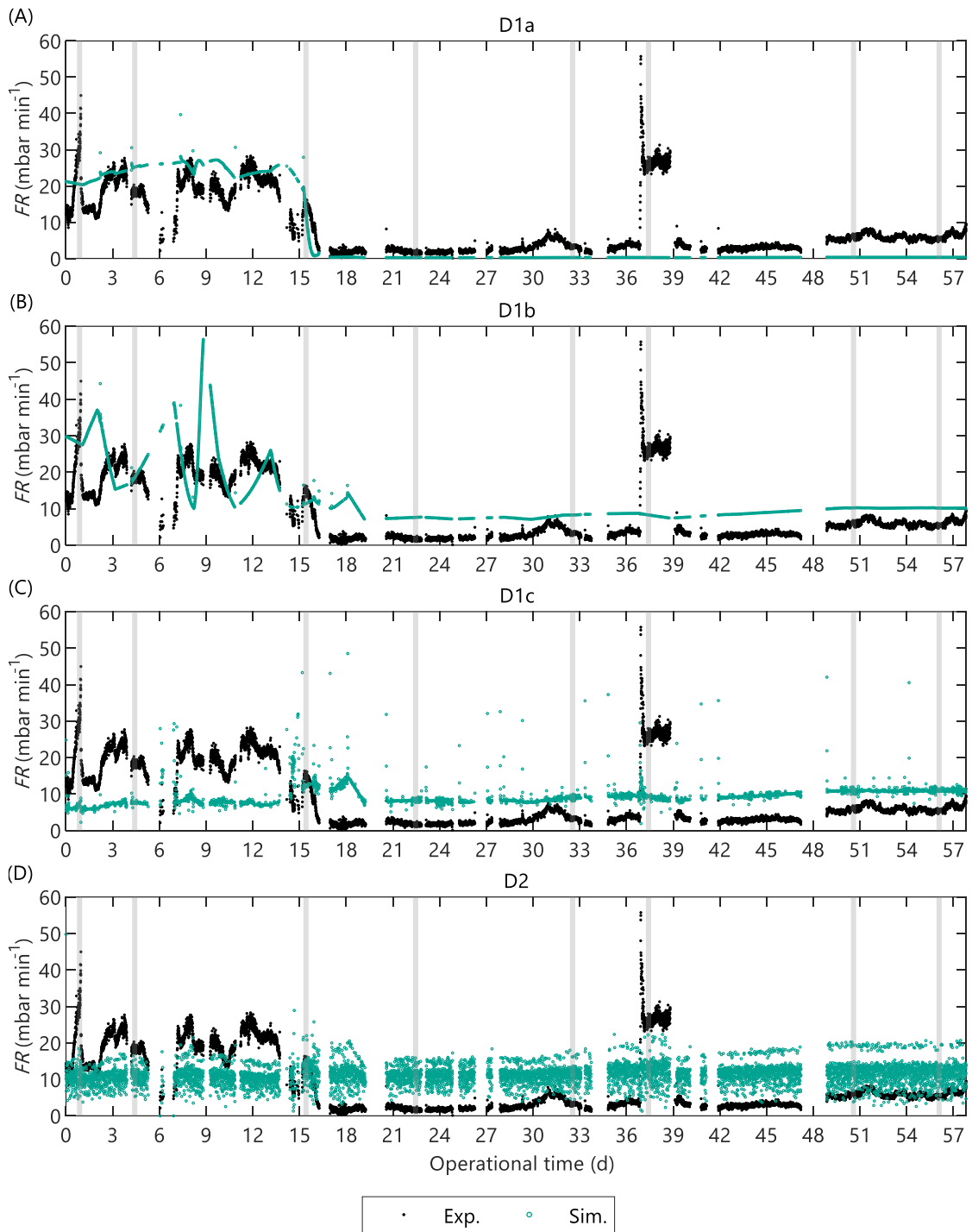
Figure A20. Validation of the alternate AnMBR filtration models that combine the specific cake resistance submodel $\alpha_{c,3}$ with the different deposition submodels: (A) D1a, (B) D1b, (C) D1c and (D) D2.
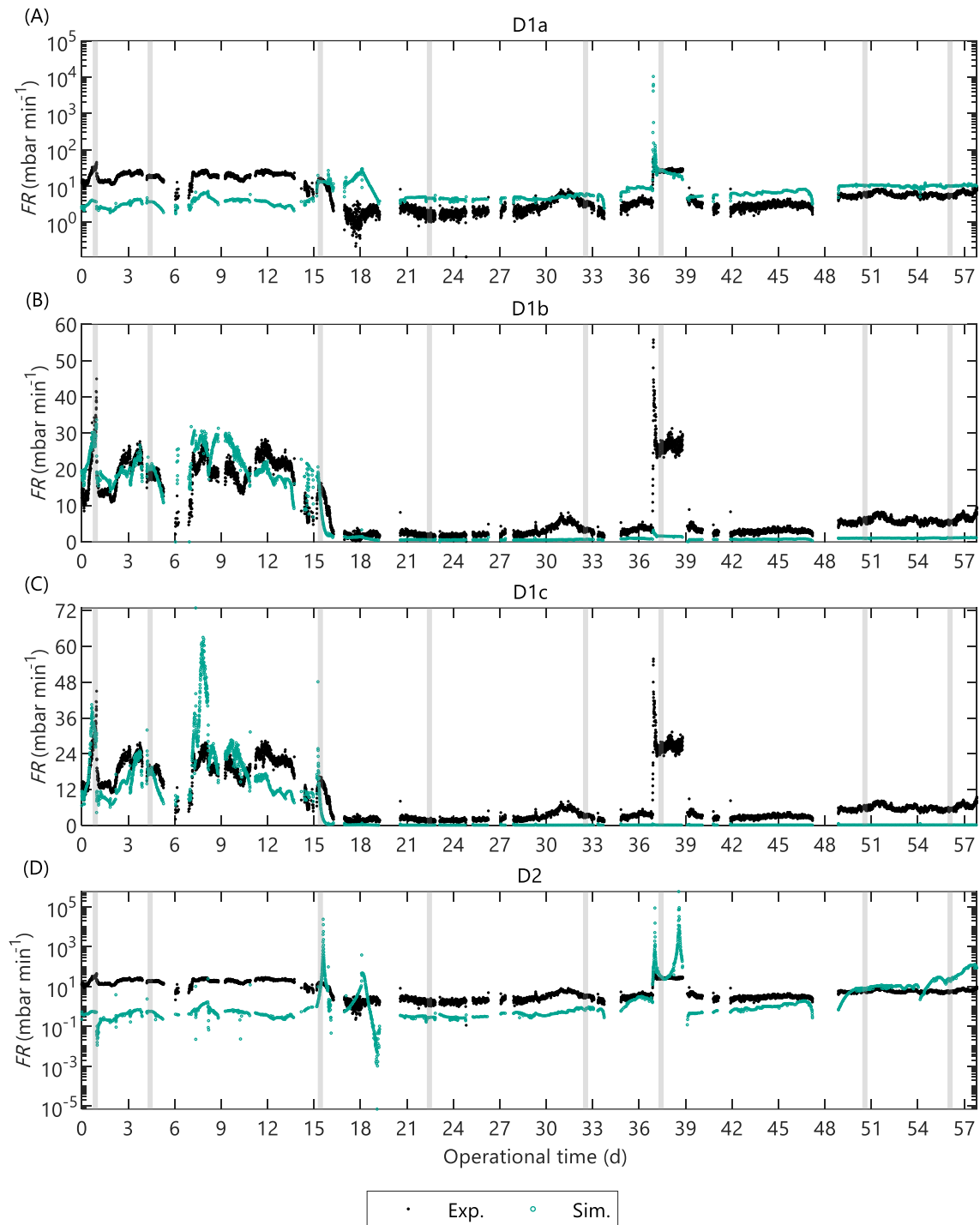
Figure A21. Validation of the alternate AnMBR filtration models that combine the specific cake resistance submodel $\alpha_{c,3p}$ with the different deposition submodels: (A) D1a, (B) D1b, (C) D1c and (D) D2.
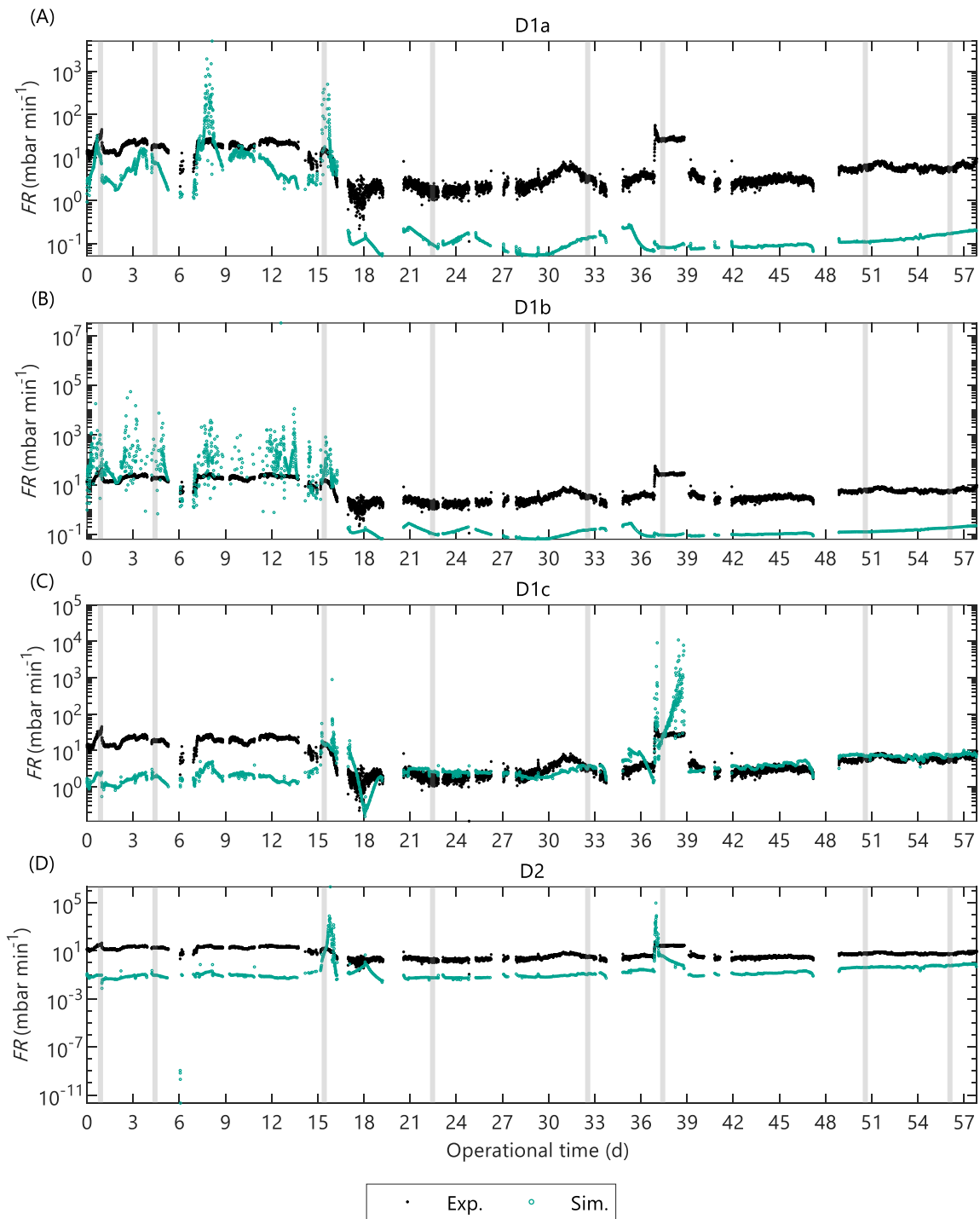
Figure A22. Validation of the alternate AnMBR filtration models that combine the specific cake resistance submodel $\alpha_{c,4p}$ with the different deposition submodels: (A) D1a, (B) D1b, (C) D1c and (D) D2.

A8. EFFECT OF SLUDGE CHARACTERISTICS ON FOULING RATE PREDICTIONS

Figure A23 show the effect of the sludge characteristics on the predicted fouling rate with three calibrated alternate AnMBR filtration models, namely FR6, D1c α_1, and D1c $\alpha_{1,p}$. The sludge characteristics were varied inside the simulation ranges in Figure A23, which were based on the observed ranges in the pilot AnMBR. The remaining variables were set to the nominal values presented in Table A1 and Table A18.

Each sludge characteristics was divided in 50 values inside its range, creating a 50x50 mesh for each plot in Figure A23, the value for each datapoint in the mesh was the predicted FR. For the empirical model, the corresponding equation to calculate FR was directly applied for each value in the mesh. For the FR_RIS models, the FR was obtained by solving the model at fixed sludge characteristics until steady state was reached, and the last FR value was used. Two hours was sufficient to reach steady state as verified by analysing the evolution of the model (results not shown).

Table A18. Nominal values and simulation range of operational conditions and sludge characteristics.

	Variable	Units	Nominal value [a]	Range in pilot AnMBR	Simulation range
c_C	Concentration of colloidal material	Kg m^{-3}	0.35	[0.14, 0.62]	[0.10, 0.65]
c_X	Concentration of particulate material	Kg m^{-3}	9.25	[4.9, 15.9]	[4.0, 16.0]
d_p	Mean particle diameter	$\times 10^{-5}$ m	2.7	[2.1, 4.5]	[2.0, 5.0]
u_G	Superficial gas velocity	$\times 10^{-3}$ m s^{-1}	3.0	[0.5, 5.7]	[0.5 6.0]

[a] Mean value during pilot AnMBR operation.
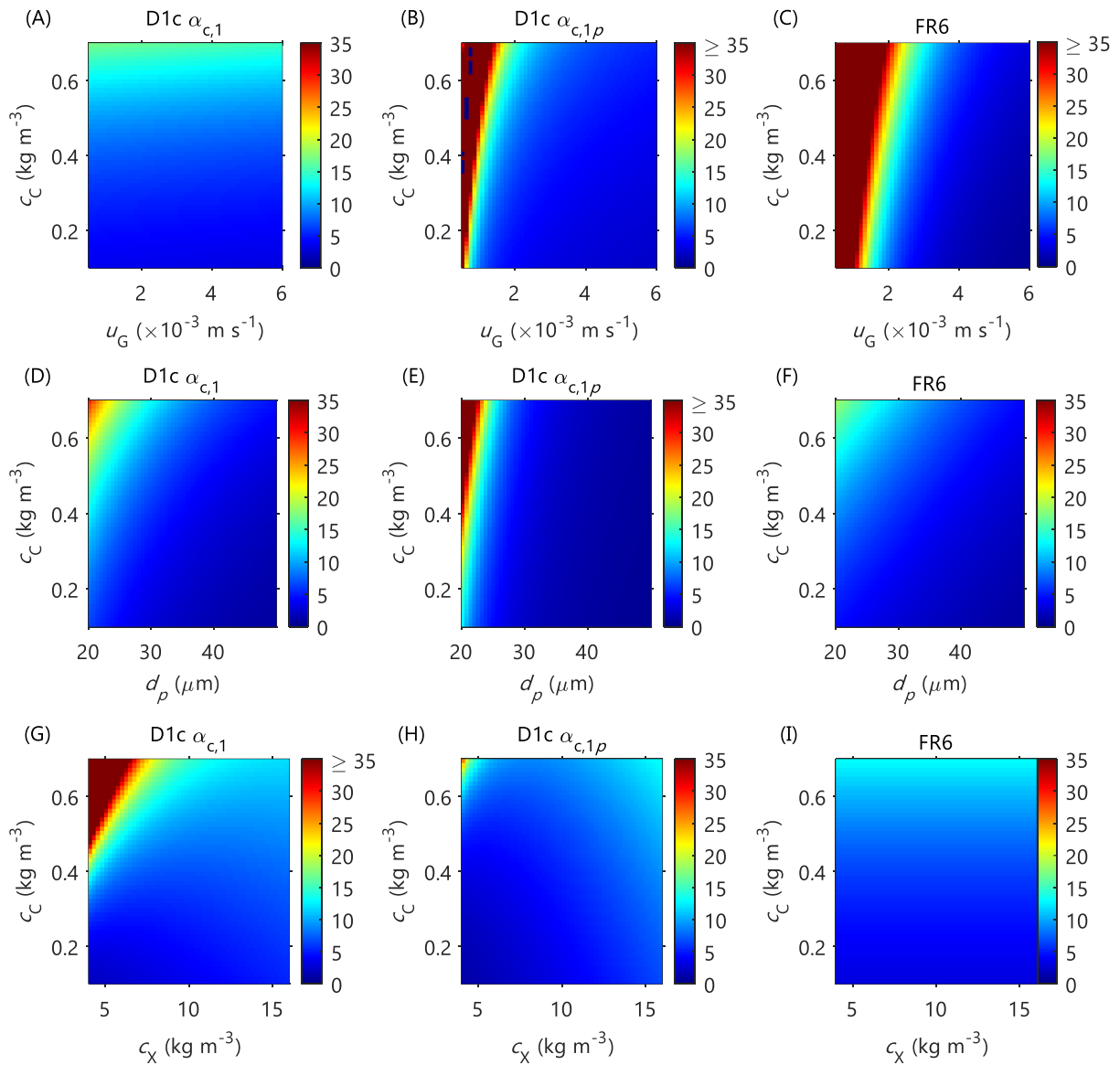
Figure A23. Effect of colloidal material concentration (c_C), particulate material concentration (c_X), mean particle diameter (d_p), and superficial gas velocity in the membrane tank (u_G) on the predicted fouling rate (FR, mbar min^{-1}) with different calibrated AnMBR filtration models: (left) D1c α_1, (middle) D1c $\alpha_{1,p}$, and (right) FR6.

A9. CALIBRATION AND VALIDATION OF ALTERNATE ANDFCM FILTRATION MODELS

Parameter estimation results

Table A19. Parameter estimation procedure for the alternate AnDFCm filtration models. Parameters contained in subset θ_{II} and θ_{II}, number of pairwise correlations above 0.50 (nCorr) and root mean square error (RMSE) at optimal parameter values.

Mode	Subset θ_{II}			Subset θ_{III}		
	Parameters	nCorr	RMSE	Parameters	nCorr	RMSE
D1c $\alpha_{c,1}$	$\{\varepsilon_{c0}\}$	NA	2.8	$\{k_{CK}, \rho_X, q_{m,MS}\}$	2	2.1
D1c $\alpha_{c,1p}$	$\{\varepsilon_{c0}\}$	NA	5.3	$\{k_{CK}, \rho_X, q_{m,MS}, K_{S,c}\}$	4	4.9
D1c $\alpha_{c,2}$	$\{\varepsilon_{c0}\}$	NA	5.6	$\{k_c, \rho_X, K_{S,c}\}$	3	4.0
D1c $\alpha_{c,2p}$	$\{\varepsilon_{c0}\}$	NA	3.8	$\{k_c, \rho_X, K_{S,c}\}$	3	2.4
D1c $\alpha_{c,3}$	$\{\zeta_3, \zeta_2, q_{m,MS}\}$	1	1.7	$\{K_{S,c}, P_b, \zeta_4\}$	ND[a]	1.6
D1c $\alpha_{c,3p}$	$\{P_b, \zeta_1, \zeta_3\}$	3	3.6	$\{q_{m,MS}, K_{S,c}\}$	1	3.6
D1c $\alpha_{c,4p}$	$\{\zeta_1, \zeta_2\}$	1	8.4	$\{q_{m,MS}, K_{S,c}\}$	1	8.4
D2 $\alpha_{c,1}$	$\{\varepsilon_{c0}\}$	NA	7.0	$\{\beta_{ST}, C_d, k_{CK}, \rho_X\}$	6	1.9
D2 $\alpha_{c,1p}$	$\{\varepsilon_{c0}\}$	NA	7.5	$\{\beta_{ST}, C_d, k_{CK}, \rho_X\}$	6	5.5
D2 $\alpha_{c,2}$	$\{\varepsilon_{c0}, C_d\}$	1	2.1	$\{\beta_{ST}, k_c, \rho_X\}$	1	2.1
D2 $\alpha_{c,2p}$	$\{\varepsilon_{c0}, C_d\}$	1	4.0	$\{\beta_{ST}, k_c, \rho_X\}$	2	4.0
D2 $\alpha_{c,3}$	$\{\beta_{ST}, C_d\}$	0	8.4	$\{P_b, \zeta_2\}$	1	8.4
D2 $\alpha_{c,3p}$	$\{\beta_{ST}, C_d\}$	1	8.4	$\{P_b, \zeta_2\}$	1	6.3
D2 $\alpha_{c,4p}$	$\{\beta_{ST}, C_d\}$	1	8.4	$\{\zeta_2\}$	NA	7.1
D3 $\alpha_{c,1}$	$\{\varepsilon_{c0}\}$	NA	2.4	$\{k_{CK}, \rho_X, f_X\}$	3	2.0
D3 $\alpha_{c,1p}$	$\{\varepsilon_{c0}\}$	NA	2.4	$\{k_{CK}, \rho_X, f_X\}$	3	2.0
D3 $\alpha_{c,2}$	$\{\varepsilon_{c0}\}$	NA	5.3	$\{k_c, \rho_X, f_X\}$	3	3.3
D3 $\alpha_{c,2p}$	$\{\varepsilon_{c0}\}$	NA	5.3	$\{k_c, \rho_X, f_X\}$	3	3.3
D3 $\alpha_{c,3}$	$\{P_b, \zeta_2, \zeta_3\}$	1	1.6	$\{f_C, \zeta_4\}$	1	1.3
D3 $\alpha_{c,3p}$	$\{P_b, \zeta_2, \zeta_3\}$	1	1.6	$\{f_X, f_C, \zeta_4\}$	3	1.2
D3 $\alpha_{c,4p}$	$\{f_X, \zeta_2\}$	1	8.6	$\{f_C, \zeta_3\}$	1	8.6

NA: not applicable

[a] Could not be determined due to numerical error: the Jacobian was zero for all values in at least one parameter resulting in division by zero when calculating the covariance matrix.

**Table A20.** Optimised parameter values ($\hat{\theta}$) for the alternate AnDFCm filtration models. Relative error $\sigma_\theta/\hat{\theta}$ shown between brackets. θ^o is the initial guess (nominal values).

↓Model	C_d	$f_{C,c}$	$f_{X,c}$	β_{ST}	$K_{S,c}$	$q_{m,MS}$
Units→	-	-	-	-	kg	-
$\theta^o\rightarrow$	0.40	0.25	0.25	1.75×10^{-4}	0.2	4.71
D1c $\alpha_{c,1}$						2.2×10^{-14} [1×10^{12}]
D1c $\alpha_{c,1p}$					1.01 [1×10^4]	2.71 [8×10^3]
D1c $\alpha_{c,2}$					0.08 [684]	
D1c $\alpha_{c,2p}$					0.05 [0.001]	
D1c $\alpha_{c,3}$					0.21 [4×10^9]	3.3×10^{-12} [5×10^9]
D1c $\alpha_{c,3p}$					5.7×10^{10} [1×10^5]	1.6×10^{11} [1×10^5]
D1c $\alpha_{c,4p}$					6.8×10^{-4} [3.78]	0.02 [2.63]
D2 $\alpha_{c,1}$	0.003 [4.3]			1×10^{-5} [33.5]		
D2 $\alpha_{c,1p}$	0.48 [545]			1×10^{-4} [1.10]		
D2 $\alpha_{c,2}$	0.10 [0.16]			2×10^{-4} [1.23]		
D2 $\alpha_{c,2p}$	0.19 [0.03]			2×10^{-4} [0.02]		
D2 $\alpha_{c,3}$	0.05 [7.9×10^3]			0.50 [7.25]		
D2 $\alpha_{c,3p}$	9.46 [44.5]			0.02 [296]		
D2 $\alpha_{c,4p}$	4.59 [0.19]			0.39 [0.51]		
D3 $\alpha_{c,1}$			0.06 [2×10^6]			
D3 $\alpha_{c,1p}$			0.06 [3×10^6]			
D3 $\alpha_{c,2}$			0.04 [1×10^6]			
D3 $\alpha_{c,2p}$			0.04 [1×10^6]			
D3 $\alpha_{c,3}$		0.13 [0.23]				
D3 $\alpha_{c,3p}$		0.12 [0.22]	0.28 [0.07]			
D3 $\alpha_{c,4p}$		0.24 [2×10^5]	0.21 [0.25]			

Table A20 continued. Optimised parameter values ($\hat{\theta}$) for the alternate AnDFCm filtration models. Relative error $\sigma_\theta/\hat{\theta}$ shown between brackets. θ^o is the initial guess (nominal values).

↓Model	k_c	k_{CK}	ε_{c0}	ρ_X
Units→	$\times 10^{17}\,\mathrm{m}^{-2}$	$\times 10^7$	-	$\times 10^3\,\mathrm{kg\,m}^{-3}$
θ^o→	1.0	4.0	0.66	1.24
D1c $\alpha_{c,1}$		0.94 [0.32]	0.33 [0.02]	4.67 [0.38]
D1c $\alpha_{c,1p}$		4.81 [186]	0.62 [0.003]	4.83 [3.61]
D1c $\alpha_{c,2}$	12.91 [342]		0.44 [0.05]	15.3 [0.26]
D1c $\alpha_{c,2p}$	8.05 [0.15]		0.66 [0.002]	5.63 [0.18]
D2 $\alpha_{c,1}$		0.69 [33.2]	0.15 [0.04]	6.7 [0.98]
D2 $\alpha_{c,1p}$		5.7 [0.75]	0.21 [0.01]	0.54 [524]
D2 $\alpha_{c,2}$	1.01 [1.27]		0.11 [0.02]	1.22 [0.17]
D2 $\alpha_{c,2p}$	1.00 [0.02]		0.19 [0.004]	1.24 [0.06]
D3 $\alpha_{c,1}$		21.1 [0.39]	0.47 [0.02]	2.05 [3×10^6]
D3 $\alpha_{c,1p}$		21.1 [0.39]	0.47 [0.02]	2.05 [3×10^6]
D3 $\alpha_{c,2}$	13.7 [0.35]		0.60 [0.04]	4.57 [1×10^6]
D3 $\alpha_{c,2p}$	13.7 [0.35]		0.60 [0.04]	4.57 [1×10^6]

Table A20 continued. Optimised parameter values ($\hat{\theta}$) for the alternate AnDFCm filtration models. Relative error $\sigma_\theta/\hat{\theta}$ shown between brackets. θ^o is the initial guess (nominal values).

↓Model	P_b	ζ_1	ζ_2	ζ_3	ζ_4
Units→	$\times 10^3\,\mathrm{Pa}$	$\times 10^3$	$\times 10^4$	-	-
θ^o→	4.1799	1.16	1.36	172.4	150.9
D1c $\alpha_{c,3}$	4.2 [∞^a]		1.57 [0.23]	248.7 [0.04]	142.4 [∞^a]
D1c $\alpha_{c,3p}$	0.85 [0.49]	73.4 [0.58]		169.6 [0.18]	
D1c $\alpha_{c,4p}$		3.69 [0.09]	0.56 [0.51]		
D2 $\alpha_{c,3}$	1.9×10^7 [0.87]		0.63 [1.05]		
D2 $\alpha_{c,3p}$	9401 [6×10^5]		570 [6×10^5]		
D2 $\alpha_{c,4p}$			7.7×10^5 [0.01]		
D3 $\alpha_{c,3}$	27.9 [0.28]		0.77 [0.32]	236.9 [0.05]	12.4 [0.69]
D3 $\alpha_{c,3p}$	27.9 [0.28]		0.77 [0.32]	236.9 [0.05]	7.60 [0.55]
D3 $\alpha_{c,4p}$			1.72 [2.54]	178 [2×10^5]	

[a] The Jacobian was zero for all values in at least one parameter resulting in division by zero when calculating the covariance matrix.
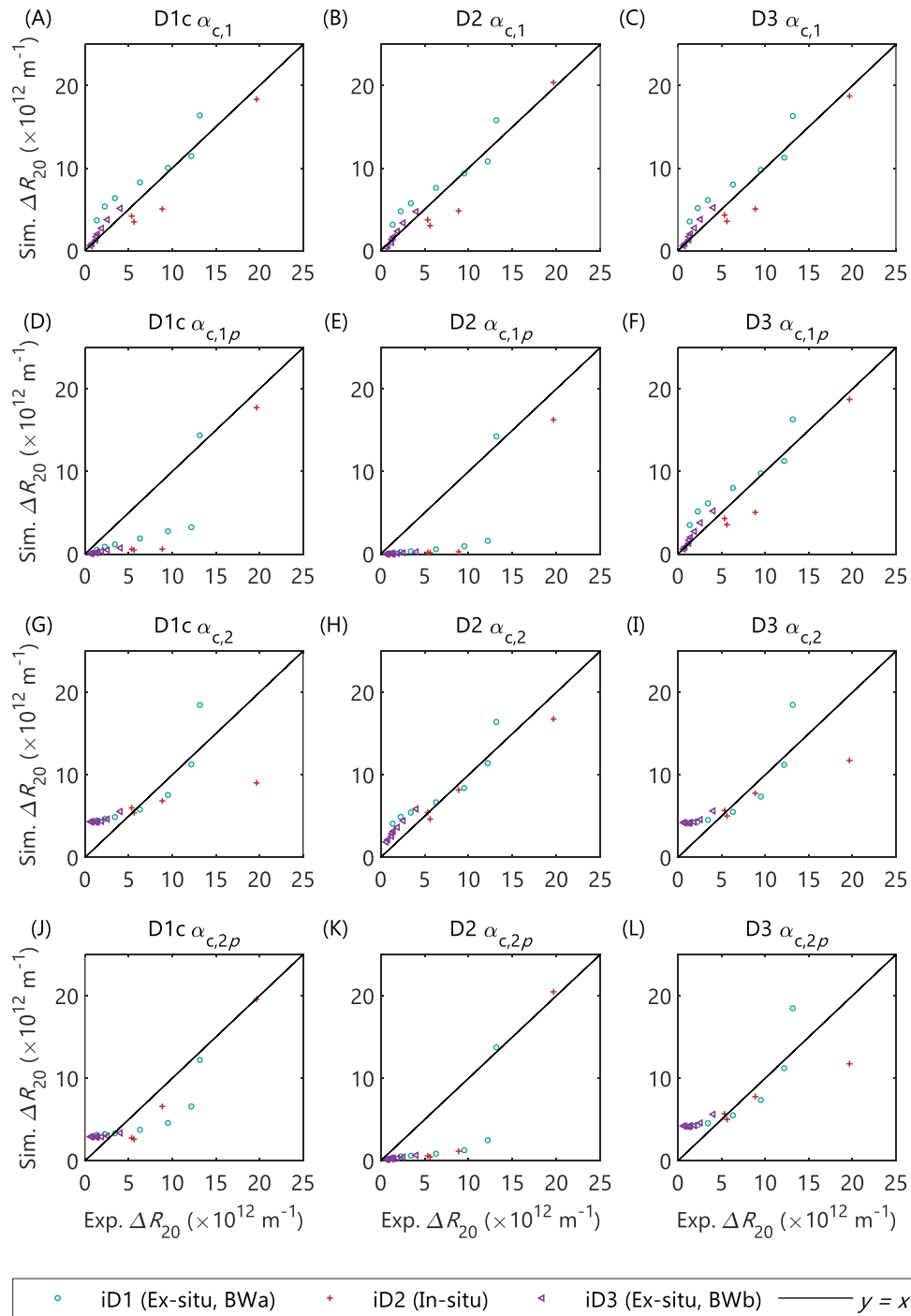
Figure A24. Calibration of the alternate AnDFCm filtration models combining the different deposition submodels (D1c, D2 and D3) with the Carman-Kozeny based specific cake resistance submodels ($\alpha_{c,1}$, $\alpha_{c,1p}$, $\alpha_{c,2}$ and $\alpha_{c,2p}$). Calibration performed using ΔR_{20} measurement during in-situ and ex-situ flux enhancer additions to the reactor and to grab samples from the pilot AnMBR, respectively.
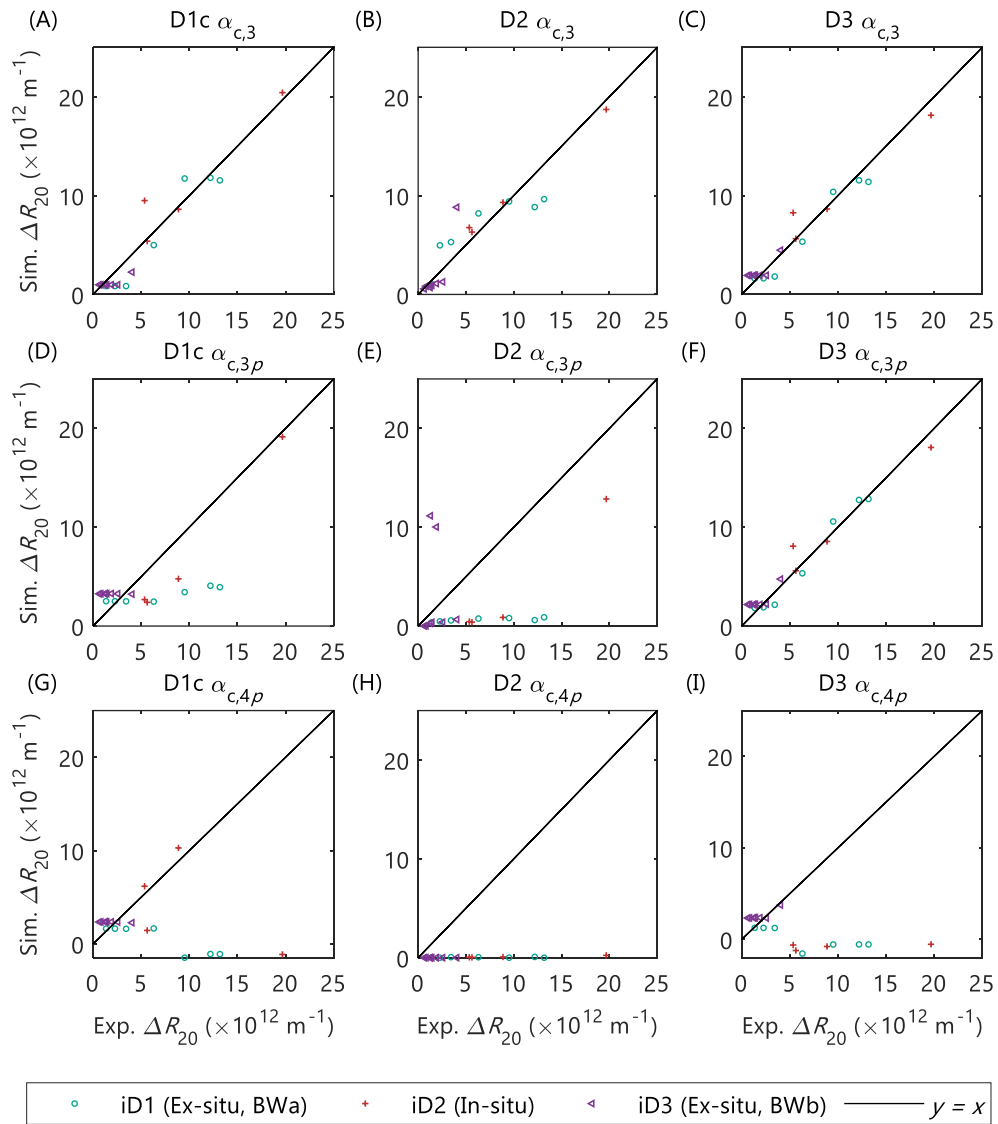
Figure A25. Calibration of the alternate AnDFCm filtration models combining the different deposition submodels (D1c, D2 and D3) with the specific cake resistance submodels based on the empirical equation by Cho et al. (2005) ($\alpha_{c,3}$, $\alpha_{c,3p}$, and $\alpha_{c,4p}$). Calibration performed using ΔR_{20} measurement during in-situ and ex-situ flux enhancer additions to the reactor and to grab samples from the pilot AnMBR, respectively.

Long-term prediction with calibrated model
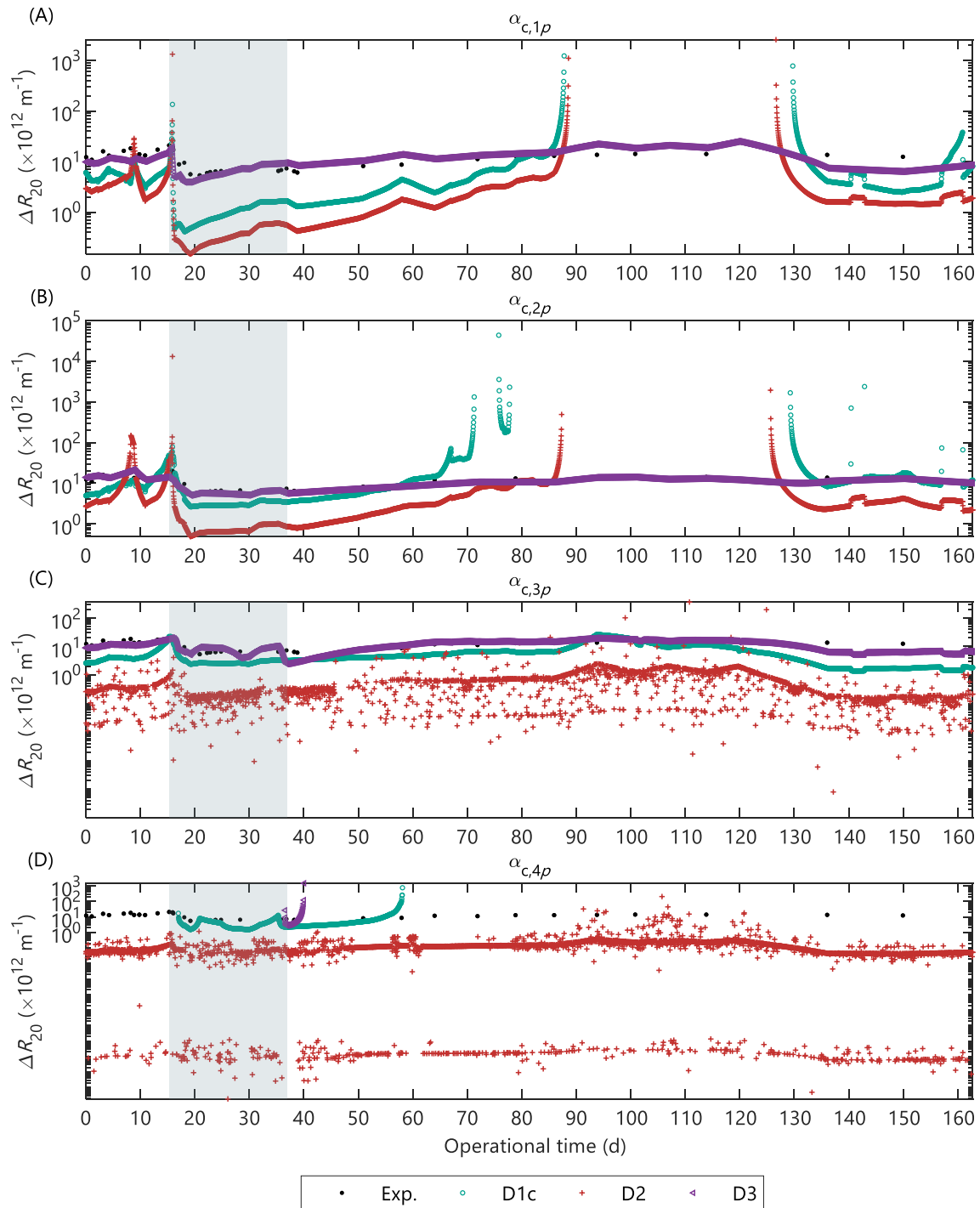
Figure A26. Validation of the alternate AnDFCm filtration models that combine the different deposition submodels (D1c, D2 and D3) with the compressible specific cake resistance submodels: (A) α_{1p}, (B) α_{2p}, (C) α_{3p}, and (D) α_{4p}. The grey area represent the in-situ data used for model calibration.
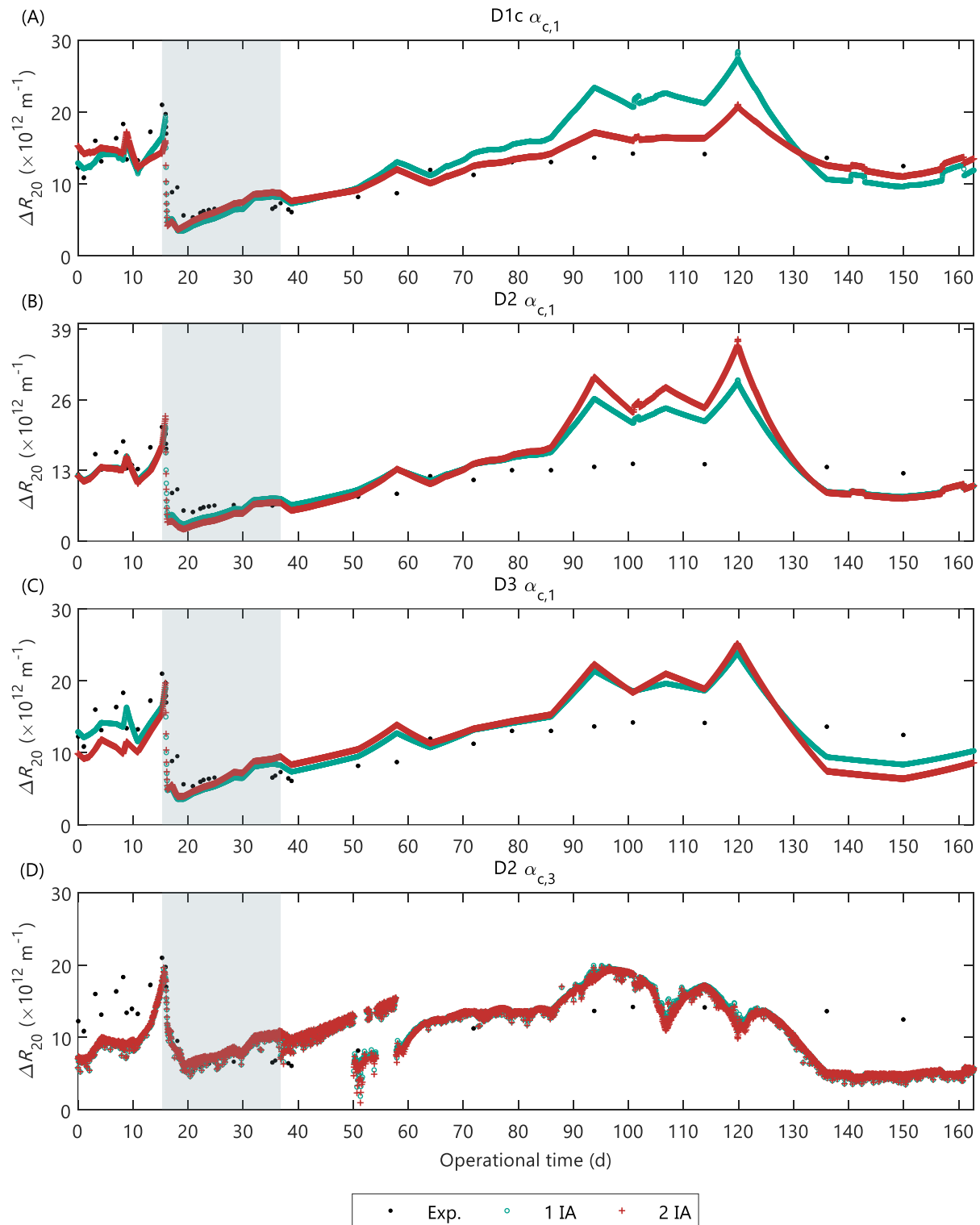
Figure A27. Comparison of alternate AnDFCm filtration models calibrated using one (1 IA) and two (2 IA) steps of identifiability analysis. Only the alternate models with different predictions for 1 IA and 2 IA are shown, as follows: (A) D1c α_1, (B) D2 α_1, (C) D3 α_1, and (D) D3c $\alpha_3 \equiv$ D3c α_{3p}. The remaining models combining the deposition submodels D1c, D2 and D3 with specific cake resistance submodels α_1, α_2, α_3, α_{1p}, α_{2p}, α_{3p} and α_{4p} presented identical predictions for 1 IA and 2 IA. The grey area represent the in-situ data used for model calibration.

A10. EFFECT OF SLUDGE CHARACTERISTICS ON FILTERABILITY PREDICTIONS

Figure A28 show the effect of the concentrations of colloidal and particulate material on the predicted ΔR_{20} with the alternate calibrated AnDFCm filtration models. The sludge characteristics were varied inside the simulation ranges in Table A21, which were based on the observed ranges in the pilot AnMBR. The remaining variables were set to the nominal values presented in the table, for example, all the ΔR_{20} simulations in Figure A28 were done at T = 296 K and d_p = 2.7×10^5 m.

Table A21. Nominal values and simulation range of operational conditions and sludge characteristics.

	Variable	Units	Nominal value [a]	Range in pilot AnMBR	Simulation range
c_C	Concentration of colloidal material	Kg m^{-3}	0.35	[0.14, 0.62]	[0.10, 0.65]
c_X	Concentration of particulate material	Kg m^{-3}	9.25	[4.9, 15.9]	[4.0, 16.0]
d_p	Mean particle diameter	×10^5 m	2.7	[2.1, 4.5]	[2.0, 5.0]
T	Sludge temperature	K	296	[292, 301]	NA

[a] Mean value during pilot AnMBR operation.
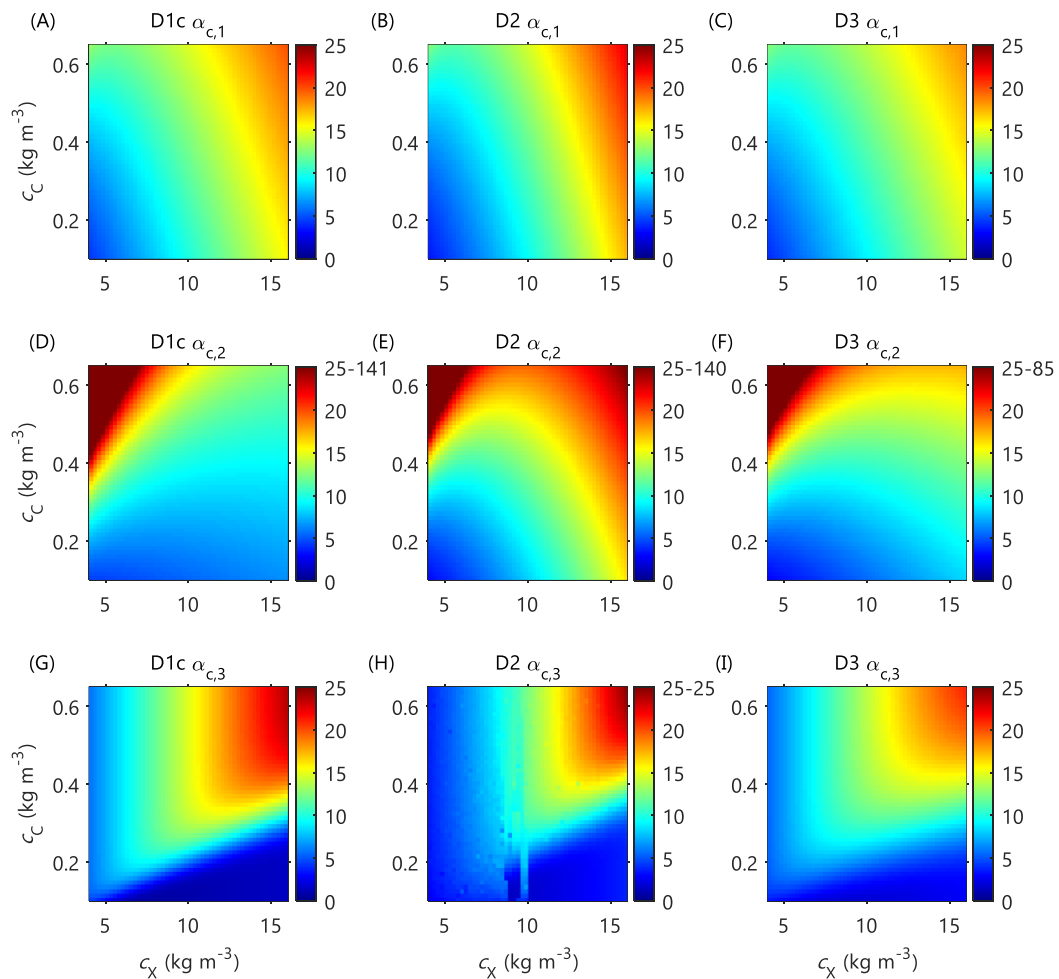
Figure A28. Effect of the concentrations of colloidal material (c_C) and particulate material (c_X) on the predicted ΔR_{20} (×10^{-12} m^{-1}) with different calibrated AnDFCm filtration models: (A) D1c $\alpha_{c,1}$, (B) D2 $\alpha_{c,1}$, (C) D3 $\alpha_{c,1}$, (D) D1c $\alpha_{c,2}$, (E) D2 $\alpha_{c,2}$, (F) D3 $\alpha_{c,2}$, (G) D1c $\alpha_{c,3}$, (H) D2 $\alpha_{c,3}$, and (I) D3 $\alpha_{c,3}$.

A11. CAKE LAYER COMPRESSION

Evenblij (2006) presented the three possible hypothetical filtration curves obtained with the Delft filtration characterization method, and Geilvoet (2010) related the filtration curves with a compressibility coefficient. The researchers qualified the cake layer by analysing the filtration curve ΔR versus ΔV_S obtained at constant flux, where ΔR is the additional resistance after production of a certain volume of permeate, and ΔV_S the volume of permeate produced per square meter of membrane surface area. Table A22 summarises the hypothetical filtration curves.

Table A22. Hypothetical filtration curves obtained with the Delft filtration characterization method (Evenblij, 2006; Geilvoet, 2010).

Cake layer type	Exponential parameter b $$\Delta R = a\,\Delta V_S^{\,b}$$	Compressibility coefficient s $$s = \frac{b-1}{b}$$
Compressible	> 1	> 0
Linear	1	0
Equilibrium	< 1	< 0

The experimental resistance-volume curves obtained with the AnDFCm were fitted to the power equation presented in Table A22 and analysed the cake layer type based on the compressibility coefficient calculated with the optimised parameter b. Figure A29 shows the histogram of compressibility coefficients obtained for the in-situ ΔR_{20} measurement performed in the pilot AnMBR; the compressibility coefficient varied between -0.39 and 0.19. In accordance with Table A22, 34% of the filtration curves corresponded to a linear cake layer ($s = 0$), 48% to an equilibrium cake layer ($s < 0$), and 18% to a compressible cake layer ($s > 0$). Furthermore, the grab sludge samples from different AnMBRs displayed in Figure A30 generated a linear or equilibrium cake layer. Therefore, results suggested that the cake layer formed with the AnDFCm when filtering anaerobic sludge samples from AnMBR is none-compressible or slightly compressible.

For aerobic sludge samples, from MBRs, the cake layer formed using the DFCm was hardly compressible, the compression coefficient varied between 0-0.3 (Lousada-Ferreira et al., 2014). The DFCm (at 80 L m^{-2} h^{-1} and 1.0 m s^{-1}) and AnDFCm (at 60 L m^{-2} h^{-1} and 1.5 m s^{-1}) differed in the flux and crossflow velocities used during filtration; therefore, the numerical values of the compression coefficients cannot be directly compared. Nevertheless, the hypothetical filtration curves were valid for both measuring methods because they were performed at constant flux.
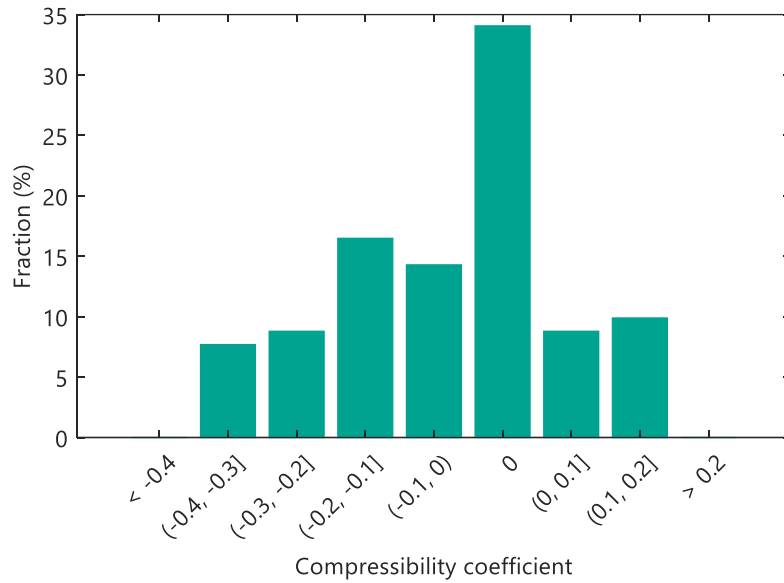
Figure A29. Distribution of the compressibility coefficient of the cake layer formed with the AnDFCm during in-situ ΔR_{20} measurements of the pilot AnMBR sludge.
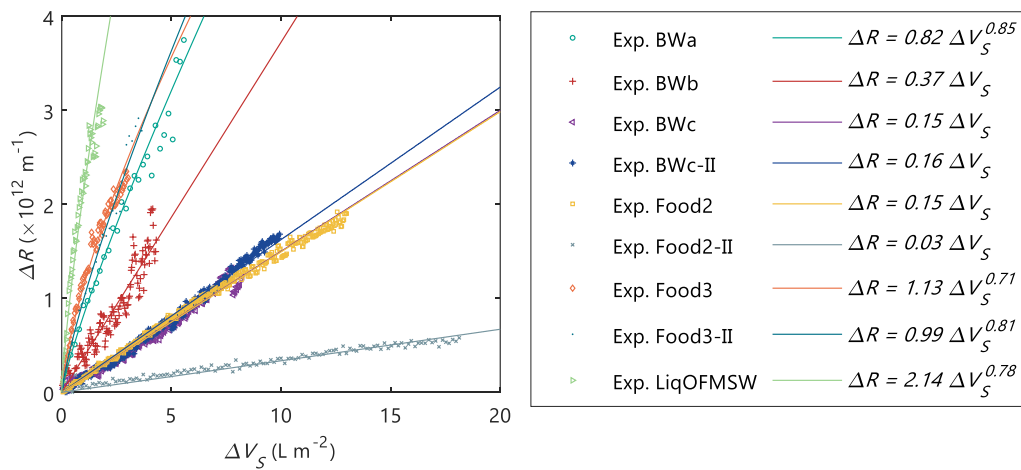
Figure A30. Added total resistance versus specific volume of permeate obtained when filtering grab sludge samples from different AnMBRs with the AnDFCm. Experimental data (markers) and fitted power curves (lines).

NOMENCLATURE

<u>Abbreviations</u>

AMP	Accumulated methane production
AnDFCm	Anaerobic Delft filtration characterization method
AnMBR	Anaerobic membrane bioreactor
COD	Chemical oxygen demand
CST	Capillary suction time
EPS	Extracellular polymeric substances
FE	Flux enhancer
FR	Fouling rate
HRT	Hydraulic retention time
HS	Humic substances
KD###	Cationic polymers from Adipap
MBR	(aerobic) Membrane bioreactor
MPE##	Cationic polymers from Nalco
PAC	Powdered activated carbon
PBM	Population balance models
PSD	Particle size distribution
RIS	Resistance in series
RMSE	Root mean square error
RSS	Residual sum of squares
SCR	Specific cake resistance
SMA	Specific methanogenic activity
SMP	Soluble microbial products
SRC	Standardised regression coefficient
SRT	Solids retention time
TMP	Transmembrane pressure
TOC	Total organic carbon
TSS	Total suspended solids
VFA	Volatile fatty acids
VSS	Volatile suspended solids

Symbols

α_c	Specific cake resistance (m kg^{-1})
$\alpha_{c,j}$	Specific cake resistance calculated with submodel j without cake compression (m kg^{-1})
$\alpha_{c,jp}$	Specific cake resistance calculated with submodel j with cake compression (m kg^{-1})
β_k	Standardised regression coefficient for parameter k
β_{ST}	Lumped parameter $\beta_{ST} = \beta(1 - K_{ST})$; β Erosion rate coefficient of the sludge cake; K_{ST} stickiness coefficient
γ	Compression coefficient for the dynamic cake layer (kg m^{-3})
γ_i	Empirical model parameter i
γ^k	Collinearity index of the parameter subset k
ΔR_{20}	Additional resistance when 20 L of permeate per m^2 of membrane surface are obtained during filtration at constant flux and crossflow velocity in the AnDFCm installation (m^{-1})
Δt_{fe}	Injection time of flux enhancer pulse-dosage (s)
ε_c	Cake layer porosity (-)
ε_{c0}	Cake layer porosity without colloidal material (-)
ζ_i	Empirical model parameters
θ	Parameter subset for estimation
$\theta°$	Initial guess
$\hat{\theta}$	Estimated parameters (optimal values)
θ_F	Total filtration time in one cycle (s)
θ_R	Total relaxation time in one cycle (s)
$\theta_{H,i}$	Temperature correction factor for Henry's law coefficient for component i (-)
θ_j	Temperature correction factor for the reaction rate of process j (-)
μ	Dynamic viscosity of the permeate at the operational temperature (Pa s)
μ_{20}	Dynamic viscosity of the permeate at 20°C (Pa s)
μ_i	Dynamic viscosity of fluid i (Pa s)
v_B	Motor frequency of the blower (Hz)
v_P	Motor frequency of the permeate pump (Hz)
$v_{i,j}$	Stoichiometric coefficients of component i in process j
ρ_j	Rate equations of process j (kgCOD m^{-3} d^{-1} or kmol m^{-3} d^{-1})
ρ_i	Density of component or fluid i (kg m^{-3})
σ_θ	Standard deviation of estimated parameters
τ	Kendall correlation coefficient
τ_w	Shear stress (Pa)
ω_i	Mass of component i deposited per membrane area (kg m^{-2})
Alk$_{BW}$	Blackwater alkalinity (KgCaCO$_3$ m^{-3})
A_m	Membrane surface area (m^2)
A_{MT}	Membrane tank cross-sectional area (m^2)
b_j	First order decay rate of microorganism in process j (d^{-1})
cCOD	Colloidal COD concentration (kgCOD m^{-3})
C_d	Drag coefficient (-)

C_i	Concentration of colloidal material i in the bulk liquid (kgCOD m^{-3})
c_i	Concentrations of component i in the liquid phase (kg m^{-3})
$c_{i,j}$	Concentration of component i in fluid j (kgCOD m^{-3} or kmol m^{-3})
c_{fe}	Total concentration of flux enhancer inside the reactor (kgCOD m^{-3})
$c_{fe,P,theo}$	Theoretical concentration of component i in the permeate (kg m^{-3})
csCOD	Submicron COD concentration (kgCOD m^{-3})
csCOD$_{BW}$	Submicron COD concentration in blackwater (kgCOD m^{-3})
$D10$	10 percentiles of the particle size distribution (µm)
$D50$	50 percentiles of the particle size distribution (µm)
$D90$	90 percentiles of the particle size distribution (µm)
D_{50}	Effective dosage 50 (kg m^{-3})
D_{crit}	Critical flux enhancer dosage (kg m^{-3})
D_{opt}	Optimal flux enhancer dosage (kg m^{-3})
d_p	Mean particle diameter (m)
$d_{p,i}$	Diameter of the i-th particle (m)
$d_{p,St}$	Mean particle diameter at stable operation (m)
E_i	Input function of component i (kgCOD m^3 d^{-1})
f_{conv}	Conversion factor
$f_{i,c}$	Fraction of material i deposited onto the membrane (-)
$f_{i,P}$	Fraction of component i that passes through the membrane and reaches the permeate (-)
$f_{i,WS}$	Fraction of component i that leaves the reactor with waste sludge flow (-)
$f_{objective}$	Objective function for parameter estimation
$f_{p,i}$	Yield of product p on substrate i (-)
g	Gravitational acceleration (m s^{-2})
G	Apparent shear rate (s^{-1})
H_{MT}	Liquid level in membrane tank (m)
$i_{C,i}$	Carbon content of component i (kmole kgCOD^{-1})
$i_{C,CXI,bio}$	Colloidal fraction of the released suspended inert material upon biomass decay (-)
$i_{COD,i}$	Theoretical chemical oxygen demand for component i (kgCOD kg^{-1})
$I_{i,j}$	Inhibition factor of component i in process j (-)
$i_{i,CSInf}$	Content of component i in the submicron material of the influent (kgCOD kgCOD^{-1})
$i_{i,SInf}$	Content of component i in the soluble material of the influent (kgCOD kgCOD^{-1})
$i_{i,XInf}$	Content of component i in the particulate material of the influent (kgCOD kgCOD^{-1})
I_{MS}	Sigmoid inhibition function during membrane scouring (-)
$i_{N,i}$	Nitrogen content of component i (kmole kgCOD^{-1})
$i_{Xac,VSS,0}$	Initial content of acetate degraders in VSS (kgCOD kgVSS^{-1})
J	Transmembrane flux (m^3 m^{-2} s^{-1})
J_{20}	20°C-normalised transmembrane flux (m^3 m^{-2} s^{-1})
$J_{20,AnDFCm}$	20°C-normalised transmembrane flux applied in the AnDFCm installation (m^3 m^{-2} s^{-1})
J_{AnDFCm}	Transmembrane flux applied in the AnDFCm installation (m^3 m^{-2} s^{-1})
$K_{a,co2}$	Acid-base equilibrium coefficient (CO$_{2,ac}$/HCO$_3^-$)

k_{ads}	Pseudo-first order reaction rate coefficient for flux enhancer adsorption (d^{-1})
k_c	Cake resistance coefficient (m^{-2})
k_{CK}	Carman-Kozeny cake resistance coefficient (-)
$k_{\mathrm{dis,bio}}$	First order reaction rate coefficient for biomass disintegration (d^{-1})
$K_{eq,\mathrm{fe},i}$	Equilibrium coefficient for flux enhancer and component i binding (kgCOD kg^{-1})
K_F	Parameter representing the fouling rate when J_{20} tends to zero (Pa s^{-1})
k_{floc}	Empirical flocculation-deflocculation rate (d^{-1})
$k_{\mathrm{floc,fe}}$	Flux enhancer induced flocculation yield (m kgCOD^{-1} m^3)
$K_{H,i}$	Henry's law coefficient for component i (kgCOD m^{-3} bar^{-1} or kmol m^{-3} bar^{-1})
k_{hyd}	Unique first order reaction rate coefficient for all hydrolysis processes (d^{-1})
$k_{\mathrm{hyd},j}$	First order reaction rate coefficient for hydrolysis of component j (d^{-1})
$K_{I,i,j}$	Concentration of inhibitor i giving 50% inhibition on process j rate (kgCOD m^{-3})
k_j	Reaction rate for process j (d^{-1})
$K_{L,\mathrm{ads}}$	Langmuir affinity coefficient (m^3 kgCOD^{-1})
$k_L a$	Dynamic gas-liquid transfer coefficient (d^{-1})
$k_{m,j}$	Monod maximum specific uptake rate for process j (d^{-1})
$K_{S,c}$	Half-saturation coefficient for cake mass during membrane scouring (kg)
$K_{S,G}$	Half-saturation coefficient for gas velocity during membrane scouring (m s^{-1})
$K_{S,\mathrm{IN}}$	Monod half saturation coefficient for inorganic nitrogen (kmol m^{-3})
$K_{S,j}$	Monod half saturation coefficient for process j (kgCOD m^{-3})
M_{fe}	Cumulative mass of flux enhancer (kgCOD)
$M_{\mathrm{fe,P}}$	Cumulative mass of flux enhancer removed with the permeate flow (kgCOD)
$\dot{m}_{\mathrm{fe}}$	Flux enhancer mass flow rate (kgCOD s^{-1})
$\mathrm{NH4}_{\mathrm{BW}}$	Ammonium nitrogen in blackwater (KgN m^{-3})
n_j	Numer of experimental observatons of the ouput variable j (-)
p	Probability value for statistical hypothesis testing
P_{a}	Pressure needed to double the specific resistance (Pa)
P_{b}	Transmembrane pressure coefficient (Pa)
pCOD	Permeate COD (kgCOD m^{-3})
p_{G}	Gas pressure in the headspace (bar)
P_i	Volume fraction (-)
$p_{i,\mathrm{G}}$	Partial pressure of gas i (bar)
$\mathrm{pH}_{\mathrm{LL},j}$	Lower pH limit where the group of organisms in process j is 50% inhibited.
$\mathrm{pH}_{\mathrm{UL},j}$	Upper pH limit where the group of organisms in process j is 50% inhibited.
$q_{e,\mathrm{ads}}$	Adsorbent phase concentration of flux enhancer after equilibrium (kgCOD kg^{-1})
Q_j	Volumetric flow rate of fluid j (m^3 s^{-1})
$q_{m,\mathrm{ads}}$	Maximum adsorption capacity corresponding to monolayer coverage (kgCOD kg^{-1})
$q_{m,\mathrm{MS}}$	Maximum membrane scouring velocity (-)
R	Gas constant (m^3 bar kmol^{-1} K^{-1})
R^2	Coefficient of determination (-)
R_{c}	Cake layer resistance (m^{-1})
R_{m}	Membrane intrinsic resistance (m^{-1})
RSS_k	Residual sum of squares for the output variable k

R_t	Total filtration resistance (m^{-1})
sCOD	Soluble COD concentration (< 0.45 μm) (kgCOD m^{-3})
$S_{fe,e}$	Concentration of soluble flux enhancer in the bulk liquid after equilibrium (kgCOD m^{-3})
SGD_m	Specific gas demand (Nm^3 h^{-1} m^{-2})
S_i	Concentration of soluble component i in the bulk liquid (kgCOD m^{-3} or kmol m^{-3})
t	Time (s)
T	Temperature (K or °C)
t_{conv}	Time conversion factor (86,400 s d^{-1})
tCOD	Total COD concentration (kgCOD m^{-3})
tCOD$_{BW}$	Total COD concentration in blackwater (kgCOD m^{-3})
t_F	Continuous filtration time in a cycle (s)
t_{fe0}	Initial time of flux enhancer pulse-dosage (s)
TMP	Transmembrane pressure (Pa)
$u_{L,AnDFCm}$	Liquid crossflow velocity in the AnDFCm installation (m s^{-1})
u_G	Gas superficial velocity (in the AnMBR membrane tank) (m s^{-1})
V_F	Volume of permeate produced within the filtration time t_F (m^3 m^{-2})
V_G	Total gas volume (m^3)
V_L	Total mixed liquor volume (m^3)
V_P	Permeate volume produced (m^3)
V_T	Total reactor volume (m^3)
w_j	Weight of output variable j (-)
$X_{fe,e}$	Adsorbed concentration of flux enhancer after equilibrium (kgCOD m^{-3})
X_i	Concentration of particulate component i in the bulk liquid (kgCOD m^{-3})
$Y_{fe,C}$	Yield of colloidal material flocculated per unit of flux enhancer adsorbed (kg kg^{-1})
$Y_{floc,fe}$	Proportionality parameter between particle diameter and flux enhancer concentration (kg kgCOD^{-1})
Y_j	Yield coefficient of biomass on substrate for process j.
$y_{e,j,i}$	i-th experimental value of the output variable j
$y_{m,j,i}$	i-th predicted value of the output variable j

Subscripts

aa	Amino acids / Amino acids degraders
ac	Acetate /Acetate degraders
bu	Butyrate
c	Cake layer
C	Colloidal
c4	Valerate and butyrate degraders
ch4	Methane
co2	Carbon dioxide
ch	Carbohydrates
fa	Long chain fatty acids (LCFA) / LCFA degraders
fe	Flux enhancer, cationic polymer
G	Gas
h2	Hydrogen / Hydrogen degraders
hs	Humic substances
I	Inert
IC	Inorganic carbon
IN	Inorganic nitrogen
Inf	Influent
L	Mixed liquor
li	Lipids
P	Permeate
pr	Proteins
pro	Propionate / Propionate degraders
S	Soluble
su	Monosaccharides
va	Valerate
W	Water
WS	Waste sludge
X	Particulate

ACKNOWLEDGEMENTS

"The individual, if left alone from birth would remain primitive and beast-like in his thoughts and feelings to a degree that we can hardly conceive. The individual is what he is and has the significance that he has not so much in virtue of his individuality, but rather as a member of a great human society, which directs his material and spiritual existence from the cradle to the grave." Albert Einstein

This dissertation would not have been possible without the collaboration and support of so many people.

I would like to start by thanking the members of my defence committee for your interest in my thesis, and for finding the time to read and assess my dissertation.

Jules, thank you for giving me the opportunity to do my PhD in a (AD)world–renowned university. I appreciate the freedom and support you gave me during this project. Although we did not meet so often, your input was always clear and relevant. Thanks for helping me improve my story telling with your feedback, and for coping with my anxiety during the "final sprint".

Henri, thank you for your guidance and support, and for helping me improve my academic writing and research skills. I highly appreciate the time, effort, and commitment in the last moths to provide feedback and help me finalise my dissertation. I know that the first draft of Chapter 5 was a though pill to swallow, but thanks to your input it improved considerably.

Maria, thank you for the professional and emotional support during the first year of my PhD. Somewhere during the second month, when I was stressed trying to complete as many GS credits as possible, you said: "the PhD is a marathon and not a race", these simple words helped me a lot during this project. I appreciated, and kind of enjoyed, our passionate and valuable weekly discussion. Thanks for teaching me about Dutch culture inside and outside academia.

Edo Abraham, I'm grateful for your collaboration on the third chapter of this dissertation. **Merle de Kreuk**, thank you for your motivation and enthusiasm during this last year, and for being part of the committee. To the students that contributed to this thesis: **Magnolia García Solano**, **Frank Mols**, **Donya Fakhravar**, and **Aditya Vir Rajaraman**, thank you for your collaboration. To **Miguel Mauricio** for the input and discussion about modelling and uncertainty analysis, for the nice trips, and for introducing the real *pulpo á galega*.

During my PhD research I had the pleasure to perform part of my experiments in the pilot plant of FCC-Aqualia located in Vigo. Thanks to the staff of Consorcio de Augas do Louro and Guillarei for their assistance during the experimental phase. A special thanks to **Nico**, **Jose**, **Ana** and **Victoria** for their infinite help and support with the experiments, and for making my stay in Spain fun and fulfilling. I hope we get the opportunity to work together in the future. Thanks to the staff of Biothane-Veolia, FCC-Aqualia, WWTP Harnaschpolder,

and Adipap SA for suppling samples and scientific insight, special thanks to **Santiago Pacheco**, **Antonio Gimenez**, **Paul Weij** and **Benjamin Viet**.

My time at TU Delft has been a fantastic journey. All the challenges, opportunities, and the people I've met throughout the journey promoted my professional and personal growth and I am extremely thankful for it. To our support staff, **Mariska, Tamara, Sabrina** and **Riëlle**, thank you for making my life easier. To the lab technicians without whom working in the lab would be more difficult and time consuming: **Armand, Mohammed, Jane, Patricia, Jasper**, and **David**. Thanks to all the colleagues from the Water Lab that made this trajectory more fun, interesting, and enriching: **Adrian, Alexander, Antonella, Beatriz, Bruno, Carina, Daniel, Dhavissen, Diana, Emiel, Felipe, Hamed, Hongxiao, Irene, Julián, Laís, Lenno, Marjet, Max, Mona, Simon, Steef, Tales,** and the ones that I might have forgotten to mention.

To my officemates, **Pamela, Víctor** and **Niels**, thank you for the *gezelligheid*, the academic input, the many interesting conversations, the nice trips and the epic phrases. After working so much from home during the pandemic I came to appreciate and value even more the amazing office environment that we had during the PhD. So amazing that it resulted in a publication in the "Journal of Office Environment Optimization". Niels, thank you for all the (un)fruitful discussions between two stubborn people, for helping with my Dutch, and for being the sunshine of the office and our "temperature-sensitive subject with proved controlling behaviour" (Odriozola & García Rea, 2020). Pamela, thanks for being there since day one of this adventure, for always clarifying all the information that I misunderstood or simply didn't know, for being my partner in our first effort to learn Dutch, for our nice trips, and for your excellent birthday speeches. Víctor, thanks for your positivity, for our always fun four-topic conversations, for co-authoring our publication, for being my microbiological encyclopaedia, and for letting me nap during our MBR course. I appreciate you teaching me the power of (creepily) smiling to people 24/7 during our adventure in Colombia, unfortunately I was not a good student.

To my paranymphs, **Javier** and **Marijke**, two extraordinary people, thanks for accepting this role without hesitation, I trust that you will not take it too far. Marijke, the woman that can do anything and do it good, except understanding the social norms over drinking tea. Thanks for your *gezelligheid*, for your constant positivity, and for all the empowering and cheering up. Looking forward to our trip to Uruguay. Javier, I am still to find a topic where you cannot enlighten me with your knowledge, in the words of Sara "que chico tan listo". Thanks for all the help and support during these last years, and for teaching me so much about the Chilean inflation. I really enjoyed sharing awkward moments with you, and co-organising the YWP conference has been so much fun, specially when we had to promote it.

Living in the Netherlands did not come without challenges. Specially at the beginning, when I had to adapt to a new job, new house, new people, new food, new ways of transportation, less benevolent weather, lack of sun light, and even opposite hemisphere. Thankfully I quickly met some amazing people that made this process exciting and interesting. To my first Boterbrug housemates, **Antonio**, **Sophie** and **Adithya**, thank you for making me feel so welcomed, for being such kind, fun and interesting people, and for the fast introduction to

fed during my PhD. For your patience and support during my long working days, and for constantly pushing me to be better. Without you, finishing this thesis would have been even more challenging, and much less fun. Thank you for convincing me to get Eris and Leia, with whom I discovered my inner crazy-cat-lady, these furry beauties kept me company during long writing days. I'd also like to thank you for all the feedback on my thesis, and for helping with the cover design and Dutch translations. I am looking forward to many more adventures in this new chapter that we are about to begin.

LIST OF PUBLICATIONS

Peer-reviewed journal publications

Odriozola, M., Abraham, E., Lousada-Ferreira, M., Spanjers, H., and van Lier, J. B. (2019). Identification of the Methanogenesis Inhibition Mechanism Using Comparative Analysis of Mathematical Models. *Frontiers in Bioengineering and Biotechnology* 7, 93. doi:10.3389/fbioe.2019.00093.

Odriozola, M., López, I., and Borzacconi, L. (2016). Modeling granule development and reactor performance on anaerobic granular sludge reactors. *Journal of Environmental Chemical Engineering* 4, 1615–1628. doi:10.1016/j.jece.2016.01.040.

Odriozola, M., Lousada-Ferreira, M., Spanjers, H., and van Lier, J. B. (2021). Effect of sludge characteristics on optimal required dosage of flux enhancer in anaerobic membrane bioreactors. *Journal of Membrane Science* 619, 118776. doi:10.1016/j.memsci.2020.118776.

Odriozola, M., Morales, N., Vázquez-Padín, J. R., Lousada-Ferreira, M., Spanjers, H., and van Lier, J. B. (2020). Fouling Mitigation by Cationic Polymer Addition into a Pilot-Scale Anaerobic Membrane Bioreactor Fed with Blackwater. *Polymers* 12, 2383. doi:10.3390/polym12102383.

Odriozola, M., van Lier, J. B., and Spanjers, H. (2022). Optimising the flux enhancer dosing strategy in a pilot-scale anaerobic membrane bioreactor by mathematical modelling. *Membranes* 12, 151. doi.org/10.3390/membranes12020151.

Lousada-Ferreira, M., Muñoz Sierra, J.D., **Odriozola, M**., Spanjers, H., and van Lier, J.B. Flux enhancers in anaerobic membrane bioreactors. *Manuscript in preparation*

Conference presentations

López, I., Borges, L. I., **Odriozola, M.**, Ramos, D., and Passeggi, M. (2011). Potassium inhibition in anaerobic treatment of distillery vinasse. in *X IWA Latin American Workshop and Symposium on Anaerobic Digestion* (Ouro Preto, Brazil).

López, I., **Odriozola, M.**, and Borzacconi, L. (2013). Modelling diffusional effects in anaerobic granules and its consequences on reactor design. in *13th IWA World Congress on Anaerobic Digestion* (Santiago de Compostela, Spain).

López, I., Passeggi, M., **Odriozola, M.**, Borges, L. I., and Borzacconi, L. (2012). Tratamiento Anaerobio de Vinaza de Destilería de Caña de Azúcar. in *V Encuentro Regional, XXVI Congreso Interamericano de Ingeniería Química* (Montevideo, Uruguay).

Lousada-Ferreira, M., **Odriozola, M.**, Spanjers, H., and van Lier, J. B. (2017a). On-line filterability measurements in Anaerobic Membrane Bioreactors. in *12th IWA Specialized Conference on Instrumentation, Control and Automation* (Québec City, Québec, Canada).

Lousada-Ferreira, M., **Odriozola, M.**, Spanjers, H., and van Lier, J. B. (2017b). Quantifying fouling in Anaerobic Membrane Bioreactors through filterability measurements. in *15th IWA World Congress on Anaerobic Digestion* (Beijing, China).

Odriozola, M., Castelló, E., Zinola, D., and Borzacconi, L. (2011). Two starting up strategies and hydrodynamic behaviour of an EGSB treating sugar cane vinasse. in *X IWA Latin American Workshop and Symposium on Anaerobic Digestion* (Ouro Preto, Brazil).

Odriozola, M., López, I., and Borzacconi, L. (2015). Modelling anaerobic reactors: integrating kinetics, mass transfer phenomena and granule growth. in *14th IWA World Congress on Anaerobic Digestion* (Viña del Mar, Chile).

Odriozola, M., López, I., and Borzacconi, L. (2016). Comportamiento de gránulos anaerobios concebidos como catalizadores heterogéneos dinámicos. in *XXV Ibero-American Catalysis Congress* (Montevideo, Uruguay).

Odriozola, M., Lousada-Ferreira, M., Morales, N., Spanjers, H., and van Lier, J. B. (2019). Fouling control by flocculant addition based on online measurement of sludge filterability in a pilot AnMBR. in *16th IWA World Congress on Anaerobic Digestion* (Delft, Netherlands). (2nd best presentation award)

Odriozola, M., Lousada-Ferreira, M., Pacheco-Ruiz, S., Baudry, M., Morales, N., Vázquez-Padín, J. R., Giménez-Lorang, A., Spanjers, H., and Van Lier, J. B. (2020). Optimal dosage of flux enhancer for sludge filterability improvement in anaerobic membrane bioreactors (AnMBRs). in *6th IWA Young Water Professionals Benelux Conference* (Luxemburg).

Odriozola, M., Lousada-Ferreira, M., Spanjers, H., and van Lier, J. B. (2017). Factors impacting particle size distribution analysis of anaerobic sludge using laser diffraction. in *5th IWA Young Water Professionals Benelux Conference* (Ghent, Belgium).

Odriozola, M., Lousada-Ferreira, M., Spanjers, H., and van Lier, J. B. (2018). Towards an automated fouling control by addition of flux enhancers to anaerobic sludge. in *XII IWA Latin American Workshop and Symposium on Anaerobic Digestion* (Medellin, Colombia).

ABOUT THE AUTHOR

Magela Odriozola Arbiza was born in Artigas, Uruguay on April 2nd, 1987. She attended her elementary, primary, and secondary education at public schools in Artigas. At age 17, she moved to Montevideo to start her university education. She completed her 5-year Chemical Engineering degree from the Universidad de la República (UdelaR) in September 2011. Immediately after, she started her MSc degree in Chemical Engineering at UdelaR with focus on modelling anaerobic granular bioreactors by integrating kinetic processes, mass-transfer phenomena, reactor hydraulics and granule development.

Next to her studies, she worked at the Biotechnological Processes for the Environment (BIOPROA) group at the Faculty of Engineering, UdelaR and at the chemical industry Sachedi Ltda. She joined BIOPROA in November 2008 and worked there for almost 8 years, until October 2016. In BIOPROA, she participated in various research projects focusing on anaerobic digestion of agro-industrial wastewaters and assisted in two undergraduate courses. At Sachedi Ltda., she worked as an operation manager of the wastewater treatment plant and junior project manager in three wastes re-valorisation projects, from June 2010 until February 2012. From May until October 2016, she worked as a technical consultant at Biotrade S.A. in the project of chemical treatment of shavings from tanned hides and skins.

In October 2016 she moved to the Netherlands to start as a PhD researcher at the Delft University of Technology in the Water Management department. Her research topic focused on fouling control in anaerobic membrane bioreactors by dosing flux enhancers. She started as a postdoc researcher at the Delft University of Technology in the Water Management department in July 2020. Her postdoc research focuses on the production of volatile fatty acid from fine sieves fermentation and improvement of municipal wastewater nitrogen and phosphorus removal by feeding the produced volatile fatty acids to the wastewater treatment plant.

Magela is passionate about innovative technologies that can help society and contribute to achieving a more sustainable world.

BIBLIOGRAPHY

Alkmim, A. R., da Costa, P. R., Moser, P. B., França Neta, L. S., Santiago, V. M. J., Cerqueira, A. C., and Amaral, M. C. S. (2016). Long-term evaluation of different strategies of cationic polyelectrolyte dosage to control fouling in a membrane bioreactor treating refinery effluent. *Environmental Technology* 37, 1026–1035.

American Public Health Association, Association, A. W. W., and Federation, W. E. (1999). *Standard Methods for the Examination of Water and Wastewater.* 20th ed. , ed. A. D. Cleseceri, Leonore S.; Greenberg, Arnold E.; Eaton Washington DC, U.S.A.: APHA/AWWA/WEF.

Astals, S., Batstone, D. J., Tait, S., and Jensen, P. D. (2015). Development and validation of a rapid test for anaerobic inhibition and toxicity. *Water Research* 81, 208–215.

Astals, S., Peces, M., Batstone, D. J., Jensen, P. D., and Tait, S. (2018). Characterising and modelling free ammonia and ammonium inhibition in anaerobic systems. *Water Research* 143, 127–135.

Barat, R., Serralta, J., Ruano, M. V., Jiménez, E., Ribes, J., Seco, A., and Ferrer, J. (2013). Biological nutrient removal model no. 2 (BNRM2): A general model for wastewater treatment plants. *Water Science and Technology* 67, 1481–1489.

Batstone, D. J., Keller, J., Angelidaki, I., Kalyuzhnyi, S. V., Pavlostathis, S. G., Rozzi, A., Sanders, W. T., Siegrist, H., and Vavilin, V. A. (2002). *Anaerobic Digestion Model No. 1 (ADM1).* London: IWA Publishing.

Batstone, D. J., Keller, J., and Blackall, L. L. (2004). The influence of substrate kinetics on the microbial community structure in granular anaerobic biomass. *Water Research* 38, 1390–1404.

Batstone, D. J., Puyol, D., Flores-Alsina, X., and Rodríguez, J. (2015). Mathematical modelling of anaerobic digestion processes: applications and future needs. *Reviews in Environmental Science and Bio/Technology*, 595–613.

Belfort, G., Davis, R. H., and Zydney, A. L. (1994). The behavior of suspensions and macromolecular solutions in crossflow microfiltration. *Journal of Membrane Science* 96, 1–58.

Ben Aim, R. M., and Semmens, M. J. (2002). Membrane bioreactors for wastewater treatment and reuse: a success story. *Water science and technology* 47, 1–5. Available at: http://www.ncbi.nlm.nih.gov/pubmed/12578166.

Benedetti, L., Claeys, F., Nopens, I., and Vanrolleghem, P. A. (2011). Assessing the convergence of LHS Monte Carlo simulations of wastewater treatment models. *Water Science and Technology* 63, 2219–2224.

BenSaïda, A. (2009). Shapiro-Wilk and Shapiro-Francia normality tests. *MATLAB Central File Exchange.* Available at: https://nl.mathworks.com/matlabcentral/fileexchange/13964-shapiro-wilk-and-shapiro-francia-normality-tests [Accessed September 1, 2018].

Benyahia, B., Sari, T., Cherki, B., and Harmand, J. (2013). Anaerobic membrane bioreactor modeling in the presence of Soluble Microbial Products (SMP) - the Anaerobic Model AM2b. *Chemical Engineering Journal.*

Bequette, B. W. (2003). *Process control : modeling, design, and simulation.* Upper Saddle River, N.J.: Prentice Hall PTR.

Bérubé, P. R., Hall, E. R., and Sutton, P. M. (2006). Parameters Governing Permeate Flux in an Anaerobic Membrane Bioreactor Treating Low-Strength Municipal Wastewaters: A Literature Review. *Water Environment Research* 78, 887–896.

Bouhabila, E. H., Ben A??m, R., and Buisson, H. (2001). Fouling characterisation in membrane bioreactors. *Separation and Purification Technology* 22–23, 123–132.

Boyle-Gotla, A., Jensen, P. D., Yap, S. D., Pidou, M., Wang, Y., and Batstone, D. J. (2014). Dynamic multidimensional modelling of submerged membrane bioreactor fouling. *Journal of Membrane Science* 467, 153–161.

Braguglia, C. M., Mininni, G., and Rolle, E. (2006). Influence of anaerobic digestion on particle surface charge and optimal polymer dosage. *Water Science and Technology* 54, 43–50.

Bratby, J. (2016). *Coagulation and Flocculation in Water and Wastewater Treatment.* Third Edit. London, UK: IWA publishing.

Brauns, E., Van Hoof, E., Huyskens, C., and De Wever, H. (2011). On the concept of a supervisory, fuzzy set logic based, advanced filtration control in membrane bioreactors. *Desalination and Water Treatment* 29, 119–127.

Bugge, T. V., Jørgensen, M. K., Christensen, M. L., and Keiding, K. (2012). Modeling cake buildup under TMP-step filtration in a membrane bioreactor: Cake compressibility is significant. *Water Research* 46, 4330–4338.

Carman, P. C. (1997). Fluid flow through granular beds. *Chemical Engineering Research and Design* 75, S32–S48.

Casolari, A. (1988). "Microbial death," in *Physiological Models in Microbiology*, eds. M. Bazin and J. I. Prosser (Boca Raton, FL, USA: CRC Press), 1–44.

Chae, S.-R., Ahn, Y.-T., Kang, S.-T., and Shin, H.-S. (2006). Mitigated membrane fouling in a vertical submerged membrane bioreactor (VSMBR). *Journal of Membrane Science* 280, 572–581.

Charfi, A., Thongmak, N., Benyahia, B., Aslam, M., Harmand, J., Amar, N. Ben, Lesage, G., Sridang, P., Kim, J., and Heran, M. (2017). A modelling approach to study the fouling of an anaerobic membrane bioreactor for industrial wastewater treatment. *Bioresource Technology* 245, 207–215.

Chianese, S., Fenti, A., Iovino, P., Musmarra, D., and Salvestrini, S. (2020). Sorption of organic pollutants by humic acids: A review. *Molecules* 25, 1–17.

Cho, J., Song, K. G., and Ahn, K. H. (2005). The activated sludge and microbial substances influences on membrane fouling in submerged membrane bioreactor: Unstirred batch cell test. *Desalination* 183, 425–429.

Choo, K. H., Kang, I. J., Yoon, S. H., Park, H., Kim, J. H., Adiya, S., and Lee, C. H. (2000). Approaches to membrane fouling control in anaerobic membrane bioreactors. *Water Science and Technology* 41, 363–371.

Christensen, M. L., Niessen, W., Sørensen, N. B., Hansen, S. H., Jørgensen, M. K., and Nielsen, P. H. (2018). Sludge fractionation as a method to study and predict fouling in MBR systems. *Separation and Purification Technology* 194, 329–337.

Collins, J. H., Yoon, S.-H., Musale, D., Kong, J. F., Koppes, J., Sundararajan, S., Tsai, S.-P., Hallsby, G. A., Cachia, P., and Kronoveter, K. (2006). Membrane performance enhancer evaluations on pilot- and full-scale membrane bioreactors. *Water and Environment Journal* 20, 43–47.

Cunha, J. R., Tervahauta, T., van der Weijden, R. D., Hernández Leal, L., Zeeman, G., and Buisman, C. J. N. (2018). Simultaneous recovery of calcium phosphate granules and methane in anaerobic treatment of black water: Effect of bicarbonate and calcium fluctuations. *Journal of Environmental Management* 216, 399–405.

De Graaff, M. S., Temmink, H., Zeeman, G., and Buisman, C. J. N. (2010). Anaerobic Treatment of Concentrated Black Water in a UASB Reactor at a Short HRT. *Water* 2, 101–119.

de La Torre, T. (2013). The Quest for a Universal Indicator for MBR Fouling. in (Technischen Universität Berlin, Germany).

de La Torre, T., Mottschall, M., Lesjean, B., Drews, A., Iheanaetu, A., and Kraume, M. (2010). Filterability assessment in membrane bioreactors using an in-situ filtration test cell. *Water Science and Technology* 61, 2809–2816.

De Temmerman, L., Maere, T., Temmink, H., Zwijnenburg, A., and Nopens, I. (2015). The effect of fine bubble aeration intensity on membrane bioreactor sludge characteristics and fouling. *Water Research* 76, 99–109.

Deng, L., Guo, W., Ngo, H. H., Zhang, H., Wang, J., Li, J., Xia, S., and Wu, Y. (2016). Biofouling and control approaches in membrane bioreactors. *Bioresource Technology* 221, 656–665.

Dereli, R. K., Ersahin, M. E., Ozgun, H., Ozturk, I., Jeison, D., van der Zee, F., and van Lier, J. B. (2012). Potentials of anaerobic membrane bioreactors to overcome treatment limitations induced by industrial wastewaters. *Bioresource Technology* 122, 160–170.

Díaz, H., Azócar, L., Torres, A., Lopes, S. I. C., and Jeison, D. (2014). Use of flocculants for increasing permeate flux in anaerobic membrane bioreactors. *Water Science and Technology* 69, 2237–2242.

Dong, Q., Parker, W., and Dagnew, M. (2015). Impact of $FeCl_3$ dosing on AnMBR treatment of municipal wastewater. *Water research* 80, 281–93.

Dong, Q., Parker, W., and Dagnew, M. (2018). Dynamic characterization of a FeCl3-dosed anaerobic membrane bioreactor (AnMBR) treating municipal wastewater. *Water Science and Technology* 2017, 481–491.

Donoso-Bravo, A., Mailier, J., Martin, C., Rodríguez, J., Aceves-Lara, C. A., and Wouwer, A. Vande (2011). Model selection, identification and validation in anaerobic digestion: A review. *Water Research* 45, 5347–5364.

Drews, A. (2010). Membrane fouling in membrane bioreactors — Characterisation , contradictions , cause and cures. *Journal of Membrane Science* 363, 1–28.

Dubois, M., Gilles, K. A., Hamilton, J. K., Rebers, P. A., and Smith, F. (1956). Colorimetric method for determination of sugars and related substances. *Analytical Chemistry* 28, 350–356.

Durán, F. (2013). Modelación matemática del tratamiento anaerobio de aguas residuales urbanas incluyendo las bacterias sulfatorreductoras. Aplicación a un biorreactor anaerobio de membranas. in (Universitat Politècnica de València).

Dvořák, L., Gómez, M., Dolina, J., and Černín, A. (2016). Anaerobic membrane bioreactors—a mini review with emphasis on industrial wastewater treatment: applications, limitations and perspectives. *Desalination and Water Treatment* 57, 19062–19076.

El-Naas, M. H., and Alhaija, M. A. (2011). "Modelling of adsorption processes," in *Mathematical Modelling*, ed. C. R. Brennan (Nova Publishers, Inc.).

Elmitwalli, T. A., van Leeuwen, M., Kujawa-Roeleveld, K., Sanders, W., and Zeeman, G. (2006). Anaerobic biodegradability and digestion in accumulation systems for concentrated black water and kitchen organic-wastes. *Water Science and Technology* 53, 167–175.

Evenblij, H. (2006). Filtration Characteristics in Membrane Bioreactors. in (Delft University of Technology, The Netherlands).

Evenblij, H., Geilvoet, S., Graaf, J. H. J. M. Van Der, and R, H. F. Van Der (2005). Filtration characterisation for assessing MBR performance: three cases compared. *Desalination* 178, 115–124.

Fan, F., Zhou, H., and Husain, H. (2007). Use of chemical coagulants to control fouling potential for wastewater membrane bioreactor processes. *Water environment research: a research publication of the Water Environment Federation* 79, 952–957.

Feng, Y. (2004). Calibration and Verification of a Mathematical Model for the Simulation of Blackwater/Biowaste Digestion (MSc thesis). in (Hamburg University of Technology).

Ferrero, G., Rodríguez-Roda, I., and Comas, J. (2012). Automatic control systems for submerged membrane bioreactors: A state-of-the-art review. *Water Research* 46, 3421–3433.

Field, A. (2009). *Discovering Statistics Using SPSS*. 3rd ed. London, UK: SAGE Publications, Limited.

Frølund, B., Griebe, T., and Nielsen, P. H. (1995). Enzymatic activity in the activated-sludge floc matrix. *Applied Microbiology and Biotechnology* 43, 755–761.

Garcia Orozco, J. H. (2008). "Toxicity," in *Biological Wastewater Treatment: Principles, Modelling and Design*, eds. M. Henze, M. C. M. Van Loosdrecht, G. A. Ekama, and D. Brdjanovic (London, UK: IWA Publishing), 273–290.

Geilvoet, S. (2010). The Delft Filtration Characterisation method Assessing membrane bioreactor activated sludge filterability. in (Delft University of Technology, The Netherlands).

Gil, J. A., Krzeminski, P., Lier, J. B. Van, Graaf, J. H. J. M. Van Der, Wijffels, T., and Prats, D. (2011). Analysis of the filterability in industrial MBRs . Influence of activated sludge parameters and constituents on filterability. *Journal of Membrane Science* 385–386, 96–109.

Gkotsis, P., Peleka, E., Zamboulis, D., Mitrakas, M., Tolkou, A., and Zouboulis, A. (2017). Wastewater Treatment in Membrane Bioreactors: The Use of Polyelectrolytes to Control Membrane Fouling. *Environmental Processes* 4, 9–21.

Gorini, D., Choubert, J.-M., le Pimpec, P., and Heduit, A. (2011). Concentrations and fate of sugars, proteins and lipids during domestic and agro-industrial aerobic treatment. *Water Science and Technology* 63, 1669–1677.

Govoreanu, R., Saveyn, H., Van der Meeren, P., and Vanrolleghem, P. A. (2004). Simultaneous determination of activated sludge floc size distribution by different techniques. *Water Science and Technology* 50, 39–46.

Guo, H., Oosterkamp, M. J., Tonin, F., Hendriks, A., Nair, R., van Lier, J. B., and de Kreuk, M. (2021). Reconsidering hydrolysis kinetics for anaerobic digestion of waste activated sludge applying cascade reactors with ultra-short residence times. *Water Research* 202, 117398.

Hamedi, H., Ehteshami, M., Mirbagheri, S. A., Rasouli, S. A., and Zendehboudi, S. (2019). Current Status and Future Prospects of Membrane Bioreactors (MBRs) and Fouling Phenomena: A Systematic Review. *Canadian Journal of Chemical Engineering* 97, 32–58.

Helton, J. C., and Davis, F. J. (2003). Latin hypercube sampling and the propagation of uncertainty in analyses of complex systems. *Reliability Engineering and System Safety* 81, 23–69.

Hendriks, A. T. W. M., van Lier, J. B., and de Kreuk, M. K. (2018). Growth media in anaerobic fermentative processes: The underestimated potential of thermophilic fermentation and anaerobic digestion. *Biotechnology Advances* 36, 1–13.

Horvath, A. E., Lindström, T., and Laine, J. (2006). On the indirect polyelectrolyte titration of cellulosic fibers. Conditions for charge stoichiometry and comparison with ESCA. *Langmuir* 22, 824–830.

Hu, Y., Cheng, H., Ji, J., and Li, Y.-Y. (2020). A review of anaerobic membrane bioreactors for municipal wastewater treatment with a focus on multicomponent biogas and membrane fouling control. *Environmental Science: Water Research and Technology.*

Huang, B. C., Guan, Y. F., Chen, W., and Yu, H. Q. (2017). Membrane fouling characteristics and mitigation in a coagulation-assisted microfiltration process for municipal wastewater pretreatment. *Water Research* 123, 216–223.

Hubbe, M. A., Wu, N., Rojas, O. J., and Park, S. (2011). Permeation of a cationic polyelectrolyte into mesoporous silica. Part 3. Using adsorption isotherms to elucidate streaming potential results. *Colloids and Surfaces A: Physicochemical and Engineering Aspects* 381, 1–6.

Huyskens, C., Brauns, E., Van Hoof, E., and De Wever, H. (2008). A new method for the evaluation of the reversible and irreversible fouling propensity of MBR mixed liquor. *Journal of Membrane Science* 323, 185–192.

Huyskens, C., Brauns, E., Van Hoof, E., Diels, L., and De Wever, H. (2011a). Validation of a supervisory control system for energy savings in membrane bioreactors. *Water Research* 45, 1443–1453.

Huyskens, C., Lenaerts, S., Brauns, E., Diels, L., and De Wever, H. (2011b). Study of (ir)reversible fouling in MBRs under various operating conditions using new on-line fouling sensor. *Separation and Purification Technology* 81, 208–215.

Iman, R., and Conover, W. (1982). A distribution-free approach to inducing rank correlation among input variables. *Communications in Statistics - Simulation and Computation* 11, 311–334.

Ishiguro, M., Tan, W., and Koopal, L. K. (2007). Binding of cationic surfactants to humic substances. *Colloids and Surfaces A: Physicochemical and Engineering Aspects* 306, 29–39.

Iversen, V. (2010). Comprehensive assessment of flux enhancers in membrane bioreactors for wastewater treatment. in (Technische Universität Berlin, Germany).

Iversen, V., Koseoglu, H., Yigit, N. O., Drews, A., Kitis, M., Lesjean, B., and Kraume, M. (2009a). Impacts of membrane flux enhancers on activated sludge respiration and nutrient removal in MBRs. *Water Research* 43, 822–830.

Iversen, V., Mehrez, R., Horng, R. Y., Chen, C. H., Meng, F., Drews, A., Lesjean, B., Ernst, M., Jekel, M., and Kraume, M. (2009b). Fouling mitigation through flocculants and adsorbents addition in membrane bioreactors: Comparing lab and pilot studies. *Journal of Membrane Science* 345, 21–30.

Iversen, V., Mohaupt, J., Drews, A., Kraume, M., and Lesjean, B. (2008). Side effects of flux enhancing chemicals in membrane bioreactors (MBRs): study on their biological toxicity and their residual fouling propensity. *Water Science and Technology* 57, 117–123.

Janssen, L. P. B. ., and Warmoeskerken, M. M. C. . (1997). *Transport phenomena data companion.* 3rd ed. Delft, Netherlands, Netherlands: Delftse Universitaire Pers.

Jeison, D., and van Lier, J. B. (2006). On-line cake-layer management by trans-membrane pressure steady state assessment in Anaerobic Membrane Bioreactors for wastewater treatment. *Biochemical Engineering Journal* 29, 204–209.

Jeldres, R. I., Fawell, P. D., and Florio, B. J. (2018). Population balance modelling to describe the particle aggregation process: A review. *Powder Technology* 326, 190–207.

Jia, X. S., Fang, H. H. P., and Furumai, H. (1996). Surface charge and extracellular polymer of sludge in the anaerobic degradation process. *Water Science and Technology* 34, 309–316.

Jørgensen, M. K., Keiding, K., and Christensen, M. L. (2014). On the reversibility of cake buildup and compression in a membrane bioreactor. *Journal of Membrane Science* 455, 152–161.

Judd, S., and Judd, C. (2011). *The MBR book: principles and applications of membrane bioreactors for water and wastewater treatment.* Second Edi. , ed. C. Judd, Simon; Judd Oxford: Butterworth-Heinemann.

Kam, S., and Gregory, J. (2001). The interaction of humic substances with cationic polyelectrolytes. *Water Research* 35, 3557–3566.

Kasper, D. R. (1971). Theoretical and experimental investigations of the flocculation of charged particles in aqueous solutions by polyelectrolytes of opposite charge. in (California Institute of Technology, US). Available at: http://thesis.library.caltech.edu/8200/1/Kasper-dr-1971.pdf.

Kooijman, G., De Kreuk, M. K., and Van Lier, J. B. (2017a). Influence of chemically enhanced primary treatment on anaerobic digestion and dewaterability of waste sludge. *Water Science and Technology* 76, 1629–1639.

Kooijman, G., Lopes, W., Zhou, Z., Guo, H., de Kreuk, M., Spanjers, H., and van Lier, J. (2017b). Impact of coagulant and flocculant addition to an anaerobic dynamic membrane bioreactor (AnDMBR) treating waste-activated sludge. *Membranes* 7, 18.

Koseoglu, H., Yigit, N. O., Civelekoglu, G., Harman, B. I., and Kitis, M. (2012). Effects of chemical additives on filtration and rheological characteristics of MBR sludge. *Bioresource Technology* 117, 48–54.

Koseoglu, H., Yigit, N. O., Iversen, V., Drews, A., Kitis, M., Lesjean, B., and Kraume, M. (2008). Effects of several different flux enhancing chemicals on filterability and fouling reduction of membrane bioreactor (MBR) mixed liquors. *Journal of Membrane Science* 320, 57–64.

Kraume, M., Wedi, D., Schaller, J., Iversen, V., and Drews, A. (2009). Fouling in MBR: What use are lab investigations for full scale operation? *Desalination* 236, 94–103.

Krauth, K., and Staab, K. F. (1993). Pressurized bioreactor with membrane filtration for wastewater treatment. *Water Research* 27, 405–411.

Krzeminski, P., Iglesias-Obelleiro, A., Madebo, G., Garrido, J. M., van der Graaf, J. H. J. M., and van Lier, J. B. (2012). Impact of temperature on raw wastewater composition and activated sludge filterability in full-scale MBR systems for municipal sewage treatment. *Journal of Membrane Science* 423–424, 348–361.

Krzeminski, P., Leverette, L., Malamis, S., and Katsou, E. (2017). Membrane bioreactors – a review on recent developments in energy reduction, fouling control, novel configurations, {LCA} and market prospects. *Journal of Membrane Science* 527, 207–227.

Kulesha, O., Maletskyi, Z., and Ratnaweera, H. (2018). State-of-the-art of membrane flux enhancement in membrane bioreactor. *Cogent Engineering* 5, 1–30.

Le Clech, P., Jefferson, B., Chang, I. S., and Judd, S. J. (2003). Critical flux determination by the flux-step method in a submerged membrane bioreactor. *Journal of Membrane Science* 227, 81–93.

Lee, W. N., Chang, I. S., Hwang, B. K., Park, P. K., Lee, C. H., and Huang, X. (2007). Changes in biofilm architecture with addition of membrane fouling reducer in a membrane bioreactor. *Process Biochemistry* 42, 655–661.

Li, X. yan, and Wang, X. mao (2006). Modelling of membrane fouling in a submerged membrane bioreactor. *Journal of Membrane Science* 278, 151–161.

Lidholm, O., and Ossiansson, E. (2008). Modeling Anaerobic Digestion. in.

Lim, K., Evans, P. J., Utter, J., Malki, M., and Parameswaran, P. (2020). Dynamic monitoring and proactive fouling management in a pilot scale gas-sparged anaerobic membrane bioreactor. *Environmental Science: Water Research & Technology* 6, 2914–2925.

Lin, H., Peng, W., Zhang, M., Chen, J., Hong, H., and Zhang, Y. (2013). A review on anaerobic membrane bioreactors: Applications, membrane fouling and future perspectives. *Desalination* 314, 169–188.

Lousada-Ferreira, M. (2011). Filterability and Sludge Concentration in Membrane Bioreactors. in (Delft University of Technology, The Netherlands).

Lousada-Ferreira, M., Krzeminski, P., Geilvoet, S., Moreau, A., Gil, J. A., Evenblij, H., van Lier, J. B., van der Graaf, J. H. J. M., Lier, J. B. Van, and Graaf, J. H. J. M. Van Der (2014). Filtration characterization method as tool to assess membrane bioreactor sludge filterability-the Delft experience. *Membranes* 4, 227–242.

Lousada-Ferreira, M., Odriozola, M., Spanjers, H., and van Lier, J. (2017). On-line fouling control tool for Anaerobic Membrane Bioreactors. in *12th IWA Specialized Conference on Instrumentation, Control and Automation* (Québec).

Lousada-Ferreira, M., van Lier, J. B., and van der Graaf, J. H. J. M. (2015). Impact of suspended solids concentration on sludge filterability in full-scale membrane bioreactors. *Journal of Membrane Science* 476, 68–75.

Malamis, S., Andreadakis, A., Mamais, D., and Noutsopoulos, C. (2014). Comparison of alternative additives used for the mitigation of membrane fouling in membrane bioreactors. *Desalination and Water Treatment* 52, 5740–5747.

Mannina, G., Di Bella, G., and Viviani, G. (2011). An integrated model for biological and physical process simulation in membrane bioreactors (MBRs). *Journal of Membrane Science* 376, 56–69.

Mara, D., Horan, N., and Hao, O. J. (2003). *Handbook of Water and Wastewater Microbiology*.

Meng, F., Zhang, S., Oh, Y., Zhou, Z., Shin, H.-S. S., and Chae, S.-R. R. (2017). Fouling in membrane bioreactors: An updated review. *Water Research* 114, 151–180.

Merkus, H. G. (2009). *Particle size measurements: fundamentals, practice, quality*. Springer Science+Business Media B.V.

Metcalf, L., Eddy, H. P., Tchobanoglous, G., Burton, F. L., and Stensel, H. D. (2002). *Wastewater Engineering: Treatment and Reuse*. 4th ed. New York: McGraw Hill.

Moreau, A. (2010). Filterability assessment of membrane bioreactors at European scale. in (Delft University of Technology, The Netherlands). Available at:

http://www.narcis.nl/publication/RecordID/oai:tudelft.nl:uuid:0cc2786d-f2f3-4189-94c3-869ae05588bd.

Moreau, A. A., Ratkovich, N., Nopens, I., and van der Graaf, J. H. J. M. (2009). The (in)significance of apparent viscosity in full-scale municipal membrane bioreactors. *Journal of Membrane Science* 340, 249–256.

Muñoz Sierra, J. D., Oosterkamp, M. J., Wang, W., Spanjers, H., and van Lier, J. B. (2018). Impact of long-term salinity exposure in anaerobic membrane bioreactors treating phenolic wastewater: Performance robustness and endured microbial community. *Water Research* 141, 172–184.

Munz, G., Gori, R., Mori, G., and Lubello, C. (2007). Powdered activated carbon and membrane bioreactors (MBRPAC) for tannery wastewater treatment: long term effect on biological and filtration process performances. *Desalination* 207, 349–360.

Naessens, W. (2018). Towards improved membrane fouling modelling: from an empirical to a spatially explicit framework, PhD Thesis. in (Ghent University, Belgium).

Naessens, W., Maere, T., and Nopens, I. (2012a). Critical review of membrane bioreactor models - Part 1: Biokinetic and filtration models. *Bioresource Technology* 122, 95–106.

Naessens, W., Maere, T., Ratkovich, N., Vedantam, S., and Nopens, I. (2012b). Critical review of membrane bioreactor models - Part 2: Hydrodynamic and integrated models. *Bioresource Technology* 122, 107–118.

Nam, K., Heo, S., Rhee, G., Kim, M., and Yoo, C. (2021). Dual-objective optimization for energy-saving and fouling mitigation in MBR plants using AI-based influent prediction and an integrated biological-physical model. *Journal of Membrane Science* 626, 119208.

Odriozola, M., Abraham, E., Lousada-Ferreira, M., Spanjers, H., and van Lier, J. B. (2019). Identification of the Methanogenesis Inhibition Mechanism Using Comparative Analysis of Mathematical Models. *Frontiers in Bioengineering and Biotechnology* 7, 93.

Odriozola, M., Lousada-Ferreira, M., Spanjers, H., and van Lier, J. B. (2021). Effect of sludge characteristics on optimal required dosage of flux enhancer in anaerobic membrane bioreactors. *Journal of Membrane Science* 619, 118776.

Odriozola, M., Morales, N., Vázquez-Padín, J. R., Lousada-Ferreira, M., Spanjers, H., and van Lier, J. B. (2020). Fouling Mitigation by Cationic Polymer Addition into a Pilot-Scale Anaerobic Membrane Bioreactor Fed with Blackwater. *Polymers* 12, 2383.

Ozgun, H., Dereli, R. K., Ersahin, M. E., Kinaci, C., Spanjers, H., and van Lier, J. B. (2013). A review of anaerobic membrane bioreactors for municipal wastewater treatment: Integration options , limitations and expectations. *Separation and Purification Technology* 118, 89–104.

Padhye, L., Luzinova, Y., Cho, M., Mizaikoff, B., Kim, J.-H., and Huang, C.-H. (2011). PolyDADMAC and Dimethylamine as Precursors of N-Nitrosodimethylamine during Ozonation: Reaction Kinetics and Mechanisms. *Environmental Science & Technology* 45, 4353–4359.

Perry, R. H., and Green, D. W. (2008). *Perry's Chemical Engineers' Handbook.*

Remy, M. J. J. (2012). Low concentration of powdered activated carbon decreases fouling in membrane bioreactors. in (Wageningen University, the Netherlands).

Robles, A., Ruano, M. V., Charfi, A., Lesage, G., Heran, M., Harmand, J., Seco, A., Steyer, J.-P., Batstone, D. J., Kim, J., and Ferrer, J. (2018). A review on anaerobic membrane bioreactors (AnMBRs) focused on modelling and control aspects. *Bioresource Technology* 270, 612–626.

Robles, A., Ruano, M. V., Ribes, J., and Ferrer, J. (2013a). Advanced control system for optimal filtration in submerged anaerobic MBRs (SAnMBRs). *Journal of Membrane Science* 430, 330–341.

Robles, A., Ruano, M. V., Ribes, J., Seco, A., and Ferrer, J. (2013b). A filtration model applied to submerged anaerobic MBRs (SAnMBRs). *Journal of Membrane Science* 444, 139–147.

Robles, A., Ruano, M. V., Ribes, J., Seco, A., and Ferrer, J. (2014a). Model-based automatic tuning of a filtration control system for submerged anaerobic membrane bioreactors (AnMBR). *Journal of Membrane Science* 465, 14–26.

Robles, A., Ruano, M. V., Ribes, J., Seco, A., and Ferrer, J. (2014b). Global sensitivity analysis of a filtration model for submerged anaerobic membrane bioreactors (AnMBR). *Bioresource Technology* 158, 365–373.

Sander, R. (2015). Compilation of Henry's law constants (version 4.0) for water as solvent. *Atmospheric Chemistry and Physics* 15, 4399–4981.

Shen, L. G., Lei, Q., Chen, J. R., Hong, H. C., He, Y. M., and Lin, H. J. (2015). Membrane fouling in a submerged membrane bioreactor: Impacts of floc size. *Chemical Engineering Journal* 269, 328–334.

Shi, Y., Huang, J., Zeng, G., Gu, Y., Hu, Y., Tang, B., Zhou, J., Yang, Y., and Shi, L. (2018). Evaluation of soluble microbial products (SMP) on membrane fouling in membrane bioreactors (MBRs) at the fractional and overall level: a review. *Reviews in Environmental Science and Biotechnology* 17, 71–85.

Shin, C., and Bae, J. (2018). Current status of the pilot-scale anaerobic membrane bioreactor treatments of domestic wastewaters: A critical review. *Bioresource Technology* 247, 1038–1046.

Sin, G., and Gernaey, K. (2016). "Data Handling and Parameter Estimation," in *Experimental Methods in Wastewater Treatment*, eds. M. C. M. van Loosdrecht and D. B. P.H. Nielsen, C.M. Lopez-Vazquez (London, UK: IWA Publishing), 201–234.

Sin, G., Gernaey, K. V., Neumann, M. B., van Loosdrecht, M. C. M., and Gujer, W. (2009). Uncertainty analysis in WWTP model applications: A critical discussion using an example from design. *Water Research* 43, 2894–2906.

Sin, G., Gernaey, K. V., Neumann, M. B., van Loosdrecht, M. C. M., and Gujer, W. (2011). Global sensitivity analysis in wastewater treatment plant model applications: Prioritizing sources of uncertainty. *Water Research* 45, 639–651.

Skouteris, G., Hermosilla, D., López, P., Negro, C., and Blanco, Á. (2012). Anaerobic membrane bioreactors for wastewater treatment: A review. *Chemical Engineering Journal* 198–199, 138–148.

Skouteris, G., Saroj, D., Melidis, P., Hai, F. I., and Ouki, S. (2015). The effect of activated carbon addition on membrane bioreactor processes for wastewater treatment and reclamation – A critical review. *Bioresource Technology* 185, 399–410.

Smith, A. L., Stadler, L. B., Love, N. G., Skerlos, S. J., and Raskin, L. (2012). Perspectives on anaerobic membrane bioreactor treatment of domestic wastewater: A critical review. *Bioresource Technology* 122, 149–159.

Song, K., Kim, Y., and Ahn, K. (2008). Effect of coagulant addition on membrane fouling and nutrient removal in a submerged membrane bioreactor. *Desalination* 221, 467–474.

Sørensen, B. L., and Sørensen, P. B. (1997). Structure Compression in Cake Filtration. *Journal of Environmental Engineering* 123, 345–353.

Spanjers, H., and Vanrolleghem, P. A. (2016). "Respirometry," in *Experimental Methods in Wastewater Treatment*, eds. M. C. M. van Loosdrecht and D. B. P.H. Nielsen, C.M. Lopez-Vazquez (London, UK, UK: IWA Publishing).

Stuckey, D. C. (2012). Recent developments in anaerobic membrane reactors. *Bioresource Technology*.

Suh, C., Lee, S., and Cho, J. (2013). Investigation of the effects of membrane fouling control strategies with the integrated membrane bioreactor model. *Journal of Membrane Science* 429, 268–281.

Tan, S., Jiang, S., Li, X., and Yuan, Q. (2018). Factors affecting N-nitrosodimethylamine formation from poly(diallyldimethylammonium chloride) degradation during chloramination. *Royal Society Open Science* 5, 180025.

Tan, W.-F. F., Norde, W., and Koopal, L. K. (2011). Humic substance charge determination by titration with a flexible cationic polyelectrolyte. *Geochimica et Cosmochimica Acta* 75, 5749–5761.

Teli, A., Antonelli, M., Bonomo, L., and Malpei, F. (2012). MBR fouling control and permeate quality enhancement by polyaluminium chloride dosage: a case study. *Water Science and Technology* 66, 1289–1295.

Tervahauta, T., van der Weijden, R. D., Flemming, R. L., Hernández Leal, L., Zeeman, G., and Buisman, C. J. N. (2014). Calcium phosphate granulation in anaerobic treatment of black water: A new approach to phosphorus recovery. *Water Research* 48, 632–642.

The MathWorks, I. (2018). Curve Fitting Toolbox^{TM} User's Guide. R2018a ed. Natick, Massachusetts, United States, Massachusetts, United States: The MathWorks, Inc. Available at: https://nl.mathworks.com/help/releases/R2018a/pdf_doc/curvefit/curvefit.pdf.

Tran, P. L., Huynh, E., Hamood, A. N., de Souza, A., Schultz, G., Liesenfeld, B., Mehta, D., Webster, D., and Reid, T. W. (2017). The ability of quaternary ammonium groups attached to a urethane bandage to inhibit bacterial attachment and biofilm formation in a mouse wound model. *International Wound Journal* 14, 79–84.

Tugtas, A. E., Tezel, U., and Pavlostathis, S. G. (2006). An extension of the Anaerobic Digestion Model No. 1 to include the effect of nitrate reduction processes. *Water Science & Technology* 54, 41–49.

van Lier, J. B., Mahmoud, N., and Zeeman, G. (2020). "Anaerobic Wastewater Treatment," in *Biological Wastewater Treatment, Principles, Modelling and Design, 2nd Edition*, eds. M. C. M. van Loosdrecht, G. A. Ekama, and D. Brdjanovic (IWA Publishing, London, UK).

Wang, H., Chen, Z., Miao, J., and Li, Y. (2016). A novel approach for mitigation of membrane fouling: Concomitant use of flocculant and magnetic powder. *Bioresource Technology* 209, 318–325.

Wang, H., Zhang, L., Li, Y., and Hu, C. (2014). Influence of Filtration Aids on Continuous Filtration in Membrane Bioreactors. *Industrial & Engineering Chemistry Research* 53, 7202–7208.

Wang, L., Chen, S. S., Tsang, D. C. W., Poon, C. S., and Ok, Y. S. (2017). Enhancing anti-microbial properties of wood-plastic composites produced from timber and plastic wastes. *Environmental Science and Pollution Research* 24, 12227–12237.

Wang, Z., Mei, X., Ma, J., Grasmick, A., and Wu, Z. (2013). Potential Foulants and Fouling Indicators in MBRs: A Critical Review. *Separation Science and Technology* 48, 22–50.

Wendland, C. (2008). Anerobic Digestion of Blackwater and Kitchen Refuse. in (Technischen Universität Hamburg-Harburg).

Wendland, C., Deegener, S., Behrendt, J., Toshev, P., and Otterpohl, R. (2007). Anaerobic digestion of blackwater from vacuum toilets and kitchen refuse in a continuous stirred tank reactor (CSTR). *Water Science and Technology* 55, 187–194.

Wozniak, T. (2010). MBR design and operation using MPE-technology (Membrane Performance Enhancer). *Desalination* 250, 723–728.

Wu, J., Chen, F., Huang, X., Geng, W., and Wen, X. (2006). Using inorganic coagulants to control membrane fouling in a submerged membrane bioreactor. *Desalination* 197, 124–136.

Wu, J., He, C., and Zhang, Y. (2012). Modeling membrane fouling in a submerged membrane bioreactor by considering the role of solid, colloidal and soluble components. *Journal of Membrane Science* 397–398, 102–111.

Xiong, Y., Harb, M., and Hong, P.-Y. (2016). Characterization of biofoulants illustrates different membrane fouling mechanisms for aerobic and anaerobic membrane bioreactors. *Separation and Purification Technology* 157, 192–202.

Yoon, S., and Collins, J. H. (2006). A novel flux enhancing method for membrane bioreactor (MBR) process using polymer. *Desalination* 191, 52–61.

Yoon, S. H., Collins, J. H., Musale, D., Sundararajan, S., Tsai, S. P., Hallsby, G. A., Kong, J. F., Koppes, J., and Cachia, P. (2005). Effects of flux enhancing polymer on the characteristics of sludge in membrane bioreactor process. *Water Science and Technology* 51, 151–157.

Zarragoitia-González, A., Schetrite, S., Alliet, M., Jáuregui-Haza, U., and Albasi, C. (2008). Modelling of submerged membrane bioreactor: Conceptual study about link between activated slugde biokinetics, aeration and fouling process. *Journal of Membrane Science* 325, 612–624.

Zhang, J. S., Zhou, J. T., Su, Y., and Fane, A. G. (2010). Transient Performance of MBR with Flux Enhancing Polymer Addition. *Separation Science and Technology* 45, 982–992.

Zhang, Q., Singh, S., and Stuckey, D. C. (2017). Fouling reduction using adsorbents/flocculants in a submerged anaerobic membrane bioreactor. *Bioresource Technology* 239, 226–235.

Zhao, X., Ma, J., Ma, H., Gao, D., Lv, X., and Zhang, J. (2016). Adsorptive removal of vinyl polymer tanning agents from aqueous solution using wastewater activated sludge. *Desalination and Water Treatment* 57, 11422–11432.

Zhou, J.-H., Wu, C.-H., Cheng, G.-F., Hong, Q.-K., Li, Y.-Z., and Wang, H.-Y. (2019). Impact of poly dimethyldiallylammonium chloride on membrane fouling mitigation in a membrane bioreactor. *Environmental Technology* 40, 1043–1049.

Zuthi, M. F. R., Ngo, H. H., Guo, W. S., Li, J. X., Xia, S. Q., and Zhang, Z. Q. (2013). New proposed conceptual mathematical models for biomass viability and membrane fouling of membrane bioreactor. *Bioresource Technology* 142, 737–740.